Biochar based amendments in the environment; different modeling approaches

PhD Thesis

Thesis supervisor: doc. Mgr. Lukáš Trakal, Ph.D.

Czech University of Life Sciences Prague

Faculty of Environmental Sciences

Department of Environmental Geosciences

Prague, 2022

Biochar based amendments in the environment; different modeling approaches

Petr Ouředníček

Thesis

This thesis is submitted in fulfillment of the requirements for the PhD degree at the Czech University of Life Sciences Prague, Faculty of Environmental Sciences.

Biochar based amendments in the environment; different modeling approaches.

Petr Ouředníček

Czech University of Life Sciences Prague (2022)

Acknowledgement

I would like to thank my supervisor, assoc. prof. Lukáš Trakal, for the opportunity to participate in this research. At the same time, I would like to thank the whole department, headed by prof. Komárek, for their patience and support. During my studies, I was also involved in sports (top-level athlete), so combining sport and science, especially during PhD. studies were often challenging, and a lot of support and tolerance of our department's collective was required. I would also like to thank Barbora Hudcová for her valuable advices during the writing of this thesis and special thanks to Luke Beesley for checking the translation, although he only had three days to do so. I would also like to thank my family, to my parents Petr and Zdeňka and to my wife Veronika for the support and energy they provided to me.

Abstract

This thesis presents a compilation of work on biochar based amendments through the investigation of their key properties and the application of suitable modeling approaches. Initially, the effect of biochar on the hydraulic parameters in contrasting soils was investigated, showing significant differences between biochar-treated soils and the control variant, i.e., an increase in water holding capacity, and bulk density and saturated hydraulic conductivity decrease. The effect can be explained by the interaction of H_2O molecules with the biochar surface facilitated by polar hydrogen bonds of O–H and C–O–H groups. These interactions caused intense swelling even at higher doses of biochar. The application of biochar to soils appears to be broadly suitable for addressing drought in drought-prone sandy soils. Other parts of the study were focused on the investigation and improvement of sorption parameters using biochar based materials, which are also necessary for subsequent modelling and general usability of materials. To this end, synthesized Mn oxide-biochar composites (AMO-char) were able to remove significantly greater quantities of various metal(loid)s from the aqueous solutions, especially at a ratio 2:1 (AMO:biochar), compared to pristine biochar. The combination of AMO and biochar resulted in a significant reduction of Mn leaching that is commonly observed after AMO application. The reduced Mn leaching was observed for both AMOchar composite and also AMO + biochar mixture. In order to increase the feasibility of AMO-based materials preparation for subsequent engineering applications, the replacement of the original reactants with less expensive ones and testing of materials against different metal(loid)s was performed in the next part of the thesis. Here, lower water content and different sugars (glucose, sucrose, and molasses) were used. Despite the fact that glucose-based AMOs (original) presented higher sorption efficiency for As(V), similar sorption efficiency toward Zn(II) and Cd(II) was observed, compared to the original AMO. Replacing glucose by molasses as a reducing agent during AMO synthesis dramatically decreased the total cost of the final materials, which suggested that such prepared (modified) biochar amendments could represent bespoke alternatives to standard remediation technologies. In the last part of the thesis, biochar based amendments were added to soil and tested in a dynamic system

(column experiments) during single metal and bimetal competitive sorption experiment using two contrasting metals, i.e., Pb(II) and Zn(II),showing a significant reduction of metal leaching from the treated soil. Subsequently, a speciation model in PHREEQC was constructed to elucidate dominant forms of major elements and the possible precipitation of mineral phases. Finally, the Hydrus 1D model was successfully calibrated, demonstrating that in a well-defined system at a constant pH, even dynamic processes can be partly modeled by a simple equilibrium solute transport model. Such an approach may be beneficial for straightforward experiments. However, a more comprehensive geochemical reaction-transport model (PHREEQC + HYDRUS) with the implementation of the Humic Ion-Binding Model VII is recommended and planned for future studies.

Abstrakt

Tato práce předkládá souhrn studií materiálů na bázi biocharu (biouhel) prostřednictvím zkoumání jejich klíčových vlastností a použití vhodných modelovacích přístupů. Nejprve byl zkoumán vliv biocharu na hydraulické parametry kontrastních půd, přičemž se ukázaly významné rozdíly mezi půdami ošetřenými biocharem a kontrolní variantou, tj. zvýšení vodní kapacity, snížení objemové hmotnosti a nasycené hydraulické vodivosti. Pozorovaný proces lze vysvětlit interakcí molekul H_2O s povrchem biocharu usnadněnou polárními vodíkovými vazbami skupin O–H a C–O–H. Tyto interakce způsobily intenzivní bobtnání i při vyšších dávkách biocharu. Aplikace biocharu do půdy se jeví jako vhodná pro řešení sucha, zvláště pak v písčitých půdách, které jsou na půdní sucho náchylné. Následující části studie byly zaměřeny výzkum a zlepšování sorpčních parametrů při použití materiálů na bázi biocharu, které jsou rovněž nezbytné pro modelování a také pro posouzení využitelnosti materiálů obecně. Za tímto účelem byly syntetizované kompozity oxidů Mn a biocharu (AMOchar), které byly schopny odstranit z vodných roztoků signifikantně větší množství studovaných (polo)kovů, zejména při poměru 2:1 (AMO:biochar), ve srovnání s čistým biocharem. Kombinace AMO a biocharu vedla k výraznému snížení uvolňování Mn z materiálu, které je běžně pozorováno po aplikaci AMO. Snížení loužení Mn bylo pozorováno jak u kompozitu AMOchar, tak i u směsi AMO + biochar. Za účelem zvýšení proveditelnosti přípravy materiálů na bázi AMO pro inženýrské aplikace byla v další části práce provedena náhrada původních reaktantů levnějšími (sacharóza, melasa) a byly provedeny testy těchto materiálů vůči různým (polo)kovům. Přestože AMO na bázi glukózy (původní) vykazovalo vyšší sorpční efektivitu pro As(V), sorpční efektivita vůči Zn(II) a Cd(II) nebyla významně odlišná ve srovnání s původními AMO. Nahrazení glukózy melasou jako redukčního činidla při syntéze AMO dramaticky snížilo celkové náklady na finální materiály, což naznačuje, že takto připravené (modifikované) materiály na bázi biocharu by mohly představovat nadějnou alternativu ke standardním sanačním technologiím. V poslední části práce byly do půdy přidány materiály na bázi biocharu, které byly testovány v dynamickém systému (kolonové experimenty) v prostředí s kompetitivní sorpce dvou kontrastních kovů (Pb(II) a Zn(II)). Výsledky prokázaly významné snížení vyplavování kovů z půdy ošetřené studovanými materiály. Následně byl sestaven speciační model v programu PHREEQC, který objasnil dominantní formy hlavních prvků a možné srážení minerálních fází. Nakonec byl úspěšně kalibrován model Hydrus 1D, což ukazuje, že v dobře definovaném systému při konstantním pH lze i dynamické procesy částečně modelovat jednoduchým modelem rovnovážného transportu rozpuštěných látek. Takový přístup může být přínosný pro jednoduché experimenty. Pro budoucí studie je v plánu používat komplexnější geochemický reakčně-transportní model (PHREEQC + HYDRUS) s implementací modelu vazby huminových iontů VII (WHAM VII).

Table of contents

CHAPTER 5

Modelling transport of Zn and Pb through the soil profile using laboratory columns

CHAPTER 6

Chapter I

General introduction

Content

5

Current environmental concerns

The beginning of the 21st century is defined by global water scarcity, pollution, and increasing soil and water salinization. Other risks to agricultural sustainability are the growing human population and the shrinking amount of land available for production (Shahbaz and Ashraf, 2013). Pollution can be divided into several categories, e.g., air (emissions), water (effluents), and land pollution (dumps and disposals). Various natural phenomena can lead to environmental pollution, including floods, cyclones, drought, earthquakes, and other environmental processes, whilst anthropogenic pollution mainly concerns human activities (Bolan et al., 2014a). The constant increase in environmental pollution represents one of the major concerns for science and the public (Simonich and Hites, 1995).

Diffuse industrial or agricultural sources of anthropogenic pollution play an essential role in water and soil quality, including groundwater pollution along with air deposits. For example, in 2000, around 90 million tons of fertilizers were used worldwide (Winiwarter et al., 2013), which is expected to be even more than 150 million tons in the next 30 years by 2050. These substances in high concentrations negatively affect water quality (Bezirtzoglou et al., 1997; Vasiliki Maipa, Yannis Alamanos, 2001). The release of chemicals and the disposal of waste, such as pesticides, hydrocarbons, and potentially hazardous metal(loid)s, are the major sources of soil pollution. Air pollution also plays an important role, contributing to water and soil pollution because of precipitation, which falls directly on the soil and water resources. In particular, acid rain can change soil chemistry, affecting plants and water quality (Singh et al., 2011). Soil acidity level is crucial because soil pH is a major driver of the mobility of metal(loid)s, which results in the possible movement of these hazardous substances into the aquatic environment. For example, soils with low levels of calcium carbonate, are also exposed to a high risk of leaching into water bodies due to acid (Manisalidis et al., 2020). In addition soils might be polluted due to the accumulation of metals and metalloid discharged from the growing industrial areas, atmospheric deposition, pesticides, land fertilizers, leakage of petrochemicals, leaded gasoline, mine tracks, animal dung, wastewater, coal ignition filtrates, irrigation and paints (Antoniadis et al., 2019).

Soil as the basis of life

Soil is an essential and irreplaceable component necessary for life. It is the most important source and sink of many nutrients and microflora. Soil quality is threatened by various factors (**Fig. 1-1**) that cause soil degradation. Soil degradation refers to the loss of intrinsic physical, chemical and/or biological properties of soil due to natural or anthropogenic processes, resulting in the reduction or extinction of critical ecosystem functions. Erosion, organic matter loss, biodiversity loss, compaction sealing, point and diffuse contamination, pollution, and salinization are the main factors in soil degradation and consequently the main risks to its ecological functions (Trakal et al., 2017a). The initial state of the land determines the degree of soil and landscape degradation, the magnitude of the pressures exerted on it, the system responses of the land and the impact of natural processes from these consequences on land resources. These factors are often interconnected and negatively synergistic. The soil becomes unusable for crop production and can also be dangerous for living organisms. Many of these processes occur naturally in the soil and are an integral part of the cycle of life (Bolan et al., 2014a).
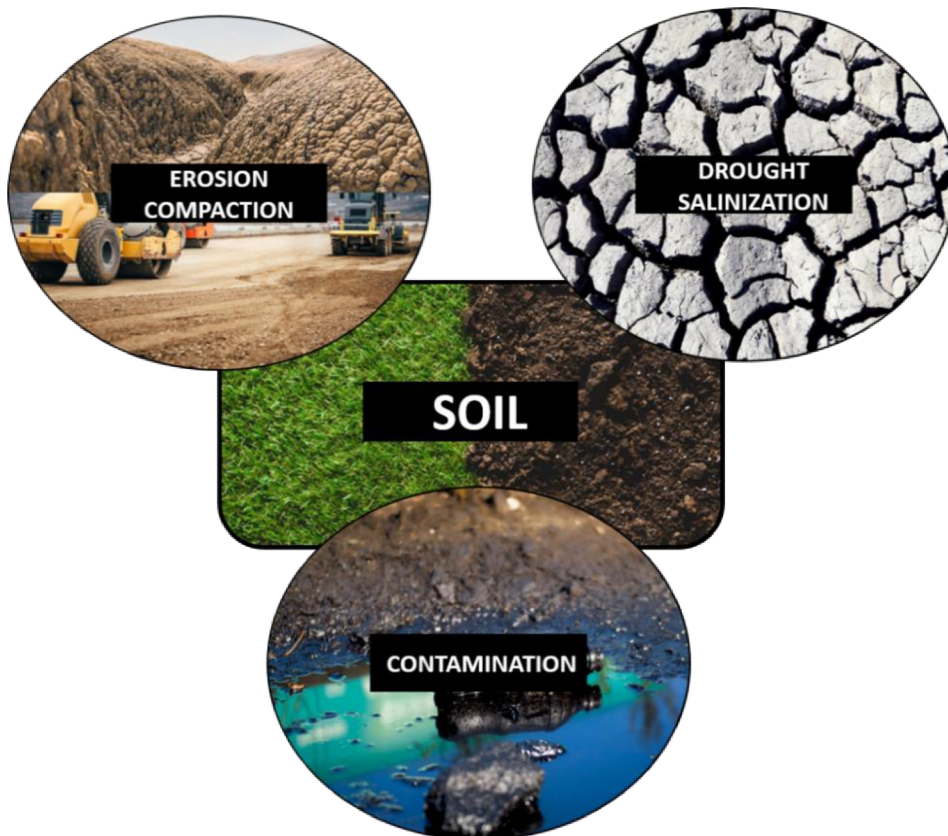
Fig. 1-1 Some negative impacts on soil

Soil contamination

Soil contamination with various potentially toxic organic or inorganic elements (PTEs) is a global problem for human health and food (Antoniadis et al., 2019; Kong et al., 2021; Qin et al., 2021). PTEs, such as metals and metalloids, are problematic due to their non-(bio)degradability and ability to accumulate in living organisms (Bolan et al., 2014a). Anthropogenic sources of metal(loid)s in soils, such as mining operations, smelters, metal-containing compounds, industrial usage of metal(loid)s waste sludge, fossil fuel burning, military training, and electronics (production, use, and disposal) belong to the most common examples (Liu et al., 2012; Antoniadis et al., 2019; Palansooriya et al., 2020). Higher concentrations of metal(loid)s, such as As, Cr, Zn, Ni, Co, Cd, Cu, Mn, and Pb, can be also found in industrial wastewater (Ahmed et al., 2019). Arsenic, Cd, Cu, Zn, and Pb are often found in the soil due to the application of fungicides and pesticides, resulting in the accumulation of PTEs in agricultural products (Khan et al., 2022). PTEs supplied by human activities usually have higher bioavailability compared to pedogenic inputs (Lamb et al., 2009). These substances have harmful consequences for the environment and human health. By biomagnifying food sources, metal(loid)s can disrupt the natural ecosystem and ultimately affect human health (Antoniadis et al., 2019; Sharma and Naushad, 2020). As a result, environmental measures are required to reduce the risk of soil metal(loid) contamination. In recent years, several studies have been published dealing with metal(loid) contaminated soils and the principle of their remediation (e.g, Palansooriya et al., 2020). Although there are a lot of separate studies dealing with remediation methods for metal(loid)-contaminated soils, none of them compares all current strategies or provides advice on technological feasibility (Khan et al., 2019).

Solution to the current problem

Various methods are used to reduce soil degradation. These techniques aim to remove contaminants from the environment or transform them into less dangerous forms. Although the aim of these techniques is similar, the mechanism by which these techniques remove/degrade the contaminants is different (Song et al., 2014). Methods can also be defined according to the position (place) where they are practically applied (Fig. 1-2)

The treatment can be implemented directly on the site (in-situ) where the pollution exists. In this case, it is not necessary to move the soil elsewhere. Conversely, the remediation can also take place at another location (not on the contaminated area), which requires the transport of the contaminated soil to the processing plant and back to the original locality (ex-situ). Several in-situ and ex-situ soil remediation methods have been developed to repair, remediate, excavate or clean metal(loid)-contaminated (Antoniadis et al., 2019; Palansooriya et al., 2020; Xiao et al., 2022). These soil remediation techniques use a great variety of working procedures. However, each method has its own specifics and associated benefits and limitations for implementation. More importantly, in practice, the effectiveness and costs of different methods vary considerably. Due to the enormous time and financial requirements, ex-situ methods are often complicated to implement. For this reason, in-situ methods are increasingly coming to the fore, especially in-situ methods using soil amendments (Bolan et al., 2014b).
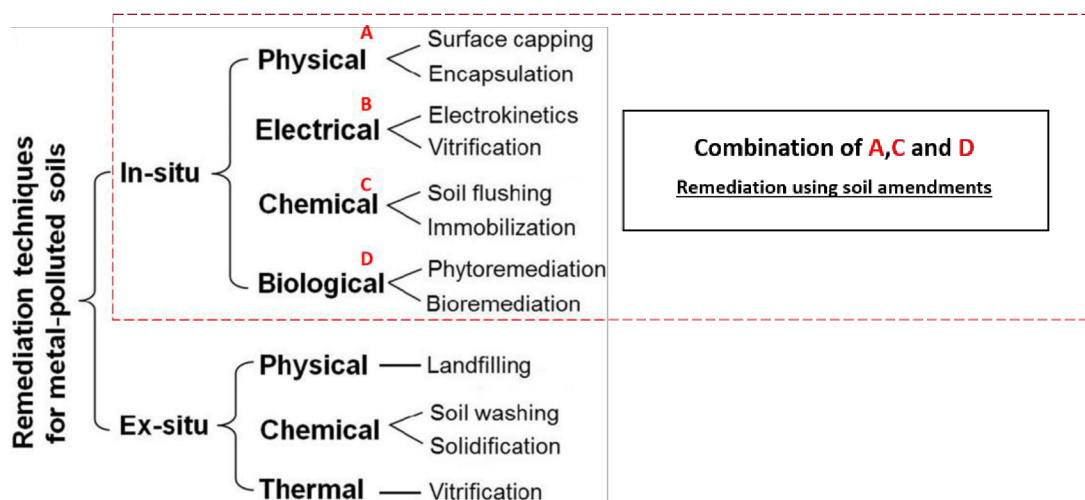
Fig. 1-2. **The most common remediation methods** (adapted from Liu et al., 2018).

In general, the remediation technology for optimal soil recovery is determined by the type of contamination, the concentration of risk elements, and their availability in the soil. As already mentioned, one of the suitable methods is the remediation using soil amendments based primarily on adsorption onto solid materials. Many organic and inorganic solid materials, such as biochar (pyrolyzed biomass), Fe/Al/Mn oxides, nanocomposites, forest residues, sewage sludge or silica, have been shown to be effective in soil stabilization, i.e., reducing the availability of pollutants for living

organisms (Bernal et al., 2007; Bolan et al., 2011). Moreover, such techniques can be further combined with other physical/chemical, bioremediation, or phytostabilization techniques directly on the site supporting the overall remediation efficiency. Organic soil amendments, such as biochar and compost, can also enhance physical and chemical soil properties, i.e., not only immobilize risk metal(loid)s and consequently reduce the contaminant absorption by crops and seepage into groundwater, but also improve soil properties in general (Beesley et al., 2010).

Soil amendments

The following section provides a brief review of some commonly utilized soil amendments.

Inorganic (mineral) amendments

Inorganic (mineral) amendments added to the soil can significantly improve the soil properties and thus further support its usability. Several minerals related to soil fertility can be commonly found or added to the soil. For example, gypsum is widely used to increase soil pH by combining high sodium salts with lime or limestone. Coal combustion by-products, such as fly ash, have become widely used as soil amendments, although they may contain many PTEs. The addition of inorganic soil amendments has been found to significantly impact soil properties, leading to a reduction in metal(loid) solubility and associated availability (Pérez et al., 2021). Hudcová et al. (2018) showed very high sorption of Zn and Pb from aqueous solutions using Mg-Fe layered double hydroxides (LDH). However, if the pH is not controlled, the primary removal mechanism was precipitation on the material surface (i.e., surface-induced precipitation). Similarly, this study also showed that the pH value can influence both removal efficiency and stability of the material. Subsequently, Hudcová et al.(2018)also studied the application of LDH to soils, which confirmed the high efficiency of materials against metal(loid)s and the partial release of Mg from LDH in soil conditions. Finally, high removal efficiency while increasing pH were also observed with synthetic zeolites by Hudcová et al., 2021. However, the application of these materials led to the release of Na into soils, which may be inappropriate in some cases.

Therefore, inorganic amendments are only applicable in specific situations. They can often increase the pH value, which can be a major disadvantage in non-acidic environments. Increasing the pH in these environments can, for example, damage the

organic component and reduce soil fertility. In addition, inorganic substances are susceptible to the physicochemical properties of the environment and can be very unstable in unsuitable conditions.

Organic amendments

Organic amendments are produced from biomass and/or living organisms. The most common examples of organic amendments are compost, wood chips, charcoal, animal manure, straw, husk, geotextiles, and sewage sludge or biochar. These substances have a high organic matter content and other macro- and microelements, which can improve soil fertility by enhancing microclimatic conditions and can also serve as substrates for microbial growth. Some of these amendments are also known to have immobilizing effects on metal(loid)s. Humic acids can efficiently bind metals like Cd, Pb, Cu, and Cr (Bernal et al., 2007). The impact of organic residues on metal(loid) mobility and bioavailability in soils vary depending on the type of metal(loid), type of soil, and overall amendment properties (Walker et al., 2003). Organic materials, such as biochar, are a popular alternative for metal(loid) stabilization. The main advantage is its biological origin, i.e., production by pyrolysis of biomass (various types, including waste). Such amendment can be directly added to soils with only a little pretreatment (Beesley et al., 2010). Biochar can be deemed advantageous over other organic materials in two ways: firstly, it has high stability, which offers long-term benefits to the soil, and secondly, it has a more remarkable ability to retain nutrients. Biochar also improves soil quality by improving soil pH, moisture retention, cation-exchange capacity (CEC) and microbial flora (Mensah and Frimpong, 2018).

Biochar

Biochar (BCH) is pyrogenic black carbon produced in an oxygen-limited environment by carbon-rich biomass thermal decomposition (pyrolysis). For the preparation of biochar, a wide range of organic materials can be used as a feedstock, such as grass, cow manure, wood chips, rice husk, wheat straw, cassava rhizome, and other agricultural leftovers (Cha et al., 2016)The type of raw material used and the pyrolysis conditions affect the final properties of biochar, such as the structure of material and nutrient content].

The temperature to which the feedstock is heated and the time for which the plant material is exposed to this temperature significantly affect the physical and chemical

properties of biochar (**Table 1-1**). Depending on the heating rate and exposure time, the heating process can be fast or slow. Slow pyrolysis (for seconds or minutes) is a continuous process in which purified (i.e., oxygen-free) feedstock biomass is transferred to an externally heated kiln or furnace (**Table 1-2**). On the contrary, fast pyrolysis relies on extremely rapid heat exchange (approx. 100–1000 °C/s) (Meyer et al., 2011). Biochar has typically very fine particles if the heating process is fast and the feedstock material is heated to a high temperature (> 650 °C) for a short time. Contrarily, larger biochar particles are produced by a long process that exposes the plant material to lower temperatures (450-650 °C) and slower heating rates. At higher production temperatures, smaller and more porous biochar particles with a correspondingly larger surface area, CEC and pH are produced (B. Duwiejuah et al., 2017). The effect of temperature on the physicochemical properties of biochar is illustrated in **Fig. ,** showing scanning electron (SEM) images and infrared (FTIR) spectra of rice husk biochar produced at different temperatures. In the case of FTIR spectra of biochar, the broad band close to the wavenumber 3300 cm^{-1} (**Fig.** 350 and 500) is visible due to the stretching of hydrogen-bonded hydroxyl groups, indicating the presence of phenols and alcohols (Pütün et al., 2005; Cantrell et al., 2012). This band decreased significantly with increasing pyrolysis temperature (**Fig. 1-3** 650). Among these effects, the pH value of biochar increases with the pyrolysis temperature and, conversely, the CEC value shows the opposite effect (**Table 1-2**) (Claoston et al., 2014).

14
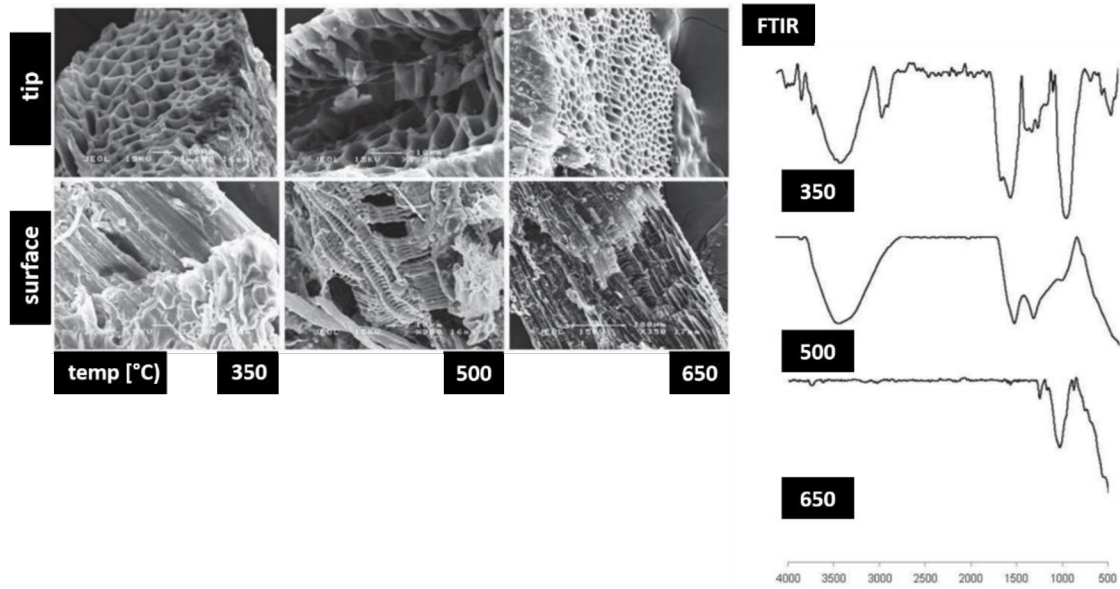
Fig. 1-3 SEM images and FTIR spectra of biochar (Claoston et al., 2014)

Table 1-1 **Physiochemical properties of rice husk biochar** (adapted from Claoston et al., 2014)

Chemical property	Rice husk		
	350	**500**	**650**
pH	6.66	7.99	8.88
EC (mS cm^{-1})	0.52	0.92	1.11
CEC (cmol.kg^{-1})	10.80	9.39	8.35
Elemental analysis (wt%)			
C	47.99	44.64	42.95
N	0.73	0.77	0.53
S	0.03	0.02	0.02
H	5.27	3.96	2.11
O[a]	46.01	50.63	54.41
H/C molar ratio	1.32	1.06	0.59
O/C molar ratio	0.72	0.85	0.95
Al	0.011	0.018	0.019
Ca	0.124	0.154	0.189
Fe	0.039	0.154	0.049
Mg	0.095	0.135	0.175
Si	0.014	0.040	0.015
Na	0.061	0.066	0.079
P	0.074	0.142	0.196
K	0.735	1.120	1.195

[a]Estimated by difference: %O = 100% − (%C + %H + %N).

Table 1-2 **Biomass feedstock products of different types of pyrolysis** (adapter from studies in **Table 1.4**)

Process	Liquid (Biooil) (%)	Solid (BCH) (%)	Gas (Syngas) (%)
Fast pyrolysis: moderate temperature (600 ℃), short hot vapor residence time	75	12	13
Intermediate pyrolysis: low moderate temperature, moderate hot vapor residence time	50	25	25
Slow pyrolysis: low moderate temperature, long hot residence time	30	35	35

Another important property commonly used to describe BCHs is specific surface area (measured by Brunauer, Emmett, and Teller method; BET). Surface area, pore-volume, and average pore size increase with pyrolytic temperature and residence time (Hasan Khan Tushar et al., 2012). A basic overview is given in **Table 1-3**. However, Trakal et al., (2014a) showed that the surface area of well-developed BCH generated at a higher pyrolytic temperature is higher. Nevertheless, the adsorption capacity is usually lower and vice versa. Thus, a higher specific surface area does not necessarily mean better sorption properties.

Table 1-3 **Fast and slow biochar production processes and resulting biochar characteristics** (adapter from studies in **Table 1.4**)

Heating Process	Temperature	Exposure Time	Biochar Particle Size	CEC	pH
Fast	(>650 °C)	Short (Seconds)	Fine and porous	Greater	Higher
Slow	(450-650 °C)	Long (min/hrs)	Large	Smaller	Lower

Versatility of biochar

Biochar is a material that can help solve many soil/environmental problems. **Table 1-4** summarizes the universal use of biochar in recent studies, which can be roughly divided into 3 main groups, i.e., (1) increase of the soil organic matter and soil stability, (2) influence of biochar on the soil hydraulic and fertility and (3) sorption or stabilization of risk element

t.

Table 1-4 **Versatility of the biochar**

USAGE OF BIOCHAR	PROBLEM	TYPE OF BIOCHAR	MAIN RESULT	STUDY
ORGANIC MATTER, STABILITY AND FERTILITY INCREASE	Release of dissolved organic matter in acidic soils.	Chemically modified biochar	Soil properties (pH, CEC and WHC) were positively enhanced.	Smebye et al., 2016
	Sustainable approach for improving plant growth and soil properties.	Biochar and biochar amendments	Promotion of microflora and plant growt when biochar added to the soil.	Rawat et al., 2019
	Organic matter degradation and humification.	Biochar and biochar amendments	Enrichment of poultry manure with biochar reduced the losses of nitrogen in the mature composts and increase organic matter in soil.	Bruno et al., 2010
	Poor soil quality and low fertility.	Corncob biochar & compost	Soil quality was enhanced after a mixture of compost and biochar was applied.	Albert et al., 2018
	Soil erosion and degradation.	Various types of biochar	Soil fertility was improved and contamination was reduced after biochar application.	Ding et al., 2019
SOIL SALINIZATION & DROUGH PROTECTION	Drought and metal toxicity negatively affect soil fertility and plant growth.	Various types of biochar	Drought stress was reduced by increasing WHC of soil.	Mansoor et al.,2021
	Impact of biochar on water retention.	Various types of biochar	Water retention capacity with limited capacity of water storage was increased.	Wang et al., 2019
	Drought and salt stress negatively affect soil fertility and plant growth.	Various types of biochar	Biochar increased the WHC, and improved the physical and biological properties in drought stress . Biochar decreased Na+ uptake, while increased K+ uptake by plants in salt stress.	Ali et al., 2017
	Soil water retention characteristics (SWRC).	Various types of biochar	Water retention capacity of the studied soil was improved.	Hussain et al., 2020

USAGE OF BIOCHAR	PROBLEM	TYPE OF BIOCHAR	MAIN RESULT	STUDY
UNIVERSAL SORBENT	Soil remediation of some organic and inorganic contaminants.	Biochar	Effective to immobilize organic and inorganic contaminants in soil	Zama et al., 2018
	Treatment of water contaminated by selenium.	Biochar modified by Fe(NO3)3	Was effective in removing Se(VI) from water.	Godlewska et al., 2020
	Adsorption of As in red soil.	Biochar modified by Mn-oxides	Sorption of As in case of modified biochar was increased.	Yu et. al, 2015
	Different metal(loid)s sorption in soil.	Biochar	Sorption of risk metal(loid)s in soil were increased after adding a biochar.	Minori et al., 2011
	Sorption of risky metal(loid)s and removal from wastewater.	Biochar	Contaminant bioavailability reduction, biochars could potentially be used in decontamination applications	Doumer et al., 2016
	Low sorption of biochar for metal(loid)s, especially As.	Biochar modified by Mn-oxides	Mn oxide-biochar composites were able to remove significantly greater quantities of various metal(loid)s from the aqueous solutions.	Trakal et al., 2018
	Soil pollution problem/ bioavailability of metal(loid)s and organic pollutants in soils.	Various types of biochar	Safe and sustainable use of biochar as a soil amendment for remediation of contaminated soils.	Zhang et al., 2013
	Adsorption and immobilization of As and Cd in water and soil.	Biochar modified by Mn-oxides	Can be used as an effective sorbent for simultaneous immobilization of As and Cd, in environmental and agricultural systems.	Wang et al., 2019
	Sorption of metal(loids).	Biochar from manure	Sorption efficiency of Cd, Cu, and Zn from aqueous solutions was increased.	Xu et al., 2013
	Adsorption of As(III) on biochar and reduce the toxicity of As(III).	Biochar modified by Fe-oxides	Iron-modified biochar beads can be promising adsorbents.	Kim et al., 2019
	Adsorption of potentially toxic elements in water.	Biochar modified by Fe-oxides	As and Cr orption capacity was increased,	Zhang et al., 2020
	Sorption of arsenate and lead.	Biochar modified by Mn-oxides	Sorption of observed risk elements was positively enhanced.	Wang et al., 2015
	Contaminant management in soil and water.	Various types of biochar	Biochar can effectively remediate polluted water and soil.	Ahmad et al., 2014

19

Increase of the soil organic matter, soil stability and fertility

Adding biochar to the soil can improve soil quality and help plants retain nutrients and thus increase plant growth (Cesarano et al., 2017). Biochar increases soil pH, electric conductivity (EC), organic carbon (C), total nitrogen (TN), accessible phosphorus (P) and cation-exchange capacity (CEC) because it contains organic matter and nutrients (Bayu et al., 2016). Biochar as a soil amendment results in significant changes in the redox state of soils. The predominant functional group species generally determine the redox properties of biochar (Dong et al., 2015).The presence of plant nutrients and ash in biochar, as well as its large surface area, porous structure, and ability to function as a medium for microorganisms, have been identified as the primary causes of improved soil properties and increased nutrient absorption by plants in biochar-treated soils (Nigussie et al., 2012). In terms of other soil properties, biochar reduces soil acidity by increasing pH (also known as the liming effect) (Lehmann et al., 2006).

Additionally, biochar promotes soil fertility by providing nutrients to the soil (such as K, to a lesser extent P and a variety of other micronutrients) and retaining nutrients from other sources (e.g., fertilizers), including nutrients directly from the soil. Because biochar adsorbs and slowly releases nutrients, it increases the availability of C, N, Ca, Mg, K, and P to plants (DeLuca et al., 2015). It also reduces agricultural and environmental pollution by allowing fewer fertilizers and preventing them from draining and leaching (Cao et al., 2018).

However, biochars are hardly effective at maintaining long-term soil fertility, except for the most heavily exposed soils. This is partly because the total and bioavailable nutrient and trace element concentrations in biochars are often lower than in their source, i.e., pre-pyrolyzed biomass feedstock (J. W. Gaskin et al., 2008). This is especially true for plant-based biochars compared to manure-based ones (Cantrell et al., 2012) and where biochars have aged or weathered before their soil application. Weathering of this nature can cause residual ash to remain within biochar structures after pyrolysis, which is rich in Ca, Mg, K, and other elements, which are otherwise easily and rapidly leached when exposed to the environment. After that, biochars are relatively stable in soils (Zimmerman et al., 2011). The increased surface area containing oxygen-rich functional groups can attract supplementary cations (e.g.,

Ca^{2+}, Cu^{2+}, Mg^{2+}, Zn^{2+}) when biochars are added to soils (Major et al., 2012). As such, biochars can be added to metal(loid) contaminated soils together with fertilizing agents to effectively retain trace elements present in the soils (Beesley et al., 2011)In this sense, biochars have been put forth under consideration as organic amendments to help soil remediation from a geochemical point of view (Santos et al., 2018).

The consensus on the general impacts of biochars on the leaching of nutrients from amended soils is not settled and existing studies present contrasting results depending on soil and biochar properties, application rates, and durations. For example, large meta-analyses have demonstrated a wide range of effects on crop yields due to the addition of biochar addition to the soils (Crane-Droesch et al., 2013). Nonetheless, it can be said that the increased moisture retention afforded by the biochar addition, as explained previously, and application especially to coarse-textured soils, can affect nutrients that are soluble and reside in pores. Because most biochars have poor anion-exchange capacity compared to CEC, their effects on N in soils vary. For example, NO3– has been somewhat mobile within biochar-amended soils compared to NH+ (Laird and Rogovska, 2015). Likewise, meta-analyses of available P have demonstrated a significant dose-dependent increase of P after biochar application to acidic agricultural soils (pH < 6.5). However, this is also highly variable depending on the pyrolysis temperature during the biochar preparation (Glaser and Lehr, 2019). In the case of potassium (K), the large surface areas of biochars and strongly negative charges on their surfaces generally favor the retention of K in soils. However, this is dependent on other factors, such as soil texture (Jindo et al., 2020).

Influence of biochar on the soil hydraulics

Biochar modifies the water-retaining properties of the soil by changing its textural and structural properties. Furthermore, the internal micrometer-scale porosity of biochar affects water retention in soils, which can directly hold readily available plant water. Several studies have shown that incorporating biochar into soil modifies soil hydrological and hydraulics parameters, including water retention factors (e.g., Peake et al., 2014; Esmaeelnejad et al., 2016; Głąb et al., 2016)

An important parameter of soil hydraulics is bulk density , and it is one of the most studied soil physical properties after biochar application (Blanco-Canqui, 2017). It has previously been demonstrated that biochar application has reduced bulk density with a linear (Głąb et al., 2016) or, in some cases,a quadratic relationship (Rogovska et al., 2014). However, such changes in bulk density were significantly and negatively correlated to those associated with porosity (Omondi et al., 2016). According to Blanco-Canqui (2017), biochar can increase soil porosity by reducing soil bulk density, increasing soil aggregation and/or reducing soil packing, and interacting with mineral soil particles. These effects are attributed to the highly porous internal structure of biochar, its large particle surface area, and its very low bulk density.

For example, the indirect proportional relationship of applied biochar to soil bulk density has been demonstrated on an experimental sandy loam Fluvisol presented in detail in Jačka et al.(2018). These results are consistent with other studies showing that reduced bulk density increases the total pore volume of amended soil samples, from coarse-textured sandy to silty clay loam soils (Blanco-Canqui, 2017), mainly when woody biochars were applied (Omondi et al., 2016). The influence of biochar on bulk density reduction is more pronounced in coarse-textured soils (Blanco-Canqui, 2017; Razzaghi et al., 2020)

Because soil water retention affects water uptake and transport by plants, which can alter plant physiology and yield, soil water retention is critical for agricultural productivity. Water retention by biochar applications is, according to experimental investigations, mainly related to high porosity, the presence of hydrophilic domains, and a large specific surface area of biochar. Pore sizes of coarse-textured soils respond to the biochar addition more profoundly than finer-textured soils (Razzaghi et al., 2020), resulting in an increased water content at saturation after biochar application (Głąb et al., 2016). This increased amount of water can be retained by the strong forces arising from the capillarity and sorption potential of biochar, although this can make part of the water unavailable for plants (Verheijen et al., 2010).

In the soils described in Jačka et al. (2018), water retention curves were plotted after application of 5% (w/w) biochar, compost, and manure applications. Water retention increased most significantly at the wet end of the soil water retention curve. The

biochar-amended sandy loam Fluvisol returned to the shape of the original/control curve at higher suction pressures (~ pF 3). In contrast, the same soil amended with compost displayed higher water contents in the drier part of the soil water retention curve. Consequently, compost addition to the Fluvisol resulted in a 20% increase in available water capacity (AWC) , compared to 35% with the addition of biochar. When a loamy sand Regosol was amended with manure, the entire profile of the water retention curve changed compared to the soil amended with biochar, which remained similar to the nonamended control samples. The total porosity estimated from the saturated water capacity at a matric potential of 0 kPa reached the highest values for soil samples with 5% manure. However, the water content at field capacity (FC) was significantly greater in all cases where organic amendments were added. Biochar-enriched samples increased AWC compared to control samples and manure-enriched samples by 84% and 103%, respectively.

In general, the effect of organic matter application on water retention showed a significantly more pronounced strengthening in the case of the loamy sand Regosol than its effect on the sandy loam Fluvisol The increased water retention after the application of organic amendments was determined by a higher frequency of pore sizes between 0.1 and 20 μm (Bird et al., 2008). This is in agreement with studies documenting the increased water retention in sandy and loamy soils after biochar application (Blanco-Canqui, 2017). Contradictory results obtained in sandy soil (Jeffery et al., 2015) can be attributed to specific hydrophobicity of biochar or the differences in application rates (Jačka et al., 2018). Significant differences have also been observed when comparing field experiments with laboratory studies (Rabbi et al., 2021).
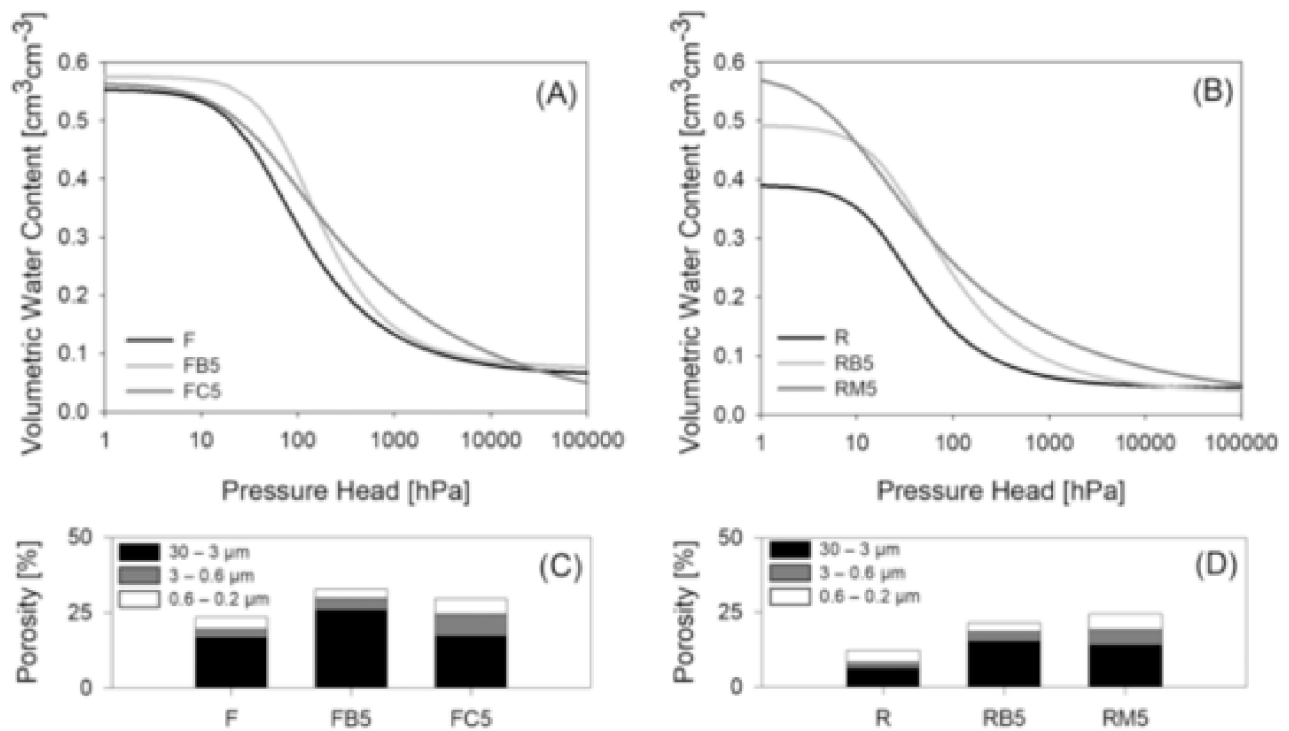
Fig. 1-4 . **Influence of biochar application on water retention (A) and pore-size distribution (C) of sandy loam Fluvisol and water retention (B) and pore-size distribution (D) of loamy sand Regosol. The biochar application is contrasted with the control soil sample and commonly used organic matter amendments represented by compost (A) and manure (B)** (adapted from Trakal, 2021 pre-proof)

Saturated hydraulic conductivity (K_S) was determined to decrease in sandy soil and increase in clay-rich soils after biochar addition (Barnes et al., 2014; Edeh et al., 2020). However, the effect of biochar on the K_S is still not fully understood. It probably depends on the particle size distribution, bulk density of the soil, and the application rate, size, and structure of the biochar (Jeffery et al., 2015; Omondi et al., 2016; Rabbi et al., 2021). Decreasing K_S in sandy soils has been observed by many authors (Omondi et al., 2016; Edeh et al., 2020). On the other hand, Barnes et al. (2014) reported an increase of K_S in clay soil (classified as clay loam). The type of clay may explain the discrepancies between the results described here and other studies conducted in loamy soils, which do not indicate any significant changes in K_S (Rogovska et al., 2014). However, the results of these studies dealing with the influence of biochar on the soil hydraulics are still inconclusive, and the processes need to be further tested (Atkinson, 2018). Moreover, the effect of biochar on the

soil hydraulic parameters, such as soil water retention, hydraulic conductivity, and aggregate stability, is highly inconsistent. Jeffery et al. (2015) found no significant effects of biochar application to sandy soil (which could benefit the most) on soil water retention and hydraulic conductivity or aggregate stability in two separate field experiments at application rates up to 50 t^{-1}. The presented results thus add further evidence that biochars and their environmental and physical effects should be investigated on a "char by char" basis. However, due to the high level of heterogeneity in biochar characteristics due to relatively small changes in production, there is a strong need to move beyond studies showing overall effects and to move to a mechanistic understanding of effects related to biochar (or lack of such effects results) when applied to a soil (Jeffery et al., 2015).

Sorption or stabilization of risk elements

Biochar can remediate soil and water contaminated by various organic and inorganic pollutants, including risk metal(loid)s. Adding biochar to the soil increases the total carbon content in the soil, affecting the organic matter content of the soil. As indicated by Amoah-Antwi et al. (2020) active primary constituents, such as clays and organic matter, generally determine the 'physical and chemical characteristics of the soil, including pH and redox potential. These characteristics usually improve after the addition of biochar to the soil, but the extent depends in part on the biochar production characteristics. In particular, high pyrolysis temperatures result in the decomposition of organic compounds, higher pH, and increased concentrations of Na, K, Mg, and Ca oxides and carbonates of on the surface of the biochar (Jindo et al., 2014). These alkaline cations can be easily exchanged with Al^{3+} and H^+ on negatively charged soil surface sites with an overall impact on increasing soil pH (Shetty and Prakash, 2020).

The ability of BCH to act as a green environmental sorbent has been established in recent studies. However, the long-term effect of biochar treatment on soil needs to be considered. This was demonstrated by Burrell et al. (2016), when in their study the soil with biochar was compared to control soil during 3 years of the experiment. Stabilization was more significant in soils amended with biochars produced at higher temperatures (525 °C) than at lower temperatures (400 °C), partly attributed to the flocculating effect on soil colloids. In this flocculated state, biochar and soil surfaces

act as more efficient environments for soil microorganisms, including mycorrhizal fungi, whose metabolic processes result in the production of mucus, which helps to maintain soil aggregate stability and reduces salt stress (Werdin et al., 2020). However, it should be considered that the biochar impact on the soil depends not only on these key physicochemical characteristics of the applied biochar, but also on the extent to which these differ from the characteristics of the non-amended soils. Hailegnaw et al. (2019) compared the effect of 5% (w/w) biochar treatment on soils with significantly different characteristics and observed a 23% increase in pH after biochar treatment in soils with the original pH of 3.9. The same biochar treatment resulted in only a 6% increase in soil pH with a starting pH of 7.3. However, it is noteworthy that in acidic soils, the effects on pH are maintained for a long time, while in alkaline soils this increase in pH is somewhat transient and likely to decrease in the long term (Farkas et al., 2020).

In general, sorption of metal(loid)s by biochar has been identified as a valuable, long-term, and cost-effective way to remove risk substances compared to standard processes or other standardly used materials (El-Shafey et al., 2002; Yousaf et al., 2016). Mitchell et al. (2018) demonstrated an increase in Cr mobility due to application of biochar produced at 750 °C, partly due to an increase in pH after soil treatment. In this case, the soil treatment with biochar notably resulted in the predominant occurrence of Cr in the form of Cr(VI). The opposite was true when the soils were amended with the non-pyrolyzed source material. The non-pyrolyzed organic materials were characterized by an increased presence of unaltered carboxylic and hydroxyl groups, which promote the reduction of aqueous Cr(VI) into Cr(III). Biochar as a soil amendment affects the toxicity, transport, and fate of several risk metal(loid)s in the soil and thus improves the overall soil adsorption capacity (Verheijen et al., 2010). Based on Trakal et al.(2014a, 2014c) biochar has been successfully used for the Cu, Cd, Pb and Zn sorption with high efficiency

Biochars can also be added to agricultural soils to reduce the leaching of metal(loid)s present as a result of legacy fertilization practices with metal-rich materials. The rapid effects of biochar on Cu and Zn mobility, for example, and the extent to which other geochemical factors affect it, can be assessed by accelerated laboratory loop (column) leaching tests. **Fig. 1-5**, for example, shows the rapid leaching of labile dissolved organic carbon (DOC) from biochar-treated soil at concentrations on the

order of magnitude higher than the metal-rich agricultural sandy clay loam Stagnosol to which it added. During the successful pore-volume leaching, surface sorption processes rapidly immobilize Zn as the pH of the soil with biochar gradually shifts this closed-loop system toward equilibrium.
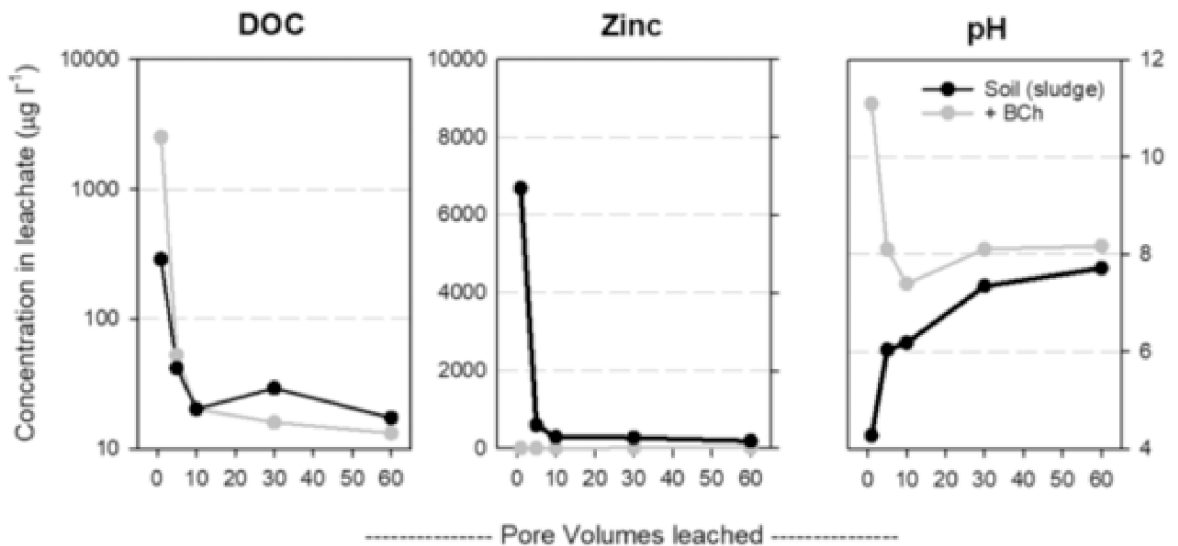

Fig. 1-5 **Dissolved organic carbon (DOC), Zn concentration, and pH of leachates from column testing of biochar derived from hardwoods (BCH) in contact with a metal-enriched, sludge-derived soil.** (adapted from Trakal, 2021 pre-proof.)

Similar effects can be observed when evaluating chemical parameters of soil pore waters, which represent one of the most environmentally relevant geochemical pools in soils (Moreno-Jiménez et al., 2011). Pot tests have been used to sample pore waters from agricultural soils, having received metal-rich materials as fertilizers and being amended with various biochar types and doses (Trakal et al., 2017a; Mitchell et al., 2018). For example, different dosage of three biochars derived from different feedstock materials were added to a sandy loam Podzol and a sandy clay loam Stagnosol, which in the past received Cu- and Zn-rich ash and sewage sludge, respectively. Here, Cu and Zn behaved differently in solution when biochars were applied, with Cu being mobilized somewhat by higher biochar dosage. In contrast, Zn concentrations were further reduced by the highest biochar dosage. When metal(loid)-rich soils were amended with biochars, Cu was often mobilized due to the strong complexation (and co-mobility) with DOC (Beesley et al., 2011). This effect has

been observed when biochars are incorporated into soils and applied as stabilizing amendments (Beesley and Dickinson, 2011) . This effect is further exacerbated when crops are grown, with exuded organic acids (rhizosphere) leading to biochars having a weak impact on Cu concentrations in soil pore waters despite their strong metal sorption qualities, in contrast to a strong immobilizing effect on Zn, overriding the influence of crops. Similar trends have also been observed where biochars have been added into mining and industrially contaminated soils to reduce phytotoxicity, metal(loid) leaching, and revegetation. In such studies, the strong immobilization effects of biochars on metals in solution have contrasted with the impact on As (Beesley et al., 2011), so that modified biochar composites, including Fe and Mn oxides, have been developed as bio-sorbents for multimetal-contaminated scenarios (Trakal et al., 2018a).

Advantages and potential drawbacks of pure biochar

As already mentioned, the application of biochar to soil provides several agricultural advantages. The economic analysis presented by Keske et al. (2020) illustrates the high probability of biochar profitability. However, the profitability is demonstrated at intensive agricultural production (potato and beet crops) and in the study area highly suitable for biochar production. In short, an sustainable strategy for biochar application to soils without severe fertility problems will require that the biochar benefits for climate change mitigation, groundwater protection and/or soil restoration have to be connected with a decrease of biochar production costs, e.g., by increasing the production processes or increasing nutrient recovery by recycling wastes.(Soja et al., 2014).

The addition of biochar to soil provides an excellent environment for beneficial soil bacteria, improving soil fertility and crop productivity (Mankasingh et al., 2011; Lehmann et al., 2015). On the contrary, biochar causes the binding and inactivation of agrochemicals, such as herbicides and nutrients, in the soil. The study of Nag et al. (2011) showed that the addition of biochar to the soil reduced the effectiveness of herbicides approx. 3.5 times compared to untreated soil and, at the same time, increased their persistence. Therefore, the addition of biochar to the soil would require an increased supply of herbicides and thus may have a direct economic impact (Nag et al., 2011). Moreover, biochar also increases soil EC and pH, which can negatively affect highly alkaline soil (Miheretu, 2020).

Another problem may be the ash content. Biochar produced at high temperatures usually contains more ash than biochar produced at low temperatures. It was hypothesized that negative effects on growing plants in soils could be generated in soils treated with biochar produced at high temperatures (Butnan et al., 2015).

A significant drawback of biochar is its ability to adsorb nitrogen and other important elements (nutrients) such as Fe, which can be harmful to plant growth (Kim et al., 2015). Furthermore, instead of supplying nutrients to plants, biochar can bind soil nutrients and thus make it more difficult for plants to absorb them (Joseph et al.,

2018). For example, when biochar and phosphorous fertilizer are applied simultaneously to saline-sodic soil, phosphate precipitation and sorption reactions may be promoted, eventually reducing the number of available nutrients to plants, such as phosphorus (G. Xu et al., 2016).

Although recent studies **(Table 1-4 A**) have demonstrated the benefits of adding biochar for improving soil quality/fertility, increasing plant development/yield, lowering agronomical diseases, helping to retain nutrients/water, and enhancing precipitation/adsorption processes, the importance of biochar in agricultural soils remains still controversial and is still not fully resolved for the common application.

Moreover, the efficiency of one type of biochar in soil may be limited due different properties of individual biochars and also due to the complexity of real systems (Shakoor et al., 2020). In general, biochar properties are soil specific and thus biochar treatment may not be beneficial for all soil types (Hussain et al., 2017) . Therefore, such "weak" properties of biochar need to be improved. One possibility is to prepare various biochar modifications making the biochar more complex and compelling.

Modified biochars

The modification of biochar in this view means an effort to improve some properties of the pure material and, conversely, suppress all undesirable properties. The modification process can be applied at the beginning as a pretreatment of feedstock, e.g., washing, drying or chemical activation, during the biochar production, e.g., different conditions of pyrolysis, and as a post-treatment after pyrolysis. A simplified diagram is shown in **Fig. 1-6.** The modification of biochar can enhance processes including surface complexation, chemical adsorption, electrostatic interaction and ion exchange or metal precipitation, especially in the case of anions, which are not easily removed by pristine biochar (Kong et al., 2021).
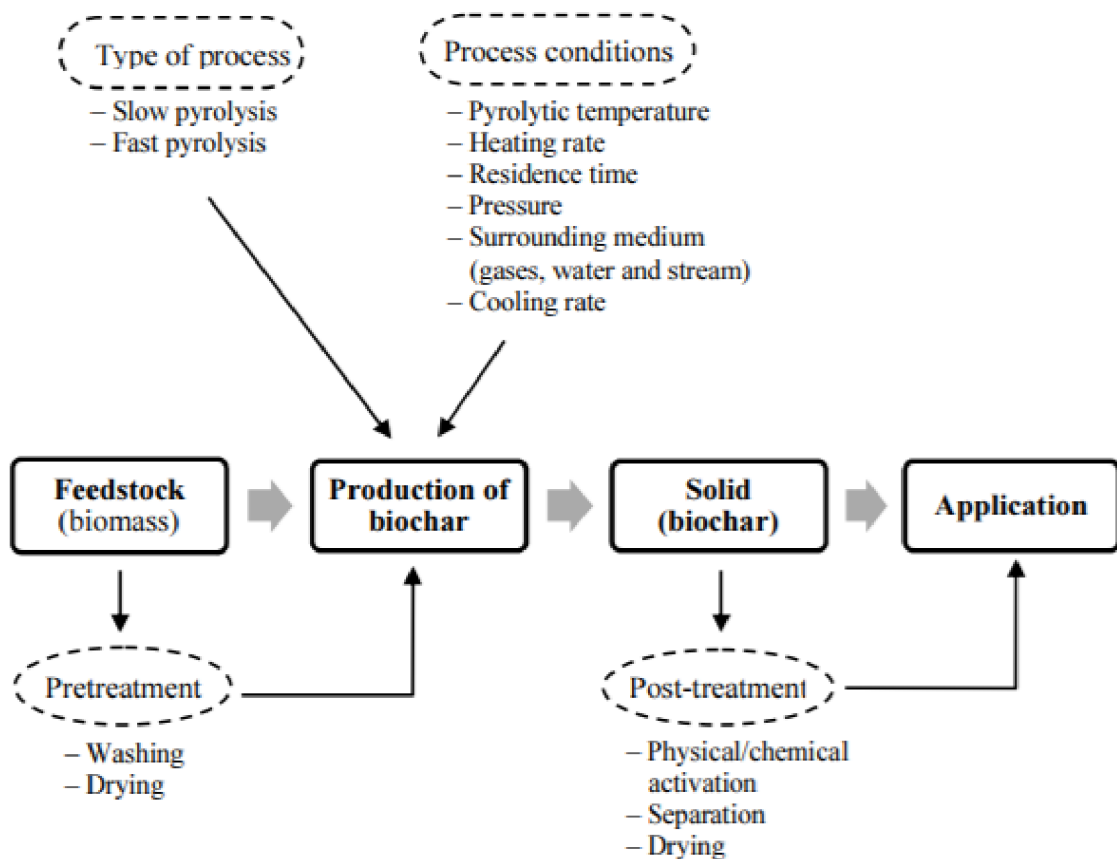
Fig. 1-6 **Biochar modification diagram** (adapted from *Chemerys and Baltrėnaitė, 2016)*

Most of the modifications are performed as chemical post-treatment of biochar. Studies focused on such modifications are depicted in

Table 1-5. For example, the application of Mn-modified biochar in As-contaminated soil reduced As uptake by plants (Yu et al., 2017). Furthermore, when biochar was combined with other chemicals, such as limestone, Cd uptake by wheat and rice straw and grain decreased by more than 80% (Rehman et al., 2017). Similarly, sewage sludge biochar combined with fulvic acid and phosphor-gypsum reduced the uptake of hazardous metal(loid)s by corn plants (Huang et al., 2017). Studies have shown that modifications of biochar significantly improve the performance of this material for sorption, stabilization and removal of inorganic and organic pollutants.

Table 1-5 **Research of studies using biochar modification**

MODIFICATION METHOD	RAW MATERIAL (FEEDSTOCK)	TEMPERATURE OF PYROLYSIS [°C]	MAIN GOAL (i.e., to increase sortpion of)	STUDY
Activated with HCl, and coated with iron ($FeCl_3.6H_2O$)	Wheat straw	450	NO_3^-, PO_4^{3-}	Li et al. (2014)
KOH	Switchgrass	300	Cu^{2+}, Cd^{2+}	Regmi et al. (2012)
KOH	Municipal solid waste	400, 500, 600	As^{5+}	Jin et al.(2014)
H_2SO_4, KOH	Rice husk	$450-500$	Tetracycline	Liu et al. (2012)
$H_2SO_4 + HNO_3$, $NH_4OH + Na_2S_2O_4 +$ acetic acid	Saw dust	500	Cu^{2+}	Yang and Jiang (2014)
H_2O_2	Peanut hull	300	Pb^{2+}, Cu^{2+},Ni^{2+}, Cd^{2+}	Xue et al. (2012)
Methanol-modified biochar	Rice husk	$450-500$	Tetracycline	Jing et al. (2014)
Carbon-nanotube modified biochar	Hickory	600	Pb^{2+}	Inyang et al. (2015b)
Fe^{3+} - coated biochar	Risk husk	700	$As^{5+,}As^{3+}$	Samsuri et al. (2013)
Chitosan-modified biochar	Bamboo	600	Pb^{2+}, Cu^{2+} , Cd^{2+}	Zhou et al. (2013)
Mg-biochar nanocomposite	Tomato	600	PO_4^{3-}	Yao et al. (2013)
MgO-biochar nanocomposite	Sugar beet,cottonwoods, pine woods	600	PO_4^{3-},NO_3^-	Zhang et al. (2012)
Biochar/AlOOH nanocomposite	Cottonwood	600	As, PO_4^{3-}	Zhang et al. (2013)
Ca and Fe-modified biochar	Rice husk	300	As^{5+}, Cr^{6+}	Agrafioti et al. (2014)
Biochar-supported zerovalent iron	Bamboo	600	Pb, Cr, As,PO_4^{3-}	Zhou et al. (2014)
Fe-impregnated biochar	Hickory chips	600	As	Hu et al. (2015)
Magnetic biochar/γ-Fe2O3 composite	Cotton wood	600	As	Zhang et al. (2013)
Magnetic biochar	Oak wood and bar	$400-450$	Cd^{2+}, Pb^{2+}	Mohan et al. (2014b)
Magnetic biochar	Pinewood	600	As^{5+}	Wang et al. (2015)
Mg-Fe LDH-coated biochar	Wood, wheat straw, grape stalks	$600-700$	Zn^{2+}, As^{5+}	Hudcová et al. (2022)

Manganese oxide-modified biochar

Della Puppa et al. (2013) used amorphous manganese oxide (AMO) and birnessite to study the sorption of Cu, Cd, Pb, and Zn in aqueous solutions. This study showed that AMO is a potentially effective sorbent. However, its stability and sorption capacity is strongly influenced by the pH value. Michálková et al. (2016a) further studied the application of AMO to soils, which lead to a significant reduction in metal(loid) leachability but also there was a partial dissolution of the material. By these studies Mn-oxides have also been demonstrated to have very high immobilization potential for metal(loid)s including the more common divalent metals (e.g. Pb(II), Cd(II), Cu(II), etc.). However associated dissolution of AMO has resulted in excessive Mn leaching, which has been highlighted as the major drawback of the application of such materials in a remediation context, due to phytotoxicity (Della Puppa et al., 2013; Ettler et al., 2014a; Michálková et al., 2016c). Concerning the natural (multi-metal(loid)s contaminated) wastewater treating, we will selectively treat solely those bivalent metals using pristine biochar and/or treat all dissolved metal(loid)s with a secondary Mn-leaching from the pure AMO. Because of that, an AMO-modified biochar, combining the advantageous properties of both AMO and pristine biochar with decreased Mn leaching and thus improved sorbent longevity, is an ideal biosorbent for multi-metal(loid)s contaminated wastewater treating.

The most important advantages of these (oxo)hydroxides are: a) high sorption efficiency towards a wide range of soil contaminants, b) large specific surface area, c) high amount of active surface sites, and d) amphoteric nature allowing sorption of both cations and anions (Komárek et al., 2013). Such oxides strongly bind metal(loid)s through different mechanisms, such as specific sorption (formation of inner-sphere complexes) or co-precipitation. For soil remediation purposes, naturally occurring (oxo)hydroxides, synthesized (oxo)hydroxides, or (oxo)hydroxides derived from industrial by-products can be used. Therefore, it is suggested that biochar modification may promote immobilization and thus stabilization of risk metal(loid)s in soils compared to biochar alone (Ahmad et al., 2014).For example, manganese (oxo)hydroxides play an essential role due to their strong ability to immobilize a great variety of metal(loid)s and high oxidation potential. Therefore, biochar modified with manganese oxides is offered as a suitable alternative to take advantage of both

materials. Such composite can be used as a potentiality cost-efficient adsorbent for the remediation of metal(loid) contaminated soils (Gregory et al., 2014).

Different approaches applicable to model soil process

Soil is a highly heterogeneous matrix. However, a simplified definition can be used to describe and model soil processes. Soil (i.e., soil matrix, porous media) is defined over a domain as a heterogeneous system of solid particles forming pores. It is assumed that the pore space must be interconnected, distributed throughout the entire domain, and occupied by fluid phases (gas, liquid, solid). It can be studied at various levels of spatial resolution corresponding to a specific scale: i.) molecular (movement of particular molecules; e.g., chemical reactions), ii.) microscopic (level of individual pores, only 1 phase) and iii.) macroscopic. The individual levels are not scale-transferable. In this study, a macroscopic approach only is considered. Phases are uniquely separated and definable. It is assumed that the whole porous medium is formed by superposition of partial phases of the macro continuum.

Macroscopic variables

Macroscopic state variables can describe the movement of liquid phases at a constant temperature (density, velocity, and pressure). These state variables should be obtained from measuring relative elementary volume (REV, **Fig. 1-7**), which may on average reflect the studied domain. The size of REV is achieved by successive averaging over arbitrary elementary volume (AEV), which is a small spherical volume centered at the selected fixed point. After a slight increase in volume, the value of the macroscopic state variable does not change (more or less). This AEV can be then considered a REV with several constraints.
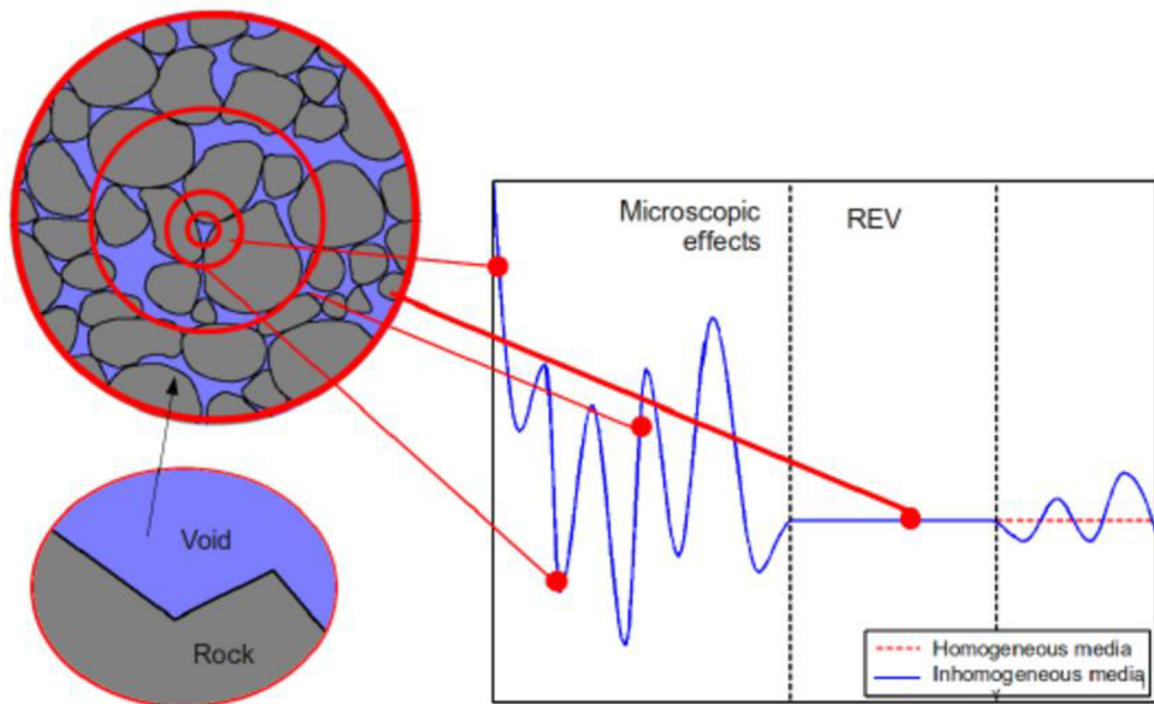
Fig. 1-7. **Concept of representative elementary volume (REV)** *(Lie and Mallison, 2015)*

Based on the relationship between state variables, the driving forces for water movement (adhesive, retention, and capillary forces), and the hydraulic parameters of the porous medium (hydraulic conductivity, shape of the retention curve, porosity, and bulk density of the soil), equations for water and solute transport are formulated. Due to the heterogeneity of the environment and a large number of parameters, it is necessary to simplify the calculations and build a suitable model. A model should simulate values closed to the observed data, although the complexity of the system is greatly simplified.

Today, the advanced soil models use convection–dispersion, the continuity equation, and Darcy's law to explain water and solute motility through soils, and preferential flow and transport (Šimůnek et al., 2003). Many numerical models are now available to describe various physical and chemical processes that affect water flow and solute transport in the vadose soil zone. There are some primary principles and values for modeling water flow and solute transport in the vadose zone and a number of the most significant procedures existing in it. Soil water content, pressure head, soil

porosity, and water flow are all considered and deal with soil water dynamics. The explanation of the basic advection-dispersion equation and the enforcement of boundary and first conditions in the quantitative model and the soil water retention curve (SWRC) elaborates the state between content of soil water and soil water potential (Lal and Shukla, 2004). The earliest mathematical and synthetic models in soil science date back to the last century and deal primarily with the simulation of water flow, heat flow, solute transport methods, soil organic carbon dynamics, and nutrient dynamics (Bresler and Hanks, 1969). Substances present in the soil can be dissolved and transported by the transport medium. Such transport is usually called miscible flow. On the other hand, immiscible flow refers to the transport of substances that are not dissolved in the transport medium and can move simultaneously in different immiscible phases. The description of solute transport can be expressed using a stochastic method based on a so-called transfer function, or it can be implemented deterministically, i.e. using a convection-dispersion equation (Moene and van Dam, 2014).

This description of the transport of substances in soil is the most commonly used in software for modeling metal transport problems through soil profiles or, in general, fluid flow through porous media, which have the following equations implemented in them(Moene and van Dam, 2014). The Richards equation (**Eq 1-1**) implements the transport of water in soil.

$$\frac{\partial \theta}{\partial t} = div\ (K(h) grad\ H),$$

$$H = h + z$$

Eq. 1-1 **Richards equation**

where H is the total potential [L], K(h) is the unsaturated hydraulic conductivity, h is the pressure head [L] and z is the geodetic head [L].

For one-dimensional flow, the equation is simplified to the following form (**Eq. 1-2**).

$$\frac{\partial \theta}{\partial t} = \frac{\partial}{\partial z}\left(K(h)\frac{\partial H}{\partial z}\right)$$

Eq. 1-2 **Simplified form of Richards equation in 1D**

And conservative solute transport is based on the continuity equation as follows

(**Eq. 1-3**).

$$\frac{\partial(\theta c)}{\partial t} = \frac{\partial(q_d + q_a)}{\partial z}$$

Eq. 1-3 **Conservative solute transport**

Substituting advection q_a and dispersion q_d flux , the equation to describe the conservative transport is obtained (**Eq. 1-4**).

$$\frac{d(\theta c)}{dt} = \frac{\partial}{\partial z}\left(\theta D \frac{\partial c}{\partial z}\right) - \frac{\partial(qc)}{\partial z}$$

Eq. 1-4 **Advection-dispersion equation (conservative transport)**

In non-conservative flow, the transport of substances is affected by sorption, degradation, volatilization and other physicochemical processes in addition to advection and dispersion. The flux of substances that are sorbed onto soil particles during non-conservative transport is expressed by the following equation (**Eq. 1-5**).

$$\frac{\partial(\theta c)}{\partial t} + \frac{\partial(\rho_d s)}{\partial t} = \frac{\partial}{\partial z}\left(\theta D \frac{\partial c}{\partial z}\right) - \frac{\partial(qc)}{\partial z}$$

Eq. 1-5 **Advection-dispersion equation (non-conservative transport)**

where s is the adsorbed concentration on the solid phase [-], $\boldsymbol{\rho_d}$ is the bulk mass [ML^{-3}], D is the dispersion coefficient [L^2T^{-1}]

Initial and boundary conditions

To find the numerical solution of differential equations, it is necessary to define initial and boundary conditions. Initial conditions are essential to determine the domain at the beginning of the flow process for the distribution of an unknown function (h ,θ):

$$h(\mathbf{x},0) = h_{\circ}(\mathbf{x})$$

$$\theta(\mathbf{x},0) = \theta_{\circ}(\mathbf{x})$$

where h_0 and θ_0 are the fields of initial pressure head and moisture content) in the whole flow domain at time 0.

Boundary conditions are the requirements that must be met in order to solve a boundary value issue. The boundary value problem is a differential equation (or series of differential equations) that must be solved in a region with defined boundaries. The domain boundary can be exposed to various boundary conditions (**Fig. 1-8**). The selection of boundary conditions is critical for solving the computational problem.
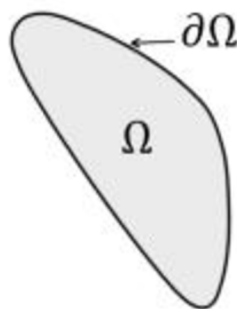

Fig. 1-8 **Resolution domain and boundary**

There are two types of boundary conditions that were further used in this study. The first type represents the value of the domain boundary solution.

Dirichlet Boundary Conditions

The Dirichlet boundary requirements specify the value that the function f (**Eq. 1-6**) of solving the differential equation must have on the boundary of domain Ω(Ω is the most used abbreviation for the boundary). The boundary is usually expressed as ∂Ω. A typical Dirichlet boundary condition in a two-dimensional domain defined by x and y would be:

$$f(x, y) = g\ (x, y, ..), where\ (x, y) \in \delta\Omega$$

$$f(x, y) = g\ (x, y, ..), where\ (x, y) \in \delta\Omega$$

Eq. 1-6. **Dirichlet boundary condition definition**

Neumann Boundary Conditions

Neumann boundary conditions are the second important form of boundary condition. According to Neumann boundary conditions, the derivative of the function f of the differential equation solution (**Eq. 1-7**, **Eq. 1-8**) must have a specific value at the boundary of domain Ω. The following example shows the Neumann boundary condition:

$$\delta f(x, y)\delta x = g\ (x, y, ..), where\ (x, y) \in \delta\Omega$$

Eq. 1-7 **Neumann boundary condition definition**

or

$$\delta f(x, y)\delta y = g\ (x, y, ..), where\ (x, y) \in \delta\Omega$$

Eq. 1-8 **Neuman boundary condition definition**

42

The function g can be affected not only by x and y, but also by other factors such as time (Rapp et al., 2016).

Models

In general, models can be divided by type and by scale. The scale can be temporal (seconds - years) or spatial (micro-processes, macro-processes). Models can be further divided into mathematical and mechanistic (Fig. 1-9).
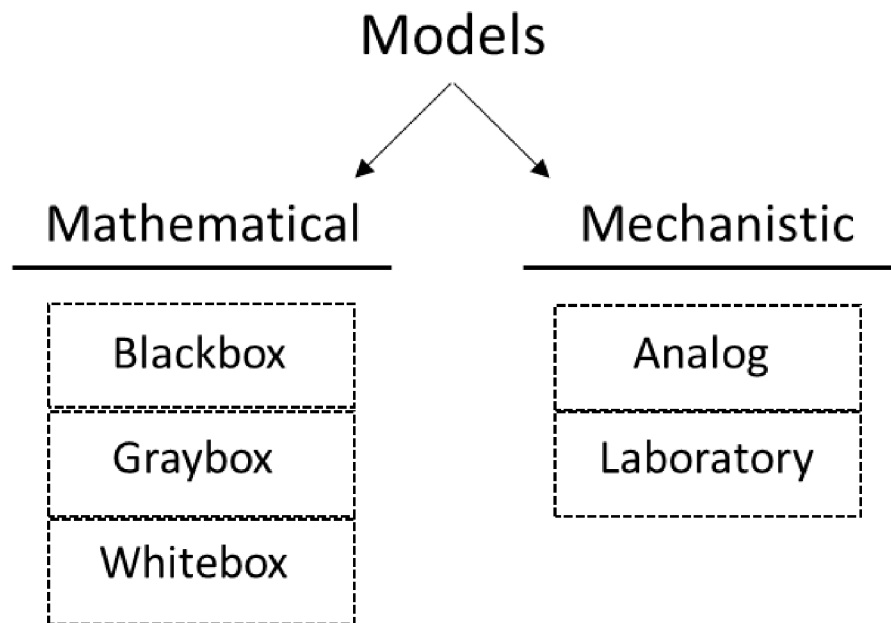
Fig. 1-9 Type of models

Analog models are based on modeling an analogous situation represented by similar physical laws and quantities (e.g., a model of the potential flow of water through a porous medium, characterized by an electric field). Laboratory or physical models are usually a scaled-down model of reality, for example, a laboratory column representing a soil profile (Kodešová, 2012). On the other hand, mathematical models are abstract models and are characterized by mathematical relations and functions that model the corresponding outputs from the given inputs. The simplest models in

this category are called blackbox or empirical models and are based only on superficial empirical relationships (e.g., Freundlich and Langmuir isotherm model). Graybox or conceptual models generally greatly simplify the physical laws and are built based on a concept related to the modeled system. The most complex models are the so-called whitebox or theoretical models, which attempt to represent actual physical regularities. They are based on the numerical solution of the differential equations of a given problem. These models are generally demanding in terms of input parameters and computational capacity of the hardware (Horgan, 1996).

Model of sorption isotherm

The primary evaluation of sorption systems is based on sorption isotherms obtained under predefined and controlled conditions. Quantitative comparison of two different sorption systems is only possible when the equilibrium metal concentration in solution and the environmental conditions (pH, temperature, concentration of other ions) are identical (Ahalya et al., 2005). An important aspect of sorption studies is the equipment in which the process is carried out. There are two types: equilibrium batch and the dynamic column systems. In the batch equilibrium system, a certain amount of sorbent is mixed with a specific volume of metal(loid) solution and allowed to interact until an equilibrium concentration between the solution and the surface of the material is reached. However as the concentration of metal in solution decreases, the rate of sorption also decreases, and it is only possible to predict it based on sorption at equilibrium, which is often not fulfilled under natural conditions (Volesky and Holan, 1995). Sorption systems using dynamic columns do not have this disadvantage. The sorbent is in continuous contact with the fresh solution, and the concentration of the solution in contact with a given layer is constant. Using these column experiments, the parameters of non-equilibrium sorption isotherms can be obtained, i.e., those that more closely match natural conditions. These nonlinear adsorption isotherms are based on the integration, called breakthrough curves, which express the ratio of the final and initial concentrations as a function of time. The main disadvantage of these experiments is the necessity to establish a local equilibrium in the experimental column, which can lead, in some cases, to an increase in the total experimental time (Buergisser et al., 1993).

In general, the main advantage of using simple adsorption isotherms is to describe the sorption equilibrium that allows a quantitative evaluation of the sorption properties of the sorbent for a single metal system (e.g., affinity or maximal adsorbed amount). Sorption isotherms express the dependence of the adsorbed amount on its residual concentration in solution at equilibrium at a constant temperature. The most used models are the Langmuir isotherm and the Freundlich isotherm. The Langmuir model assumes a homogeneous material surface, constant sorption surface properties, and adsorption on only one layer. The Freundlich model is a more complex model, which already assumes a heterogeneous material surface and a course of adsorption on multiple layers. However, the evaluation parameter S_{max}, which represents the maximum sorption capacity of a given sorbent for a given ion and is expressed as the ratio of sorbed metal in milligrams per dry weight of sorbent in grams, can only be obtained from the Langmuir model or if Langmuir and Freundlich models are combined (Volesky and Holan, 1995; Nurchi and Villaescusa, 2008). In general, the sorption is not affected by temperature unless it is outside 20 °C - 35 °C. Contrarily, one of the most important parameter influencing the sorption process is the pH value, which affects the ability of metal ions in solution and the charge of the binding groups on the sorbent surface. Other factors affecting the sorption are the concentration of the sorbent and the interactions between the various ions in the solution (Ahalya et al., 2005).

Reactive transport and geochemical models

HYDRUS

Hydrus 1D is a software for simulating water, energy, and solute movements in saturated and unsaturated porous media, developed by the U.S. Salinity Laboratory. It has been widely used to analyze the processes of water movement and solute migration in unsaturated and porous media (Šimůnek et al., 2003, 2008). The HYDRUS models can be used for both direct problems when the initial and boundary conditions for all involved processes and corresponding model parameters are known

and inverse problems when some of the parameters need to be calibrated or estimated from observed data. Hydrus-1D is a model widely used by the international center of groundwater simulation with 5 modules used for different calculations, including water movement, solution migration, heat conduction, plant-root water uptake, and plant-root growth (Chen et al., 2021). The water movement module can be explicitly used for unsaturated soil water movement simulation. It considers plant-root water uptake, but it also modifies the lagging of soil water holding capacity (Chen et al., 2021).The boundary conditions of the model are complex, with the upper boundary conditions including a constant water head, a constant water flow, an atmospheric boundary condition, variable water head, variable water flow, and atmospheric boundarycondition with surface with run-off.

In contrast, the lower boundary conditions include constant waterhead, constant water flow, variable water head, variable water flow, freedom drainage, deep layer drainage, leached surface, and horizontal drainage. Some boundary conditions are variable and the corresponding variable conditions should be imputed (WU et al., 2019). For the calculation of water movement, the standard Richards equation (**Eq. 1-9**) was used, taking the soil surface as the abscissa while the direction of the *Z*-axis is downwards.

$$\frac{\partial \theta}{\partial t} = \frac{\partial}{\partial z}\left(D(\theta)\frac{\partial h}{\partial z}\right) + \frac{\partial k(\theta)}{\partial z} + S$$

Eq. 1-9 **Form of Richards equation used in Hydrus 1D**

Where θ is soil water content, h is suction head, K is unsaturated soil water conductivity, S is plant-root water uptake, which would be 0 when no plants are present in the soil surface and D(θ) is soil water diffusivity.

The model can be divided into a single pore model and a double pore model and the Van Genuchten-Mualem model, which was developed from the single models of Van Genuchten (1980) and Mualem (1975)., expressed by **Eq. 1-10.**

$$\theta\left(h\right)=\begin{cases}\theta_r+\dfrac{\theta_s-\theta_r}{\left(1+\left|\alpha h\right|^n\right)^m},h<0\\[3mm]\theta_s,h\geq 0\end{cases}$$

Eq. 1-10 **Van Genuchten and Mualem formula**

Where, θ_r is the residual soil moisture content; θ_s is saturated soil moisture content and h is pressure water head.

Considering the effect of suction head on plant-root water uptake, Feddes function was used to calculate the actual transpiration rate according to the potential transpiration rate. According to Eq.1-11

$$\alpha\left(h\right)=\begin{cases}0,h\geq h_4,h\leq h_1;\\[2mm]\dfrac{h_1-h}{h_1-h_2},h_2\leq h\leq h_1;\\[3mm]1,h_3\leq h\leq h_2;\\[2mm]\dfrac{h-h_4}{h_3-h_4},h_4\leq h\leq h_3;\end{cases}$$

Eq.1-11 **Feddes function for transpiration rate**

where, h is soil water potential [cm], h_1 is the negative pressure value when the soil pores are full of water, h_2 is a negative value when the soil water reaches the water holding capacity, h_3 is a negative value when the capillary bond is disrupted due to plant consumption and evaporation from the soil surface and h_4 is a negative pressure value when permanent wilting occurs.

47

The Hydrus 1D application also allows a numerical simulation of solute transport in one-dimensional soil environments. Convection-dispersion equation (**Eq. 1-12**) for solute transport, where in addition to sorption, gas flow, degradation of defined substances in soil, heat transport, root zone extraction rate and zero-second order rate constants for sources and sinks in the gas, liquid and solid phases are also included (Kodešová, 2012).

$$\underbrace{\frac{\partial \theta c_1}{\partial t}}_{\text{FUNCTION OF VOLUME}} + \underbrace{\frac{\partial \rho s_1}{\partial t}}_{\text{SORPTION}} + \underbrace{\frac{\partial a_v g_1}{\partial t}}_{\text{VOLATILIZATION}} = \underbrace{\frac{\partial}{\partial x}\left(\theta D_1^w \frac{\partial c_1}{\partial x}\right)}_{\text{DISPERSION}} + \underbrace{\frac{\partial}{\partial x}\left(a_v D_1^g \frac{\partial g_1}{\partial x}\right)}_{\text{VOLATILIZATION}} - \underbrace{\frac{\partial q c_1}{\partial x}}_{\text{ADVECTON}} - \underbrace{r_{a,1}}_{\substack{\text{ROOT}\\\text{EXTRACTION}}} -$$

$$-(\mu_{w,1} + \mu'_{w,1})\theta c_1 - (\mu_{s,1} + \mu'_{s,1})\rho s_1 - (\mu_{g,1} + \mu'_{g,1})a_v g_1 + \gamma_{w,1}\theta + \gamma_{s,1}\rho + \gamma_{g,1}a_v$$

Rate constant of 0.-2. order for sources, sinks a linking among phases (solid, liquid, gas)

Eq. 1-12 **Convective dispersion equation** (adapted from *Kodešová, 2012)*.

PHREEQC

PHREEQC is a program designed to simulate processes in a geochemical system. Phase interactions can define the geochemical system during specific reactions (**Fig. 1-10**).
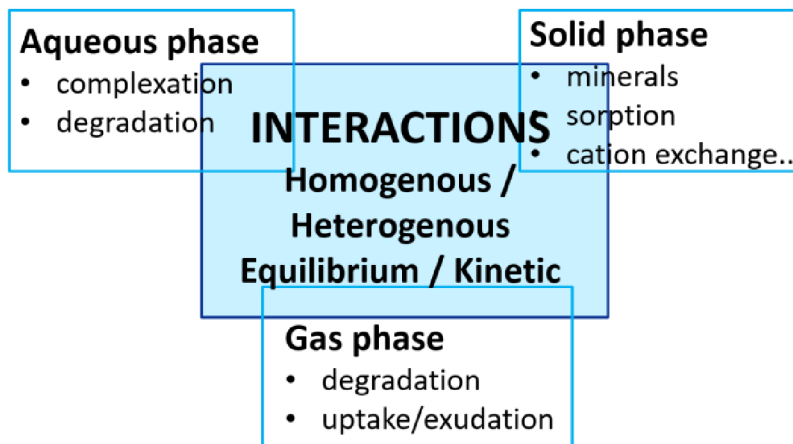

Fig. 1-10 **Geochemical system**

48

Geochemical modelling aims to find a specific form (speciation) in which an element exists in solution (water). The calculation of the above-mentioned processes, including the major species of elements, composition of surfaces, saturation states of mineral phases and many others, are based on principles stored via data structures and coefficients in thermodynamic databases.

$$\sum_{i=1}^{N} W_i v_{ir} = 0 \qquad\qquad \sum_{i=1}^{N} z_i v_{ir} = 0$$

Eq. 1-13 Reaction must be in balance

All reactions have to be in the balance as shown on **Eq. 1-13** and the ionic species in an electrolyte solution remain charge balanced on a macroscopic scale (**Eq. 1-14**)

$$\sum_{i} z_i c_i + \sum_{i} z_j c_j = 0$$

Eq. 1-14 Charge balance

The reaction can be defined by an equilibrium constant expressing that product of concentrations of products over product concentration of reactants is constant (**Eq. 1-15**).

$$K = \frac{[C]^c [D]^d}{[A]^a [B]^b}$$

Eq. 1-15 Reaction equilibrium constant

Governing equation for total molarity of element is shown in (Eq. 1-16).

$$M_i = m_{H_2O} \left(c_i + \sum_{j=1}^{N_{sa}} v_{ji} K_j \prod_i c_i^{v_{ji}} \right)$$

Eq. 1-16 Governing equation for molarity calculation

where M_i is total molar concentration of the observed component, v_{ji} represents stoichiometric coefficient of i-th component for j secondary species, K_j is an equilibrium reaction constant and c_i is concentration of i-th component in the iterative calculation. N_{sa} is total number of secondary species which are calculated according to Eq. 1-17

$$N_{SA} = N_S - N_R$$

Eq. 1-17 Total number of secondary species

where N_S is the total number of components and N_R is the total number of linearly independent reactions.

Above mentioned definitions are valid for calculations in a non-ideal geochemical system. In the non-ideal (closer to reality) system, the interaction between species cannot be neglected, chemical potential does not depend only on a mole fraction and other species will affect free energy in the solution, i.e., an activity correction coefficient must be implemented to a calculation based on Eq. 1-18.

$$a_i = \gamma_i * m_i$$

Eq. 1-18 Activity reacalculation

where γ represents an activity coefficient and m is a molar concentration. Examples of several activity models that can be implemented in the model are shown in Table 1-6. Activity models

Table 1-6. Activity models

Model	Main equation
Extended Debye–Hückel	$\log \gamma = -\dfrac{A\sqrt{m}}{1+Ba\sqrt{m}} + cm + dm^2 - \log(1+0.002mM) + \text{Ext}$ $A = \dfrac{1.8247 \times 10^6 \sqrt{\rho}}{(\varepsilon_r T)^{3/2}}$ $B = \dfrac{50.2901 \times 10^6 \sqrt{\rho}}{\sqrt{\varepsilon_r T}}$
Pitzer	$\ln \gamma = f^\gamma + B^\gamma m + C^\gamma m^2$ $f^\gamma = -A_\phi \left[\dfrac{\sqrt{m}}{1+b\sqrt{m}} + \dfrac{2}{b}\ln\left(1+b\sqrt{m}\right) \right]$ $B^\gamma = 2\beta^0 + \dfrac{2\beta^1}{\alpha^2 m}\left[1 - \left(1 + \alpha\sqrt{m} - \dfrac{\alpha^2 m}{2}\right)\exp\left(-\alpha\sqrt{m}\right)\right]$ $A_\phi = \dfrac{1.4006 \times 10^6 \sqrt{\rho}}{(\varepsilon_r T)^{3/2}}$

For calculation of saturation states, is used **Eq. 1-19.**

$$SI = log\,\frac{IAP}{K_{SP}}$$

Eq. 1-19 Saturation index calculation

where K_{SP} is a solubility constant related to an equilibrium reaction constant (K) and calculated products of free ions in solution (IAP) based on the activity model. If SI = 0, solution is in equilibrium and no reaction is running. SI > 0 reflects precipitation of a mineral phase. SI < 0 reflects dissolution of a mineral phase.

Recent studies

Hydrus and Phreeqc are widely used for modeling transport and speciation processes shown in **Table 1-7**. Chen et al. (2021) used Hydrus-1D software to examine the long-term stability of immobilized Cr in soil treated by Fe modified biochar. Results showed that Fe-BCH-amended soil could remove about 71% Cr from contaminated groundwater.

Hydrus 1D simulations were used to estimate changes in water fluxes. and calculation of the soil water content (SWC) by Altdorff et al., (2019). Horel et al. (2019) used HYDRUS 1D soil hydrological model to simulate changes in SWC, using the control treatment without biochar as a reference data source for model calibration. The simulated SWC dynamics fitted well the measured ones in all treatments and the HYDRUS 1D was proved as an exceptionally valuable tool to predict the hydrological response of different amount of biochar addition to silt loam soil including plant growth.

Study presented by Berns et al. (2018) combined batch sorption experiments of Cs^+ and Sr^{2+} in agricultural soils of differing soil texture with numerical experiments using PHREEQC to identify key processes of sorption at different temperatures. Sorption was simulated for both radionuclides using cation exchange models. In addition, surface complexation was integrated into the reaction network for Sr^{2+}.

Liu et al. (2019) modelled aqueous data from batch-style experiments using PHREEQC, incorporating thermodynamic constants between Hg and DOM (dissolved organic matter)

Table 1-7. **Recent studies on biochar using transport and speciation software**

PROBLEM	AMENDMENT	SOFTWARE/MODEL	STUDY
Remediation of chromium-contaminated soil and groundwater.	Iron-modified biochar	HYDRUS-1D	Chen et al., 2021.
Soil hydraulic properties and enhancement of nutrient retention.	Biochar	HYDRUS-1D	Altdorff et al., 2019
Changes in soil water content (SWC).	Biochar	HYDRUS-1D	Horel et al., 2019
Sorption and transport of Sr and Cs in agricultural soils.	Biochar	PHREEQC	Berns et al., 2018
Hg complexation with DOM	Biochar	PHREEQC	Liu et al., 2019

Presented studies confirmed that PHREEQC is mainly used not for more complex geochemical while HYDRUS is mostly used for simulations of changes and evolution of hydraulic properties of materials or soil amendments

Chapter II

Biochar presence in a soil significantly decreased the saturated hydraulic conductivity due to swelling

Lukáš Jačka, Lukáš Trakal, Petr Ouředníček, Michael Pohořelý, Václav Šípek

Content

Abstract

The application of biochar on two contrasting soils was tested to assess its effects on soil hydraulic properties (SHP) and study the interaction between water and the biochar surface (e.g., the swelling effect).

Two contrasting soil types were enriched with 0, 2 and 5% (wt.) doses of grape stalks biochar in order to prepare soil samples for a 14-days continually saturated laboratory experiment. H_2O bonds to the biochar surface were detected using FTIR spectroscopy.

Results show that water molecules were bound through polar hydrogen bonds to O–H and C–O–H, and these interactions caused (i) intensive swelling, which decreased the bulk density and enhanced the water holding capacity (up to 5% in the case of sandy loam and 5% biochar dose), and (ii) significantly decreased K_s in both soils (with a maximum difference of 82.6%).

The results of this laboratory experiment provide useful information about the significant effect of presented biochar in two contrasting soils, and its application appears to be a potential option for addressing drought (especially in coarser soils). Nevertheless, these findings must be verified under field conditions where the presence of biota and long-term effects can be considered.

Introduction

Among other advantages, biochar has also been recently tested for its potential to affect soil hydraulic properties (SHP) such as saturated hydraulic conductivity (K_s) and soil water retention curve (RETC). Lim et al. (2016) and Barnes et al. (2014) reported that biochar addition decrease K_s in sandy soils and increase K_s in clay-rich soils. Furthermore, water holding capacity (WHC) can be increased (although not always significantly) by the biochar application (see Herath et al., 2013; Rogovska et al., 2014; Burrell et al., 2016; Głąb et al., 2016). The observed decreasing effect of biochar on K_s has been explained by (i) the obstruction of water flow through effective soil pores by biochar particles (Barnes et al., 2014; Lim et al., 2016); (ii) the gradual clogging of soil pores by moving biochar particles (Wang et al., 2013; Barnes et al., 2014); (iii) a decrease in the volume of effective pores by sorbed water (Uzoma et al., 2011; Hardie et al., 2014; Lim et al., 2016); and (iv) an increase in the number of micropores (< 1 μm), which bind to water by strong capillary and/or adsorptive forces (Hillel, 1998; Hardie et al., 2014; Lim et al., 2016).

The latter two relate to the interactions of biochar surface and water molecules. In more details, water can be sorbed on the biochar surface: (i) using physical sorption through π interaction to the carbon surface (Shi et al., 2015); (ii) by hydrogen bonds on carboxyl groups (Ettler et al., 2014b); and/or (iii) by hydration interaction with cations (Kutílek et al., 1994; Shi et al., 2015). As a result, such water-biochar interactions can also significantly affect the swelling effect which has been usually omitted in the recent studies reflecting the effect of biochar to SHP. As a novel approach we will, therefore, try to fill the gap of knowledge to deeply understand and describe the effect of swelling caused by presented biochar as well as to confirm consequent response in the form of decreased K_s value. Specifically, one selected biochar from previous study of Trakal et al., 2014 with high CEC value was tested **Table 2.1.**

The aims of this paper are, therefore, (i) to reveal the biochar effect (with high CEC) on K_s variability in two soils of contrasting texture over the period; (ii) to evaluate the

effect of biochar on water holding capacity at saturation; and mainly (iii) to describe mechanism(s) of the swelling caused by presented biochar.

Table 2.1**Initial characteristics of the materials used; data shown are means ± SD (n=3)**

Material Used	P^a (g cm^{-3})	Texture (%)			CEC	pH
		Clay (<2μm)	Salt (2.50μm)	Sand (0.05-2mm)	(Cmol$_{(+)}$kg^{-1})	(-)
Soil	1.21±0.005[b]	8.7±1.0	34.8±43	56.5±4.4	9.08±0.42	5.95±0.01
Kaolin day	0.46±0.007	68.5±2.1	31.5±2.1	<DL	8.51±0.21	5.43±0.04
Biochar	0.16±0.004[c]	I^c	I^c	I^c	40.2±0.3[d]	10.0±0.1[d]

[a]bulk density, [b]undisturbed dried soil sample, [c]100 % of particles are < 0.50 mm

[d]value presented in Trakal et al.(2014b).

Materials and methods

Biochar preparation and analysis

Grape stalks, a common by-product of wine production, were used in this study for the biochar preparation. The production methodology and initial characteristics of the biochar is/are described by Trakal et al., 2014. Additionally, the interaction (i.e., chemical bonds) between water molecules and the biochar surface was identified using an ATR technique (Fourier Transform Infra-Red (FTIR) Nicolet Avatar 360,1.92 cm^{-1} resolution) to more precisely describe the swelling effect (bindings of the sorbed H_2O molecules on the biochar surface). The preparation procedure for FTIR analysis is written in the supplement of this paper.

Soil and sample ring preparation

The Fluvisol (classified as sandy loam; hereinafter CS) was collected from an uncultivated alluvium (= unaffected soil properties; for more information see the supplement) and such soil was air-dried, sieved (< 2 mm) and homogenized. For the preparation of the contrasting clay-enriched soil (classified as loam; hereinafter CSK), the same soil was thoroughly mixed with 20% (wt.) of kaolin clay with lower plasticity and swelling compared to most other clay minerals (Hillel, 1998). Next, milled biochar (< 0.50 mm) was then applied to each of the contrasting soils (CS and CSK) at two doses, 2% and 5% (wt.), by careful mixing. The following system was used throughout the experiments to label the samples: control soil (CS); soil amended by 2% and 5% biochar (S2B) and (S5B); kaolin clay-modified control soil (CSK); kaolin clay- modified soil amended by 2% and 5% biochar (SK2B) and (SK5B). Each prepared soil variant was then repacked into a standard stainless-steel ring (volume of 100 cm^3), where five sample rings were filled for each variant.

Laboratory measurements

The samples were first gradually saturated from bottom in order to eliminate the effects of entrapped air (Jačka et al., 2014). Next, the K_s of the samples were

measured using the constant head method and calculated according to its primary defining Darcy's equation. The 5 control samples were always measured in parallel against the 5 samples amended by the biochar for each measuring at 10 regular time intervals during the 14-day experiment of continual water flow through the samples. Subsequently, each saturated sample was immediately weighed and dried to a constant weight. From the difference in weights, the water holding capacity at saturation (WHC) was then calculated. At the end of experiment, swelling effect was measured as an increase of soil sample over the edge of randomly selected sample rings. The increase in volume of sample was then responsible for the swelling.

Results and discussion

The effect of swelling caused by the biochar presence

The interaction of H_2O molecules with the biochar surface is presented in **Fig. 2.1** The FTIR spectra confirmed water binding on O–H and C–O–H functional groups through polar (hydrogen) bonds which is in agreement with the results presented by Chen et al. (2014). Furthermore, the 4 individual FTIR spectra showed decreasing intensity of the O–H peak, reflecting the release of water during the continuous drying process. The intensity decrease was not visible in the case of water bonded to the C–O–H group **Fig. 2.1**) probably due to creation of stronger 'double hydrogen bonds' (under steric conditions). Additionally, a significant amount of these hydrophilic oxygen-containing groups (reflected by the higher cation exchange capability; Mohamed et al., 2016) can enhance the binding of H_2O molecules. Specifically, the high content of fixed K^+ in functional groups (e.g., in grape stalks; Trakal et al., 2014) could have been responsible for the higher polarity, and consequently stronger binding to H_2O, of the functional groups observed in this experiment. Study of Shi et al. (2015) demonstrated so called 'molecular-thick aqueous salt-solution pancakes' on a surface of originally hydrophobic carbon-based material such as biochar. Furthermore, the prevalence of basic reactions over acidic reactions could result in increased water retention of the biochar surface, by which the protons in water molecules can be exchanged with Na^+, K^+ and Ca^{2+} (de Pasquale et al., 2012). The effect of these cations (mainly K^+) on water absorption to the biochar surface could not be verified directly due to the absence of an identical biochar (to the one used in this study) lacking these cations. The effect was therefore assumed according to our previous study (Trakal et al., 2014b), in which the sorption efficiencies of various biochar (cation-poor and -rich) were compared. Furthermore, the CEC value is strongly pH dependent when under basic pH the CEC of biochar is significantly higher compared to acidic conditions (Mukherjee et al., 2011). In this study, the pH value of biochar was 10.0 ± 0.1, which was therefore reflected by the prevalence of basic reactions over acidic ones.
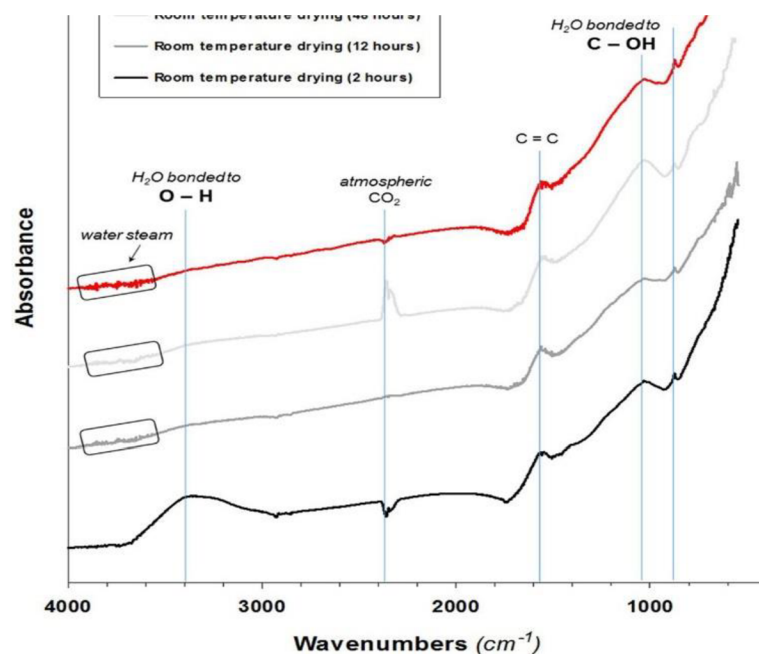
Fig. 2.1 **FTIR spectra of the biochar dropped by pure water at four stages (after 2, 12 and 48 drying under atmospheric conditions and oven drying at 60 °C in vacuum and consequent putting above the water table).**

Following the already mentioned facts such as (i) possibility of H_2O to sorb on the biochar surface; as well as (ii) the specific biochar characteristics (such as high CEC and/or very basic pH), this biochar was, therefore, predisposed to significantly influence overall swelling of such amended soils. **Fig. 2.2** and Table A1 show the swelling effect of the biochar in both soils. The 2% biochar dose showed negligible swelling effects in comparison with the 5% biochar dose (for both contrasting soils), and even stronger effects were observed in the case of biochar application to CS. Specifically, the highest swelling in this study.

Furthermore, the water holding capacity showed that biochar contained from 1.5% to 4.7% (depending both on the amount of biochar and soil type) more water at saturation than the untreated soil (CS). The WHC increase was most pronounced in the case of the highest biochar dose and sandy loam soil (S5B). In clayed soil, the effect on WHC was also statistically significant, yet this increase after the biochar

application was less intensive (Table A2). Similar impact of biochar on soil water retention (including WHC) is documented in several studies (e.g. Uzoma et al., 2011; Peake et al., 2014; Głąb et al., 2016). It can be explained mainly by the increased volume of soil samples (due to observed swelling) and the general ability of natural organic carbon to increase soil water retention (Rawls et al., 2003). However, this increased amount of water can be held by strong forces arising both from the capillarity (caused by small biochar intra-pores) and sorption potential of biochar, and thus may not be available for plants (Hardie et al., 2014). Streubel et al. (2011) concluded that the biochar influence on soil WHC depends on the biochar and soil types that are used.
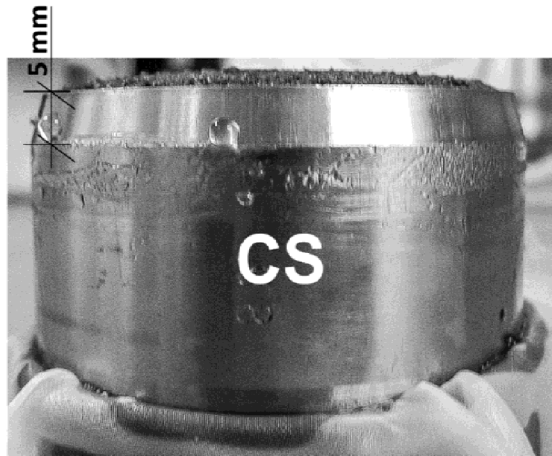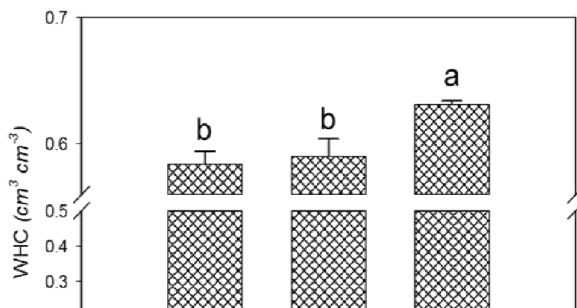
Fig. 2.2 The swelling effect in case of soil samples (CS – control non-clayed soil; S2B – 2% biochar dose to non-clayed soil; S5B – 5% biochar dose to non-clayed soil); graph shows measured WHC values at saturation for non- clayed soil; different letters following means (n = 5) indicate significant differences between treatments (Tukey HSD test at α = 0.05).

Differences in K$_s$ after the biochar application

The addition of biochar to both soils resulted in the decrease of saturated hydraulic conductivity (compared to non-amended soils). This decrease is more significant when higher biochar doses are applied. The soil samples, in order from least to greatest pores difference in K$_s$ values, are as follows: SK2B > > S2B > SK5B > > S5B (**Fig. 2.**). The rate of K$_s$ decrease ranged from 10% to 50% in biochar amended soils (Table A3 and A4). This could be explained by the addition of smaller biochar particles (< 0.50 mm) and above documented swelling which may clog the existing coarser pores and make them finer (Ajayi et al., 2016). Moreover, this overall decrease was accompanied by the temporal stabilization of K$_s$ values, which were significantly decreasing over time in the control soil (by 50%–80% in the case of CSK and CS, respectively). This temporal variability of K$_s$ values is probably caused by particle transport within the sample, with pores becoming continuously clogged by finer particles when such effect was suppressed by the amended biochar and kaolin clay, respectively. The small biochar and clay particles obviously clogged larger pores at the very beginning of the experiment and only limited particle transport was further possible. Barnes et al. (2014) and Lim et al. (2016) observed similar decreases in K$_s$ over time using several soil types. In contrast with the results of this study, Barnes et al. (2014) observed increased K$_s$ in clay- rich soil (classified as clay loam) but the clay type was not specified. The kaolin clay used in this study (less prone to swelling) may be the reason of discrepancies between the results of our study and other studies conducted in loamy soils reporting no significant changes in K$_s$ (Laird et al., 2010; Rogovska et al., 2014). The CSK soil in this study exhibited decreased K$_s$ after the biochar application; however, this decrease was significantly smaller in comparison to CS (**Fig. 2.**). Such limited effect of the K$_s$ decrease could be explained by the (artificial) presence of kaolin clay which partly suppressed the effect of presented biochar in this case.

Besides the decrease in K$_s$, the decline in bulk density was simultaneously observed. This reduction in bulk density was more evident for the 5% doses than for the 2% doses of biochar, as well as for non-clayed soil (CS; Table A1). This is in contradiction with their generally inverse relationship. Similar behavior was reported by Barnes et

al. (2014), who attributed it to the internal structure of biochar. Frequently, biochar has significantly lower bulk density and higher porosity than soils, but this porosity is mainly formed by micropores (and/or mesopores up to 50 nm) with limited ability to conduct water and, hence decreasing K_s.
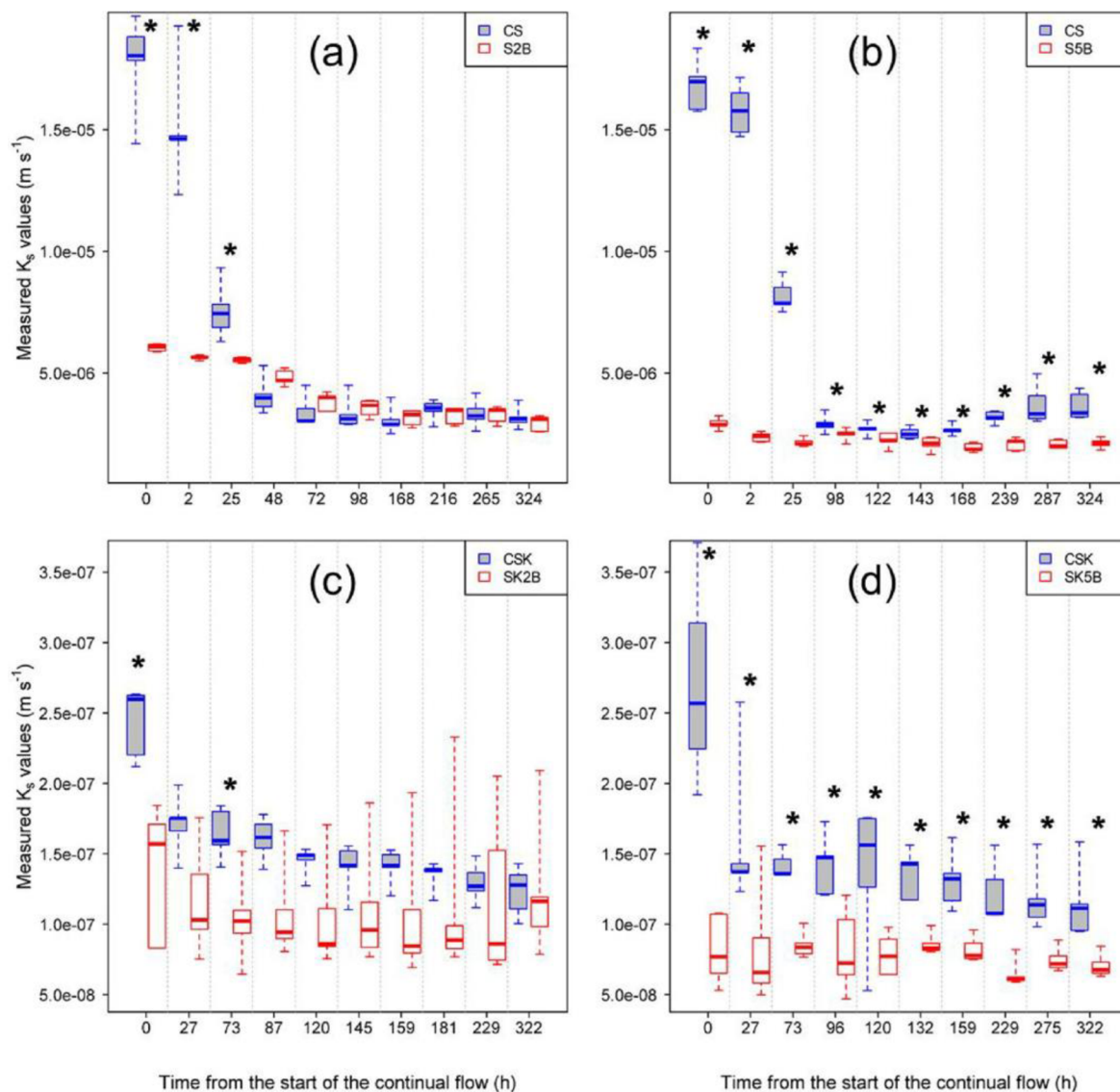
Fig. 2.3 **Time variable differences of saturated hydraulic conductivity (K_s) between biochar amended and control soils (a) soil vs. treated soil by 2% biochar; (b) soil vs. treated soil by 5% biochar; (c) clayed soil vs. treated soil by 2% biochar; and (d) clayed**

soil vs. treated soil by 5% biochar. Set of data pairs (each boxplot reflecting five replicas) with asterisk are statistically significant (Tukey HSD test at α = 0.05).

The applicability and limitation of this research

The application of biochar reduced water flux in both soils, which was reflected by the decrease in K_s (representing crucial dynamic parameter). In soils with a coarser texture (exhibited by higher K_s values), this observation can be beneficial, especially for plants that are in contact with pore water and dissolved nutrients for long periods of time (Lim et al., 2016). Biochar can be especially beneficial during cycles of extreme drought and intensive rainfall by mitigating both soil eluviation during wet periods and soil pore water deficiency during dry periods. However, the selection of biochar dose is very important. Specifically, the amount of biochar that is applied has been directly proportional to the effect on SHP. Appropriate dose of biochar seems to be 2% (wt.). Concerning the field application of biochar and its consequent effect on SHP, soil compaction has also shown to be critically important (Zhang et al., 2006).

The results of this laboratory study may be difficult to compare with field experiments, as the soil samples were repacked (a standard laboratory procedure), and interaction with the surrounding soil was restricted during the experiment. Specifically, the swelling effect could be different under field conditions because swelling would not be restricted by the walls of the sample rings. Furthermore, it is impossible to uniformly distribute biochar during field applications (Tammeorg et al., 2014).

Additionally, the influence of the biochar application to SHP may be masked by the activity of biota in the case of long-term field experiments (Jeffery et al., 2015). Hardie et al. (2014) reported minor impacts of the biochar (applied to sandy loam, Planosol) on available water capacity and a significant increase in both K_s and water retention close to saturation (as a result of more intensive earthworm burrowing in biochar-enriched soil).

In summary, many studies have shown that the effects of adding specific biochars (mainly in specific doses) to particular soils are valid only for the tested biochar and soil (see e.g., Herath et al., 2013; Głąb et al., 2016). The addition of biochar could, therefore, increase or decrease K_s according to the individual experimental design (field vs. laboratory; long-term vs. short-term study.

Conclusions

The interaction of H_2O molecules with a biochar surface was facilitated through polar hydrogen bonds of O–H and C–O–H, with C–O–H groups forming stronger bonds. These interactions caused intensive swelling, even in the case of a higher dose of biochar being applied to non-clayed soil, which caused a decrease in bulk density and an enhancement of WHC (up to 5%). The presence of biochar also significantly decreased K_s in the cases of both contrasting soils, where this decrease was most obvious in the S5B variant. As a result of these findings, the application of biochar to soils appears to be a plausible option for addressing drought (especially in problematic sandy soil.

Supplementary material

Materials and Methods

Additional information of all material used

Fluvisol (CS) from the Litavka River near Trhové Dušníky (49°43'N, 14°0'E, 440 m above sea level) at depths of 10 to 30 cm below the surface. Kaolin clay was supplied by Eijkelkamp (Art. No. 08.02.04, Batch No. 51359712).

Based on the particle size analysis performed using the hydrometer method (CEN ISO/TS 17892-4, 2004), the soil (CS) was classified as sandy loam (according to the USDA textural triangle). The clay-enriched soil (SCK), which contains a 20% higher amount of kaolin clay, was classified as loam (21.6% clay, 35.9% silt, 42.5% sand; calculated values based on the texture of kaolin clay and CS soil). All initial characteristics of the soil, kaolin clay and biochar are presented in Table 1. More detailed characteristics of the biochar used in this study have been presented by Trakal et al. (2014).

The initial K_s value of non-clayed soil (1.78-1.68 × 10^{-5} m s^{-1}) was significantly higher than that of soil with clay presence (2.73-2.44 × 10^{-7} m s^{-1}), which demonstrated the 'hydraulic contrast' of both examined soils.

Moistening procedures of biochar

Distilled water was dropped onto the pure biochar, and the moistened biochar was allowed to dry under atmospheric conditions for 2, 12 and 48 hours. Additionally, the biochar sample was dried by a final time at 60°C in a vacuum oven, and such completely dried sample was then placed above a water table for 3 days. The absorption of low amounts of water vapor (from the atmosphere) was detected, mainly after drying and consequent placement above the water table (see the red line in Fig. 1). The C-H and C=C peaks confirmed the presence of biochar in the form of polynomic organic chains (Trakal et al., 2014), and the peak at 2350 cm^{-1} reflected the absorption of atmospheric CO_2.

Procedure of sample rings filling

Force of tamping (tapping on the wall of the ring by hand) was used in order to ensure such bulk density (in case of CS) equal to that of undisturbed soil sample (sampled and measured previously in the field; see value of the soil in Table 1). The filling procedure of other rings though the all remaining variants was then designed in order to ensure identical force of tamping which was previously used for CS variant.

Table A1. Comparison of initial (measured) and final (calculated) bulk densities (means ± SD recalculated for dry soil) of the soil samples, including the swelling effect of the final soil samples obtained from the K_s experiment; different letters following means (n = 5) for the initial bulk density indicate significant differences between treatments (Tukey HSD test at α = 0.05).

Sample	Measured initial bulk density (g cm^{-3})	Measured height of the swelling (mm)	Calculated final values[a]	
			Soil sample volume (cm^3)	Bulk density (g cm^{-3})
CS	1.236 ± 0.003a	0.90 ± 0.10	102.2	1.209
S2B	1.234 ± 0.005a	2.90 ± 0.30	107.1	1.152
S5B	1.208 ± 0.005b	5.40 ± 0.60	113.3	1.066
CSK	1.145 ± 0.002c	<DL	100.0	1.145
SK2B	1.141 ± 0.002c	1.40 ± 0.20	103.4	1.103
SK5B	1.140 ± 0.002c	3.40 ± 0.40	108.4	1.052

[a]values were calculated from means of measured height of swelling and known volume (100 cm^3) and height (4.06 cm) of standardized sample ring.

Table A2. A statistical description of the measured WHC values at saturation (n = 5). Different letters following means indicate significant differences between treatments (Tukey HSD test at $\alpha = 0.05$).

Treatment	Mean ± SD $(cm^3\,cm^{-3})$	Minimum $(cm^3\,cm^{-3})$	Maximum $(cm^3\,cm^{-3})$
CSK-2B*	0.552 ± 0.005e	0.547	0.558
CSK-5B**	0.554 ± 0.005e	0.550	0.561
SK2B	0.567 ± 0.004d	0.560	0.570
SK5B	0.595 ±0.009b	0.582	0.605
CS-2B***	0.575 ±0.013cd	0.561	0.597
CS-5B****	0.584 ± 0.010bc	0.572	0.595
S2B	0.590 ± 0.014b	0.578	0.612
S5B	0.631 ± 0.004a	0.628	0.637

*Control soil measured together with SK2B

**Control soil measured together with SK5B

***Control soil measured together with S2B

****Control soil measured together with S5B

Table A3. Measured K_s values (n = 5) in the soil enriched by kaolin at selected hours after the start of the continual flow. Different letters following means indicate significant differences between treatments within each time step (Tukey HSD test at $\alpha = 0.05$). Mean value of control soil is compared against treated one for each specific time step (CSK-2B vs. SK2B and CSK-5B vs. SK5B).

	Mean ± SD ($m\ s^{-1} \times 10^{-7}$)						
	Hours after the start of the continual flow						
Treatment	0	27	73	120	159	229	322
CSK-2B*	2.44 ± 0.254a	1.71 ± 0.212a	1.64 ± 0.179a	1.45 ± 0.102a	1.41 ± 0.127a	1.30 ± 0.139a	1.23 ± 0.176a
CSK-5B**	2.73 ± 0.907a	1.60 ± 0.553a	1.43 ± 0.119ab	1.37 ± 0.512ab	1.31 ± 0.201ab	1.24 ± 0.282ab	1.15 ± 0.259ab
SK2B	1.36 ± 0.491b	1.17 ± 0.392ab	1.05 ± 0.315bc	1.06 ± 0.387ab	1.08 ± 0.504ab	1.18 ± 0.589ab	1.24 ± 0.501a
SK5B	0.82 ± 0.248b	0.84 ± 0.427b	0.85 ± 0.095c	0.79 ± 0.149b	0.82 ± 0.090b	0.65 ± 0.097b	0.71 ± 0.085b

*Control soil measured together with SK2B; **Control soil measured together with SK5B

Table A4. Measured K_s values (n = 5) in the soil at selected hours after the start of the continual flow. Different letters following means indicate significant differences between treatments within each time step (Tukey HSD test at α = 0.05). Mean value of control soil is compared against treated one for each specific time step (CS-2B vs. S2B and CS-5B vs. S5B).

Treatment	Mean ± SD $(m\ s^{-1} \times 10^{-6})$					
	Hours after the start of the continual flow					
	0	2	25	98	168	324
CS-2B*	17.8 ± 1.997a	15.1 ± 2.531a	7.56 ± 1.150a	3.34 ± 0.674a	3.08 ± 0.558a	3.17 ± 0.444a
CS-5B**	16.8 ± 1.071a	15.8 ± 1.035a	8.17 ± 0.654a	2.92 ± 0.371ab	2.68 ± 0.230a	3.65 ± 0.559a
S2B	6.05 ± 0.154b	5.64 ± 0.091b	5.54 ± 0.106b	3.56 ± 0.359ab	3.17 ± 0.333a	2.95 ± 0.326a
S5B	2.93 ± 0.237c	2.37 ± 0.194c	2.16 ± 0.170c	2.49 ± 0.249b	1.95 ± 0.180b	2.12 ± 0.204b

*Control soil measured together with S2B; **Control soil measured together with S5B

Chapter III

AMOchar: Amorphous manganese oxide coating of biochar improves its efficiency at removing metal(loid)s from aqueous solutions

Lukáš Trakal, Zuzana Michálková, Luke Beesley, Martina Vítková, Petr Ouředníček, Andreu Piqueras Barceló, Vojtěch Ettler, Sylva Číhalová, Michael Komárek

Content

Abstract

A novel sorbent made from biochar modified with an amorphous Mn oxide (AMOchar) was compared with pure biochar, pure AMO, AMO + biochar mixtures and biochar + birnessite composite for the removal of various metal(loid)s from aqueous solutions using adsorption and solid-state analyses. In comparison with the pristine biochar, both Mn oxide-biochar composites were able to remove significantly greater quantities of various metal(loid)s from the aqueous solutions, especially at a ratio 2:1 (AMO:biochar). The AMOchar proved most efficient, removing almost 99, 91 and 51% of Pb, As and Cd, respectively. Additionally, AMOchar and AMO + biochar mixture exhibited reduced Mn leaching, compared to pure AMO. Therefore, it is concluded that the synthesis of AMO and biochar can produce a double acting sorbent ('dorbent') of enhanced efficiency, compared with the individual deployment of their component materials.

Introduction

Modern technologies for the remediation of wastewaters polluted by metal(loid)s are often based on sorption to high-binding materials such as various forms of activated carbon, because of their unique surface chemistry and highly porous structure (Song et al. 2014). However, the utilization of such pristine biochar as sorbents for metal(loid)s in aqueous solution has usually resulted in a few milligrams of metal(loid) sorption per gram of biochar (Mohan, et al. 2014). The efficiency can further be enhanced by various modifications as reviewed by Ahmed et al.(2016). One such improvement is the inclusion of secondary oxides, such as Fe-oxides (e.g. magnetite or γ-Fe_2O_3; (Han et al. 2015; Mohan, et al. 2014). We have demonstrated in our previous study (Trakal et al., 2016) that metal sorption of biochars with well-developed structures (i.e. those with greater BET surface) were significantly improved after such modification whilst, in contrast, biochars with lower BET surface (< 100 m^2 g^{-1}) showed negligible response to modification in terms of their sorption capacity.

In addition to Fe oxides, Mn oxides have also been demonstrated to have very high immobilization potential for metal(loid)s including the more common divalent metals (e.g. Pb(II), Cd(II), Cu(II), etc.), through adsorption processes onto amphoteric surface groups of the Mn-oxide, and also As(V) and/or Cr(VI), due to the initial oxidation/reduction process and consequent sorption, surface complexation and/or coprecipitation with birnessite and hydrous manganese oxide (Lenoble et al., 2004; Komárek et al., 2013). Among various types of Mn oxides, we have previously used the modified sol-gel procedure of Ching et al. (1997) for the preparation of amorphous manganese oxide AMO (Della Puppa et al., 2013). Such material has been previously established as very suitable sorbent for various metal(loid)s but associated dissolution of AMO has resulted in excessive Mn leaching in low pH environments, which has been highlighted as the major drawback of the application of such materials in a remediation context (Della Puppa et al., 2013; Michálková et al., 2014; Ettler et al., 2015).

In the following study, we will selectively treat solely those bivalent metals using pristine biochar and/or treat all dissolved metal(loid)s with a secondary Mn-leaching from the pure AMO. Because of that, the main aim of the present study was (i) to

produce an AMO-modified biochar combining the advantageous properties of both AMO and pristine biochar, with emphasis on the decrease of Mn leaching, improved sorbent longevity and (ii) to test their metal(loid) sorption properties in comparison with pure AMO and BC. Furthermore, AMOchar was also tested using a case column study where the source of metal(loid)s is contaminated ash, i.e., multi-metal(loid)s 'natural' solution under fluctuating pH.

Materials and methods

In the following study, we will selectively treat solely those bivalent metals using pristine biochar and/or treat all dissolved metal(loid)s with a secondary Mn-leaching from the pure AMO. Because of that, the main aim of the present study

Sorbent's preparation

Biochar produced from grape stalks was selected according to its proven high sorption capacity for Cd(II) and Pb(II) caused by dominancy of chemisorption (represented mainly by ion exchange sorption mechanism; (Trakal et al., 2014b). Specifically, the source material was pyrolysed at 600 °C in a muffle furnace under a nitrogen flow rate of 16.7 mL min^{-1} at atmospheric pressure with a retention time of 30 min. The pyrolysed product was then cooled overnight (under the same nitrogen flow), ground, homogenized, sieved (< 0.50 mm), washed with ultra-clean water (MilliQ Integral; Merck Millipore Corp., USA), and dried at 60 °C for 24 h until constant weight. The pure amorphous Mn oxide (AMO) was prepared according to Della Puppa et al.(2013) when 0.5 L of dissolved 0.4 M KMnO$_4$ was mixed with 0.5 L of 1.4 M glucose solution in beaker. Resulted gel was at first washed by 2.0 L of pure water and later dried at room temperature. Next, two AMO-modified biochars were prepared in two different ways and at three AMO/BC ratios: 1:2, 1:1 and 2:1 (w/w). In the first method, the AMO and biochar were mixed and agitated then together in deionized water (20/1; L/S) for 24 h at pH 9.00 (mean pH value between pH$_{ZPC}$ of pristine BC and pure AMO, respectively; denoted herein as AMO + BC; **Fig. 3.3**a). The desired pH value was maintained using 0.1 M KOH. In the second method, biochar was added directly into the reaction mixture for the synthesis of AMO (denoted herein as AMOchar; **Fig. 3.3**b). Specifically, biochar was mixed with 0.4 M KMnO$_4$ solution and subsequently 1.4 M glucose solution was added (Della Puppa et al., 2013). The resulting gel was then washed several times with deionized water, dried at laboratory temperature and milled in agate mortar. By way of comparison, a biochar-birnessite composite (BCB; synthetized according to S. Wang et al. (2015a) was prepared in

order to provide a reference sorbent after which the newly synthesized AMO-biochar modifications could be compared.

Sorbents characterization

All newly synthetized biochars were analyzed for the following characteristics: (i) pH value (at 1:10 (w/V) after 1 h of mixing) using an inoLab® pH meter (pH 7310, WTW, Germany); (ii) pH of the point of zero charge (pH_{ZPC}) determined using the immersion technique (IT) (Fiol and Villaescusa, 2008) and (iii) cation exchange capacity (CEC) determined according to Trakal et al.(2012). Specifically, 0.2 g of biochar (in duplicates) was mixed with 10 mL of $BaCl_2$ solution at 0.1 M of concentration and consequently was agitated in a GFL Shaker 3006 at 300 rpm for 24 h. The solution was then filtered and analyzed using ICP-OES (ICP-OES, Agilent 730, Agilent Technologies, USA). All these data were then compared with those of the pure AMO and the pristine biochar, respectively (see supplement)

The mineralogical composition of the studied sorbents was determined by X-ray diffraction analysis (XRD; PANalytical X'Pert Pro diffractometer with X'Celerator detector). The Mn oxide binding energies on the structure of biochar were then measured though X-ray photoelectron spectroscopy (XPS; Omicron Nanotechnology, Ltd.) and the Casa XPS program (for spectra evaluation). The SEM images of Mn-oxide-biochar composites were provided using high-resolution scanning electron microscope JEOL JSM-7401F Fesem (USA) and the SEM TESCAN VEGA3XMU (TESCAN Ltd., Czech Republic) equipped with a Bruker QUANTAX200 energy dispersive X-ray spectrometer (EDS). This was conducted to confirm the physical binding of AMO with biochar and the distribution of Mn oxide phases. Additionally, high-resolution transmission electron microscopy (HRTEM) using a JEOL JEM-3010 instrument (LaB_6 cathode; accelerating voltage of 300 keV) coupled with EDS and selected area electron diffraction (SAED) was applied to investigate the AMOchar particles under high resolution with special focus on the biochar surface coating.

Sorption experiments

Two sorption experiments were carried out in this study. The first was a static batch sorption test using synthetic solution (implemented in duplicate) to evaluate the kinetics of As(V), Cd(II) and Pb(II) sorption where all sorbents were tested under

optimized condition (concentration, dose and pH) for pristine biochar presented elsewhere by Trakal et al. (2014b). Specifically, all these sorbents were agitated in 1 mM solution of As(V), Cd(II) and Pb(II) (supplied as $Na_2HAsO_4 \cdot 7H_2O$, $Cd(NO_3)_2 \cdot 4H_2O$ and $Pb(NO_3)_2$, respectively; analytical grade; Lach-Ner, Czech Republic) using the ratio of 500/1 (L/S). The 0.01 M $NaNO_3$ was used as a background electrolyte. The pH was continuously adjusted (by 0.1 or 0.01 M HNO_3) to the aimed value of 5.00 (Cd(II) and Pb(II)) or 7.00 (As(V)) to avoid precipitation of the studied metal(loid)s using automatic titration device (TitroLine alpha plus, SI Analytics, Germany). The suspension was collected at given time intervals (3–450 min) and filtered immediately through 0.45-µm nylon filter (VWR, Germany). The content of the studied metal(loid)s (also including Mn and K) in solution was then determined using ICP-OES (Agilent 730, Agilent Technologies, USA). Additionally, the concentration of dissolved organic carbon (DOC) in solutions was determined using the carbon analyzer TOC-L CPH (Shimadzu, Japan).

The second sorption test (Fig. A.1) was a dynamic leaching test (not replicated) using one selected sorbent and a case contaminated material under non-buffered pH conditions. A metal(loid) rich wood ash collected from a biomass boiler of a farm, burning various waste-wood materials containing CCA-Chromated Copper Arsenate was selected as the source of As in solution (Mollon et al., 2016). This ash had a total As content of ~10,000 mg kg^{-1} (*aqua-regia* digestion after (Mollon et al., 2016)). Glass columns (dimensions 8 cm length and 1.5 cm internal diameter) were filled with 10 g of ash (control column) and 5 g of additional AMOchar (test column; Fig. A.1b). The AMOchar was placed above the ash in the column so that, in the direction of flow, ash leachate passed through the AMOchar layer. To avoid movement of material out of the columns during leaching, glass-wool was packed into the column at both ends and a 0.45 µm filter paper inserted. The filter paper ensured that the analyte contained no particulates > 0.45 µm and such collected eluate should then be directly applicable for ICP-OES. The columns were leached at a flow rate of 1 mL min^{-1} from their base, whilst a second pump was attached to the top of the column to maintain neutral pressure in the columns. Leaching from the base was to ensure, as far as possible, that the whole mass of material inside the column was leached uniformly, avoiding preferential pathways of flow through the material inside the column. The columns were constantly leached for 100 min and an auto-sampler distributed 2 mL

of leachate into tubes at pre-determined intervals every 10 min, resulting in a total of 10 fractions of leachate.

Leachate samples were analyzed for pH before being diluted for ICP-MS (ICapQ, Thermo Scientific, Germany) analysis, to determine As concentration. The obtained concentration data were converted from mg L^{-1} into cumulative mass of As (mg kg^{-1}), based on the volume of eluent passed through the column in each time step and the mass of ash in the column. Additionally, using complete analyses of the column leachate, aqueous speciation and saturation indices of the possible precipitates were predicted using the Visual MINTEQ 3.1 geochemical code (Gustafsson, 2013).
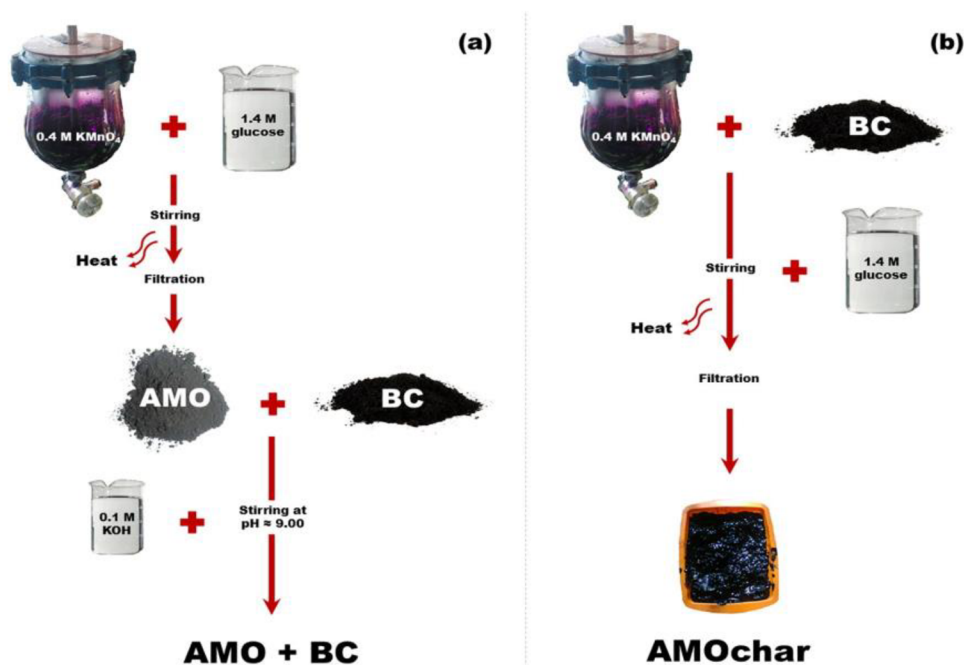

Fig. 3.3 **Scheme of AMOchar and AMO + BC composite synthesis.**

Results and discussion

Characterization of the newly synthetized AMO-biochar composites

The XRD pattern (**Fig 3.5**) of the AMOchar confirmed its amorphous character (obvious from the wide shape of the pattern), where the dominant peaks represent Mn-oxalate hydrate, a by-product of AMO synthesis ($C_2MnO_4 \cdot H_2O$; PDF-2 card 00-025-0544; as is the best reflection of the AMO, according to Ettler et al. (2014b) and by carbon (PDF-2 card 00-026-1080), showing the presence of the biochar skeleton. Apart from the presence of Mn-oxalate hydrate and carbon, the presence of rhodochrosite ($MnCO_3$; PDF-2 card 01-086-0172) was also confirmed. The formation of the rhodochrosite was previously explained by Ettler et al.(2014b) as a reaction of the removed Mn from oxalates of the AMO with atmospheric CO_2. Additionally, such leached Mn could react with CO^{2-} groups sorbed at the surface of biochar, originated from CO_2 sorption (X. Xu et al., 2016) during synthesis under atmospheric conditions. The alkaline pH conditions during the actual synthesis/reaction (pH = 9.00) also explains the rhodochrosite precipitation. Furthermore, the XPS spectra of both AMO-biochar composites (**Fig. A.2**) show the presence of Mn2p in the amount of 6.60% (atomic). The deconvolution of Mn2p band of both modified biochars shows three bands of binding energies (between 641.47 and 646.30 eV). This corresponds to the presence of Mn binding to polynomic chain of organic carbon (Mn-C_{org}), Mn_xO_y/Mn-oxalate (Mn(III), Mn(IV)), $MnCO_3$ (Mn(II)) and residual $KMnO_4$ (Mn(VII)). Additionally, a detailed scan of C1s (**Fig. A.2b**) shows three peaks corresponding to: (i) π-bond on graphite C (284.55 ± 0.32 eV); (ii) C-O bond represented mainly by CO^{2-} (286.06 ± 0.05 eV); and (iii) O_C-O bond represents carboxylic group (288.60 ± 0.10 eV). This is in agreement with the study of H. Wang et al.(2015); S. Wang et al. (2015a); Shi et al.(2015). Each Mn-biochar composite has its individual proportion of the three peaks, where AMO + BC has the highest peak of graphite C whereas AMOchar showed the highest peak of C-O bond. This reflects different synthesis of both composites, where AMO + BC show a similar C1s band as the pristine biochar (Trakal et al., 2014b). Such differences between both AMO-biochar composites were more obvious from the deconvolution of O1s, where the peak (531.08/529.75 eV) represents O(II) in oxides (eventually in carbonates) for AMOchar and AMO + BC

composite, respectively. The peaks at (532.65 and 534.03 eV) represent oxygen bound in carboxylic group and the peaks at (533.99 and 534.03 eV) then reflect absorbed H_2O.

Concerning the structure and surface morphology of AMOchar, the SEM-EDS images (**Fig. 3.5**A; A.3) shows that the AMO with Mn-oxalates coated the surface of the pristine biochar during the actual synthesis. The process of the biochar coating was further confirmed by high resolution TEM (**Fig. 3.5**B, C). Specifically, biochar particles covered by a layer of AMO were identified (**Fig. 3.5**C), showing an efficient and well-proportioned surface coating as demonstrated by EDS spectra taken from several different spots (**Fig. 3.5**B). The attraction of the AMO on the surface of pristine biochar was confirmed by XPS deconvolution of Mn bond at binding energy 641.84 eV (responsible for Mn-C_{org} bond; **Fig. 3.5**D). However, porous biochar fragments associated with irregular AMO clusters were also observed by TEM (data not shown). Additionally, the amorphous nature of the studied material was confirmed by SAED (data not shown).

On the other hand, the AMO + BC composite shows individual particles of the AMO and biochar (**Fig. A.3c**), where the surface of biochar is partly occupied by clusters of the AMO with Mn-oxalates and/or secondary precipitated rhodochrosite (**Fig A.3c, d**). The presence of the rhodochrosite (confirmed by the XRD pattern) was detectable only by the high-resolution SEM, which could be due to its very small crystal size (~ 100 nm) caused by the short time of stirring during the preparation.

Additionally, considering the biochar-birnessite material (BCB), by way of comparison to the newly synthesised sorbents, the X-ray diffraction (XRD) patterns (**Fig. 3.5**) as well as the SEM-EDS (Fig. A.3e, f) of BCB confirmed similar composition as in the study of S. Wang et al. (2015a). Partly crystalline K-exchanged birnessite ($K_{0.5}Mn_2O_{4.3}(H_2O)_{0.5}$; PDF-2 card 01-087-1497) was detected in the BCB composite. Additionally, the XPS wide scan (Fig. A.2a) showed that the amount of Mn2p on the BCB surface was 14.0% (atomic), which was a higher quantity than in the study of S. Wang et al.(2015a). (9.40%). More specifically, deconvolution of Mn2p band of BCB showed three band binding energies (641.47, 643.03, and 645.11 eV), which corresponds to the presence of Mn_xO_y or birnessite (Mn(III), Mn(IV)), and residual $KMnO_4$ (Mn(VII)).

Table 3.8 shows initial characteristics (such as BET surface, pH, pH$_{zpc}$ and CEC) of all composites used. Specifically, the BET surface of the pristine biochar is rather low as discussed in paper of Trakal et al.(2014b) whereas the BET surface of pure AMO is almost double in comparison to the BC. Birnessite is represented by similar BET surface to that of the BCH Della Puppa et al.(2013). The BET surface of newly synthetized AMOchars is similar and/or lower in comparison to the pristine biochar. Such lower surface could be caused by 'filling of free space' on the biochar surface by precipitated Mn-oxides during common synthesis. Nevertheless, in case of the BCB composite and AMO + BC composites, respectively, the resulted surface increased 2-times compared to its origin/pristine materials. Such unexpected BET surface magnification could be here explained by heterogeneity of the pristine biochar (Trakal et al., 2014b).

The pH of all sorbents (except biochar-birnessite complex) was alkaline. When the biochar was modified directly by the AMO during its synthesis (AMOchar), the resulting pH of all three mixture ratios was significantly decreased to a similar pH value (approx. 8.4) in comparison to the pristine biochar (10.0). For the AMO + BC composite, the resulting pH values vary between 9.02 (for AMO + BC 2:1) and 9.52 (for AMO + BC 1:2). In contrast, the pH of the BCB composite was neutral (6.98), which reflects the acidic conditions during the actual synthesis as well as very low pH of birnessite.

As discussed in the paper of Della Puppa et al.(2013), the pure AMO has a positively charged surface, because the pH of aqueous solution was 5.00/7.00 and the pH of the point of zero charge (pH$_{ZPC}$) was 8.30. All prepared AMO-biochar composites also showed a theoretically positively charged surface, whereas the surface of BCB was theoretically negatively charged during As(V) sorption. The cation exchange capacity (CEC) of the pristine biochar (BC) was 40 cmol kg^{-1} (Trakal et al., 2014b), which was lower in comparison to pure AMO (61 cmol kg^{-1}). The CEC of pure birnessite was > 4-times higher compared to the AMO, whilst the CEC value of the biochar-birnessite composite was equal to that of the pristine biochar. All three ratios of AMO + BC showed values within the range of 28–31 cmol kg^{-1}, which is like that of pristine biochar. Finally, the CEC values of all AMOchars significantly increased compared to the BC. This could be caused by coating of the biochar surface by the AMO which is

represented by significantly higher CEC value compared to the pristine biochar. The resulted CEC value is, therefore, like that of the pure AMO.

Table 3.8 **shows initial characteristics (such as BET surface, pH, pHzpc and CEC) of all composites used.**

Sorbent	BET (mg^{2}g^{-1})	pH (-)	pH$_{ZPC}$ (-)	CEC (cmol kg^{-1})	Reference
AMO	134[a]	8.10±0.30	8.30±0.10	60.8±1.0[a]	(Della Puppa et al., 2013)
Birnessite	76.5	3.30±0.10	2.70±0.30	247±29	(Della Puppa et al., 2013)
BC	72.0	10.0±0.10	9.92±0.10	40.2±0.3	(Trakal et al., 2014b)
AMO+BC 1:2	141	9.52±0.02	8.89±0.10	28.1±0.6	This study
AMO+BC 1:1	171	9.36±0.04	8.49±0.10	24.5±0.1	This study
AMO+BC 2:1	72.0	9.02±0.06	8.09±0.10	31.2±0.3	This study
AMOchar 1:2	67.0	8.40±0.02	7.94±0.10	65.3±2.4	This study
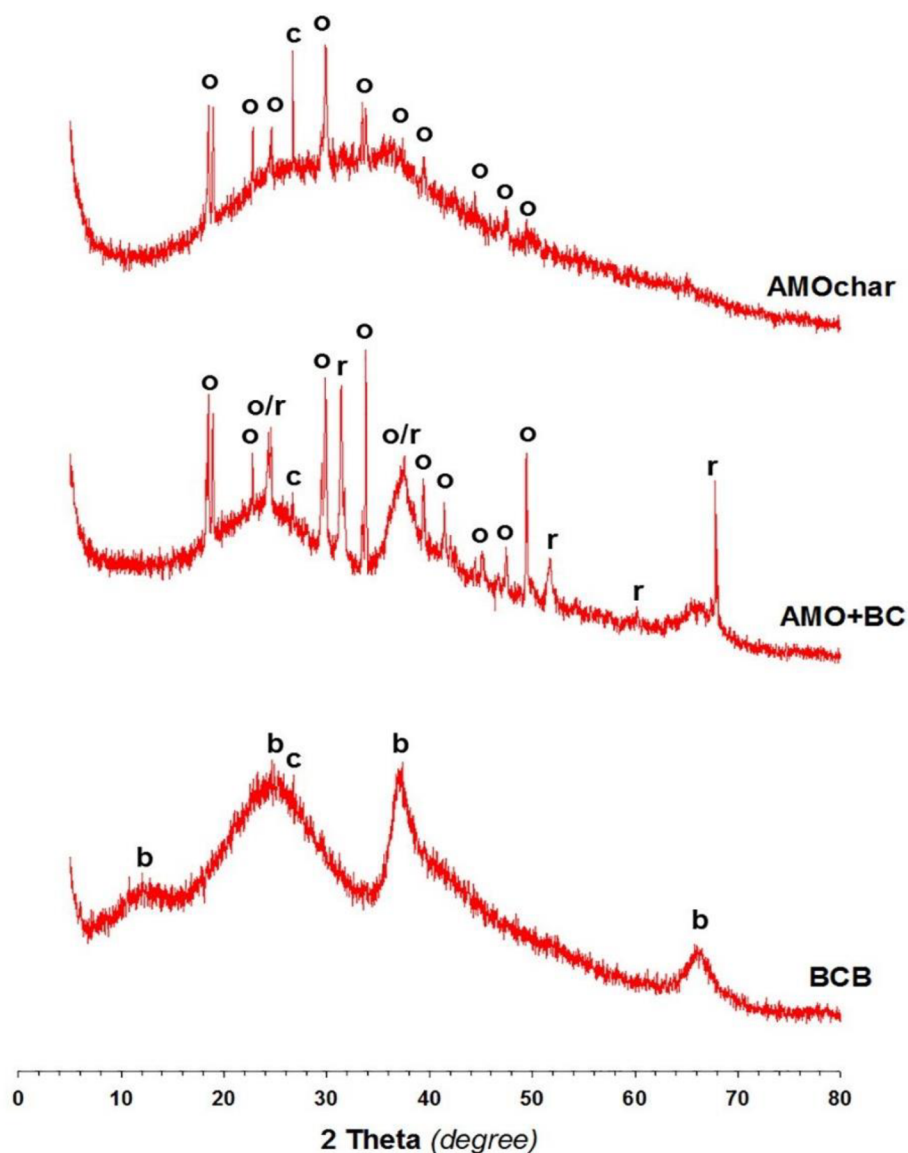
o – Mn-oxalate hydrate (C$_2$MnO$_4$•2H$_2$O); PDF-2 card: 00-025-0544
r – rhodochrosite (MnCO$_3$); PDF-2 card: 01-086-0172
b – birnessite K-exchanged (K$_{0.5}$Mn$_2$O$_{4.3}$(H$_2$O)$_{0.5}$); PDF-2 card: 01-087-1497
c – carbon; PDF-2 card: 00-026-1080

Fig. 3.4 The AMO + BC composite, AMOchar, and the biochar-birnessite material (BCB), by way of comparison to the newly synthesized sorbents, the X-ray diffraction (XRD) patterns.
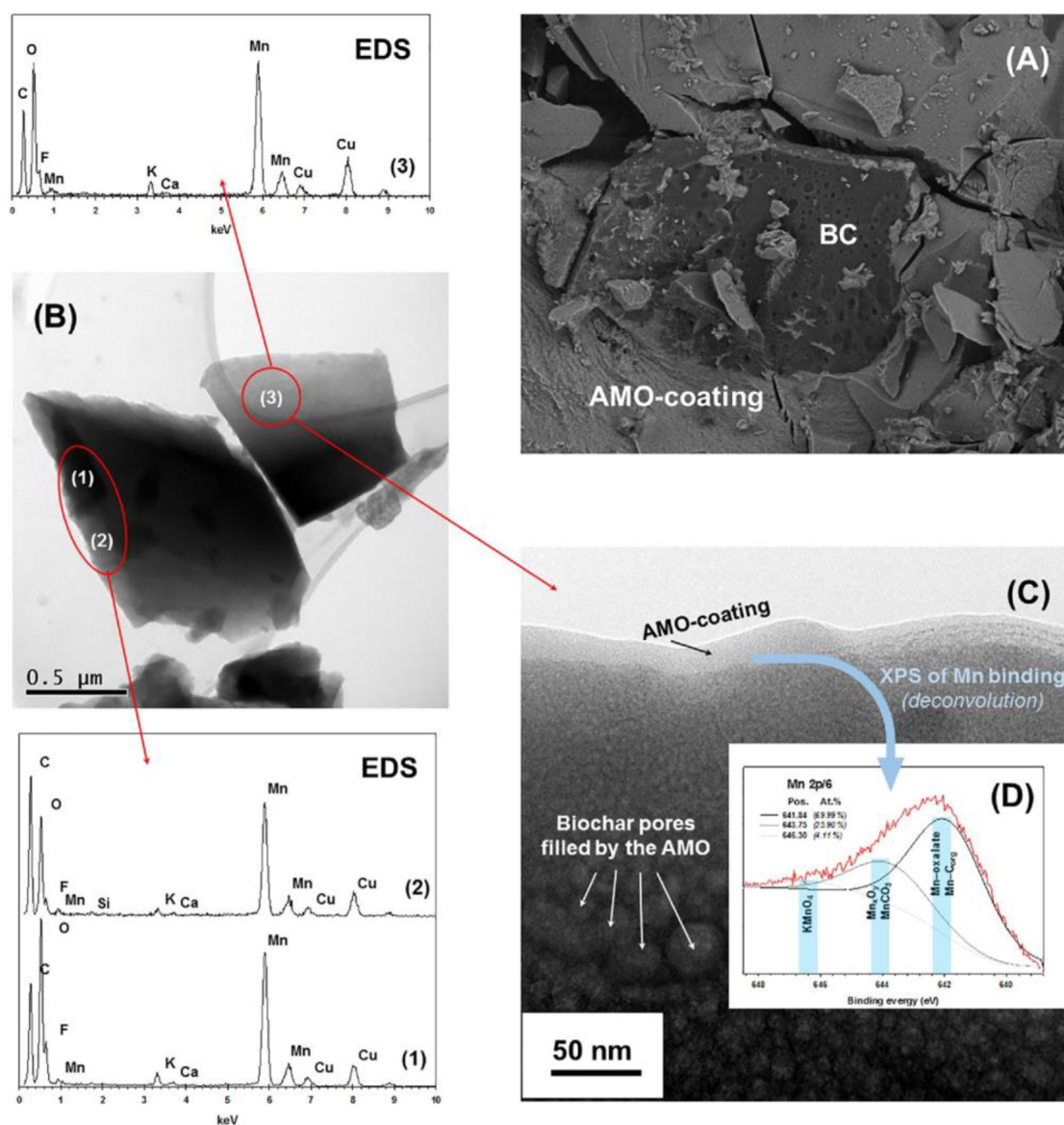
Fig. 3.5 (Fig. 3A) shows that the AMO with Mn-oxalates coated the surface (Fig. 3B, C) showing the process of the biochar coating (Fig. 3C), showing EDS spectra taken from several different spots (Fig. 3B). The attraction of the AMO on the surface of pristine biochar coating (Fig. 3C), showing EDS spectra taken from several different spots (Fig. 3B). The attraction of the AMO on the surface of pristine biochar was confirmed by XPS deconvolution of Mn bond Fig. 3D).

Removal of various metal(loid)s from aqueous solutions – batch experiments

In the static batch tests, pristine biochar (BC) showed the lowest sorption for As(V) and Cd(II) of all tested sorbents. In the case of As(V), this was due to rather low affinity of this metalloid to bond on the surface of organic matter (as against e.g. iron oxides).

The amount of sorbed Cd(II) and Pb(II) was approximately 15% and 60% from the total, respectively (**Fig. 3.6**) and the removal rate of both Cd(II) and Pb(II) continuously decreased with time (Fig. A.4). This was caused by the initial precipitation of both metals at the start of the experiment caused due to impossibility of maintaining pH-stat conditions (pH = 5.00) at the beginning of experiment when non-buffered pH conditions; therefore, prevailed as discussed in our previous study (Trakal et al., 2014b).

In contrast, pure AMO was very efficient in removing both metals and As (especially Pb; **Fig. 3.6**) as shown also previously by Della Puppa et al.(2013); Ettler et al. (2015); Michálková et al. (2016b). Equilibrium (under optimized conditions) was reached after several minutes for Pb(II), after 1 h for Cd(II), and after 7 h for As(V) (Della Puppa et al., 2013). The removal efficiency of the BCB has been previously described by S. Wang et al.(2015a) and the present study confirmed a similar trend, although maximum sorption of 3.42 g kg^{-1} for As(V) and 105 g kg^{-1} for Pb(II) was 3x and 2x times greater, respectively. Such differences could be explained by woody origin of the biochar (reflected by well-developed structure) used in the study of S. Wang et al.(2015a) against the biochar with poorly developed structure exploited for this case.

AMOchar was able to remove > 98.5% of dissolved Pb(II), 34–51% of dissolved Cd(II) and 64–91% of dissolved As(V) (**Fig. 3.6**). Generally with increased amounts of AMO in the AMOchar, greater amounts of metal(loid)s were removed, which reflects a high affinity of all tested metal(loid)s to sorb on the surface of Mn oxides (Komárek et al., 2013). Furthermore, the biochar stirred with AMO under given pH conditions (AMO + BC) also showed significant enhancement in metal(loid)s sorption compared to the BC alone (**Fig. 3.6**). The improvement was more obvious at the ratio 2:1 (AMO:BC), where the surface of the pristine biochar was intensively occupied by Mn oxides which formed oxalates as well as rhodochrosite (as discussed earlier). The Mn oxides

in the biochar composites provide sorption sites that appear to play more important roles than specific surface area (of the pristine biochar) during metal(loid)s sorption (Li et al., 2017). The presence of biochar in these composites, could therefore, indicate the adverse effect on resulted sorption efficiency. This could be caused by: (i) basic pH of the biochar (valid for As); (ii) mutual interaction of both sorbents during stirring under given pH conditions; and (iii) leachate/dissolution of crucial components such as Mn and DOC during common stirring. Generally, various Mn oxide-biochar composites provided materials which have been very suitable to sorb metal(loid)s from aqueous solution at very high quantities. The improvement of metal(loid) sorption efficiency (compared to its pristine biochar) has been usually several times higher as presented in the studies of Song et al.(2014); H. Wang et al.(2015); M. C. Wang et al.(2015); S. Wang et al.(2015a); Li et al.(2017).

The reaction speed of metal(loid)s sorption on selected biochars is presented in **Fig. A.4.** In general, the equilibrium state was reached within 1 h or less for Pb(II) and Cd(II), respectively, but within 8 h for As(V). This is in agreement with other studies (e.g. Trakal et al., 2014; S. Wang et al., 2015a, 2015b) mainly due to similarity of metal(loid)s sorption mechanisms where chemisorption (reflected mainly by high CEC value responsible for ion exchange related to the biochar and/or Mn oxides) together with precipitation (at the beginning of the experiment) were here a predominant sorption mechanisms. Additionally, the sorption mechanism of identical pristine biochar has been previously described in the study of Trakal et al.(2014b) and the improvement of this metal mechanism using biochar modification by secondary metal-oxides (Fe and Mn) has then been previously discussed (H. Wang et al., 2015; S. Wang et al., 2015a; Trakal et al., 2016)

The fastest metal(loid)s sorption (except the pure AMO) was detected on the AMOchar, especially where a higher amount of AMO was present (data not shown), followed by the biochar-birnessite composite (with the greatest contrast observed for Pb; **Fig. A.4**). The kinetics of the AMO + BC composite shows similar behavior as the BC, where the removal rate continuously decreased for both Cd(II) and Pb(II). As already explained above, the initial precipitation of both metals was caused by the highly alkaline pH of the sorbent.

Finally, **Table 3.9** shows the leaching of selected elements during metal(loid)s sorption with all the chosen sorbents that were tested. The standard deviation

reflects the concentration changes in K, Mn and DOC that had occurred during the experiment which tested sorption of individual metal(loid)s. Potassium leaching did not change significantly in time and the leaching proceeded in the following order (BC

≈ AMOchar > AMO > BCB > AMO + BC). The high content of K in the BC was described previously by Trakal et al.(2014b) and is caused by composition of the source material, i.e., grape stalks (fertilization of vineyards). Manganese leaching was negligible from the pristine biochar, but a very high quantity of Mn was leached from the pure AMO (60–351 mg L^{-1}). Additionally, Mn leaching continuously increased in time during metal(loid)s sorption, which could be caused by the gradual dissolution of the Mn-oxalates (Ettler et al., 2014b) also reflected here by increased DOC leaching compared to pristine biochar; **Table 3.9**). Nevertheless, both AMO-biochar composites show the reduction in Mn leaching, compared to the AMO (more intensive for AMO + BC). This demonstrates that (i) total Mn content in all AMOchar composites was lower compared to the AMO (see Table A.1) when such lower Mn content has no effect to resulted metal(loid) sorption for all AMOchars; and (ii) some Mn was leached during the stirring of all AMO + BC composites. Additionally, the BCB composite reduced Mn leaching, probably caused by the higher stability of birnessite compared with readily soluble Mn-oxalates. DOC leaching was also measured during metal(loid)s sorption. The pristine biochar showed very similar DOC concentrations over the period of the experiment (**Table 3.9**). On the other hand, more variable and significantly higher DOC concentrations were observed in the pure AMO (described also by Michálková et al. (2014). The DOC leaching was significantly decreased in the AMO + BC and the BCB composites, compared to the other materials, possibly due to: (i) pre-leaching during the preparation of AMO + BC and (ii) higher stability resulting from acidic conditions during the BCB synthesis.
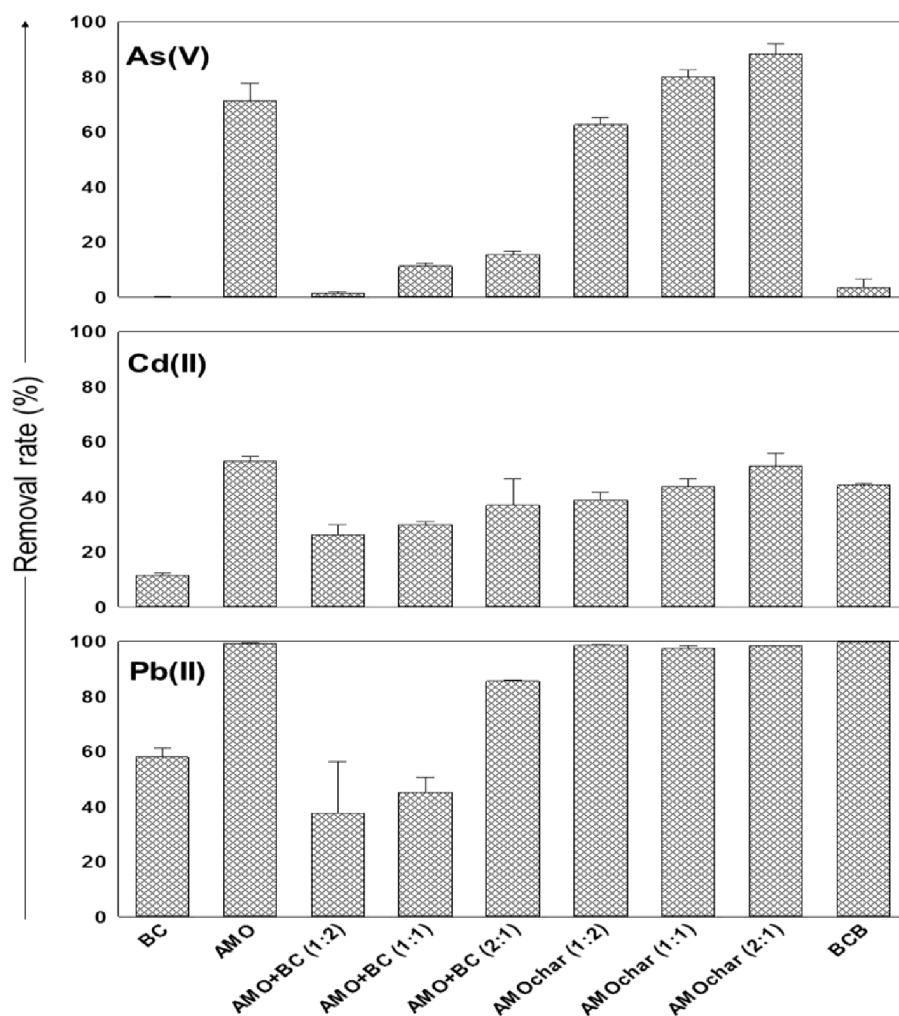
Fig. 3.6 **Removal of various metal(loid)s from aqueous solutions using batch experiments**

Table 3.9 **Leaching of selected elements during metal(loid)s sorption with all the chosen sorbents**

	Mn (mgL^{-1})	K (mgL^{-1})	DOC (mgL^{-1})
BC	0.13 ± 0.39 e	116 ± 7 a	127 ± 7 b
AMO	186 ± 88 a	30.9 ± 2.7 b	181 ± 41 a
AMO + BC^a	56.2 ± 43.6 c	15.5 ± 2.8 d	97.4 ± 16.0 c
AMOchar^a	109 ± 49 b	63.1 ± 6.1 a	242 ± 51 ab
BCB	14.0 ± 11.2 d	25.0 ± 4.9 c	78.7 ± 34.6 c

Removal of As from solutions contaminated by waste wood ash – column experiments

In order to validate the efficiency of the tested AMO-biochar composites, the most efficient composite from previous batch experiments (AMOchar at ratio 2:1) was tested in a continuous flow column system simulating the treatment of solutions contaminated by waste wood ash (for detailed characteristics see the study of Mollon et al. (2016)). Unlike soils, or other materials with a more complex organo-mineral matrix, wood ash consists primarily of carbonates, Ca, Mg, K and some metal-oxides, thence its high pH (pH = 11.7). The waste wood derived ash used in the current experiment additionally contains high concentrations of As, which is highly mobile under such basic condition.

The results of the leaching test confirmed that the presence of AMOchar was able to reduce the concentration of As compared to the control throughout the course of the leaching test (**Fig. 3.7**). This was due to the occurrence, in the first case, of mainly $HAsO^{-2}$ species induced by the lower pH in the AMOchar column. This is in contrast to the column without AMOchar where ~ 60% of As species were present in the form of AsO^{-3} due to very high initial pH (**Fig. 3.7**). Leachate pH changed after ~ 70 min and the pH value from each column was ~ 10 and dropped further by 0.5 units by the end of the experiment (100 min; **Fig. 3.7**). At this stage, the abundance of AsO^{-3} decreased. In the case of the column containing AMOchar, a small amount of H_2AsO^- occurred at the end of the test (**Fig. 3.7**). Therefore, by the end of the leaching test, the cumulative amount of removed As was approx. 6-fold lower as a result of the addition of AMOchar to the column (**Fig. 3.7**) with limited amount of released Mn from the AMOchar (~3 mg kg^{-1}; data not shown).

The saturation indices of different minerals in the initial and final column leachates were also calculated using Visual MINTEQ 3.1 (Table A.2). The saturation indices for initial ash leachate (Ash_{10}) show oversaturation (> 2 values) of Cr-precipitates (e.g. $Cr(OH)_3$; Cr_2O_3; or $MgCr_2O_4$) and (hydroxyl)apatite and values close to saturation for calcite and dolomite, respectively (see Table A.2). Various combinations of $Ca(Mg)^{2+}$, Al^{3+}, $Cr^{3(6)+}$ and Mn^{2+} together with OH^-, CO^{2-} and PO^{3-} can precipitate minerals as (hydroxy)apatite, rhodochrosite, various Cr-precipitates, calcite/dolomite, gibbsite or pyrochroite. Furthermore, the presence of Mn in the AMOchar leachate caused a

precipitation of As in a form of As-Mn-precipitates. The final ash leachate (Ash$_{100}$) then show only limited amount of minerals close to saturation (Cr-precipitates and calcite and Ca(Mg)-CO$_3$), probably due to the release of the metals and As and pH decreases during the dynamic column test (**Fig. 3.7**). On the other hand, the final AMOchar leachate (AMOchar$_{100}$) was more or less oversaturated by several mineral phases as a result of lower metal(loid)s release in combination with Mn presence, which results into the precipitation of various Mn-minerals and other various amorphous phases (Sparks, 2003). In summary, this dynamic leaching test shows practical utilization of the AMOchar to stabilize not only bivalent metals but also metal oxyanions in various contaminated materials such as Copper Chromated Arsenate (CCA)- contaminated ash (Mollon et al., 2016).

Engineering implications

The use of biochar for metal(loid)s removal has been shown to be an effective technology for the remediation of various mining wastewaters which are often highly acidic. As many bivalent metals have a solubility that is strongly pH dependent, then acidic mine waters represent a situation where the efficiency of sorbents can be tested with multiple metals at once, at their most mobile within the environment. Such biochars are usually very suitable for selective sorption of particular bivalent metal as well as for multi-metal loading mainly due to their overall basic pH and negatively charged active surface (Mohan et al., 2014c). Nevertheless, when various bivalent metals are sorbed to the same biochar the sorption efficiency of some metals (e.g. Cd or Zn) is usually diminished by the sorption of metals with higher affinity to organic matter such as Pb or Cu (Trakal et al., 2012, 2014b).

Furthermore, their effectiveness to sorb oxyanions is usually limited, especially under alkaline conditions when such oxyanions are very mobile. In order to ensure complexity of this material to sorb various metal(loid)s as well as to ensure its universality (when the sorbent will be suitable under various pH or Eh conditions), the biochar has been previously amended using numerous modifications, e.g., mineral impregnations (Rajapaksha et al., 2016). In our study, we propose a biochar coated with the amorphous Mn-oxide, which can provide very complex and efficient universal sorbent for not only bivalent metals (Cd(II) and Pb (II)), but also for oxyanions (e.g. As(V)). Such composite appears to be a very suitable candidate for

treating multi-metal(loid) contaminated wastewaters, e.g., acid mine drainage. Another practical advantage of this material lies in the use of solely waste material. Specifically, biochar is synthesised from waste biomass and the AMO could also be prepared from organic waste materials reacting with potassium permanganate. Therefore, the synthesis of AMOchar should be very reliable in practice, and still can provide excellent performance under the severe operating conditions of complex metal(loid)s loading. Additionally, (i) the concurrence during multi-bivalent-metal sorption; and/or (ii) the necessity of various conditions during common sorption of bivalent metal(s) together with metalloid(s) (in form of oxyanions) could be suppressed when such material will be used due to its complexity. On the other hand, the composite has to be further tested for its long-term stability in order to preclude Mn leaching (especially dissolution of Mn oxalates coming for the AMOchar mainly under acidic conditions and/or its unknown stability under reduction conditions) which may then pose a risk of secondary contamination. Therefore, more extensive studies testing the AMOchar long-term effect using some field experiment (under changing redox conditions) as well as the response to biota are also needed.
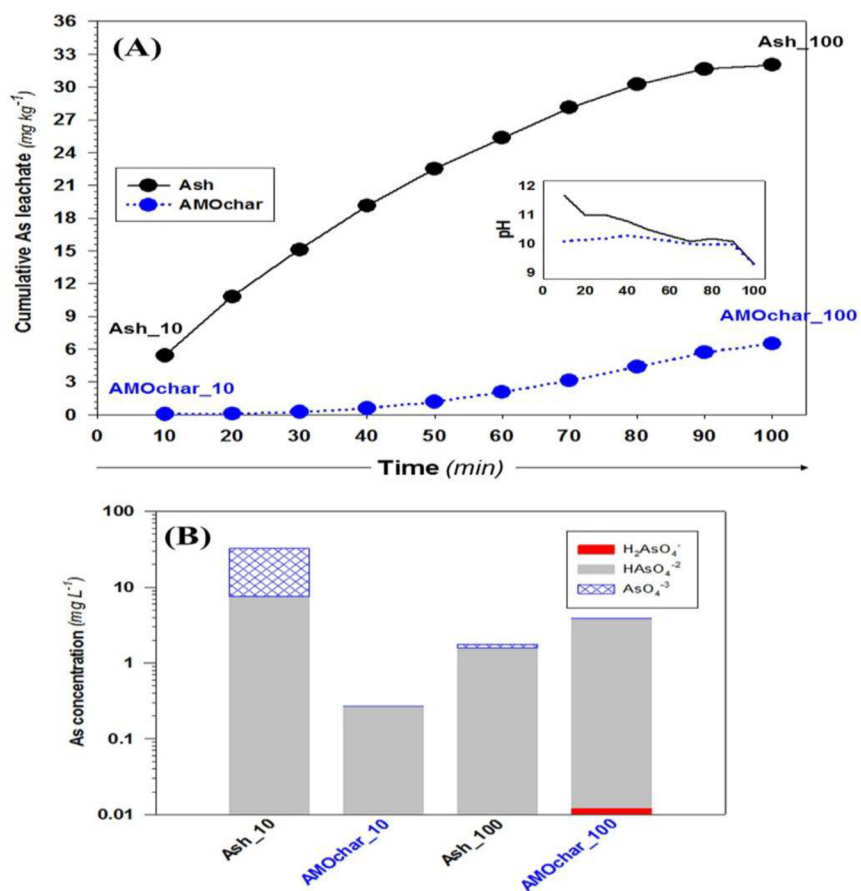
Fig. 3.7 **Removal of As from solutions contaminated by waste wood ash by using column experiments and the results of the leaching test confirmed that the presence of AMOchar**

Conclusions

This study shows that AMOchar - a composite sorbent produced from biochar (char) and amorphous Mn-oxide (AMO) was a highly efficient sorbent for selected metal(loid)s in waste waters with removal rates of 99% (Pb), 91% (As) and 51% (Cd). In column leaching tests, using an As-contaminated ash, the predominance of $HAsO^{-2}$ species was confirmed, resulting from the lower pH induced by the AMOchar addition compared to AsO^{-3} predominantly leached from the ash alone. Thus, in comparison with individual sorbent materials tested, and other composites, such as pristine biochar and a biochar-birnessite comparison material, the AMOchar was the most suitable sorbent for removing various metal(loid)s from aqueous solution whilst avoiding excessive Mn leaching associated with the use of AMO.

Supplementary material

Table A.1. Overview of used sorbents

Symbol	Mn content *(%)*	Component *(%)*		Comment/Reference
		Mn-oxide	*Biochar*	
AMO	50.6 ± 0.78	100	0	Synthesis according to Della Puppa et al. (2013)
BC	1.16 ± 0.10	0	100	Pyrolysis of grape stalks Trakal et al. (2014)
AMO+BC 1:2	14.9 ± 0.36	33	66	Agitation under pH = 9.00 (mean pH value between pH_{zpc} of the BC and AMO, respectively)
AMO+BC 1:1	20.4 ± 0.29	50	50	
AMO+BC 2:1	26.1 ± 0.42	66	33	
AMOchar 1:2	14.1 ± 0.23	33	66	Application of the BC during the actual syntheses of the AMO
AMOchar 1:1	16.8 ± 0.48	50	50	
AMOchar 2:1	19.5 ± 0.57	66	33	
BCB	14.4 ± 0.40			Biochar modification by birnessite according to Wang et al. (2015a)

Table A.2. Saturation indices of selected minerals in the leachate obtained from the ash and ash treated by the AMOchar after 10 and 100 minutes of the column leaching test.

Mineral	Ash$_{10}$	Ash$_{100}$	AMOchar$_{10}$	AMOchar$_{100}$
Al(OH)$_3$ (Soil)	/	/	1.407	2.226
Al$_2$O$_3$(s)	/	/	-0.259	1.380
Aragonite	-0.518	0.672	0.646	1.150
Boehmite	/	/	1.119	1.938
Brucite	-0.340	-3.874	-1.457	-2.848
Ca$_3$(PO$_4$)$_2$ (am)	-1.684	/	-1.270	1.642
Ca$_3$(PO$_4$)$_2$ (beta)	-1.014	/	-0.600	2.312
Ca$_4$H(PO$_4$)$_3$·3H$_2$O (s)	/	/	-3.843	0.715
CaCO$_3$·H$_2$O (s)	-1.710	-0.519	-0.546	-0.042
Calcite	-0.374	0.816	0.789	1.294
Cr(OH)$_3$ (am)	2.48	1.121	3.935	1.724
Cr$_2$O$_3$ (c)	5.301	2.582	8.209	3.788
Diaspore	/	/	2.824	3.643
Dolomite (disordered)	-1.327	0.297	1.774	1.774
Dolomite (ordered)	-0.777	0.847	2.324	2.324
FCO$_3$-Apatite	13.17	/	22.94	28.48
Fluorite	/	/	0.834	-0.235
Gibbsite (C)	/	/	1.957	2.776
Huntite	/	/	1.051	0.042
Hydroxyapatite	7.892	/	7.567	11.74
Magnesite	-1.553	-1.120	0.384	-0.120
MgCr$_2$O$_4$(s)	4.54	-1.712	6.331	0.520
Mn$_3$(AsO$_4$)$_2$·8H$_2$O (s)[§]	/	/	0.259	0.140
MnCO$_3$ (am)	/	/	3.105	2.439
MnHPO$_4$ (s)	/	/	3.422	3.898
Pyrochroite	/	/	0.129	-1.423
Rhodochrosite	/	/	3.605	2.939
Vaterite	-0.941	0.250	0.223	0.727
pH	*11.70*	*9.30*	*10.10*	*9.30*

[§]As-Mn-precipitate

Fig. A.1. Leaching columns showing the location of (a) As contaminated ash and (b) AMOchar. Note that the direction of leaching is from the base to the top of the column.

Fig. A.2. XPS analyses of newly synthetized Mn oxide-biochar composites, (a) wide scan of the AMOchar, AMO+BC, and BCB; (b) deconvolution of C1s, O1s and Mn2p.
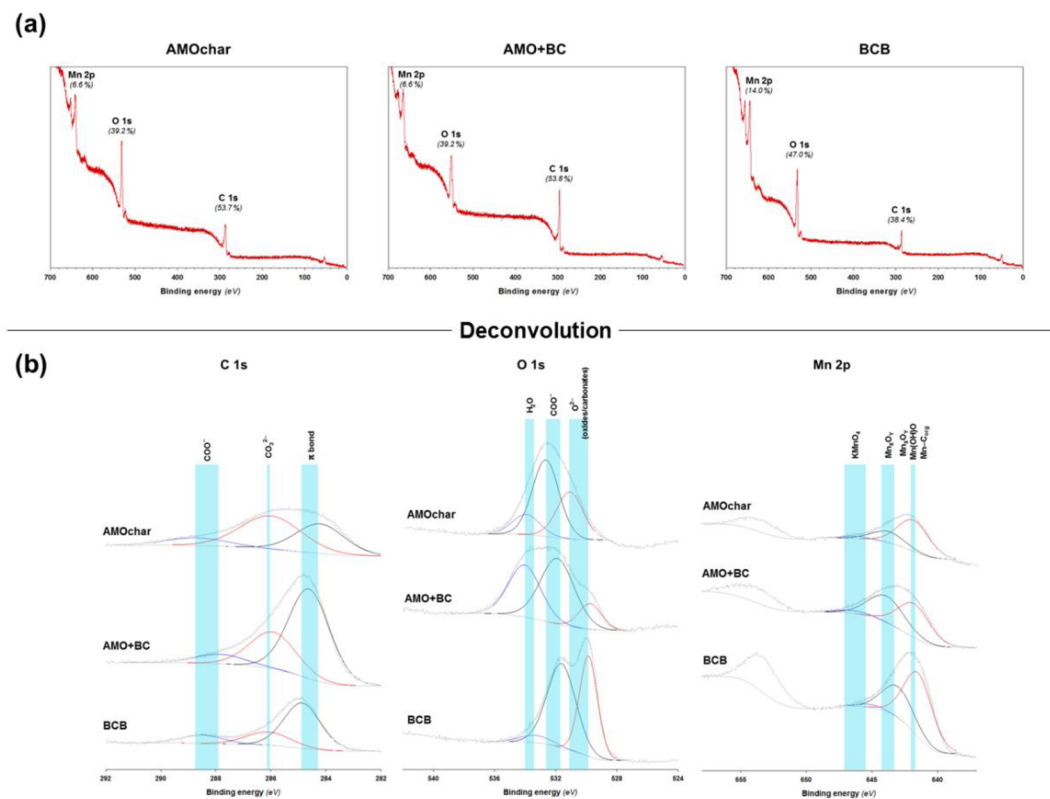
Fig. A.3. The SEM-EDS images in back-scattered electrons (BSE) with corresponding EDS spectra and the high-resolution SEM, respectively, of the AMOchar (a, b), AMO+BC composite (c, d) and biochar-birnessite (BCB) complex (e, f).
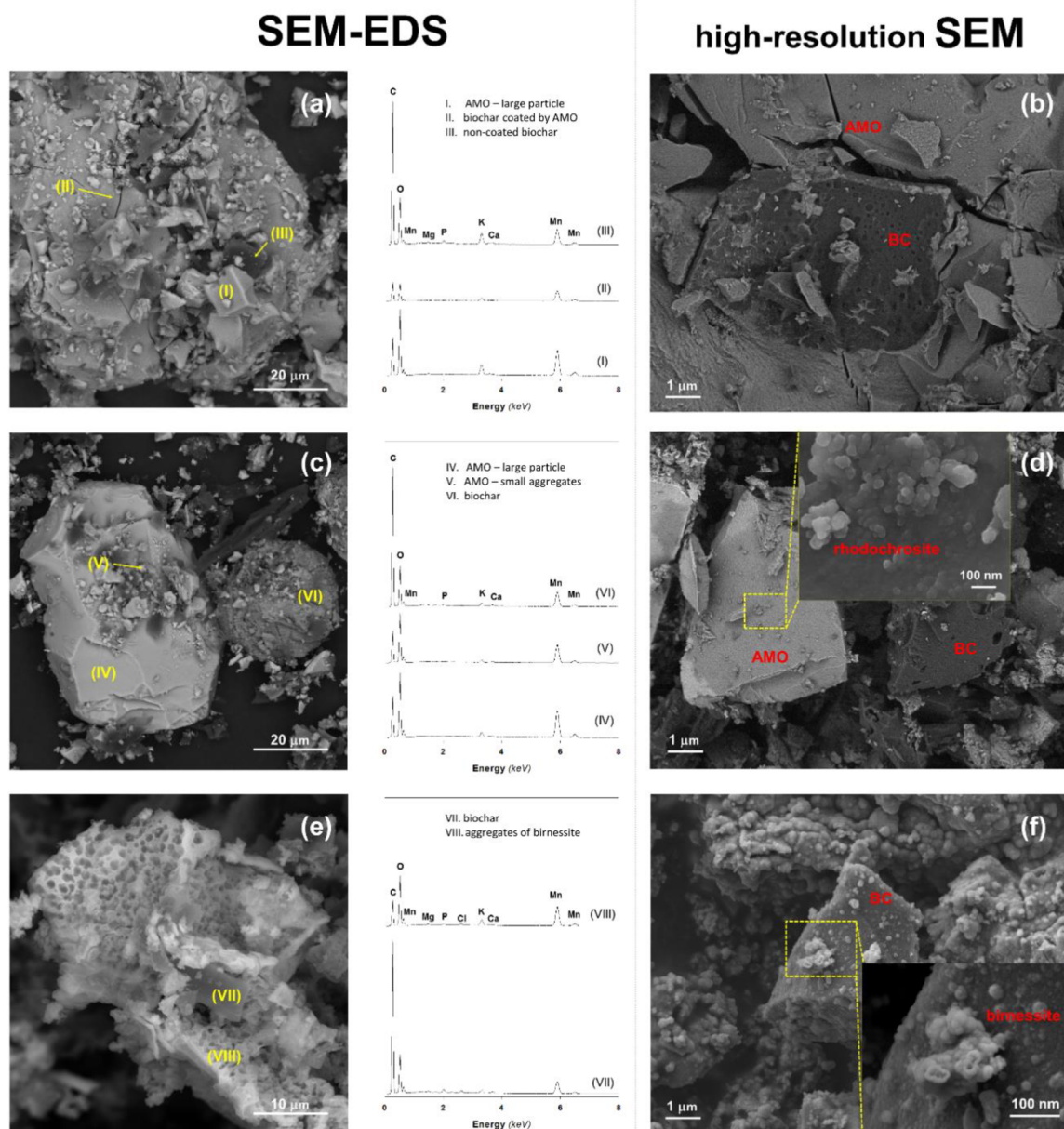
Fig. A.4. Metal(loid)s sorption onto selected sorbents under constant pH value.
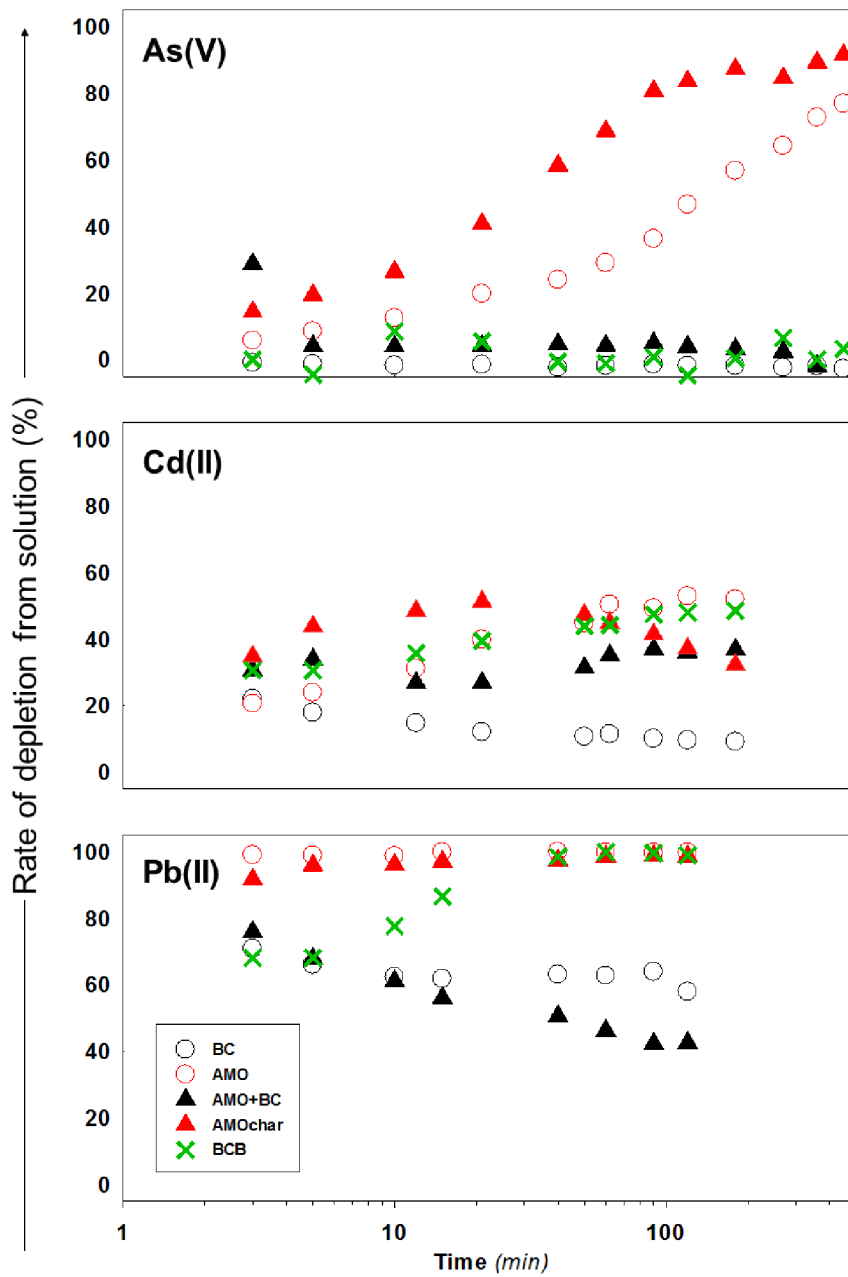
Chapter IV

Synthesis of modified amorphous manganese oxide using low-cost sugars and biochars: Material characterization and metal(loid) sorption properties

Petr Ouředníček, Barbora Hudcová, Lukáš Trakal, Micheal Pohořelý, Michael Komárek

Content

Abstract

In this study, amorphous Mn oxides (AMOs) and their composites with biochar (BC) were synthesized using different sugars (glucose, sucrose, and molasses), and their sorption efficiency toward Zn(II), Cd(II), and As(V) was tested. Additionally, detailed characterization of synthesized materials using various solid-state analysis methods (e.g. XRD, FTIR-ATR, and/or SEM-EDX) was also performed. Despite glucose-based AMOs presented higher sorption efficiency for As(V), i.e., 0.73 mmol g^{-1} (glucose) > 0.27 mmol g^{-1} (sucrose and molasses), similar sorption efficiency toward Zn(II), i.e., 0.80 mmol g^{-1} (glucose and molasses) > 0.66 (sucrose) and Cd(II) (0.71–0.74 mmol g^{-1} (sucrose and molasses) > 0.36 mmol g^{-1} (glucose), was observed for sucrose and molasses-based AMOs under the given conditions. Next, the sorption efficiency of all AMO/BC composites was proportional to their AMO content. Finally, Mn(II) leaching from the structure of the new AMOs was negligible compared to that observed for the glucose-based AMOs, in this study as well as in other similar studies. Moreover, using molasses as reducing agent during AMO synthesis dramatically decreased the total cost of the final materials, which suggested that these new AMOs could represent interesting alternatives for standard remediation technologies. The AMOs synthesized using low-cost sugars could, therefore, be promising materials for real field applications, since the main disadvantages of using standard AMOs are mitigated. Nevertheless, the efficiency and stability of these composites under real-life conditions must be tested prior to their direct application for remediation technologies.

Introduction

During the last decades, Mn oxides have been used for water and/ or soil treatments (Ociński et al., 2016; Xie and Zhao, 2016; Jian et al., 2019). Mn oxides are present in nature as coatings and/or fine-grained aggregates in soils, and influence the speciation and mobility of metal (loid)s even at low concentrations (Su et al., 2010). Moreover, Mn oxides are often more effective than Fe oxides for the stabilization of some metal(loid)s, since the formation of inner-sphere complexes, which results in strong bonds between the metal(loid)s and Mn oxide surface (Hettiarachchi et al., 2000; Michálková et al., 2014, 2016b, 2016d), is the prevailing stabilization mechanism. Poorly crystalline Mn oxides or amorphous Mn oxides (AMOs) have been previously considered to be highly effective stabilizing amendments of metal(loid)s in water and soil (Kanungo et al., 2004; Della Puppa et al., 2013; K. Xu et al., 2013; Ettler et al., 2014b; Michálková et al., 2014; Ettler et al., 2015; Michálková et al., 2016b, 2016d; Huang et al., 2017). In general, AMOs can be relatively easily prepared using the modified birnessite synthesis method described by Ching et al. (1995, 1997)which uses potassium permanganate ($KMnO_4$) and simple sugars as reducing agents. Such synthesis methods (using glucose) have been previously described by Della Puppa et al.(2013), Ettler et al. (2014b, 2015) and Michálková et al.(2014, 2016b, 2016d).

The previously synthesized AMOs have presented high sorption efficiencies for various metal(loid)s, such as Cu, Cd, Zn, Pb, and As from water and soil over a wide range of pH values, and a particularly high sorption efficiency toward As(V) has been observed at higher pH values (Michálková et al., 2016b). However, the use of the standardized AMOs could have potential drawbacks: (1) Mn leaching (especially at lower pH values and/or under reducing conditions); (2) the reactions could generate considerable amounts of secondary products (e.g., Mn oxalates) or unreacted compounds (e.g., glucose) due to the inappropriate $KMnO_4$ to sugar molar ratio; and (3) resulted the high costs of the final AMO product. The mentioned aspects could complicate the large-scale preparation of AMOs. Moreover, low yields of the final product (approx. only 12%) using the standard would result in a significant increase of the final material costs.

Moreover, the leached Mn could cause secondary contamination of water and soil when using these materials for remediation technologies (Pinsino et al., 2012). Two

different approaches on increasing the stability of AMOs (i.e., decrease Mn leaching) have been presented so far: (1) surface modification of AMOs using $MnCO_3$ (Michálková et al., 2016d)and (2) synthesis of AMO/BC composites (Trakal et al., 2018b). According to the surface modification approach, the differences between the synthesized and surface modified standardized AMOs were not significant, i.e., similar stabilities were observed (Michálková et al., 2016d). By contrast, the synthesized AMO/BC composites generated significantly lower amounts of leached Mn compared to the pristine AMOs (Trakal et al., 2018b). In general, BC (a pyrolyzed biomass), is a low-cost material that can be used In agriculture to improve soil properties (Liu et al., 2013; Jeffery et al., 2015) and/or as a sorbent for various metals. The sorption efficiency of pristine BCs strongly depends on the biomass source (Trakal et al., 2014b) and on its physical (Trakal et al., 2016, 2017b) or chemical activation (Cha et al., 2016). To further improve the sorption properties of BCs, which are attributed to the large specific surface area and porous structure of pristine BCs (Mohan et al., 2014a) modification using secondary oxides can be performed (Li et al., 2018b). Previously, modification of BCs using nano particles (by zerovalent Fe impregnation (Dong et al., 2017), by nano MgO decoration (Li et al., 2018a) or by nano CeO_2 hybridization (Li et al., 2019) has been studied and tested for metal(loid) sorption. Another type of BCs modification using $KMnO_4$ impregnation (Li et al., 2017), poorly crystalline/amorphous Mn oxides impregnation (H. Wang et al., 2015; M. C. Wang et al., 2015; Trakal et al., 2018b) or crystalline Mn oxides decoration (S. Wang et al., 2015a; Huang et al., 2018) has been used and tested as well.

The main aim of this study was to synthesize AMOs and AMO/BC composites using different sugars, while emphasizing the use of molasses as low-cost, waste sugar source. The individual steps of the study were as follows: (1) finding an appropriate Mn/sugar molar ratio for the AMO synthesis; (2) detailed characterization of synthesized materials using various solid-state analysis methods and (3) testing the sorption efficiencies of all materials for Zn(II), Cd(II), and As(V). In summary, we hypothesize that the AMO (originated from glucose) will be fully substituted by that one originated from low-cost sugars (i.e. molasses or sucrose). Additionally, the AMO/biochar composites (mainly that originated from molasses or sucrose) will be more stable in regard to Mn-leaching.

Materials and methods

All chemicals used in this study were of analytical grade (Lach-Ner, Ltd.; Czech Republic) and were used without any modifications. All solutions were prepared using deionized water (0.01 µS/cm). The pH values of the solutions during the sorption experiments were adjusted using HNO_3 and NaOH (0.001, 0.01, and 0.1 M).

Preparation and synthesis of studied materials

Synthesis of AMOs

The synthesis of AMOs was preformed according to the methods described by Ching et al.(1995) and Della Puppa et al. (2013) (i.e. a simple reaction between $KMnO_4$ and the reducing agent (glucose). The individual steps of this study were modified to: (1) maximize the yield of the final product (maximum soluble concentration of chemical reagents); (2) minimize the amount of residual secondary products (appropriate molar ratio of chemical reagents); and (3) render the synthesis more economical (utilization of low-cost sugars as reducing agents). Nine different samples of AMOs were prepared (see **Table 4.10**). More detailed description of AMOs' synthesis is presented in the supplement.

The yield of the AMO synthesis used in this study (54%) increased compared to the yield of the final product (approx. 10%) mentioned in Della Puppa et al.(2013) and, moreover, the residual water content during the synthesis decreased by approx. 86% compared to above mentioned study. In general, the use of cheaper sugars (sucrose and molasses) decreased the price of the final products compared to glucose-based AMOs used in this study by 40% and more than by 80% compared to Della Puppa et al.(2013).

Agro-waste biochar preparation

The source materials (mixture of rape, wheat, and barley straw/grass hay in the form of commercially available pellets) for the pyrolysis of BC were obtained from Bropel Biopaliva Ltd. (Czech Republic). The pyrolysis process was carried out in a fixed-bed reactor under nitrogen flow of 1 m^3 h^{-1}, at atmospheric pressure, and for the exposure time of 120 min at the final designed temperature of 550 °C. The initial

moisture content was 5%. The pyrolyzed product was then cooled overnight (under the same nitrogen flow), milled, homogenized, and sieved (<250 μm).

Synthesis of AMO/BC composites

The AMO/BC composites were prepared using the AMO/biochar ratio of 2:1, according to the method described by Trakal et al. (2018b).

Table 4.10 **Nine different samples of AMOs were prepared.**

Ratio	Glucose	Sucrose	Molasses
1:1	AMO-G1	AMO-S1	AMO-M1
1:1.5	AMO-G2	AMO-S2	AMO-M2
1.5:1	AMO-G3	AMO-S3	AMO-M3

In brief, BC was added to $KMnO_4$ before the AMO synthesis. The appropriate of Mn/sugar molar ratio for the AMO/ BC composite synthesis was chosen according to the obtained results, i.e., characterization of synthesized AMOs and their sorption efficiencies (see **Fig. S2**). Based on these results, the molar ratio of 1:1 was used, therefore the AMO-G1, AMO-S1, and AMO-M1 (where G, S, and M are glucose, sucrose, and molasses, respectively), and mixtures were prepared. The mixtures were further used to synthesize the composite materials. The resulting AMO/BC composite gels (AMO-G1-BC, AMO- S1-BC, and AMO-M1-BC) were filtered using a vacuum pump and dried at room temperature (25 ± 2 °C) to constant weight. Afterwards the newly synthetized materials were milled to fine particles and homogenized by sieving (b250 μm).

Characterization of studied materials

The pH values of all newly synthetized materials were determined according to ISO 10390:2005 using an inoLab® 7310 pH meter (WTW, Germany). The CEC values of the materials were measured in suspension according to ISO 11260:2018. The specific surface areas were measured using the Brunauer–Emmett–Teller (BET) method (N_2 adsorption at −196 °C) using an ASAP 2050 (Micrometrics Instrument Corporation, USA) instrument. The structure of all materials was characterized using XRD analysis using a PANalytical X'Pert Pro diffractometer equipped with an X'Celerator detector

(Cu K$_\alpha$ radiation, 40 kV, 30 mA, and measuring step of 0.02° s^{-1} in the 2θ range of 10–80°). The individual phases of the materials were identified using the PANalytical X'Pert HighScore Plus software (version 3) and ICDD PDF-2 database (2003). To describe the morphologies and chemical compositions of the individual materials a *TESCAN VEGA 3 XMU* microscope was used for the SEM measurements, and EDX analysis was performed using a QUANTAX 200 spectrometer, respectively. The functional groups were characterized using FTIR-ATR using a diamond crystal and Nicolet 6700 spectrometer.

Sorption experiments

Sorption efficiencies of studied materials

Initial sorption experiments that did not involve controlling the pH were performed to evaluate the sorption efficiencies of all studied materials toward the selected metal(loid)s. Based on these results, appropriate materials were selected for further experiments. In general, zinc (Zn(NO3)$_2$·6H$_2$O), cadmium (Cd(NO$_3$)$_2$·4H$_2$O) and arsenate (HAsNa$_2$O$_4$·7H$_2$O) solutions at concentrations of 1 mM in the background electrolyte (0.01 M NaNO$_3$) were prepared, and the appropriate amounts of individual materials (solid/liquid ratio of 1 g L^{-1}) were added to the individual solutions and stirred at room temperature for 24 h using an end-to-end shaker at 200 rpm. Afterward, the samples were filtered (0.45 μm pore sizes membrane) and the resulted supernatant was analyzed using inductively coupled plasma-optical emission spectrometry (ICP-OES) (Agilent Technologies 700 Series).

*Sorption kinetics and equilibrium exp*eriments

Sorption kinetics and equilibrium experiments were performed to evaluate the removal rates and maximum sorption capacities, respectively, of the selected AMOs (AMO-G1, AMO-S1, and AMO-M1) and AMO/BC composites (AMO-G1-BC, AMO-S1-BC, and AMO-M1-BC) according to the methods described by Hudcová et al. (2017, 2018). In brief, individual batches containing Zn(II), Cd(II), and As(V) solutions with concentrations of 0.1 mM (kinetic experiments) and 0.05–7.00 mM (equilibrium experiments) in the background electrolyte (0.01 M NaNO$_3$) were mixed with the appropriate amounts of individual materials (solid/liquid ratios of 1 g L^{-1}) for 180 min at pH = 5 in the case of Zn and Cd (to avoid metal precipitation in the solution) and pH

= 7 in the case of As (to achieve a higher mobility of studied metalloid). Subsequently, the samples were filtered and analyzed using ICP-OES. The non-linear forms of the Langmuir and Freundlich isotherms were used to model the obtained equilibrium sorption data. Moreover, the samples obtained after the sorption of Zn(II), Cd(II), and As(V) at two different concentrations were filtered using a vacuum pump, dried at room temperature, and consequently analyzed using XRD and SEM/EDX to characterize the removal mechanism of individual materials and describe the possible effect of surface precipitation on sorption, respectively. To estimate the influence of potential precipitation during sorption, the initial metal concentrations under the given conditions, i.e., pH of 5 for Zn and Cd and 7 for As, oxic atmosphere (Eh = 622.3 mV), and room temperature (25 ± 2 °C), were modeled using the PHREEQC 3 and MINTEQ 3.1 software. The alkalinities of all solutions containing analyzed materials (1 g L^{-1}) were obtained by titration according to ISO 9963-1:1994.

Stability modeling

The stabilities and model calibration of the selected materials (AMO-G1, AMO-S1, AMO-M1, AMO-G1-BC, AMO-S1-BC, and AMO-M1-BC) were determined using the concentration values of the leached Mn in the background electrolyte (0.01 M NaNO$_3$) at pH 5 and 7 (solid/liquid ratio of 1 g L^{-1}) at different time intervals (1–180 min). The amount of leached Mn was recalculated to percentage loss of Mn, according to

$$measured\,loss\,of\,Mn\,(\%) = 10\left(\frac{C_{Mn}}{r_{Mn}}\right)$$

Eq. 4.1

where c_{Mn} is the leached amount of Mn (mg g^{-1}) and r_{Mn} is a relative representation of Mn (mg g^{-1}) based on the total decomposition of the material. Total decomposition was performed using a microwave-assisted aqua regia extraction process using the Multiwave PRO SOLV microwave reaction system (Anton Paar, Germany). For each material, 0.250 g was digested according to EPA 3051A (2007) (" Z. Für Anal., 2007). The decomposition of each material was performed in duplicate. The calculated absolute loss (%) values were fitted using a simple logarithmic model to predict the time dependence of Mn loss, according to **Eq. 4.2**

Eq. 4.2

$$Simulated\ loss\ of\ Mn(\%) = a\ ln(t) + b$$

where *t* is the time (min) and *a* and *b* are model parameters. The individual modeling parameters and amounts of individual elements (%) based on the total decomposition of the individual materials are listed in **Tables S3** and **S4**.

Statistical analyses

All experimental data were normalized (Tufféry, 2011) and pretreated using the Shapiro–Wilks test of normality at the significance level of 0.05. If data were normally distributed,

ANOVA including Post-Hoc statistical analysis (Turkey's honestly significant difference and Fisher's least significant difference) were performed using the Statistical 13 software (TIBCO Software Inc.).

Results and Discussions

Characterization and elemental sorption efficiencies of studied materials

Newly synthesized Mn oxides

The basic characteristics of the studied materials are listed in **Table 4.11**. In general, the differences among the specific surface areas of AMOs synthesized using different Mn/sugar ratio were not significant (except molar ratio 3:1). More specifically, the specific surface area increased based on the Mn/sugar ratio in order: Mn/sugar ratio 3:1 > Mn/sugar ratio 1:1 > Mn/sugar ratio 1:1.5. By contrast, the specific surface area of AMO-G1 was the lowest, and that could be attributed to the formation of crystalline phases such as rhodochrosite or glucose (Della Puppa et al., 2013; Ettler et al., 2014b). Since the AMOs synthesized using glucose presented lower pH values, the general structure of the material (including the secondary phases) probably influenced the final pH values (see **Table 4.11**, **Fig. 4.8** and **Fig. 4.9**). Moreover, the structure of the individual sugar could also influence the final properties of the synthesized materials. The pH and CEC values increased as follows: AMO-G1 < AMO-G2 < AMO-G3. While the pH values of the AMOs synthesized using sucrose and molasses, were higher, their CEC values were significantly lower than those of the AMOs synthesized using glucose. However, we concluded that Mn leaching (Ettler et al., 2014b, 2015; Michálková et al., 2016b) could also influence the final CEC values, especially for AMO-G1.

The diffractograms of the newly synthesized AMOs are illustrated in **Fig. 4.8A**. The broad peaks at 37° and 65° were assigned to the structure of hydrous Mn oxide/birnessite (PDF-2 cards 00-023-1239 and 01-087- 1497) and were in agreement with the diffractograms reported by Lenoble et al. (2004) and K. Xu et al. (2013). Compared to the birnessite synthesized by Ching et al. (1997) all studied materials presented amorphous structure. Although no additional peaks were observed in the diffractograms of the AMOs obtained using the Mn/sugar molar ratios of 1:1, new peaks corresponding to glucose and Mn oxalate (PDF-2 cards: 00-002-0224 and 00-014-0713, respectively) were detected in the diffractograms of AMOs with higher glucose and Mn contents, i.e., AMO-G2, and AMO-G3, respectively. Moreover,

rhodochrosite (PDF-2 card: 00-002-0224) was detected when both lower and higher molar ratios were used. Such phases, which represented secondary products (Mn oxalates, rhodochrosite) or unreacted input compounds (glucose), have been previously observed (Della Puppa et al., 2013; Ettler et al., 2014b; Michálková et al., 2016b; Trakal et al., 2018b) and were attributed to the excess of glucose or $KMnO_4$ during the synthesis of AMOs.

More specifically, the precipitation of rhodochrosite corresponded to the reaction between free Mn(II) and atmospheric CO_2, which was favored at neutral/basic conditions (Ettler et al., 2014b, 2015). The AMOs synthesized using glucose, exhibited higher Mn(II) leaching, which resulted in a higher probability for the formation of rhodochrosite at the given conditions. Conversely, the materials in the present study (especially at the molar ratio of 1:1) exhibited minimum amounts of these phases. Moreover, the use of other sugars, i.e., saccharose and molasses, significantly decreased the formation of such phases at all studied molar ratios.

The FTIR-ATR spectra of the newly synthesized AMOs are presented in **Fig. 4.8B**. The spectra of all materials presented similar bands, which corresponded to the metal‑oxygen and oxygen‑hydrogen binding arrangements. Such as the stretching vibrations of water and lattice O-H groups at 3650–3000 cm^{-1} (Eren and Gumus, 2011), O-H bending vibrations combined with those of Mn atoms at 1597–1572 cm^{-1} (Di Leo et al., 2012), and stretching vibrations of Mn-O at 800–500 cm^{-1} In general, compared to the AMOs synthesized using other sugars, those synthesized using glucose presented significantly higher intensities of the individual bands, and featured a significant band at 767–742 cm^{-1} (Ching et al., 1997). Regardless, the intensities of the individual bands for the binding arrangements of the AMOs synthesized using sucrose and molasses were similar. Glucose bands were detected at 1032–1028 cm^{-1} in the spectra of AMO-G1-3 (Adina et al., 2010), and were in agreement with the XRD results. The intensity of the glucose band decreased as follows: AMO-G3<AMO-G1<AMO-G2 following the Mn/sugar molar ratio for the synthesis of the individual materials. Although sucrose was not detected in the XRD spectra of AMO-S1-3 and AMO-M1-3, corresponding sucrose bands at 1052–1047 and 995–991 cm^{-1} Adina et al. (2010) were observed in the FTIR-ATR spectra of these composites. Similarly, the intensities of these bands decreased as follows: AMO-S3/M3< AMO-S1/M1<AMO-S2/M2, following the sugar content during synthesis. Moreover, the bands attributed to Mn oxalates at approximately 1600 and 1300 cm^{-1}, which corresponded to the

vibrations of the C=O and C-O bonds of oxalate, respectively (Manigandan et al., 2015; Chen et al., 2020) and/or the band ascribed to rhodochrosite at approximately 1300 cm^{-1}, which was ascribed to the vibration of the planar CO^{2-}(Duan and Sorescu, 2010) were detected in the FTIR-ATR spectra, particularly for AMO-G1–3, and were confirmed the XRD results. In general, both AMO-S1-3 and AMO-M1-3 presented significantly lower intensities of these bands (especially AMO-M1–3). Moreover, such phases were not observed in the XRD spectra, therefore, only minor amounts of these phases were expected to form.

The SEM images and EDX analysis results of the newly synthesized AMOs are presented in **Fig. S1** and Table S5, respectively. The morphologies of the individual materials were similar, and involved the agglomeration of individual particles without the formation of any visible crystalline phases, which was characteristic for materials prepared using the sol-gel procedure (Della Puppa et al., 2013). The distribution of individual elements, such as Mn, O, and K was homogeneous, and the elemental composition reported by Ching et al. (1997) confirmed the partial formation of birnessite during the syntheses of AMOs, as described by XRD analysis. Compared to the AMOs synthesized using glucose, slightly higher amounts of K were detected for AMO-S1-3 and AMO-M1-3. Additionally, a low amount of Na (approximately 0.5 wt.%) was detected for AMO-M1-3, which originated from the pristine molasses (see Table S1). No secondary phases or non-reacted compounds were observed using SEM/EDX.

The sorption efficiency values of the newly synthesized AMOs for Zn (II), Cd(II), and As(V) are illustrated in **Fig. S2A**. In general, similar sorption efficiencies toward individual metal(loids) were observed for the AMOs synthesized using the same sugar at different molar ratios of Mn/sugar, and the efficiencies decreased as follows: Cd(II) > Zn(II) < As(V). Since the resulting pH, which was not adjusted, was approximately 7 for all metals, the precipitation of $CdCO_3$, $Zn_5(CO_3)_2(OH)_6$, and/or $ZnCO_3$ influenced the removal mechanism. This was confirmed using the Visual MINTEQ 3.1 software. Surprisingly, Mn leaching was significantly decreased after the sorption of As(V) compared to the sorption of Zn(II) and Cd(II), in particular for AMO-G1–3 (see **Fig. S2B**). Based on the experimental conditions (**Fig. S2C**), the decrease in Mn leaching was probably caused by the precipitation of Mn(II) alongside As(V), which was further confirmed using the Visual MINTEQ 3.1 software, and resulted in the possible formation of Mn_3 $(AsO_4)_2 \cdot 8H_2O$ (manganhörnesite). Significantly lower sorption efficiencies were observed for AMO-S1-3 and AMO-M1-3, which were attributed to

119

their slightly higher pH values as well as lower Mn leaching. Based on the Visual MINTEQ 3.1 software, the probability of the Mn-As precipitation increased as the pH and Mn concentration increased. However, pH values higher than 8.5 lead to the subsequent decrease in the precipitation probability (data not shown). In general, the decrease in Mn leaching during the sorption of As(V) as well as its increase owing to the increase in pH were observed by Michálková et al. (2016b). Nevertheless, these effects have not been sufficiently described or explained.

Table 4.11 **Basic characteristics of the studied materials and the influence of the final pH on general structure of the material**

Material	BET ($m^2\,g^{-1}$)	pH (−)	CEC ($cmol\,kg^{-1}$)
AMO-G1	13	7.18 ± 0.1	271.63 ± 9.4
AMO-S1	54	9.07 ± 0.3	117.53 ± 1.4
AMO-M1	29	9.07 ± 0.2	120.20 ± 1.9
AMO-G2	b1	7.65 ± 0.1	310.66 ± 3.5
AMO-S2	36	8.55 ± 0.1	99.67 ± 0.9
AMO-M2	23	8.68 ± 0.2	118.31 ± 6.6
AMO-G3	12	7.39 ± 0.2	386.77 ± 4.7
AMO-S3	93	9.39 ± 0.1	111.82 ± 1.3
AMO-M3	79	9.29 ± 0.2	122.89 ± 2.3
AMO-G1-BC	b1	8.08 ± 0.1	105.00 ± 1.9
AMO-S1-BC	45	9.23 ± 0.2	99.15 ± 2.8
AMO-M1-BC	33	9.40 ± 0.3	109.97 ± 0.6
BC	235.96	11.01 ± 0.1	66.48 ± 3.3
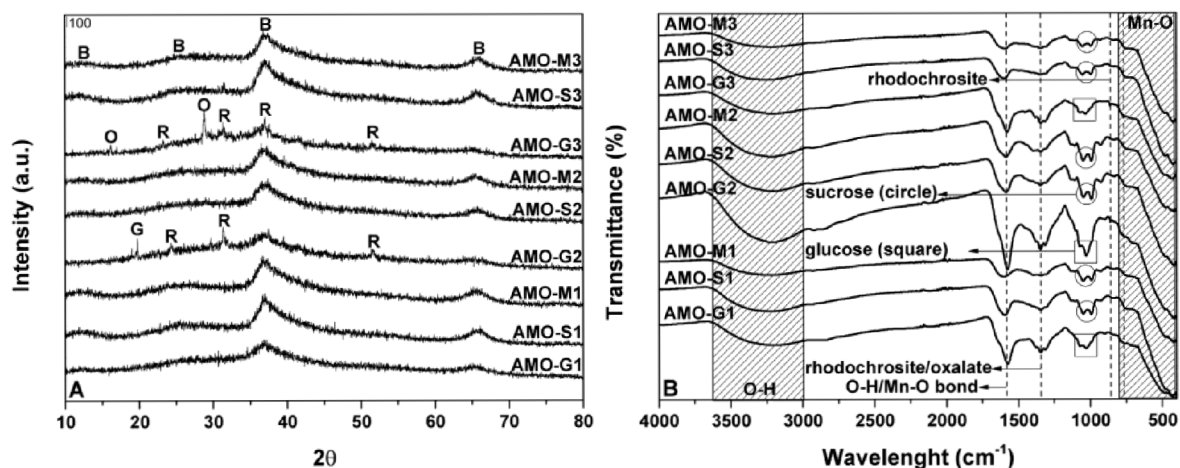
Fig. 4.8 **Diffractograms of the newly synthesized AMOs are illustrated in A and the FTIR-ATR spectra of the newly synthesized AMOs are presented in B.**
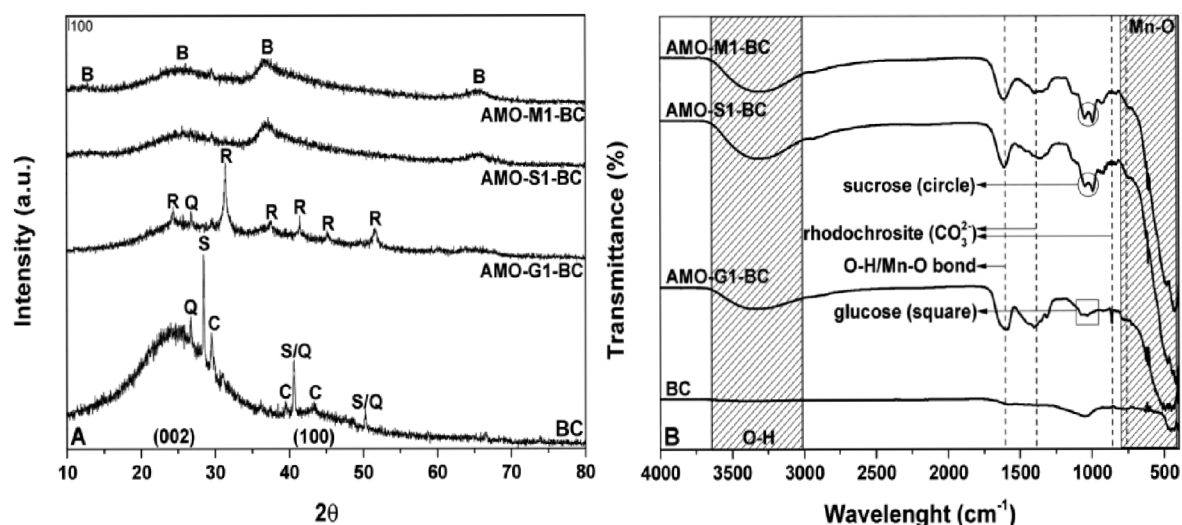
Fig. 4.9 **Diffractograms of pristine BC and the AMO/BC composites are illustrated in A and the FTIR-ATR spectra of pristine BC and the AMO/BC composites are illustrated in B.**

AMO/BC composites

To further minimize Mn leaching, AMO/BC composites were prepared. The lowest Mn/sugar ratio (which generated the minimum amounts of secondary products and nonreacted compounds,) was chosen for the synthesis of the composites (sorption efficiencies of the individual AMOs were similar. The basic properties of the

121

synthesized AMO/BC composites are listed in **supplement**. The specific surface area of the BC used in this study was similar to those of other wheat straw BCs (Trakal et al., 2014b, 2016). In addition, the AMO/BC composites exhibited significantly lower specific surface areas than BC, which corresponded to the precipitation of AMOs on the BC surface as well as possible clogging of pores (Trakal et al., 2018b). The pH values of the AMO/BC composites were comparable to those of the pristine AMOs, but lower than that of pristine BC. This was most likely caused by the interaction of BC with the synthetized Mn oxides. The CEC value of pristine BC was significantly lower than those of the AMOs and corresponding AMO/BC composites, as previously reported by Trakal et al. (2018b). The diffractograms of pristine BC and the AMO/BC composites are illustrated in **Fig. 4.9A**. The diffractogram of pristine BC exhibited two broad peaks at approximately 25° and 45°, which were attributed to the (002) and (100) planes of amorphous carbon, respectively (Liu et al., 2012). The broadening of the peak at 25° was ascribed to the stacking structure of the aromatic layers and presence of small crystallites located vertically from these layers (Takagi et al., 2004). Since the obtained value of the layer distance, d$_{(002)}$, (0.364 nm), was larger than that of graphite, it was concluded that the randomly oriented layers in the structure of BC contributed to its amorphous structure (Xu et al., 2017; Tran et al., 2018). Moreover, the presence of crystalline phases, such as quartz (PDF2 card: 00-003-0427), calcite (PDF2 card: 00-004-0636), and sylvite (PDF2 card: 01-073-0380) was also detected in the structure of BC. Such phases have been previously observed by Trakal et al. (2014b); Lawrinenko and Laird, (2015); Domingues et al. (2017) and were attributed to the biomass sources of the studied BCs. The diffractograms of the AMO/BC composites presented peaks that corresponded to birnessite. Surprisingly, the diffractogram of AMO-G1-BC exhibited an even higher amount of secondary-formed rhodochrosite compared to that of pristine AMO- G1, which suggested that a reaction occurred between the BC and/or species composing BC (e.g., calcite) and Mn(II) that leached or did not react during the synthesis of AMOs. The possible co-effect of the CO^{2-} of calcite on the precipitation of rhodochrosite was further confirmed by the disappearance of the calcite peaks from the diffractogram of AMO-G1-BC compared to that of BC. For the other AMOs, the birnessite peaks were more significant and no secondary phases were observed. Since Mn(II) leaching from these materials was significantly lower than that from AMO-G1 and AMO-G1-BC, the formation of rhodochrosite through the reaction of Mn(II) with CO^{2-} from calcite was negligible.

The FTIR-ATR spectra of pristine BC and the AMO/BC composites are illustrated in **Fig. 4.9**B. The spectrum of pristine BC, especially at higher resolution (see **Fig. S3**) presented bands corresponding to the stretching vibrations of the O-H bonds of the phenolic/carboxylic group at 3358 cm^{-1} (the low intensity of the bands was caused by the dehydration that occurred during pyrolysis), stretching vibration of the C=C bonds of the aromatic rings and carboxylic groups at 1564 cm^{-1}, stretching vibration of the C -O and bending vibrations of the C–OH bonds at 1063 cm^{-1}, and bending vibrations of the C -H bond at 874 cm^{-1}. Moreover, the broad and sharp bands at 1063 and 454 cm^{-1}, respectively, were attributed to the O–Si–O bonds in quartz (Liu et al., 2012; Trakal et al., 2014b)These data were in agreement with the XRD results. The presence of calcite was confirmed by the bands observed at 1371 and 878 cm^{-1} (Butto et al. 2018). Significant changes were observed in the spectra of the AMO/BC composites. Since the intensities of the individual bands attributed to the BC structure were low, only the bands of pristine AMOs were observed at certain resolutions. The intensities of the individual bands of AMO-G1-BC were comparable with those of AMO-S1-BC and AMO-M1-BC. Furthermore, the sharp band at 861 cm^{-1} in the spectra of AMO-G1-BC confirmed the formation of rhodochrosite, as described by XRD analyses.

The SEM images and EDX analysis results of pristine BC and the AMO/BC composites are presented in **Fig. 4.10**. The pristine BC exhibited well developed porous structure, which resulted in a high specific surface area, as described above and reported by Trakal et al. (2014b). As can be seen in **Fig. 4.10**., several inorganic phases were observed on the BC surface, such as pure SiO$_2$ coating (point 1), calcite coating (point 2) and individual KCl particles (point 3), which were confirmed by the XRD and FTIR results. For the AMO/BC composites, AMO covered the surface of BC, and larger clusters were also observed. The proportional Mn coating on the surface of BC has been previously observed by Trakal et al. (2018b). Additionally, other studies demonstrated both the presence of the Mn coating and agglomeration of larger Mn particles on the BC surface (Song et al., 2014; Li et al., 2017). Moreover, AMO-G1-BC and AMO-M1-BC exhibited two different types of Mn distribution sites on the surface of BC: high and low K/Mn concentrations (points 5 and 8 and points 6 and 9, respectively). By contrast, homogenous distribution of Mn was observed for AMO-G1-BC. Compared to pristine BC, the presence of inorganic impurities was negligible for AMO-G1-BC, which suggested that such impurities were removed during the synthesis procedure.

The sorption efficiencies of pristine BC and AMO/BC composites for Zn(II), Cd(II), and As(V) are illustrated in **Fig. S4**. Pristine BC exhibited significantly lower metal sorption and higher pH values compared to all AMO/BC composites, which indicated that the pH was not the key factor for metal removal, and removal was strongly influenced by the general structure of the material. Additionally, the sorption of As

(V) on BC was not observed. Insignificant changes were observed for the AMO/BC composites compared to the pristine AMOs. Since the pH values of the AMOs and AMO/BC composites were also similar, the possible influence of BC on metal sorption was expected. The pH value near the surface of BC, which usually corresponded to the pH of the point of zero charge (pH_{PZC}) of the material (Hou and Zhang, 2007) can be higher than that in bulk solution, which is approximately 9–10 for BCs (Trakal et al., 2014b). Since the surface precipitation could strongly influence the metal removal at these conditions, the sorption properties of studied materials need to be tested under controlled conditions. Compared to the Mn leaching of the pristine AMOs, that of the AMO/BC composites was only slightly limited after the removal of Zn(II) and Cd(II), i.e., approximately 10–15 mg g^{-1} for AMO-G1-BC and 5 mg g^{-1} for AMO-S1-BC and AMO-M1-BC. No changes were observed in the case of As(V) sorption onto AMO/BC composites compared to that of the pristine AMOs.
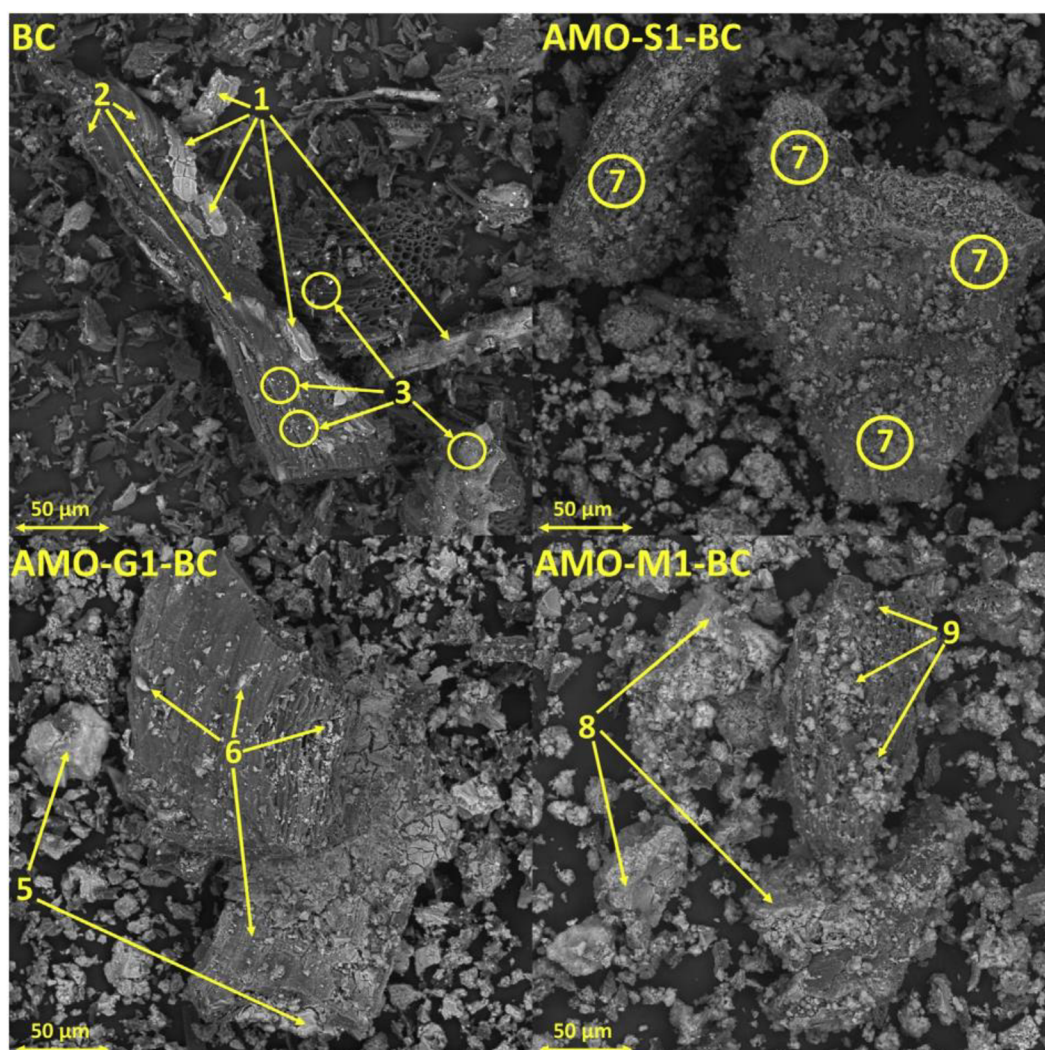
Fig. 4.10 **SEM images and EDX analysis results of pristine BC and the AMO/BC composites.**

Kinetic experiments

The sorption of Zn(II), Cd(II), and As(V) onto selected AMOs, BC, and AMO/BC composites at pH 5 (Cd and Zn) and pH 7 (As) are presented in **Fig. 4.11**. However, the precipitation of leached Mn during the sorption of As(V) was still expected. The equilibrium time was different for different materials and metal(loid)s. For the sorption of Zn(II), pseudo-equilibrium was reached within 15 and 5 min for the AMOs and AMO/BC composites, respectively. Afterward, desorption occurred, and equilibrium was reached after 60 min. No post-desorption of Cd(II) was detected for

any materials except for pristine BC and AMO-G1-BC, where equilibrium was reached within 15 min. Similarly, no post desorption was observed after the sorption of As(V), and equilibrium was reached within 180 min. Slightly longer equilibrium time has been previously observed for Cd(II) sorption (Della Puppa et al., 2013; Michálková et al., 2014, 2016b) and for As(V) sorption (Trakal et al., 2018b) at similar pH values. Moreover, different Mn oxide/BC composites exhibited significantly longer equilibrium times for the sorption of Cd (II) and As(V) compared to the materials in this study (H. Wang et al., 2015; S. Wang et al., 2015a). In general, the sorption efficiency decreased as follows: As(V) > Cd(II) > Zn(II). Therefore all AMOs and AMO/BC composites in this study exhibited the highest affinity for As(V), and these conclusions were in agreement with the results reported by Michálková et al. (2016b) However, these results contravened the sorption efficiency data obtained when the pH was not controlled and therefore demonstrated the effect of pH on the removal process (especially for metals). To further evaluate the sorption efficiencies of individual materials, statistical analyses were performed. For the sorption of Zn(II), significant differences were observed between pristine BC, individual AMOs, and AMO/BC composites. Among the studied materials, AMO-S1 was established to be the most effective material for the sorption of Zn(II). While no significant differences were observed between the Zn(II) sorption of AMO -S1, AMO-G1, and AMO- M1, significantly lower amounts of sorbed Zn(II) were detected for all AMO/BC composites (except for AMO-S1-BC). Similarly, while AMO- S1 was determined to be the most effective for Cd(II) removal (significantly more effective than AMO-G1 and AMO-G1-BC), no significant differences were observed between the Cd(II) removal properties of AMO -S1, AMO-M1, AMO-S1-BC, and AMO-M1-BC. Pristine BC exhibited the lowest Cd(II) removal efficiency of all materials analyzed in this study. In general, AMOs prepared using sucrose and molasses appeared to be more effective for metal sorption compared to the standard AMOs prepared using glucose. However, contrasting results were obtained for the sorption of As(V), since AMO-G1 was found to be the most effective material for that purpose. The pristine BC exhibited no sorption for As(V), while the As(V) sorption efficiencies of the AMO/BC composites were almost the same as those of the pristine AMOs. 2: Mn leaching during sorption kinetics experiments is illustrated in **Fig. S5**. Significantly higher Mn leaching was observed for the sorption of Zn(II) and Cd(II) onto AMO-G1 compared to that onto the AMOs synthesized using sucrose and molasses. Mn leaching decreased by

approximately 20% when AMO-S1 and AMO-M1 were used, compared to AMO-G1 after the sorption of As(V). This study also demonstrated that Mn leaching was lower after the sorption of Zn(II) and Cd(II) onto AMO-G1-BC but observed effect was still significantly lower compared to pristine AMO-S1 and AMO-M1. In general, the AMOs synthesized using sugars other than glucose were more stable compared to the AMOs synthesized using glucose and AMO/BC composites as well as controlled pH values.

Sorption equilibrium experiments

Sorption equilibrium data that describes the sorption of Zn(II), Cd (II), and As(V) onto selected AMOs and AMO/BC composites at pH 5 (Cd and Zn) and 7 (As) are presented in **Fig. 4.12**. Pristine BC was not included in **Fig. 4.12** owing to its extremely low observed sorption. The pH value was controlled for the entire duration of the kinetic experiments. The possible precipitation of Zn(II) and Cd(II) in the bulk solution was excluded using the Visual MINTEQ 3.1 and PHREEQC 3 software (see Table S10). The precipitation of As(V) alongside the leached Mn(II) was expected, although the precipitation of As(V) in the bulk solution, i.e., without Mn leaching from the structure of AMOs, was excluded. The equilibrium data were further modeled using the Langmuir and Freundlich isotherms, and the results are listed in Tables S7 and S8 (for the AMOs and AMO/BC composites, respectively). All data describing the sorption of Zn(II) and Cd(II) onto AMOs were better fitted using the Langmuir model. By contrast, the sorption of As(V) followed the Freundlich model. Similarly, most data describing the sorption onto AMO/BC composites were better fitted using the Langmuir model, while the sorption of As(V) and Cd(II) onto AMO-S1- BC and AMO-M1-BC, respectively, exhibited slightly higher coefficients of determination using the Freundlich model. Most studies on metal (loid) sorption for Mn-based materials reported that the Langmuir model represented a better fit for the data (Huang et al. 2017; Li et al. 2017; Michálková et al. 2014, 2016; Della Puppa et al. 2013; H. Wang et al. 2015) compared to the Freundlich (Huang et al. 2017; S. Wang et al. 2015). In general, non- significant changes were observed for the sorption of Zn(II) onto different pristine AMOs. However, the pristine AMOs were significantly more effective compared to the AMO/BC composites (AMO-G1 was nearly two times more effective). Among the AMO/BC composites, slightly higher Zn(II) sorption efficiency was observed for AMO-M1-BC. Similar results were obtained for the sorption of Cd(II). Nevertheless, the AMOs synthesized using sucrose and molasses presented

slightly better sorption properties compared to AMO-G1. Similarly, AMO-M1- BC exhibited better sorption properties compared to the other AMO/ BC composites, although these results were not statistically significant. By contrast, a significantly higher amount of sorbed As(V) was observed for AMO-G1 and AMO-G1-BC compared to other AMOs and synthesized AMO/BC composites, respectively. However, the data describing the sorption of As(V) onto pristine AMOs were divided into two regions: the first region included the sorption and minor effect of Mn -As precipitation, which was modeled, and the second region included the prevailing effect of surface Mn -As precipitation, which was not modeled. The observed S-shaped isotherm commonly corresponds to sorption processes that are influenced by different removal mechanisms, such as sorption and precipitation (Román-Ross et al., 2006). For the sorption of As(V) onto AMO/BC composites, only one region was observed, which indicated lower or no effect of precipitation. That was probably caused by the lower Mn leaching, especially for AMO-G1-BC compared to the pristine AMOs. Based on these results, the sorption efficiencies of the AMO/BC composites were proportional to their AMO contents, which implied that the co-effect of BC was not significant at the given concentrations.

The PHREEQC model was used to estimate the prevailing forms of the major elements in solution during the sorption experiments. After stirring the materials in the electrolyte (without metals/metalloids), the prevailing forms (N94%) were represented by dissociated Mn, K, Ca, and Na cations. After the simulated reactions in solutions containing AMOs and AMO/BC composites and the selected contaminants (Zn, Cd, and As nitrates), the model indicated that Zn(II) and Cd(II) were the predominant forms of metals for the given conditions. Therefore, based on the observed saturation indices metal precipitation was not observed at pH 5. These results confirmed that the sorption of Zn(II) and Cd (II) onto the studied materials was not influenced by the precipitation of metals in the bulk solution. For the sorption of As(V) onto AMO-G1 and AMO-G1-BC (pH 7), the precipitation of manganhörnesite was observed, which further confirmed the results of the sorption experiments. The modeled precipitation of As(V) was observed from 0.03 mM of As(V), which described the real Mn(II) leaching process from AMO-G1 and AMO-G1-BC. Mn(II) leaching from other materials was significantly lower, and therefore, Mn -As precipitation was not observed for those materials.
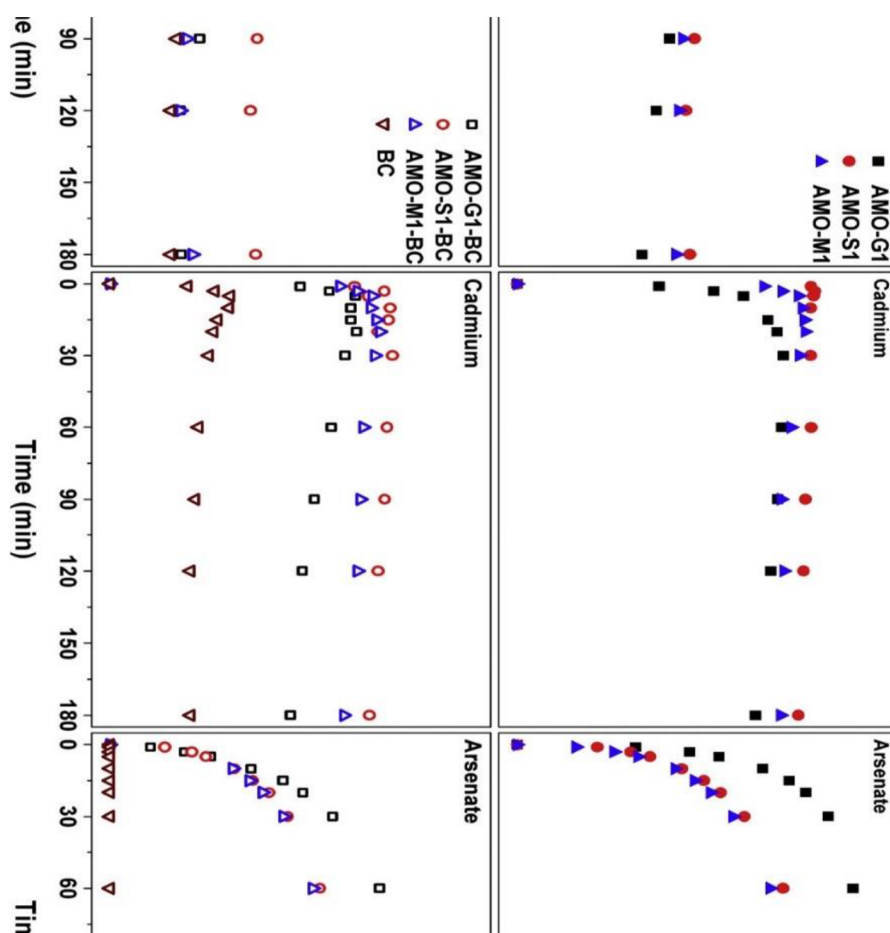
Fig. 4.11 **The sorption of Zn(II), Cd(II), and As(V) onto selected AMOs, BC, and AMO/BC composites at pH 5 (Cd and Zn) and pH 7 (As).**

Solid-state analyses

Since the sorption mechanisms of BC (Trakal et al., 2014b, 2016)and AMO/BC composites (Trakal et al., 2018b) have been intensively studied, only the fundamental sorption mechanism. of Zn(II), Cd(II), and As(V) onto the newly synthesized AMOs was analyzed in this study. Moreover, only AMO-G1 and AMO-M1 were tested since AMO-S1 exhibited the same sorption isotherm shapes and sorption capacities as AMO-G1 and AMO-M1, and therefore, similar sorption mechanisms were expected for all three AMOs. The SEM/EDX analyses of the selected AMOs after the sorption of Zn(II), Cd(II), and As(V) at two different concentrations are presented in **Fig. S6, S7**, and **S8** for Zn(II), Cd(II), and As(V), respectively. The SEM images of AMO G1 after the sorption of Zn(II) at both concentrations presented smoother surfaces compared to

those of the material before sorption. Moreover, some morphological changes ("holes") were observed on the material surface, especially at higher Zn(II) concentrations. Additionally, the amount of sorbed Zn(II) remained unchanged and no precipitates occurred on the surface (no changes in the XRD spectra; data not shown). The surface of AMO-M1 after the sorption of Zn(II) was rougher than that of AMO-G1, yet the amount of sorbed Zn(II) did not change, which excluded the possibility of precipitation. Similarly, while some morphological changes (differently shaped "holes") were also detected, no changes in the elemental composition of the materials were observed. Moreover, the SEM images of AMO-G1 and AMO-M1 at both Cd(II) concentrations did not present any precipitates (no changes were observed in the XRD spectra, either; data not shown). Despite the presence of some darker AMO-G1 particles in the absence of any sorbed Cd(II), the distribution of Cd(II) on the material surface was homogenous. The SEM images of AMO-G1 after the sorption of As(V) presented significant differences between the lower and higher As (V) concentrations since visible fiber-like precipitates were formed at higher As(V) concentrations. These results confirmed the possibility of Mn -As precipitation, as mentioned above. The precipitation of Mn -As phases commonly occurs in nature and takes place in the presence of excess free Mn(II), under oxidic conditions, and at high pH values (Adriano, 2001). In general, Mn -As precipitates present low solubility products, and therefore, high stability of the emerging phases is expected. Therefore, these precipitates could significantly influence the overall sorption efficiency of the AMOs as well as decrease Mn(II) leaching. However, the XRD spectra (data not shown) of the AMOs before and after sorption were comparable, which suggested that the emerging precipitates presented amorphous structures (Bossy et al., 2010). No Mn -As precipitates were observed in the SEM images of AMO-M1 for the lower As(V) concentration and both Mn(II) concentrations. Based on the solid-state analyses, the prevailing effect of adsorption was expected for both metals at controlled pH values. By contrast, the sorption of As(V) onto AMOs (especially those manufactured using glucose) was influenced by Mn -As precipitation owing to Mn leaching.
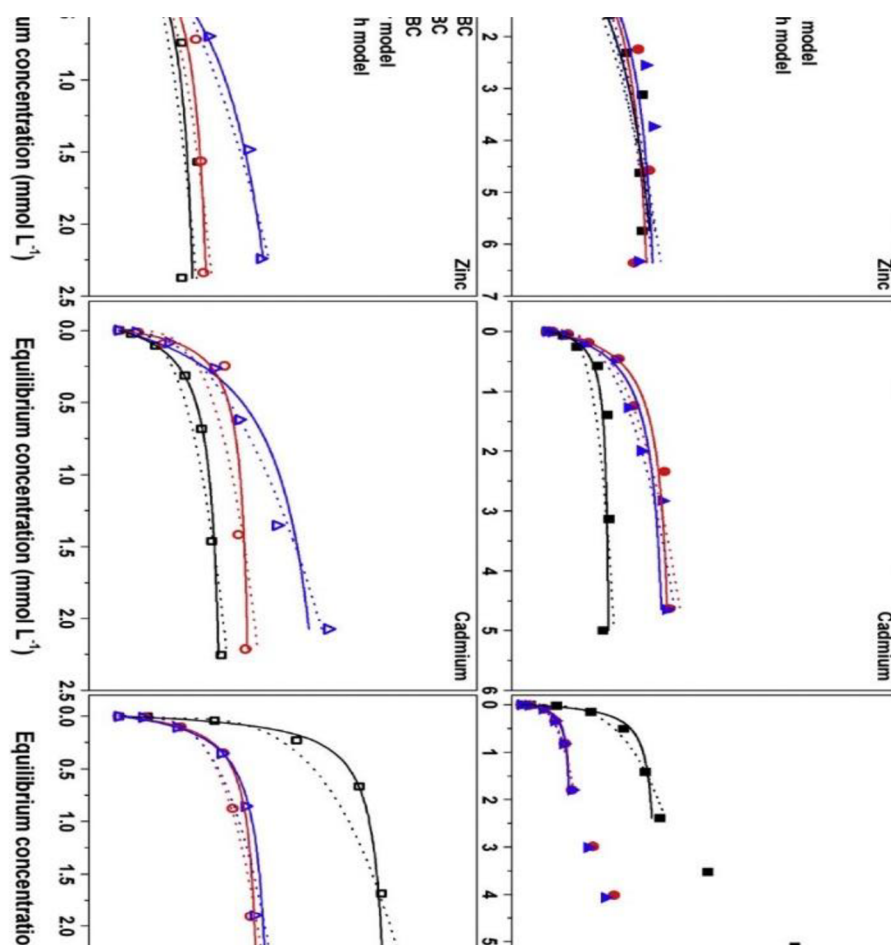
Fig. 4.12 **The sorption equilibrium data that describes the sorption of Zn(II), Cd (II), and As(V) onto selected AMOs and AMO/BC composites at pH 5 (Cd and Zn) and 7 (As)**

Material stability and short-term predictions

The stability of individual materials was tested according to the absolute loss of Mn (%) **Fig. 4.13**. Significant differences were observed for all materials at different pH values, i.e., pH 5 compared to 7 (except for AMO-G1-BC). Significantly higher Mn leaching was observed for AMO-G1 compared to other materials. The total Mn loss of AMO-G1 reached 21.5 and 11.7% at pH 5 and 7, respectively, after 180 min (this corresponded to the equilibrium time. The AMO-G1- BC composite exhibited significantly higher stability than pure AMO- G1. The decrease in Mn loss was approximately 13 and 6% at pH 5 and 7, respectively, after 180 min. However, this effect was not significant for other materials (AMO -S1, AMO-S1-BC, AMO-M1, and

131

AMO-M1- BC). As previously mentioned, the synthesis of AMOs according to the modified sol-gel procedure used in this study, utilizing sucrose or molasses as reducing agents for KMnO$_4$, significantly increased the stability of the resulting materials, and BC was not needed to stabilize their structure. Compared to AMO-G1, the Mn loss of AMO-S1 and AMO-M1 decreased by 17.6 and 17.9%, respectively, at pH 5 and by 11.5% for both materials at pH 7. The obtained results were compared to those published by Della Puppa et al. (2013) who tested the stability of AMOs synthesized using glucose in pure water at pH close to 7 for 200 h, which resulted in Mn leaching that corresponded to 5.7% of the total AMO content. Compared with the modeled results after 200 h reported in this study, the Mn loss (%) had to be recalculated according to the total loss of material content. Therefore, as can be seen in , AMO-G1 and AMO-G1-BC appeared to be less stable since their corresponding material loss values increased by 3.7 and 0.5%, respectively. However, the stabilities of the other studied materials were significantly higher compared to those of the AMOs and AMO/BC composites synthesized using glucose. More specifically, the Mn loss values of these materials were decreased by approximately 5.4% (i.e., only 0.2–0.3% material loss was observed) compared to that of the original AMO. The abovementioned results indicated promising stability of the newly synthetized AMOs compared to the standard AMOs synthesized using glucose.
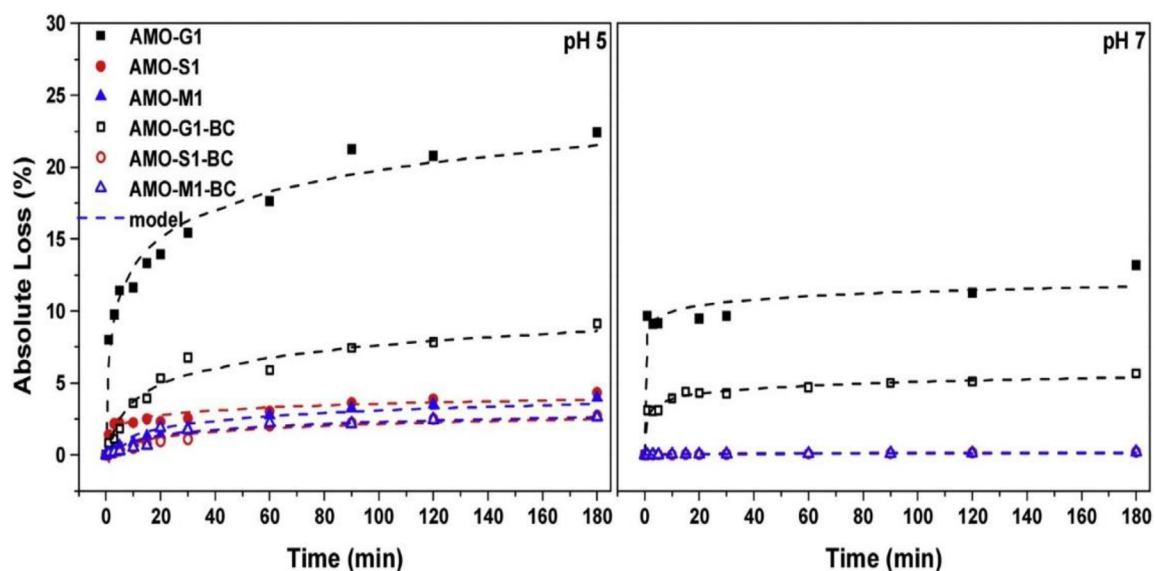
Fig. 4.13 **The stability of individual materials was tested according to the absolute loss of Mn (%)**
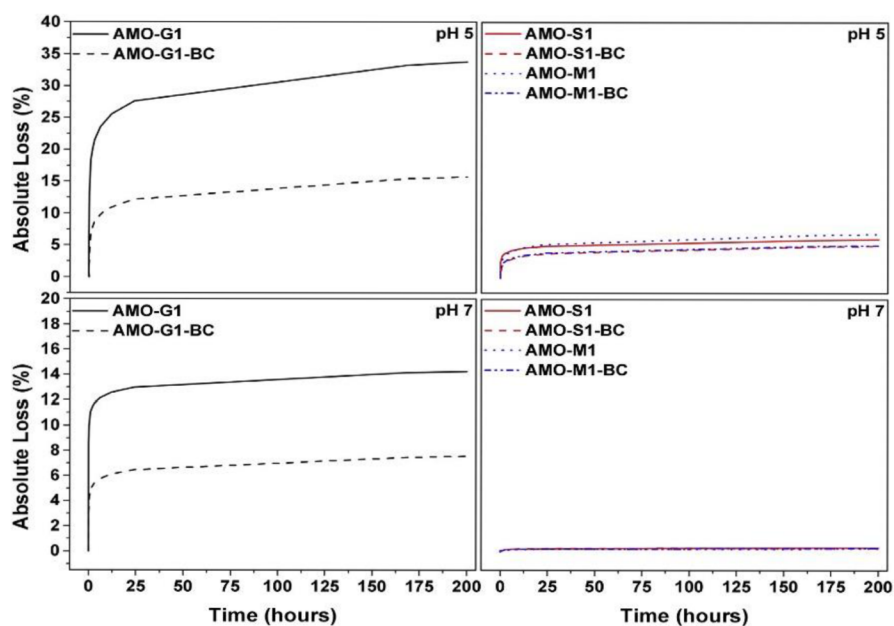
Fig. 4.14 **The AMO-G1 and AMO-G1-BC appeared to be less stable since their corresponding material loss**

Conclusion

Amorphous manganese oxides (AMOs) synthesized using different sugars (glucose, sucrose, and molasses) and their biochar (BC) composites exhibited promising results for the sorption of Zn(II), Cd(II), and As (V) in aqueous solutions. Since the sucrose and molasses-based AMOs and AMO/BC composites in this study have not been synthesized before, these materials presented similar or higher sorption efficiencies for metals in comparison to original AMO and/or modified AMO/BC (except the removal of As(V) due to the Mn -As precipitation caused by the higher Mn(II) leaching).

Next, Mn(II) leaching from the structure of the new AMOs was negligible compared to that observed for the glucose-based AMOs, in this study as well as in other similar studies. Moreover, using molasses as reducing agent during AMO synthesis dramatically decreased the total cost of the final materials, which suggested that these new AMOs could represent interesting alternatives for standard remediation technologies. These materials could, therefore, be recommended as promising sorbents, especially for metal cations. However, future studies using field conditions should be performed, when the efficiency and stability of the materials (under dynamic conditions) need to be tested.

Supplementary material

S1.1. The AMO preparation

The molarities of $KMnO_4$ and sugars were calculated as their theoretical maximum solubility for the given conditions. However, the final concentrations of all compounds were slightly smaller than their maximum solubility (by approximately 12.5 %) to avoid the presence of any potential undissolved residues. Moreover, the $KMnO_4$ solution was heated up to 40 °C before the reaction with the sugar to further increase solubility. More specifically, individual sugar solutions were prepared, and concentrations of 3.2 M for glucose monohydrate and 5 M for sucrose (recalculated for the glucose carbon content in sucrose) were used. The amount of molasses was recalculated using its density and sucrose content. During the individual synthesis processes, the calculated amounts of glucose, sucrose, or molasses (see Table S2) were slowly added to the preheated solution containing 0.7 M (90 mL) $KMnO_4$. The resulting gel was then filtered using a vacuum pump, dried at room temperature (25 ± 2 °C) to constant weight, milled, and sieved (< 250 µm).

Equation S1 Recalculation of % Mn loss to % loss of total material content.

$$Total\ material\ content\ loss\ [\%] = Mn\ loss[\%] - (\frac{(100 - tdc)}{100} * Mn\ loss[\%])$$

where *tdc* is the % content of Mn based on total decomposition.

Table S1 Physicochemical characterization of molasses.

	Analysis of molasses		
	CHARACTERISTICS	UNITS	RESULTS
Physical parameters			
	Bulk density	g mL^{-1}	1.34 ± 5.0%
	Active pH	-	8.7 ± 1.7%
	C:N ratio	-	24.6
	Combustible substances	%	70.7 ± 5.0%
	Moisture content (105°C)	%	27.0 ± 6.1%
	Dry matter (105°C)	%	72.9 ± 6.0%
Anorganic parameters			
	Total nitrogen content	mg kg^{-1}	14300 ± 20.0%
	Chlorides	mg kg^{-1}	1310 ± 10.2%
Organic parameters			
	Total sucrose content	%	54.08 ± 5%
Major ionts			
	As	mg kg^{-1}	< 5
	Ca	mg L^{-1}	273 ± 10.0%
	Cd	mg kg^{-1}	< 0.40
	Cr	mg kg^{-1}	< 0.50
	Cu	mg kg^{-1}	0.79 ± 33.6%
	Hg	mg kg^{-1}	< 0.300
	K	mg L^{-1}	27500 ± 10.0%
	Mg	mg L^{-1}	50.2 ± 10.0%
	Na	mg L^{-1}	10400 ± 10.0%
	Ni	mg kg^{-1}	1.86 ± 23.1%
	Pb	mg kg^{-1}	< 5
	Zn	mg kg^{-1}	14.3 ± 20%

Table S2 Calculated amounts of glucose, sucrose, and molasses during individual synthesis processes.

Material	V_{sugar} (mL)
AMO-G1	19.68
AMO-G2	29.53
AMO-G3	13.1
AMO-S1	6.3
AMO-S2	9.45
AMO-S3	4.2
AMO-M1	14.8
AMO-M2	22.3
AMO-M3	7.18

G - using of glucose, **S** - using of sucrose, **M** - using of molasses recalculated to its sucrose content

Table **S3** Parameters for speciation modeling.

Material	pH 5			pH 7		
	a	b	R	a	b	R
AMO-G1	2.91	6.4	0.97	0.6	8.57	0.6
AMO-S1	0.5	1.26	0.87	0.04	-0.05	0.79
AMO-M1	0.77	-0.44	0.91	0.03	-0.01	0.86
AMO-G1-BC	1.69	-0.13	0.94	0.51	2.72	0.92
AMO-S1-BC	0.58	-0.51	0.91	0.03	-0.02	0.75
AMO-M1-BC	0.57	-0.33	0.89	0.03	-0.01	0.71

Table S4 Amount (%) of individual elements based on total decomposition of individual materials.

Material	Ca	K	Mn	Mg	Na	other
			% composition			
AMO-G1	0.31 ± 0.05	33.40 ± 2.2	66.03 ± 1.2	0.03 ± 0.01	0.14 ± 0.04	0.09
AMO-S1	0.12 ± 0.02	36.70 ± 2.6	63.00 ± 1.5	0.03 ± 0.01	0.084 ± 0.03	0.07
AMO-M1	0.16 ± 0.04	32.53 ± 1.8	63.90 ± 1.7	0.04 ± 0.02	3.11 ± 0.9	0.26
AMO-G1-BC	1.86 ± 0.31	15.10 ± 1.1	82.30 ± 2.6	0.24 ± 0.05	0.19 ± 0.5	0.31
AMO-S1-BC	1.78 ± 0.33	18.74 ± 1.1	78.80 ± 2.6	0.28 ± 0.1	0.19 ± 0.4	0.21
AMO-M1-BC	1.73 ± 0.31	19.86 ± 2.4	76.05 ± 2.5	0.27 ± 0.1	1.73 ± 0.8	0.36

Table S5 EDX results (wt.%) of newly synthesized AMOs.

Material	O	Na	K	Mn
AMO-G1	38.9 ± 4.7	-	8.7 ± 1.3	45.4 ± 1.0
AMO-S1	30.7 ± 3.8	-	10.5 ± 3.4	50.5 ± 8.6
AMO-M1	33.3 ± 2.7	0.5 ± 0.0	11.4 ± 0.7	47.0 ± 2.9
AMO-G2	39.3 ± 6.9	-	8.7 ± 1.2	42.3 ± 3.2
AMO-S2	33.9 ± 3.0	-	10.3 ± 0.6	44.0 ± 2.8
AMO-M2	40.2 ± 4.9	0.6 ± 0.1	9.5 ± 1.4	42.7 ± 4.4
AMO-G3	36.6 ± 6.1	-	9.9 ± 1.8	49.4 ± 8.1
AMO-S3	37.9 ± 3.5	-	11.9 ± 0.8	46.0 ± 2.4
AMO-M3	36.9 ± 7.0	0.4 ± 0.1	11.8 ± 0.8	45.8 ± 5.2

Table S6 EDX results (wt.%) of pristine BC and AMO/BC composites.

Material	Number a	O	K	Mn	Si	Ca	Cl	Na	Mg	P	S
BC	1	23.9 ± 1.8	2.2 ± 0.7	-	30.8 ± 4.1	0.3 ± 0.2	0.2 ± 0.0	0.3 ± 0.0	-	-	-
	2	12.8 ± 2.9	4.6 ± 0.3	-	1.2 ± 0.4	5.4 ± 0.1	1.4 ± 0.1	0.2 ± 0.0	0.4 ± 0.2	0.2 ± 0.0	0.3 ± 0.0
	3	37.2 ± 2.0	11.3 ± 0.1	-	17.9 ± 1.0	0.4 ± 0.0	0.4 ± 0.0	0.5 ± 0.0	-	-	-
AMO-G1-BC	5	32.8 ± 1.6	9.4 ± 0.3	48.0 ± 0.9	2.0 ± 1.1	0.6 ± 0.0	-	-	-	0.2 ± 0.0	0.1 ± 0.0
	6	38.1 ± 4.6	6.4 ± 0.5	32.2 ± 9.5	-	0.4 ± 0.1	-	-	-	-	0.2 ± 0.0
AMO-S1-BC	7	30.5 ± 2.0	11.1 ± 0.9	43.3 ± 2.0	-	0.3 ± 0.1	-	-	-	-	-
AMO-M1-BC	8	30.2 ± 6.9	12.8 ± 0.1	43.2 ± 2.0	1.4 ± 0.3	0.3 ± 0.0	-	0.6 ± 0.0	-	-	0.2 ± 0.1
	9	34.0 ± 5.3	7.4 ± 0.6	35.4 ± 3.8	1.3 ± 0.3	1.1 ± 0.7	0.2 ± 0.0	0.2 ± 0.0	-	0.3 ± 0.0	0.2 ± 0.1

[a] points corresponded to numbers given in **Fig. 4-3**

Table S7 Non-linear modeling parameters of Langmuir and Freundlich models for sorption of selected metal(loid)s onto selected AMOs at pH 5 (Zn and Cd) and 7 (As).

Material	Metal(loid)	Langmuir model							Freundlich model				
		q_{exp} (mmol g^{-1})	S.E.	q_{max} (mmol g^{-1})	S.E.	K_L (L mmol^{-1})	S.E.	R^2	n (-)	S.E.	$K_F{}^a$	S.E.	R^2
AMO-G1	Zn	0.54		0.80	0.10	0.46	0.14	0.97	1.88	0.31	0.24	0.03	0.93
	Cd	0.32		0.36	0.02	4.75	1.08	0.98	4.02	1.00	0.25	0.02	0.86
	As	0.73		0.73	0.04	7.63	2.20	0.97	3.56	0.31	0.60	0.02	0.99
AMO-S1	Zn	0.50		0.66	0.07	0.92	0.28	0.95	2.51	0.51	0.29	0.03	0.90
	Cd	0.69		0.74	0.04	2.11	0.45	0.98	2.99	0.36	0.45	0.02	0.96
	As	0.27		0.27	0.02	8.62	2.88	0.97	3.54	0.30	0.23	0.01	0.99
AMO-M1	Zn	0.52		0.80	0.07	0.89	0.28	0.95	2.46	0.52	0.30	0.04	0.89
	Cd	0.68		0.71	0.04	2.48	0.49	0.98	2.80	0.29	0.42	0.02	0.97
	As	0.27		0.27	0.02	7.39	2.20	0.97	3.35	0.27	0.23	0.01	0.99

^{a} [(mmol g^{-1})(L mmol^{-1})$^{1/n}$]

Table S8 Non-linear modeling parameters of Langmuir and Freundlich models for sorption of selected metal(loid)s onto AMO/BC composites at pH 5 (Zn and Cd) and 7 (As).

Material	Metal(loid)	Langmuir model							Freundlich model				
		q_{exp} (mmol g^{-1})	S.E.	q_{max} (mmol g^{-1})	S.E.	K_L (L mmol^{-1})	S.E.	R^2	n (-)	S.E.	$K_F{}^a$	S.E.	R^2
AMO-G1-BC	Zn	0.11		0.14	0.02	2.61	1.01	0.94	2.60	0.73	0.09	0.01	0.86
	Cd	0.17		0.18	0.00	4.87	0.33	0.99	3.09	0.46	0.14	0.01	0.96
	As	0.45		0.46	0.02	10.5	2.04	0.99	4.19	0.65	0.38	0.02	0.96
AMO-S1-BC	Zn	0.14		0.17	0.01	2.84	0.85	0.96	2.68	0.53	0.11	0.01	0.92
	Cd	0.21		0.23	0.01	8.44	2.45	0.97	3.88	1.06	0.19	0.02	0.87
	As	0.25		0.24	0.02	7.32	2.33	0.96	3.98	0.44	0.20	0.00	0.98
AMO-M1-BC	Zn	0.24		0.34	0.02	1.11	0.15	0.99	1.89	0.17	0.16	0.01	0.98
	Cd	0.35		0.40	0.04	2.34	0.78	0.96	2.34	0.18	0.25	0.01	0.99
	As	0.27		0.26	0.01	5.54	1.34	0.98	3.62	0.43	0.20	0.00	0.97

^{a} [(mmol g^{-1})(L mmol^{-1})$^{1/n}$]

Table S9 Species of major elements in solution.

| Material | Zn sorption (pH 5) | | | | Cd sorption (pH 5) | | | | As sorption (pH 5) | | | | |
| | | | | | | % | | | | | | | |
	Zn^{2+}	K^+	Na^+	Mn^{2+}	Cd^{2+}	K^+	Na^+	Mn^{2+}	H_2AsO4^-	$HAsO4^{2-}$	K^+	Na^+	Mn^{2+}
AMO-G1	92.06	100.00	99.99	95.60	89.22	100.00	99.99	95.61	29.40	70.59	100.00	99.99	96.09
AMO-S1	92.29	100.00	100.00	95.73	89.53	100.00	100.00	95.74	29.71	70.28	100.00	100.00	96.00
AMO-M1	92.33	100.00	99.99	95.71	88.93	100.00	99.99	95.72	30.03	69.96	100.00	99.99	96.30
AMO-G1-BC	90,06	100.00	100.00	94.70	84.43	100.00	100.00	94.69	26.70	73.29	100.00	99.99	94.88
AMO-S1-BC	89.94	100.00	100.00	94.62	85.44	100.00	100.00	94.61	29.60	70.39	100.00	99.99	96.13
AMO-M1-BC	89.15	100.00	100.00	94.31	81.27	100.00	100.00	94.29	29.53	70.46	100.00	100.00	96.14

Table S10 Saturation indices of potentially precipitated minerals

A		As sorption, pH 7							Cd sorption, pH 5					Zn sorption, pH 5			
		SATURATION INDEX							SATURATION INDEX					SATURATION INDEX			
Material	c_L (mmol L^{-1})	Bs	Hn	Mt	Hr	Ns	Py	Rh	Bs	Mt	Ns	Ot	Py	Bs	Mt	Ns	Py
	0.025	4.30	8.21	3.90	0.00	4.88	6.36	1.54	0.54	0.15	1.13	0.00	2.60	0.69	0.22	1.28	2.75
	0.5	4.29	8.19	3.90	2.39	4.88	6.35	1.53	0.53	0.14	1.12	0.00	2.60	0.69	0.22	1.28	2.75
	1	4.29	8.17	3.89	2.94	4.87	6.35	1.52	0.53	0.14	1.12	0.00	2.59	0.68	0.21	1.27	2.74
	2	4.27	8.13	3.88	3.54	4.86	6.33	1.51	0.53	0.13	1.12	0.00	2.59	0.67	0.20	1.26	2.73
AMO-G1	3	4.26	8.10	3.87	3.80	4.85	6.32	1.50	0.53	0.13	1.12	0.00	2.59	0.22	0.00	0.81	2.28
	4	4.25	8.06	3.86	3.99	4.84	6.31	1.48	0.53	0.12	1.11	0.00	2.59	0.21	0.00	0.80	2.27
	5	4.24	8.03	3.85	4.13	4.83	6.30	1.47	0.53	0.12	1.11	0.05	2.59	0.20	0.00	0.79	2.26
	6	4.65	8.42	4.05	4.24	5.24	6.72	1.46	0.52	0.11	1.11	0.13	2.58	0.19	0.00	0.77	2.25
	7	4.64	8.39	4.03	4.32	5.23	6.71	1.44	0.52	0.11	1.11	0.19	2.58	0.17	0.00	0.76	2.24
	0.025	4.05	7.28	3.61	0.00	4.64	6.11	1.18	0.29	0.00	0.88	0.00	2.35	0.01	0.00	0.60	2.07
AMO-S1	0.5	4.05	7.27	3.61	1.24	4.63	6.11	1.17	0.29	0.00	0.88	0.00	2.35	0.02	0.00	0.60	2.08
	1	4.04	7.25	3.60	1.80	4.63	6.10	1.17	0.29	0.00	0.88	0.00	2.35	0.01	0.00	0.60	2.07

Material	c_L (mmol L^{-1})	Bs	Hn	Mt	Hr	Ns	Py	Rh	Bs	Mt	Ns	Ot	Py	Bs	Mt	Ns	Py
	2	4.03	7.22	3.59	2.41	4.62	6.09	1.16	0.29	0.00	0.87	0.00	2.35	0.00	0.00	0.58	2.06
	3	4.02	7.19	3.58	2.68	4.61	6.08	1.14	0.29	0.00	0.87	0.00	2.35	0.00	0.00	0.57	2.05
	4	4.01	7.16	3.57	2.87	4.60	6.07	1.13	0.28	0.00	0.87	0.00	2.34	0.00	0.00	0.56	2.04
	5	4.00	7.13	3.56	3.02	4.59	6.06	1.12	0.28	0.00	0.87	0.00	2.34	0.00	0.00	0.55	2.02
	6	3.99	7.10	3.55	3.13	4.58	6.06	1.11	0.28	0.00	0.87	0.07	2.34	0.00	0.00	0.54	2.01
	7	3.99	7.07	3.54	3.22	4.57	6.05	1.10	0.28	0.00	0.87	0.13	2.34	0.00	0.00	0.53	2.00
	0.025	2.68	3.03	2.21	0.00	3.27	4.75	0.00	0.00	0.00	0.53	0.00	2.01	0.00	0.00	0.45	1.93
	0.5	2.25	2.58	1.98	0.00	2.83	4.31	0.00	0.00	0.00	0.53	0.00	2.00	0.00	0.00	0.45	1.92
	1	2.24	2.56	1.98	0.00	2.83	4.30	0.00	0.00	0.00	0.53	0.00	2.00	0.00	0.00	0.45	1.92
	2	2.66	2.95	2.18	0.00	3.25	4.72	0.00	0.00	0.00	0.52	0.00	2.00	0.00	0.00	0.45	1.92
AMO-M1	3	2.65	2.92	2.17	0.00	3.24	4.71	0.00	0.00	0.00	0.52	0.00	2.00	0.00	0.00	0.44	1.92
	4	2.64	2.88	2.16	0.00	3.23	4.70	0.00	0.00	0.00	0.52	0.00	1.99	0.00	0.00	0.44	1.92
	5	2.63	2.85	2.15	0.00	3.22	4.69	0.00	0.00	0.00	0.52	0.00	1.99	0.00	0.00	0.44	1.92
	6	3.01	3.20	2.33	0.00	3.60	5.07	0.00	0.00	0.00	0.08	0.04	1.56	0.00	0.00	0.45	1.92
	7	3.00	3.17	2.32	0.00	3.59	5.06	0.00	0.00	0.00	0.08	0.10	1.55	0.00	0.00	0.01	1.49

B

Material	c_L (mmol L^{-1})	As sorption.pH 7 SATURATION INDEX							Cd sorption. pH 5 SATURATION INDEX					Zn sorption. pH 5 SATURATION INDEX			
		Bs	Hn	Mt	Hr	Ns	Py	Rh	Bs	Mt	Ns	Ot	Py	Bs	Mt	Ns	Py
AMO-G1-	0.025	2.63	3.07	2.20	0.00	3.22	4.69	0.00	0.00	0.00	0.00	0.00	1.47	0.00	0.00	0.03	1.51

BC	0.5	2.62	3.06	2.20	0.00	3.21	4.69	0.00	0.00	0.00	0.00	0.00	1.47	0.00	0.00	0.31	1.78
	1	2.62	3.04	2.19	0.00	3.21	4.68	0.00	0.00	0.00	0.00	0.00	1.46	0.00	0.00	0.30	1.77
	2	2.61	2.99	2.18	0.00	3.19	4.67	0.00	0.00	0.00	0.00	0.00	1.45	0.00	0.00	0.29	1.76
	3	2.60	2.96	2.17	0.00	3.18	4.66	0.00	0.00	0.00	0.00	0.00	1.45	0.00	0.00	0.28	1.75
	4	2.59	2.93	2.16	0.00	3.17	4.65	0.00	0.00	0.00	0.00	0.00	1.44	0.00	0.00	0.26	1.74
	5	2.57	2.89	2.14	0.00	3.16	4.64	0.00	0.00	0.00	0.00	0.00	1.43	0.00	0.00	0.25	1.73
	6	2.98	3.27	2.34	0.00	3.57	5.04	0.00	0.00	0.00	0.00	0.00	1.42	0.00	0.00	0.24	1.72
	7	2.97	3.24	2.33	0.00	3.56	5.03	0.00	0.00	0.00	0.00	0.00	1.42	0.00	0.00	0.23	1.70
AMO-S1-BC	0.025	2.28	2.54	1.98	0.00	2.86	4.34	0.00	0.00	0.00	0.39	0.00	1.87	0.00	0.00	0.41	1.88
	0.5	2.27	2.52	1.98	0.00	2.86	4.33	0.00	0.00	0.00	0.39	0.00	1.86	0.00	0.00	0.27	1.75
	1	2.26	2.50	1.97	0.00	2.85	4.33	0.00	0.00	0.00	0.38	0.00	1.86	0.00	0.00	0.27	1.74
	2	2.68	2.89	2.17	0.00	3.27	4.74	0.00	0.00	0.00	0.37	0.00	1.84	0.00	0.00	0.25	1.72
	3	2.67	2.86	2.16	0.00	3.26	4.73	0.00	0.00	0.00	0.36	0.00	1.83	0.00	0.00	0.23	1.71
	4	2.66	2.82	2.15	0.00	3.25	4.72	0.00	0.00	0.00	0.35	0.00	1.82	0.00	0.00	0.22	1.69
	5	3.03	3.17	2.33	0.00	3.62	5.09	0.00	0.00	0.00	0.34	0.00	1.81	0.00	0.00	0.21	1.68
	6	3.02	3.13	2.32	0.00	3.61	5.08	0.00	0.00	0.00	0.33	0.00	1.81	0.00	0.00	0.19	1.67
	7	3.01	3.10	2.31	0.00	3.60	5.07	0.00	0.00	0.00	0.32	0.00	1.80	0.00	0.00	0.18	1.65
AMO-M1-BC	0.025	2.49	3.05	2.16	0.00	3.08	4.55	0.00	0.00	0.00	0.28	0.00	1.75	0.00	0.00	0.32	1.79
	0.5	2.48	3.03	2.16	0.00	3.07	4.54	0.00	0.00	0.00	0.28	0.00	1.75	0.00	0.00	0.16	1.64
	1	2.48	3.02	2.15	0.00	3.06	4.54	0.00	0.00	0.00	0.28	0.00	1.75	0.00	0.00	0.16	1.63

2	2.46	2.97	2.14	0.00	3.05	4.53	0.00	0.00	0.00	0.27	0.00	1.74	0.00	0.00	0.14	1.61
3	2.45	2.94	2.13	0.00	3.04	4.51	0.00	0.00	0.00	0.26	0.00	1.73	0.00	0.00	0.13	1.60
4	2.44	2.90	2.11	0.00	3.03	4.50	0.00	0.00	0.00	0.25	0.00	1.72	0.00	0.00	0.12	1.59
5	2.43	2.87	2.10	0.00	3.02	4.49	0.00	0.00	0.00	0.24	0.00	1.72	0.00	0.00	0.10	1.58
6	2.85	3.26	2.31	0.00	3.44	4.91	0.00	0.00	0.00	0.23	0.00	1.71	0.00	0.00	0.09	1.57
7	2.84	3.23	2.30	0.00	3.43	4.90	0.00	0.00	0.00	0.23	0.00	1.70	0.00	0.00	0.08	1.56

Bs = Birnessite, Hn= Hausmannite, Mt = Manganite, Hr = Manganohornessite, Ns = Nsutite, Ot = Otavite, Py = Pyrolusite
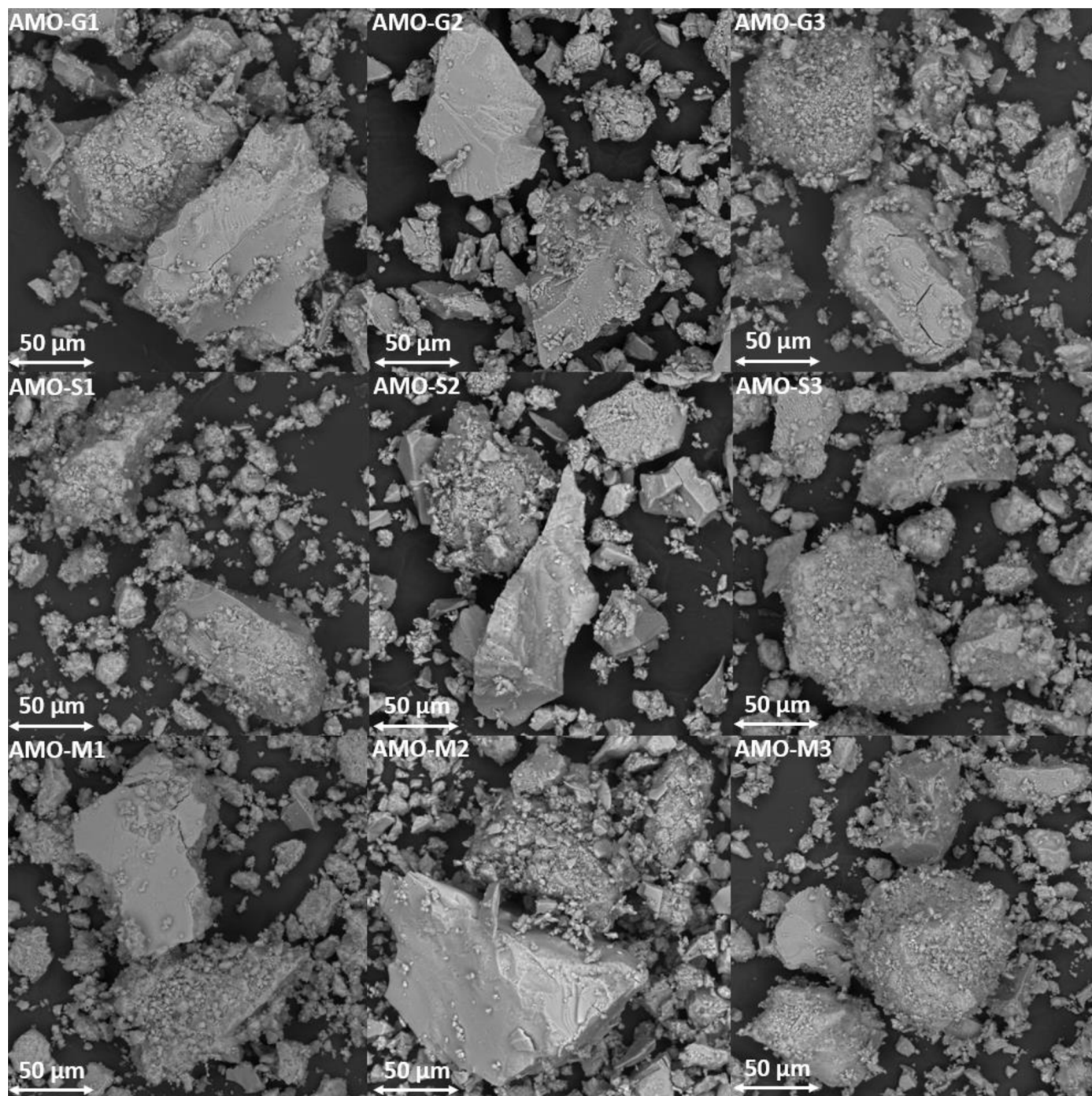
Fig. S1. SEM images of newly synthesized AMOs.
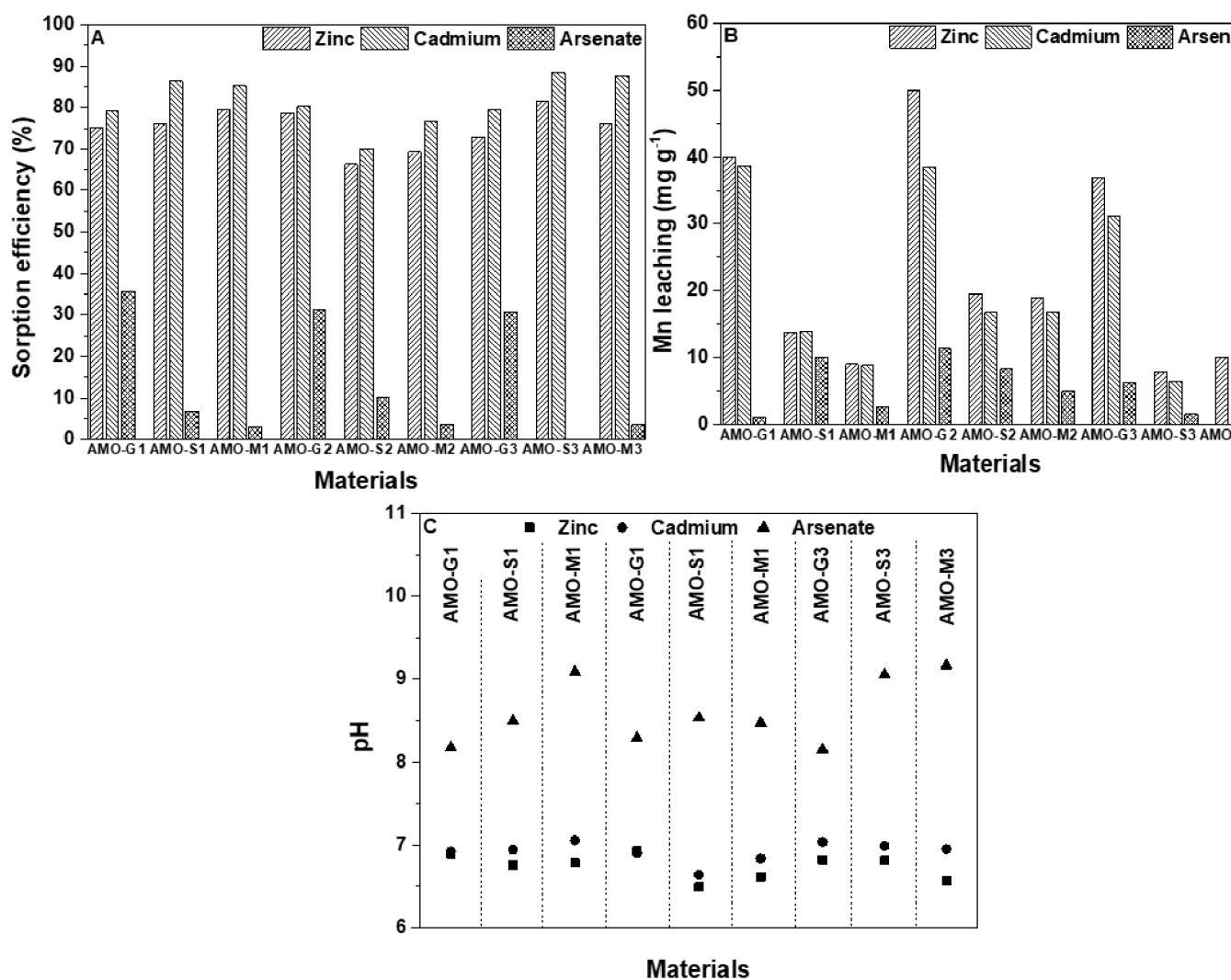
Fig. S2. (A) Sorption efficiencies of newly synthesized AMOs, (B) Mn leaching, and (C) measured pH values.
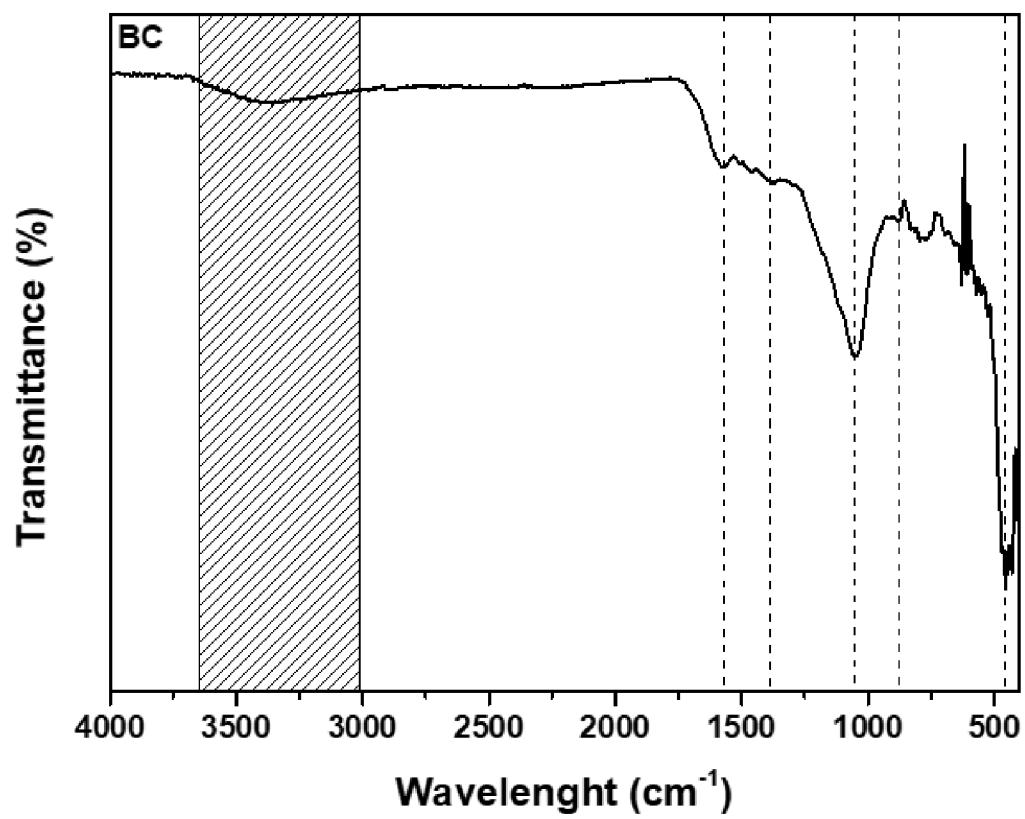
Fig. S3. FTIR spectrum of pristine BC.
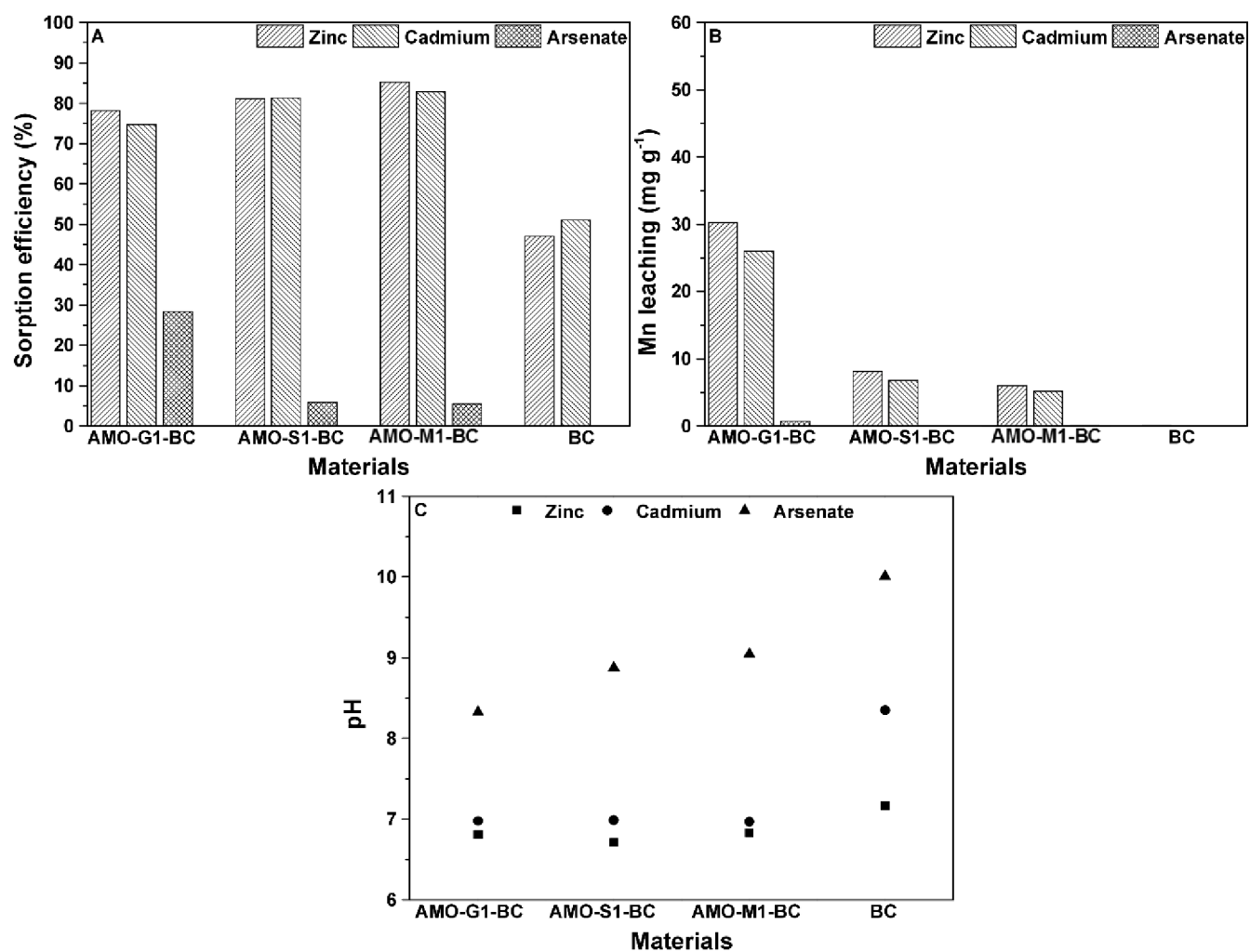
Fig. S4. (A) Sorption efficiencies of pristine BC and AMO/BC composites, (B) Mn leaching, and (C) measured pH values.
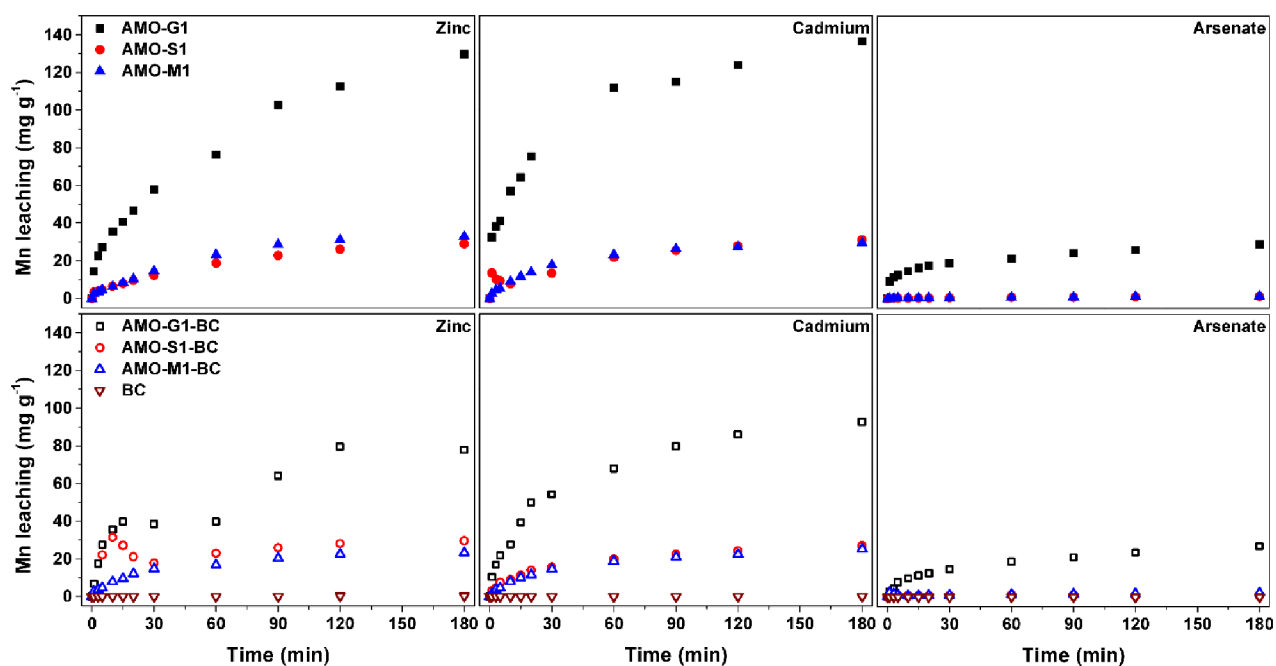
Fig. S5. Mn leaching during metal(loid)s sorption of newly synthesized AMOs, BC, and AMO/BC composites at pH 5 (Zn and Cd) and 7 (As).
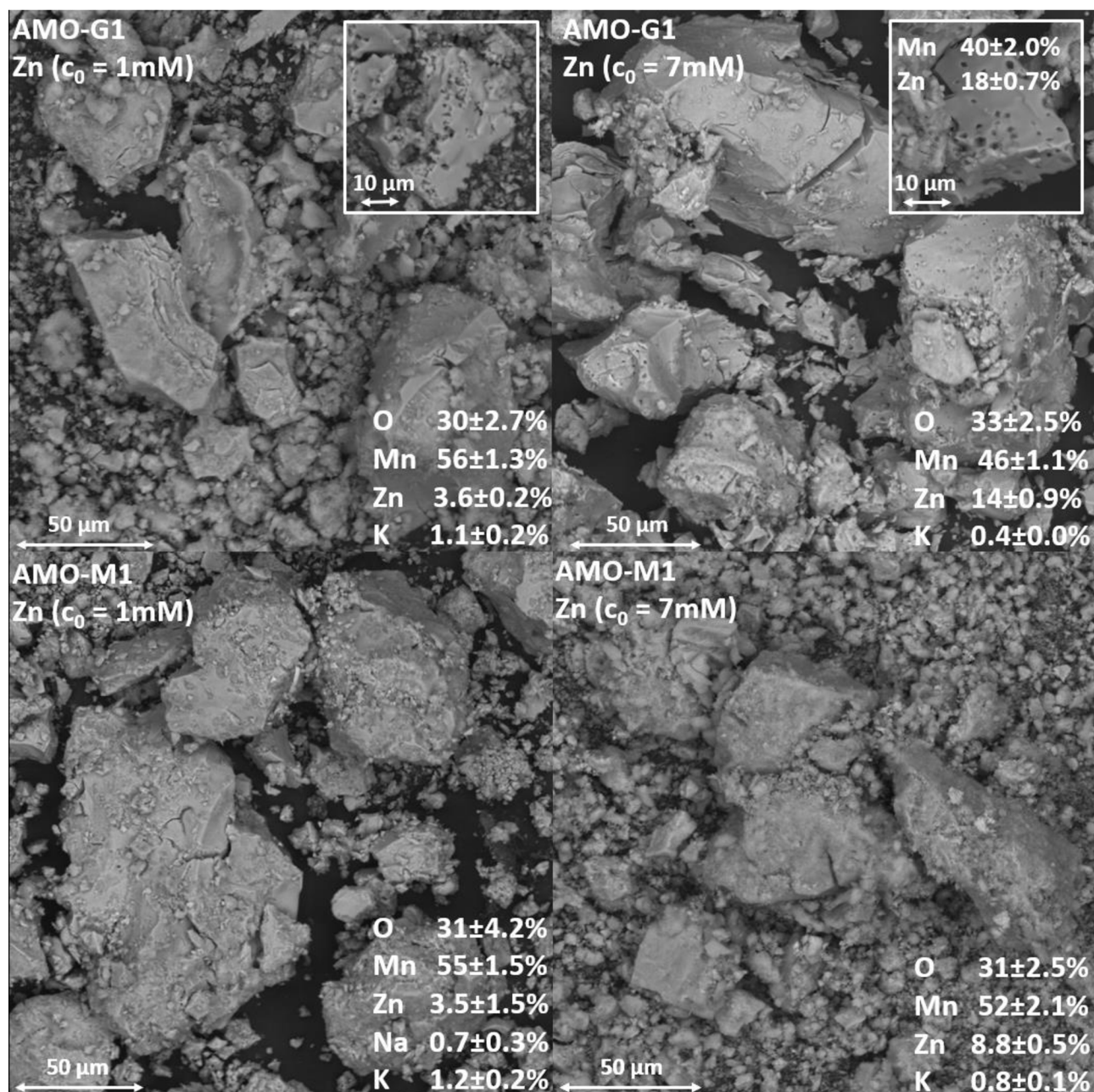
Fig. S6. SEM/EDX of AMO-G1 and AMO-M1 after Zn(II) sorption at concentrations of 1 and 7 mM.
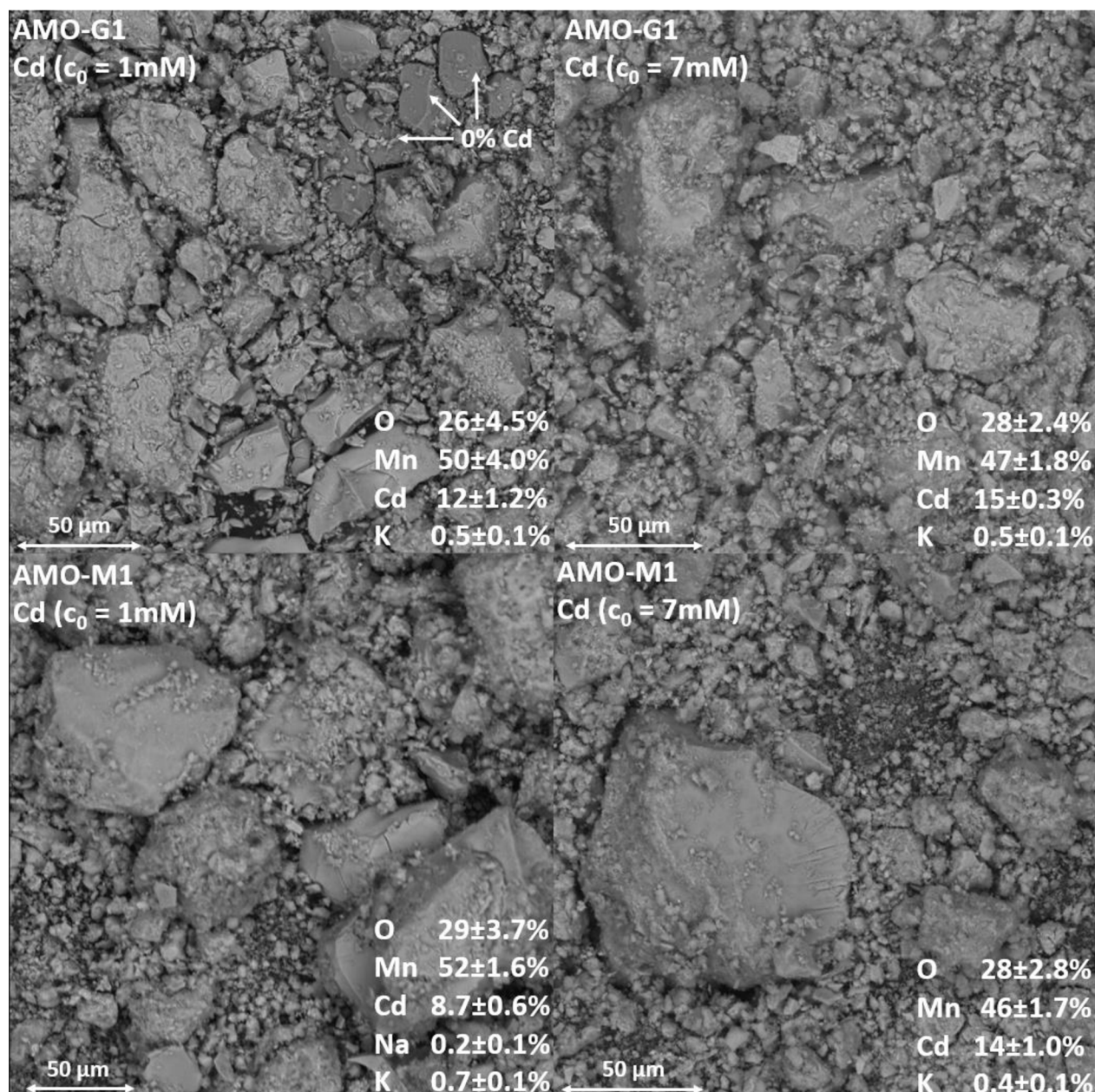
Fig. S7. SEM/EDX of AMO-G1 and AMO-M1 after Cd(II) sorption at concentrations of 1 and 6 mM.
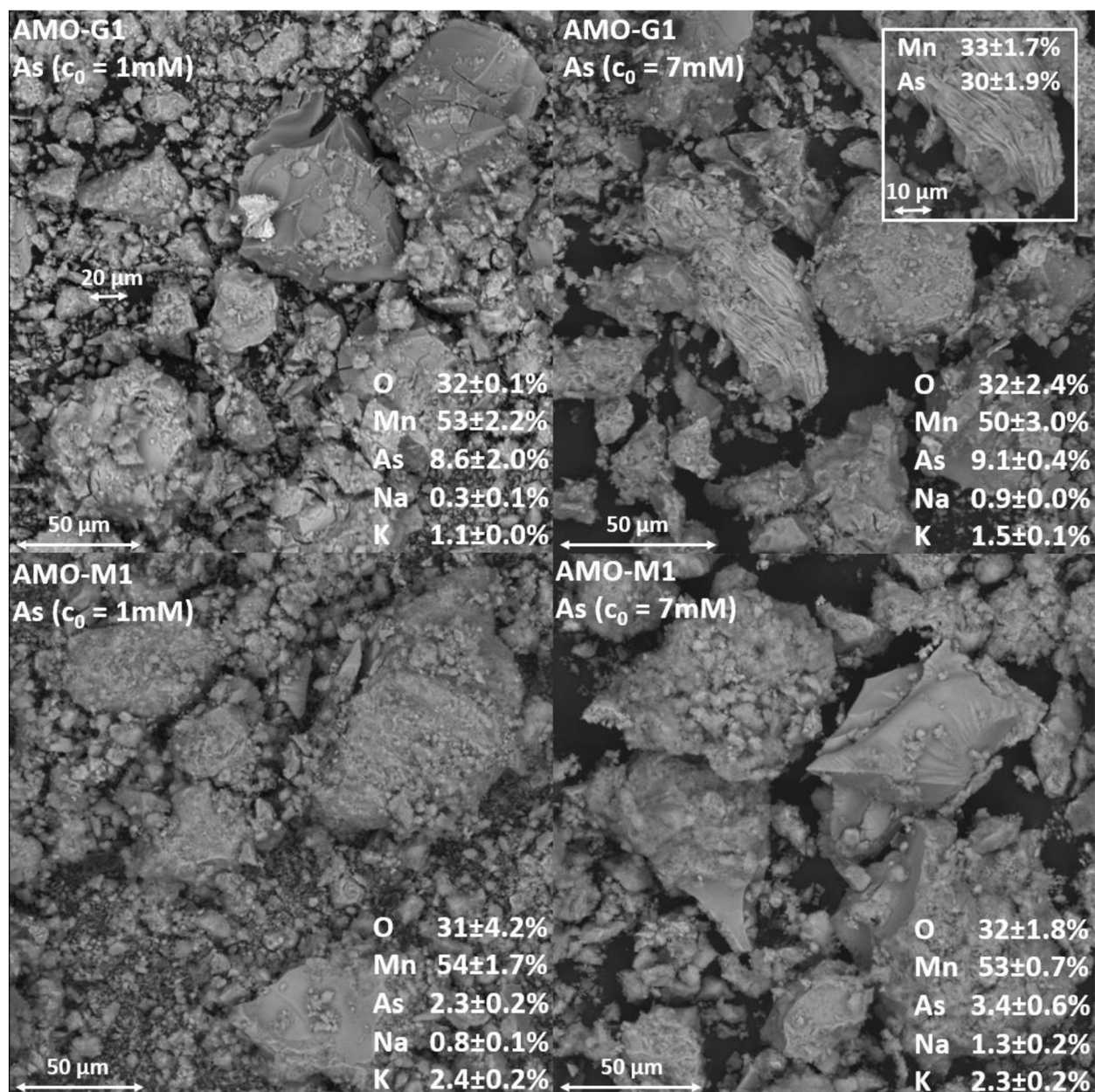
Fig. S8. SEM/EDX of AMO-G1 and AMO-M1 after As(V) sorption at concentrations of 1 and 7 mM.

Chapter V

Modelling transport of Zn and Pb through the soil profile using laboratory columns

Content

Abstract

A comprehensive study was conducted to assess the effect of biochar (BCH) and its modification with manganese oxide (BCH + AMO) as soil amendments in heavily Zn- and Pb-contaminated sandy-loam soil (CONTROL). Firstly, sorption equilibrium batch experiments were conducted to describe basic sorption properties showing high sorption efficiency of both amendments for Zn and Pb. Subsequently, column experiments, which better reflect a dynamic system close to natural conditions, were performed. During column experiments, a synthetic solution of Zn and Pb (single) and their combination Zn + Pb (bimetal) was added to the soil to fully reach the maximum sorption capacity of each material in strongly contaminated soil conditions. Significantly higher sorption efficiency was observed during single metal sorption for all studied material however the sorption of Zn during Zn and Pb competition is low for both materials. Additionally, a leaching test with water and 0.43 M HNO_3 showed significant pH increase (more than 30%), indicating potential use in acidic environments of both amendments. Subsequently, a speciation model in PHREEQC version 2 was constructed to find dominant forms of major elements and the possible precipitation of mineral phases. Finally, the Hydrus 1D model was successfully calibrated, demonstrating that in a well-defined system at a constant pH, even dynamic processes can be partly modelled by a simple equilibrium solute transport model. The measured and simulated data significantly showed an increase in sorption efficiency after adding biochar amendments up to 12 times. A significant reduction of saturated hydraulic conductivity (K_s) and increase in saturated volumetric water content (θ_s) the case of BCH and BCH + AMO was observed.

Introduction

Biochars and manganese oxides have previously been effective agents for removing a wide variety of metal(loid)s from contaminated soils (Komárek et al., 2013b; Gong et al., 2018). Biochar is an inorganic sorbent produced by the thermal decomposition of biomass, such as wood, wheat straw, sewage sludge, and many other sources, under conditions with limited access to oxygen. Biochar is characterized by high efficiency against metals, overall high specific surface area with developed porous structure, and the ability to improve soil properties, such as soil fertility or hydraulic properties (Beesley et al., 2010b; Mohan et al., 2014c). The effect of BCH on soil hydraulic properties was recently studied by Jačka et al. (2018) which proved that hydraulic parameters (K_s, porosity and bulk density) are changed after BCH addition to the soil. Synthetically prepared amorphous manganese oxides (AMO), which can be synthesized using various sugars (e.g., glucose or sucrose), have proven to be highly effective inorganic adsorbents showing high immobilization efficiency against metal(loid)s in both aqueous solutions and contaminated soils (Michálková et al., 2016c; Ouředníček et al., 2019). Because BCH metal(loid) removal efficiency is often limited, especially against anions, mixtures of BCH and AMO and/or synthesized composite materials have recently been (Trakal et al., 2018a; Ouředníček et al., 2019).

Although there are several studies on metal capture using BCH and/or AMO in both aqueous solutions and soils (e.g., adsorption kinetics, isotherms, soil incubation), their main shortcoming is the need for more (BCH) or at least some (AMO) studies in dynamic conditions including development of transport models. To simulate solute transport and geochemical changes, computational programs such as HYDRUS 1D (Šimůnek et al., 2016) or PHREEQC (Parkhurst et al., 2013), can be used. Still, few studies dealing with transport models in the system with biochar have been published. The HYDRUS 1D program has been used to describe remediation of Cr-contaminated ground water and soil using barley grass-based biochar modified with Fe (Chen et al., 2021), soil hydraulic properties and enhancement of nutrient retention by application of woody-based biochar to podzols (Altdorff et al., 2019) or changes in soil water content (SWC) by application of commercial paper fiber sludge/grain husk-based biochar to Alfisols (Horel et al., 2019). The program PHREEQC previously described Hg complexation with dissolved organic matter released from various BCs in water (Xu et al., 2017). Moreover, a combination of HYDRUS 1D and PHREEQC was used to study

the fractionation and leaching of metal(loid)s in metal-contaminated soils with nanobiocomposite of biochar, clays and chitosan (Arabyarmohammadi et al., 2018) or to describe sorption and transport of Cs and Sr in agricultural soils (Luvisol and Cambisol) after application of woody-based biochar (Berns et al., 2018). Although current studies on transport phenomena in an environment with added biochar provide important information, studies involving such a comprehensive approach (batch, columns, speciation, transport) are still insufficient.

To fill the existing research gap, the main objectives of this study were to: (i) perform basic adsorption experiments (kinetics and isotherms) to obtain sorption parameters for subsequent modeling; (ii) construct a soil column experiment to obtain information on leaching and the course of concentrations during column saturation and extraction; (iii) perform model optimization (calibration) in the HYDRUS 1Dprogram; (iv) validate the obtained model. Such a comprehensive approach was used to demonstrate the overall process and final effectiveness of the materials in dynamic soil conditions by the development of a comprehensive transport model with inverse optimization for columns filled with soil and amendments, i.e., BCH or AMO + BCH. The main advantage is the understanding of ongoing processes, which is a necessary step before the application of materials in real technologies to assess both the effectiveness of the materials themselves and the potential risks associated with the possible release of risk elements.

Materials and methods

Soil and amendments

Soil (CONTROL)

Soil for experiments was collected in Trhové Dušníky (**Fig.S. 5-1 B**). The locality is situated approx. 60 km southwest from Prague and historically belonged to an important mining site (**Fig.S. 5-1 B**). From 1786 until the 1970s, a smelter processing Pb and Ag was operated there. During this period, rainfall caused frequent breaches of the tailings dams and massive environmental contamination with Pb, Zn and other metals. After 1972, secondary mined materials were processed there for the production of car batteries(Ettler et al., 2005). The soil samples were taken from the topsoil layer (0 - 25

cm depth), dried to a constant weight and homogenized by sieving on a 2 mm mesh sieve. Physicochemical parameters (structure, bulk density, composition, pH, hydraulic conductivity K_s and soil retention curves) were determined by appropriate laboratory methods (**see page 164**) under constant conditions.

Biochar (BCH)

Biochar was produced at the Institute of Chemical Processes of the CAS by pyrolysis of grape stalks waste at 600 °C. The pyrolyzed product was crushed and sieved to a grain size < 0.5 mm, washed with deionized water (Watek, IWA 120 iol, Czech Republic) and dried at 60 °C according to the methodology described in Trakal et al. (2014c). Physicochemical parameters of the BCH corresponded to the values described for the same BCH type in Trakal et al. (2014c). This type of BCH was chosen because of its better sorption properties compared to BCHs derived from other sources. Subsequently, this material was mixed with the soil (CONTROL) at 2% w/w and the resulting mixture was incubated for 7 days at 80% WHC.

Biochar modified by manganese oxides (BCH + AMO)

Synthetic manganese oxide was prepared by reaction of 0.4M of $KMnO_4$ with 1.4M of glucose (Della Puppa et al., 2013) dried and homogenized by sieving to a grain size < 0.5 mm. Physicochemical parameters were the same as previously obtained for this material by Della Puppa et al. (2013) The synthesized material was mixed with BCH at 1% w/w. The resulting combined material was then mixed with the soil (Control) at 2% w/w and resulting mixture was incubated for 7 days at 80% WHC.

Experimental solutions

All chemicals used in this study were of analytical grade (Lach-Ner, Ltd.) and were used without any other modification. A stock solution of lead nitrate $Pb(NO_3)_2$ **(experiment Pb),** zinc nitrate $Zn(NO_3)_2 4H_2O$ **(experiment Zn)** and their combination **(experiment Zn +Pb)** at concentrations of 12 and 6 mmol/l were prepared using deionized water (0.01 µS/cm) an 0.01 M $NaNO_3$ as a background electrolyte. Solutions of lower concentrations were prepared by dilution of the stock solutions by deionized water (0.01 µS/cm). The pH value of the solutions was adjusted by HNO_3 and NaOH prior to the experiment (0.001, 0.01, 0.1 M).

Experiments

Physical experiments

For determination of soil structure, texture and grain sizes, two methods were used. Firstly, the sieving method (i.e., determination of the sandy soil fraction) and the Casagrande density test (i.e., determination of the fine-grained fraction). For the determination of the elementary content, the total soil decomposition method according to ISO 14869-1 was used. Soil extraction with EDTA was performed to determine the bioavailable fraction of metals and 0.01 M $CaCl_2$ was used as extraction reagent to determine the cation exchange capacity. Total carbon and soil organic carbon were determined using TOC analyzer (Shimadzu TOC-L Series). Soil retention curves were determined according to ISO 11274 and was fitted by van Genuchten model via software RETC (Van Genuchten et al., 1991) to obtain soil retention curve parameters. A laboratory permeameter was used to determine the saturated hydraulic conductivity according to CSN 721020. The calculation of K_s was based on the constant gradient method based on **Eq. 5-1**.

$$K_s = \frac{V_p L_v}{A_v t \Delta H}$$

Eq. 5-1. **K_s calculated according to the constant gradient method**

where A_v is flow area of the soil ring [L^2], L_v is the length of the soil ring [L], V_p is the volume of water flowing through the sample [L^3], t is the time to reach the desired level in the burette [T] and ΔH inner and outer water level differences in the permeameter [L].

Batch experiments

Batch experiments were performed to obtain (ad)sorption parameters of prepared materials (CONTROL, BCH, BCH + AMO) in case of single metal (Zn, Pb) and bimetal (Zn + Pb) synthetic aqueous solutions. Initially, a basic kinetic experiment was conducted to estimate the time to reach the equilibrium time between metal concentrations in the solutions and on the surface of the sorbent materials. 1 g of the given material (CONTROL, BCH, BCH + AMO) and 20 ml of prepared synthetic solution **(experiment Zn, Pb and Zn + Pb)** were added to a laboratory cuvette. Initial concentrations are shown on **Fig.S. 5-2**. The cuvettes were shaken (GFL 3006, Germany) at a constant speed of

200/min under room temperature (Boudesocque et al., 2007). The sampling for subsequent analysis was carried out in time steps of 10', 30', 60', 24 hours and 48 hours. Changes in pH were recorded for all samples (inoLab® pH-meter 7310 WTW,Germany).

Additionally, sorption equilibrium experiments to construct sorption isotherm were performed. To this end, 1 g of experimental material (CONTROL, BCH, BCH + AMO) and 20 ml of prepared synthetic solution **(experiment Zn, Pb and Zn + Pb)** at concentrations of 0.05 - 6 mM were added into a laboratory cuvette (**Fig.S. 5-3**). Sampling for subsequent analysis was carried out after 24 hours according to the equilibrium time obtained from the kinetic experiment. Sample processing was performed as in the case of kinetic experiments. The obtained data were further fitting using the Freudlich and the Langmuir sorption isotherm models. Fitting of measured data was performed using non-linear squares method optimization.

Column experiments

Three cylindrical polycarbonate containers (Čadek, Czech Republic), 15 cm high with an inner diameter of 6 cm, were used for the column experiments (**Fig. 5-1**). Individual columns were filled with untreated soil (CONTROL) and soil with amendments (BCH, BCH + AMO). The prepared columns were irrigated from the top (**Fig. 5-1 a**) at a constant flow rate (36 ml/h) using a peristaltic pump (PCD 82.4 K, Kouřil, Czech Republic). This constant inflow was regularly distributed by "distributor" (**Fig. 5-1 b**) to achieve that the top layer of the column with material was moistened as evenly as possible in order to minimize the preferential flow. The experiment consisted of three parts (**Fig.S. 5-4**), which followed each other smoothly: i) saturation (**Saturation**) of the columns with the given metal solution, (ii) extraction of metals from the soil with 0.01M NaNO$_3$ solution (background electrolyte, **Extraction 1**) and iii) extraction of metals from the soil with 0.43M HNO$_3$ (**Extraction 2**) solution representing the geochemically active form of metals (Tipping et al., 2003). Each part of the experiment lasted 150 h (including 68 hours pause when no flow was realized). Prior to the start of the experiment, the columns were fully saturated with distilled water to reach full saturation. Samples were collected using rhizones (Eijkelkamp, The Netherlands) from the three levels of each column (**Fig. 5-1 c**) in the following time steps: 0.3, 6, 12, 24, 48, 72 and 82 hours from the start of the experiment. The experimental solution that passed through the bottom of the column through a microfilter (50 μm; **Fig. 5-1 d**) was sampled in the following time steps: 6, 12, 24, 48, 72 and 82 hours from the start of the experiment. For all samples, pH (inoLab® pH-meter 7310 WTW, Germany), redox

potential and conductivity (Multi 3420 WTW, Germany) were measured. Concentrations of cations in the collected samples during experiments were analyzed by ICP-OES (Agilent Technologies 720 Series). Anion concentrations were analyzed by HPLC (Dionex ICS-2000, USA) and the total (TC) and total organic carbon (TOC) by TOC-L CPH Analyser (Shimadzu, Japan). In order to be able to compare measured data (in mmol/l), values were recalculated and normalized by the total mass of the material in the column and by the total volume of solution passed through the laboratory column resulting in the normalized extracted amount from the column (N* extracted amount mmol/g).

Breakthrough curves were constructed based on the concentrations of the samples taken at each time step using **Eq. 5-2**. These curves simply express the metal sorption capacity of the given material in dynamic system. The occupancy of the sorption capacity can be expressed by **Eq. 5-2**. If the c/ci ratio is equal to 1, this indicates a situation where the sorption capacity of the material is fully exhausted. For values greater than 1, this indicates desorption. At the end of the experiments, soil samples were collected from each column using a soil rings and the hydraulic conductivity (K_s) was measured following the same procedure as in the case of original bulk soil sample.

a) inflow generated by peristaltic pump

b) „splitter" – regular distribution of inflow

c) (c1-c3)* rhizones used for sampling

d) microfilter

e) outflow from column

f) container (outlfow collection)
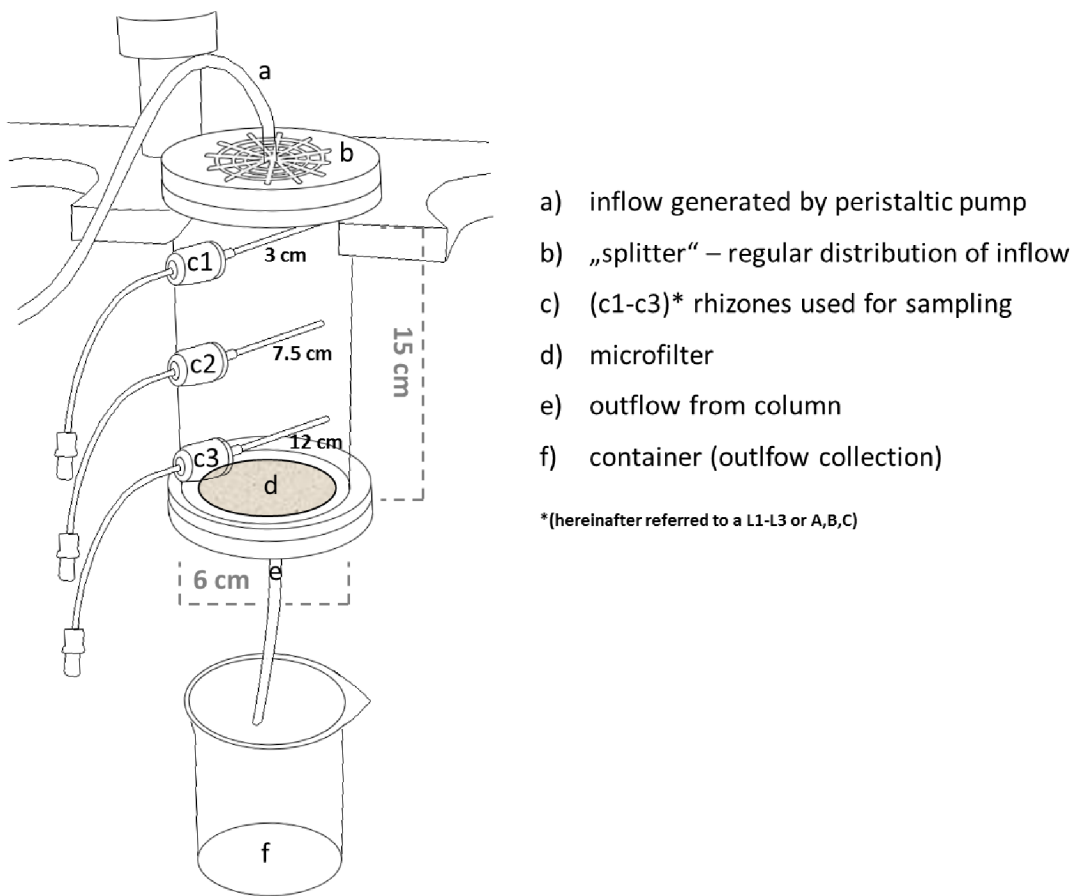
*(hereinafter referred to a L1-L3 or A,B,C)

Fig. 5-1. Scheme of the laboratory column

$$P_t = \frac{c_t}{c_i},$$

Eq. 5-2. **Breakthrough curves ratio calculation**

where c_t is the measured concentration in actual timestep and c_i is an initial concentration of the inflowing solution.

Tracer experiment

At the end of the previous experiment, the sampling rhizones were changed to soil activity probes (same column levels; see **Fig. 5-1**) with logger (Hanna Instruments, USA). First, the column was saturated with deionized water, then 25ml of NaCl tracer at 1M concentration was injected into the top of the column. The column was then continuously washed with deionized water at a constant flow rate of 2.5 ml/min using a peristaltic pump (PCD 31.2, Kouřil, Czech Republic) (**Fig.S. 5-5**). The washing was carried out until the soil activity values at all three levels returned to the initial values, i.e., before the tracer was applied. During this time, changes in soil activity were continuously recorded. In addition, the total amount of water flowing through the column was recorded and the flowing water was sequentially collected in a beaker, where the specific electrical conductivity was measured. In order to convert the measured activity values to tracer concentrations, a calibration was performed. The calibration involved measuring the activities of NaCl solutions at known concentrations $(0.01 - 1$ M in 7 steps) and then constructing plots of concentration versus soil activity and conductance. The relationship between measured NaCl solution activity and real NaCl solution concentration was plotted and fitted by logarithmical trendline model and equation for converting measured activity to concentration was obtained (**Fig.S. 5-6**).

Modelling

The data obtained from the batch (sorption isotherms parameters) and column experiments (measured concentrations in rhizones) were used as inputs for model calibration. The program Hydrus 1D was used for water and solute transport modelling. Dimensions and parameters of experimental column (Fig. 5-1) were used to define a geometry information. Each soil with or without amendment (CONTROL, BCH, BCH + AMO) was considered as a homogeneous matrix with regular capillary pores. A single porosity model with variable saturated hydraulic conductivity based on Van Genuchten – Mualem recalculation was used. Water flow parameters (K_s and θ_s) were optimized by inverse simulation with initial estimates based on the measured column bottom flux. The tortuosity parameter in the conductivity function was used as a default value. Hysteresis in the retention curve was omitted. Atmosperic boundary condition (constant flux 36 ml/h) with surface layer (h= 1) were used as an upper boundary condition. Seepage face (h = 0) was used as a lower boundary condition. The initial boundary condition reflected the full column saturation prior the experiment (h = 0). Standard solute transport equilibrium model (ADE) was used to model solute transport. Longitudinal dispersivity, D_L, was optimized by inverse simulation based on tracer experiment. Diffusion in water and in gas was neglected. The solute reaction parameters K and η were optimized by inverse simulation. The upper boundary condition of concentration flux was selected. The lower boundary condition was selected as the zero concentration gradient.

Speciation model

The measured data of elemental concentrations (cations, anions, TC) and physicochemical parameters (pH, Eh, temperature) recorded during the column experiments were transformed to PHREEQC version 2 data input. Redox potential (Eh) was recalculated to pe which is acceptable for PHREEQC version 2 model based on Eq. 5-3.

$$pe = \frac{Eh\,[V] + U_{ref.}}{0.05916}$$

Eq. 5-3. Recalculation of Eh to pe

where Eh is the measured potential and U_{ref} is the potential of the reference electrode.

Each time step of experiment (**Fig.S. 5-4**) and each observation point (**Fig. 5-1 c**) was considered as a single solution in equilibrium. In total 189 different solutions were modelled using thermodynamic database minteq.v4 (Parkhurst et al., 2013). The prevailing forms of main observed elements in term of speciation were selected. The selection limit was a modelled concentrations equal or higher than 10^{-4} M. Percentages were calculated based on the equation **Eq. 5-4.**

$$\% = \frac{modelled\ concentration\ of\ a\ specie}{total\ concentration\ of\ an\ element} \times 100$$

Eq. 5-4. **Percentage representation of individual species**

Another parameter modelled in this study was the potential precipitation of mineral phases in solution (SI). Positive values of SI indicate oversaturation of the solution with mineral phase and the mineral phase should be present in the solution in the form of crystals or mineral coatings.

Statistical tests and data treatment

Statistical tests were made using Statsoft STATISTICA. In case the normality condition was not met, the non-parametric U-test (Mann-Whitney) was used as a statistical test.

Results and discussions

Physical experiment

The results from soil analyses are given in **Table S. 5-1**. Soil without treatment (CONTROL) can be classified as a sandy loam. Results of the measured bulk density, hydraulic conductivity (K_s) and fitted measured retention curve points are shown in **Table S. 5-2.** A significant decline in the bulk density and hydraulic conductivity was recorded and increase of saturated volumetric moisture content (θ_s) after application of BCH and BCH + AMO was observed.

Reduction in bulk density and soil hydraulic conductivity could be explained by the addition of smaller biochar particles (< 0.50 mm) and above documented swelling which may clog the existing coarser pores and make them finer (Ajayi et al., 2016).

Similar behavior was reported by Barnes et al. (2014), who attributed it to the internal structure of biochar Increase of θ_s can be explained mainly by the increased volume of soil samples and the general ability of natural organic carbon to increase soil water

retention (Rawls et al., 2003).Recorded observation were in agreement with Jačka et al. (2018).

Sorption isotherms

The measured adsorbed amount and the equilibrium concentration in solution was plotted to create sorption isotherms, which can be further fitted by empirical models (e.g., Langmuir and Freundlich isotherm in this study). A graphical representation is shown in **Fig. 5-2**. Obtained parameters after fitting are given in **Table S.5-3.** In case of CONTROL and BCH after bimetal sorption (Zn + Pb) it was not possible to fit the experimental data. In case of CONTROL, only desorption was measured and in the case of BCH the measured data significantly varied and, therefore, the sufficient fitting was not possible. In case of single Zn sorption (**Fig. 5-2 A**), modelled S_{MAX} values of BCH and BCH + AMO are 1.2 and more than 2 times higher compared to CONTROL. However, in the case of single Pb sorption (**Fig. 5-2 B**), modelled S_{MAX} values of CONTROL are high (87 mmol/kg) compared to soils with pure BCH (73 mmol/kg). This could reflect to the fact that untreated soil (CONTROL) contains a high portion of organic matter, which can effectively bind Pb. BCH is still significantly more effective in single Pb sorption experiments compared to CONTROL. Modification of BCH by adding manganese oxides (AMO) enhanced S_{MAX} in the case of Pb sorption showing the highest value compared to the other materials (98.9 mmol/kg). In case of Zn sorption during bimetal sorption (Zn + Pb, **Fig. 5-2 C**), only desorption occurred in the case of CONTROL. Although the adsorbed values of soil with BCH was not able to be fitted by Langmuir model, a significantly higher Zn sorption compared to CONTROL was monitored. In case of Pb sorption in bimetal sorption experiment (Pb + Zn, **Fig. 5-2 D**), only in case of BCH + AMO significantly higher sorption compared to CONTROL was observed. It is influenced mainly by Mn oxides (AMO) which are used in BCH modification and are very effective for sorption of both Zn and Pb as confirmed by numerous studies (e.g., Michálková et al., 2016c, 2017)

However, it needs to be mentioned that the pH value during these equilibrium experiments was not fixed, which means that the sorbed amount of metals can be a sum of both surface precipitation and adsorption. Based on this fact, the sorption parameters (e.g., S_{MAX}) can be higher compared to the values obtained at fixed pH values. On the other hand, this approach can better describe the behavior in real conditions where pH is not controlled as well.
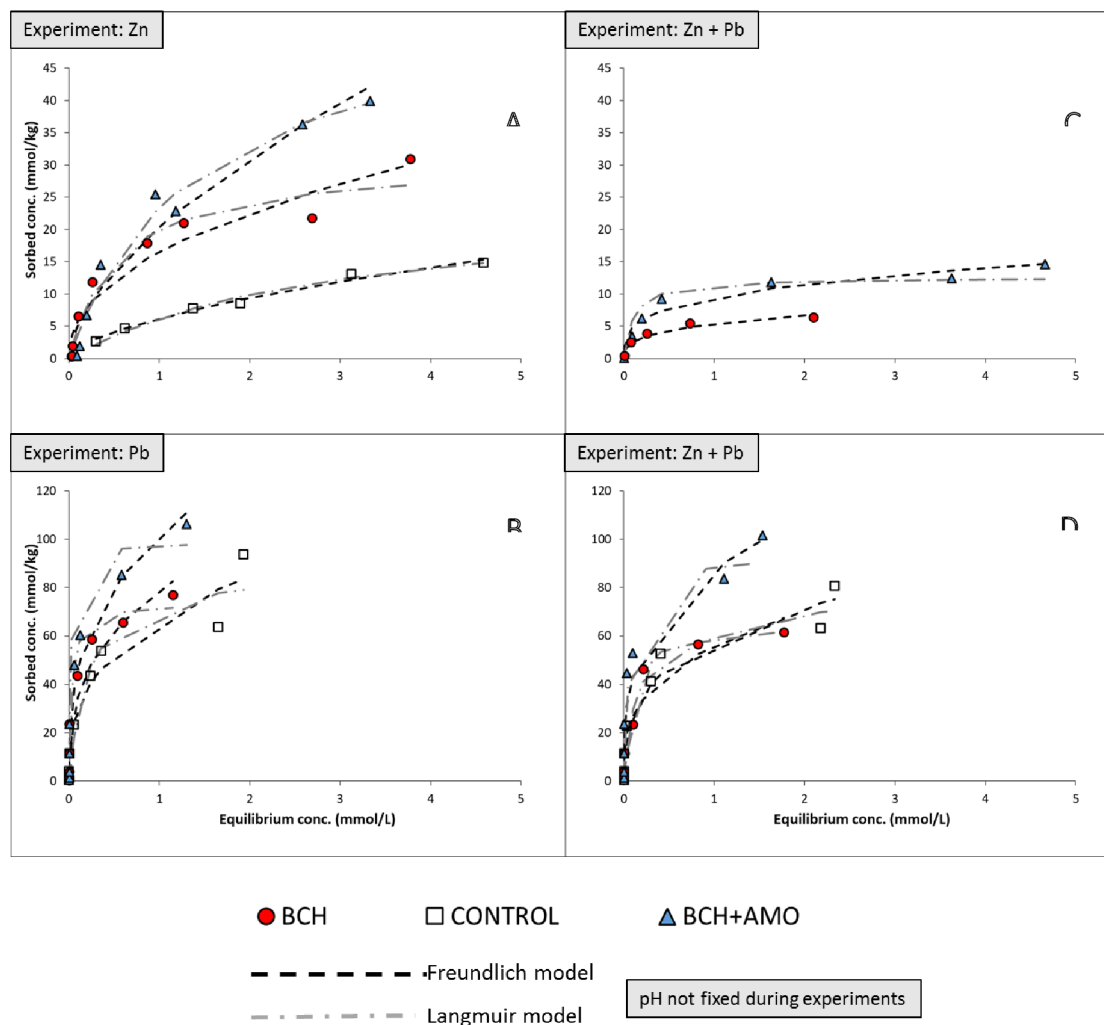
Fig. 5-2. Sorption isotherms

Breakthrough curves

The results of breakthrough curves showed a significant increase of sorption capacity in dynamic system (in columns) in case of both amendments in case of Zn and Pb single metal sorption **Fig. 5-3 A** and **B**, compared to CONTROL. The ratio between initial and final concentration was approx. 12 times lower for BCH and BCH + AMO which tentatively shows that the treated soil can take up metals in much larger quantities and over a more extended period. Moreover, treatment of the soil using BCH + AMO seems to be slightly more effective than BCH in the case of single metal sorption. However, these results are not statistically significant. In case of Zn (**Fig. 5-3 C**) and Pb (**Fig. 5-3 D**) bimetal sorption , soil with BCH and BCH + AMO treatments was significantly more effective in case of Zn bimetal sorption compared to CONTROL and the c/c_i ratio is between 3x (BCH) to 7x (BCH + AMO) lower compared to CONTROL until first 30 hours of the experiment. Afterwards, the measured concentration began to increase rapidly (**Fig. 5-3 C**). This is probably caused due to the higher affinity of Pb, which begins to displace Zn from the sorption sites when most of the sorption sites are already fully occupied could no longer be bound and was released into solution. Similar effect was observed in Chatterjee and Schiewer (2014) during Pb x Cd and Pb x Zn competitive sorption in case of citrus peel used for sorption as organic amendment. Another study confirmed higher affinity of Pb sorption in case of biochar compared Zn during competitive sorption (Esfandiar et al., 2022).

In all bimetal sorption cases, the BCH and BCH + AMO amendments are significantly more efficient in comparison to CONTROL. Moreover, the modification of biochar (BCH) by the addition of AMO (i.e., BCH + AMO) was found to be significantly more effective even compared to pristine BCH.
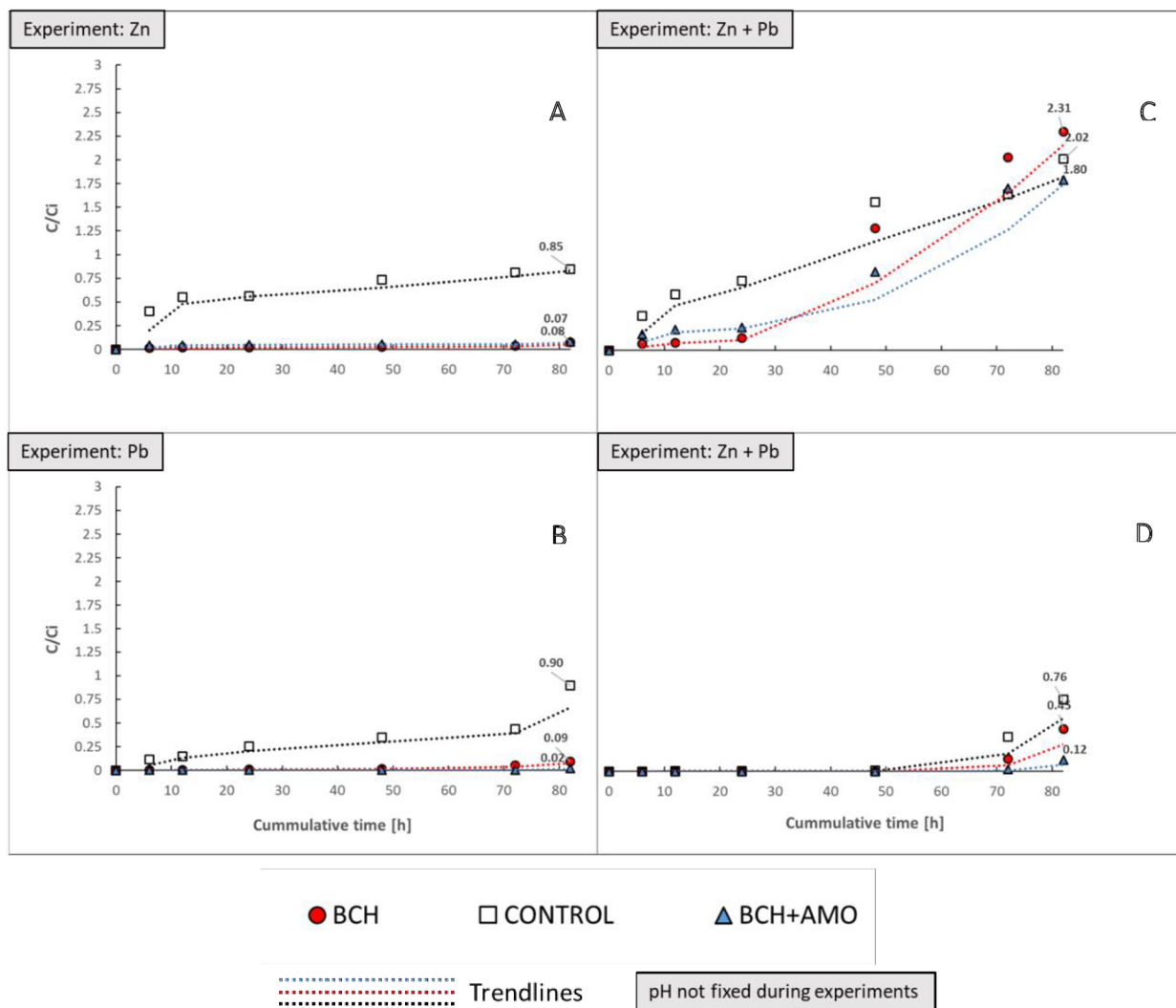
Fig. 5-3. Breakthrough curves during single metal and bimetal column saturation

Leaching from columns

The leaching of Zn and Pb from columns during single metal and bimetal sorption and extraction experiments are shown on **Fig. 5-4.A, B** and **Fig. 5-4.C, D**. Moreover, redox potential and pH trends are shown on **Fig.S. 5-7**, **Fig.S. 5-8** and the leaching of C and Mn during experiments is presented on **Fig.S 5-9** for. Extracted amount of Zn was significantly lower (20x lower) for BCH and BCH + AMO compared to CONTROL during saturation step in the case of Zn in single metal experiment (**Fig. 5-4. A, 0 − 150 hours**) as well as in case of water extraction step (**Fig. 5-4. A, 150 − 300 hours**). During the strong acid extraction step (**Fig 5.4. A-D ,350 − 450 hours**), difference between BCH and CONTROL was not significant. At very low pH values, metals started to be highly mobile and were released from the material. This process was visible after approx. 330 hours when pH dropped. In general, BCH and BCH + AMO significantly increased pH during the whole experiment as natural buffers. However, with prolonged exposure to a strong acid, this effect disappears, and the pH began to drop sharply, leading to the release of most of the adsorbed pollutants. In case of Zn sorption in bimetal experiment (**Fig. 5-4. C**), significant differences among CONTROL, BCH and BCH + AMO were not observed (leaching was lower approximately 1.3 x). This effect is probably related to the high sorption affinity of Pb, which was also observed in sorption batch experiments. A similar trend was observed in case of Pb sorption in single metal and bimetal sorption column experiments (**Fig. 5-4. B**). Amendments (BCH, BCH + AMO) significantly decreased Pb extraction from the columns in case of single (**Fig. 5-4. B**) (more than 40x for BCH + AMO) and bimetals (**Fig. 5-4. D**) sorption experiments (5x lower in case BCH and 10x lower in case of BCH + AMO), but only during saturation and water extraction steps (0 − 300 hours). In case of strong acid extraction (300 − 450 hours) differences were not significant and corresponded to results presented in **Fig. 5-2**. This is probably caused by high organic matter content in the untreated soil (CONTROL), which can adsorb Pb quite effectively in single or bimetal sorption experiments and releasing of C and Mn from material (**Fig.S. 5-9**).

In general, BCH and BCH + AMO significantly decreased Eh compared to CONTROL and increased pH values. In the case of BCH + AMO, the higher pH was probably caused due to proton adsorption on the AMO surfaces and/or proton consumption during the AMO hydrolytic dissolution, leading to acidity buffering effects in the soils (Ettler et al., 2014a). In the case of BCH, the pH increase agreed with Trakal et al. (2014a) and A slightly higher Mn leaching from columns was observed for BCH + AMO compared to

BCH and CONTROL in the case of single Zn sorption experiment, but the difference was not significant during column saturation and water extraction (**Fig.S. 5 9 A, 0 − 300 hours**) which reflects that Mn oxides in BCH + AMO in full saturated conditions are stable. During Pb single metal and bimetal (Pb + Zn) experiment, Mn extraction from columns for BCH + AMO was significantly higher compared to other materials. This process is most likely consisted of several different steps which leads to higher Mn extraction. In part, this process is generated by dissolving pure AMO in aqueous solutions, which corresponds to Ettler et al. (2014a).The of this dissolution increases with decreasing pH. It was observed that the AMO dissolution/transformation also can be responsible for the dissolution of soil organic matter and, subsequently, the dissolved organic carbon dynamics in soils can be strongly affected by the addition of the amendment (Ettler et al., 2014a). Nevertheless, it was significantly observed only in case of BCH + AMO during bimetal (Zn + Pb) sorption experiments in this study (**Fig.S. 5 9 G**).
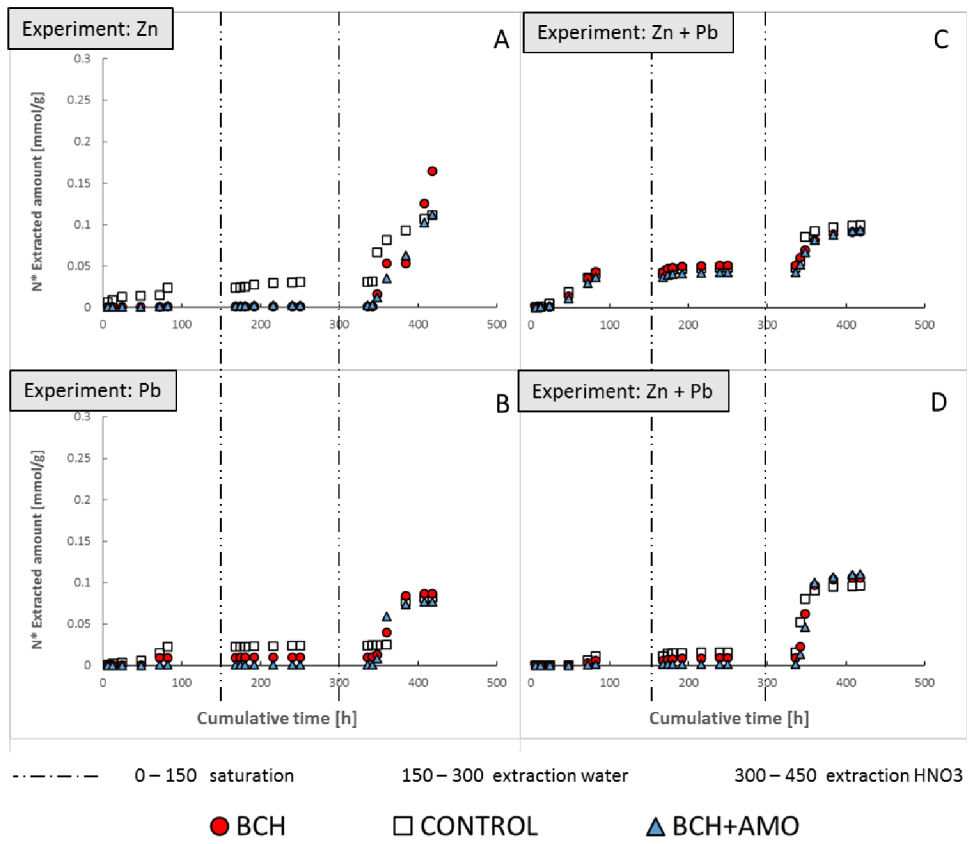
Fig. 5-4- Leaching of Zn and Pb from columns

Geochemical model

Geochemical modeling was used to evaluate the percentage changes of the dominant forms of the major elements in the column experiments (0 - 450 hours) for each horizon L1 – L3 (**Fig. 5-1 c**) for Zn and Pb during single metal experiment (**Fig.S. 5-10, Fig.S. 5-12**) and during bimetal experiments (**Fig.S. 5-14**). The observed trends of these changes were similar for all columns and all materials, and these were strongly correlated by the current pH – Eh conditions. Potential precipitation and a formation of mineral phases in the column experiments (0 - 450 hours) for each horizon L1 – L3 **Fig. 5-1 c**) was expressed on the basis of the saturation indices and can be found in **Fig.S. 5-11** for single Zn sorption experiment, **Fig.S. 5-13** for single Pb sorption experiment and **Fig.S. 5-15** for Zn and Pb bimetal experiment.

In case of BCH + AMO, Mn ions released from material resulted in precipitation of rhodochrosite, hausmannite and bixbyite, which was observed mainly during water extraction (150 – 300 hours). These mineral phases were also present in the first 50 hours of the strong acid extraction (300-350 hours). When the buffer capacity of materials was reached and pH dropped, these mineral phases disappear. During Pb single sorption experiment, mainly goethite and cerussite were formed. The formation of cerussite was significant especially in lower layers (L2, L3) in the case of BCH and BCH + AMO. This was probably caused by a higher available concentration of dissolved carbon, which is released from biochar based materials as presented in Smebye et al. (2016).

In the case of CONTROL, cerussite was not formed due to lower available concentration of dissolved carbon and pH. Adding of Mn oxides to the system (BCH + AMO) led to significant precipitation of bixbyite, hausmannite and rhodochrosite (**Fig.S. 5-15 G-I**).

Reactive Transport model

Results of inverse optimization of soil hydraulic parameters shown in (**Table S. 5-2**). Significant differences were detected between values measured by permeameter (**Table S. 5-2**) and values observed during experiments, especially in the case of BCH and BCH + AMO during Zn experiment. This was probably due to change in soil structure during experiments and extractions. Colombani et al. (2020)proved that soil conditioners as well as other chemical reagents in longer contact with soil during fully

saturation state can cause structural changes (displacement of organic matter, changes in pores structure, etc.). However, such extreme reduction observed in case of BCH during single Zn experiment was not satisfactorily explained. In general, biochar added to the soil (BCH, BCH + AMO) can caused swelling, which is discussed in detail in Jačka et al. (2018). Swelling probably led a reduction in K_s during the experiments for BCH and BCH +AMO compared to CONTROL, but the same dramatic reduction as in the case of BCH and BCH + AMO materials during the Zn experiment was no longer observed. The bottom outflux during the Zn experiment in case BCH and BCH + AMO were objectively observed to be very small due to clogging of the filter by fine particles released from the soil matrix. However, the same effect was not observed in other experiments.

For determination of longitudinal dispersion, inverse fitting of measured tracer concentration was performed (**Fig.S. 5-16**).

Optimized value was 0.549 cm. Parameters of Freundlich sorption isotherm were optimized by model based on bottom cumulative solute flux. In the last part of the experiment, calibration of solute flux parameters was performed. Results of calibration are shown on **Table S. 5-5.**

Surprisingly significant differences were not observed in quality comparison of fitting (based on R^2 coefficient) between single and bimetal sorption data. However only observation point A was able to fit properly. Other observation points (B,C) were fitted poorly and are not presented. This is probably due to the small distance of the upper edge of the experimental column (upper boundary conditions). In this case, pseudo-equilibrium can also occur in a non-equilibrium system. As the distance from the upper edge increases, the heterogeneity of the system increases and the state ceases to be in pseudo-equilibrium. Another phenomenon that must be taken into account is the dynamics of the process (here referred to as sorption), which is only described by a simplified model of the equilibrium sorption isotherm and is only valid within a constant pH value and does not account for other processes (such as cation exchange, surface sorption, chemisorption, surface complexation, etc...), which, however, apply to a large extent in the case of biochar based amendments (Ambaye et al., 2021).

The results of this study are remarkable because few similar studies have been reported. Most studies are focused mainly on water flux parameters and soil hydraulic parameters. WU et al. (2019) successfully validated HYDRUS 1D model for biochar applied to soil, but only hydraulic parameters were presented. The similar concept can be found in Altdorff et al. (2019) and Horel et al. (2019). Chen et al. (2021) used

HYDRUS 1D to predict long-term stability of immobilized Cr in soil in the case of biochar modified by Fe oxides. However, the calibration of the model is missing in their study. Focusing on modelling of metal and metalloid transport in biochar-treated soils, geochemical modelling using the PHREEQC program has been commonly used (Arabyarmohammadi et al., 2018; Berns et al., 2018; Liu et al., 2019). Although PHREEQC can simulate speciations and changes in chemistry precisely, it has only limited capabilities to model transport processes (Parkhurst et al., 2013).

In general, results of this study confirmed that it is possible to successfully calibrate the model even with ordinary equilibrium sorption isotherm data, which was not expected in a dynamic system. However, it is necessary to have valid and precise calibration data for both water and solute flux. Obtaining these datasets is relatively easy, but the model will only work under certain assumptions. The porous environment was almost homogeneous, with very low longitudinal dispersion and fully saturated. Thus, it is not possible to simply apply obtained parameters to a different computational domain, which will be different in geometry, degree of heterogeneity and with differently defined boundary conditions. In this experiment, no vegetation was considered on the surface or inside the column. Only the saturation branch (c_{Pb} = 12 mM, c_{Zn} = 6 mM) and the water extraction branch (c_{ext} = 0) could be successfully simulated by the model. In case of acid extraction physicochemical parameters were changed and model was not effective. Finally, the model was calibrated only in the pH ranges close to the natural values of the materials and the sorption parameters were measured at constant temperature and pH, as these parameters were obtained from the sorption isotherm measured using batch experiments.

The observed shortcomings of this model may be solved by coupling HYDRUS transport model and the PHREEQC speciation model. Within this coupling, the transport equation is solved in HYDRUS and developed for each component defined within PHREEQC, which can be done within HP1 (Steefel et al., 2015). A universal model of surface sorption onto biochar can then be implemented using WHAM VII (Golui et al., 2020). However, this approach requires much more complex data. Future studies should be focused on this comprehensive approach in order to concisely describe all ongoing processes, even under different environmental conditions.
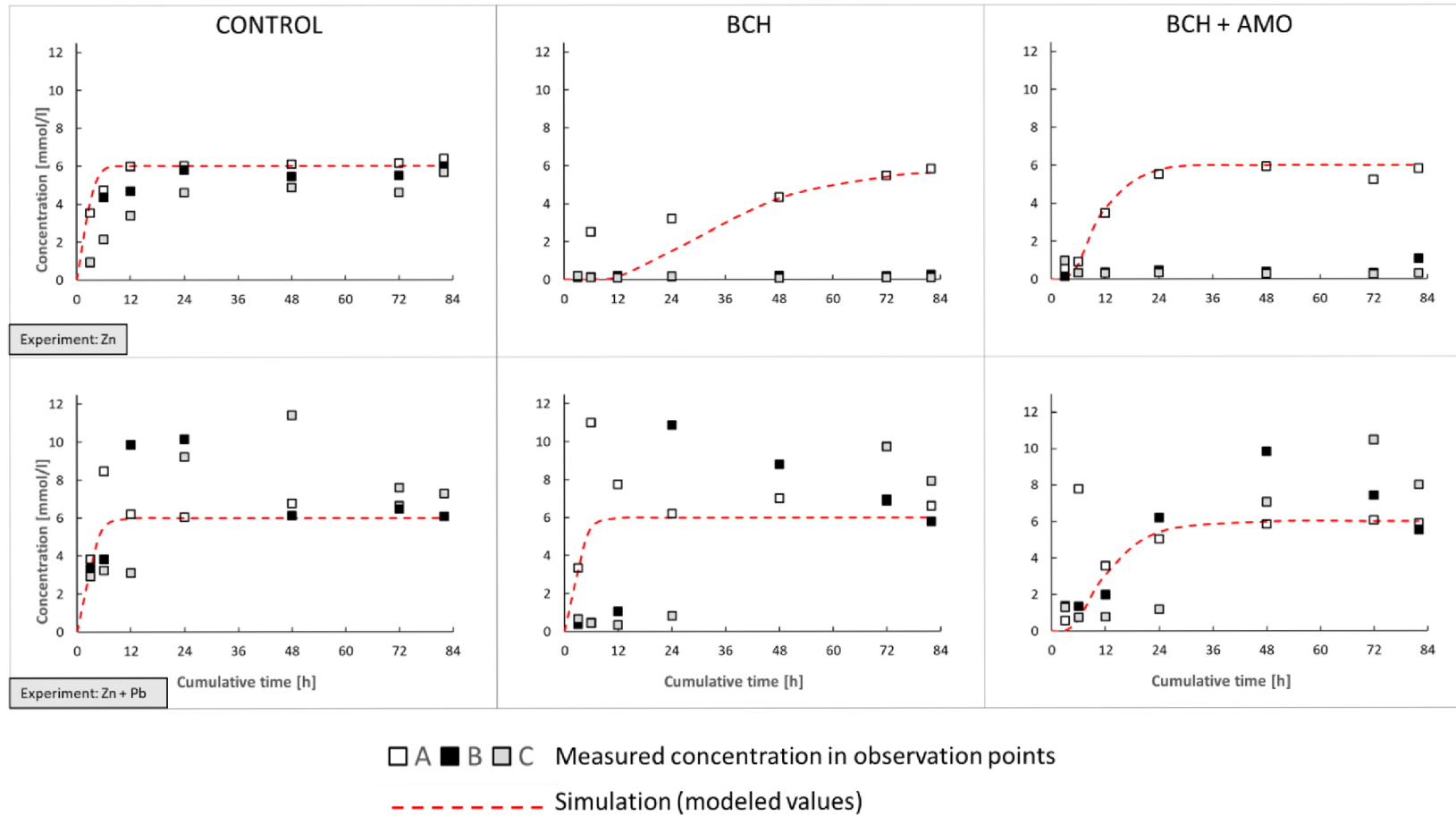
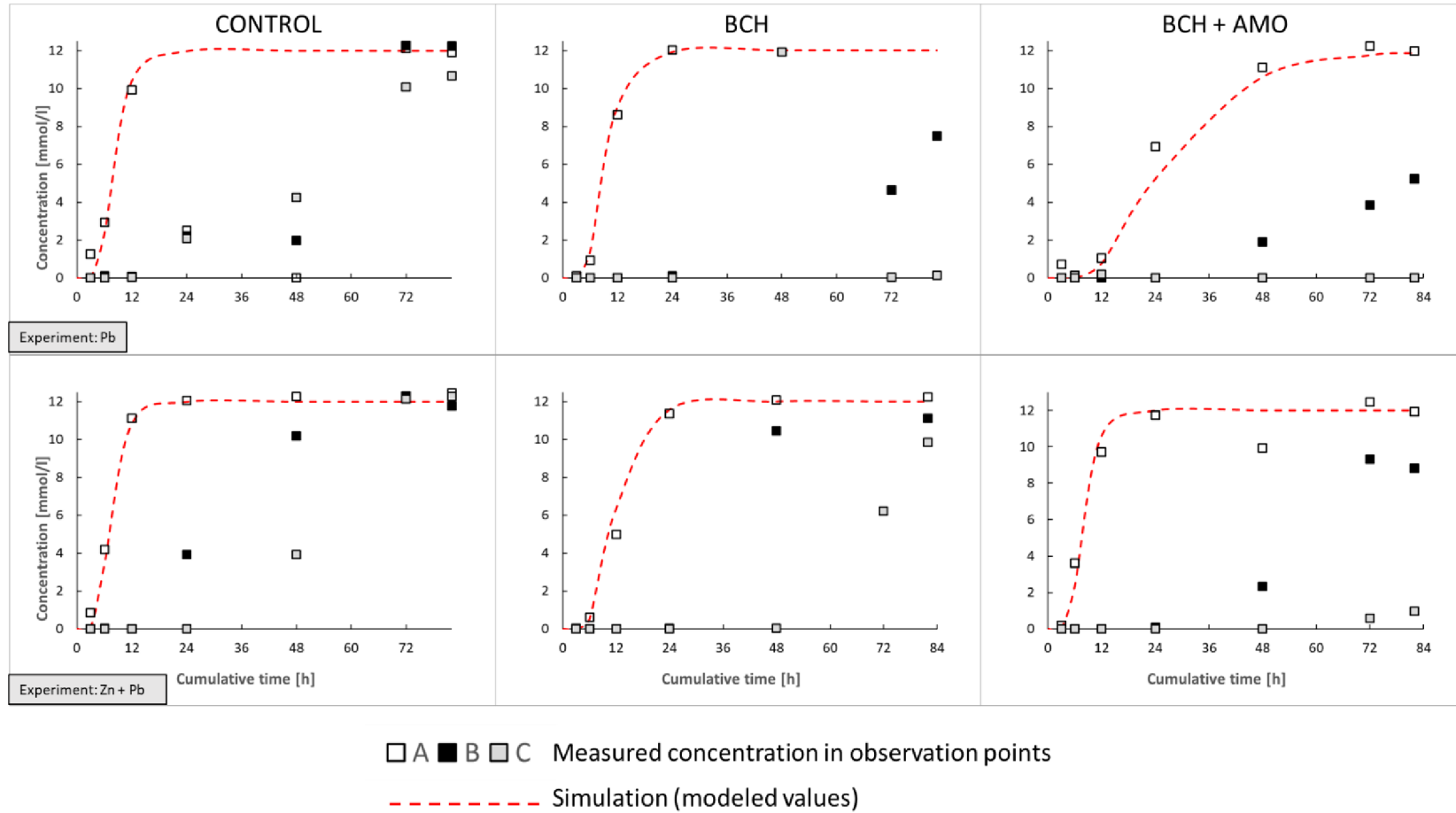Fig. 5-5 Model calibration, Zn single and bimetal (Zn x Pb) sorption

Fig. 5-6 Model calibration, Pb single and bimetal (Pb x Zn) sorption

Conclusion

In this study, the use of biochar and its modification with amorphous manganese oxides in a heavily Zn- and Pb-contaminated sandy loam soil was studied. Both batch equilibrium and dynamic column experiments showed a significant increase in sorption efficiency in the case of single sorption and bimetal sorption after soil amendments application. Similar trends were observed in the dynamic column experiments, where the leaching of both metals Zn and Pb was significantly reduced in the amendment treated soils. In the case of biochar and amorphous manganese oxide mixture, a decline in the leaching of pollutants from the column was significantly higher. The geochemical model pointed to possible precipitation of manganese mineral phases, which is based on the dissolution of Mn oxides contained in the biochar and amorphous manganese oxide modification. The study demonstrated the effectiveness of biochar and its modification on the sorption of the studied metals. Furthermore, a significant reduction in hydraulic conductivity using biochar was demonstrated. The study also showed the possibility to calibrate the Hydrus1D transport model under conditions close to natural pH at equilibrium and also that metal sorption (in both single and bimetallic systems) can be subsequently modeled using only the basic advection-dispersion model. However, it is not possible to perform simulations under different eh - pH conditions using the presented model, or to study individual changes in chemical reactions during transport. For more detailed study of these processes, a coupling of Hydrus-1D and PHREEQC using a proper surface sorption and complexation model performed by HP1 with implemented WHAM VII model will be necessary.
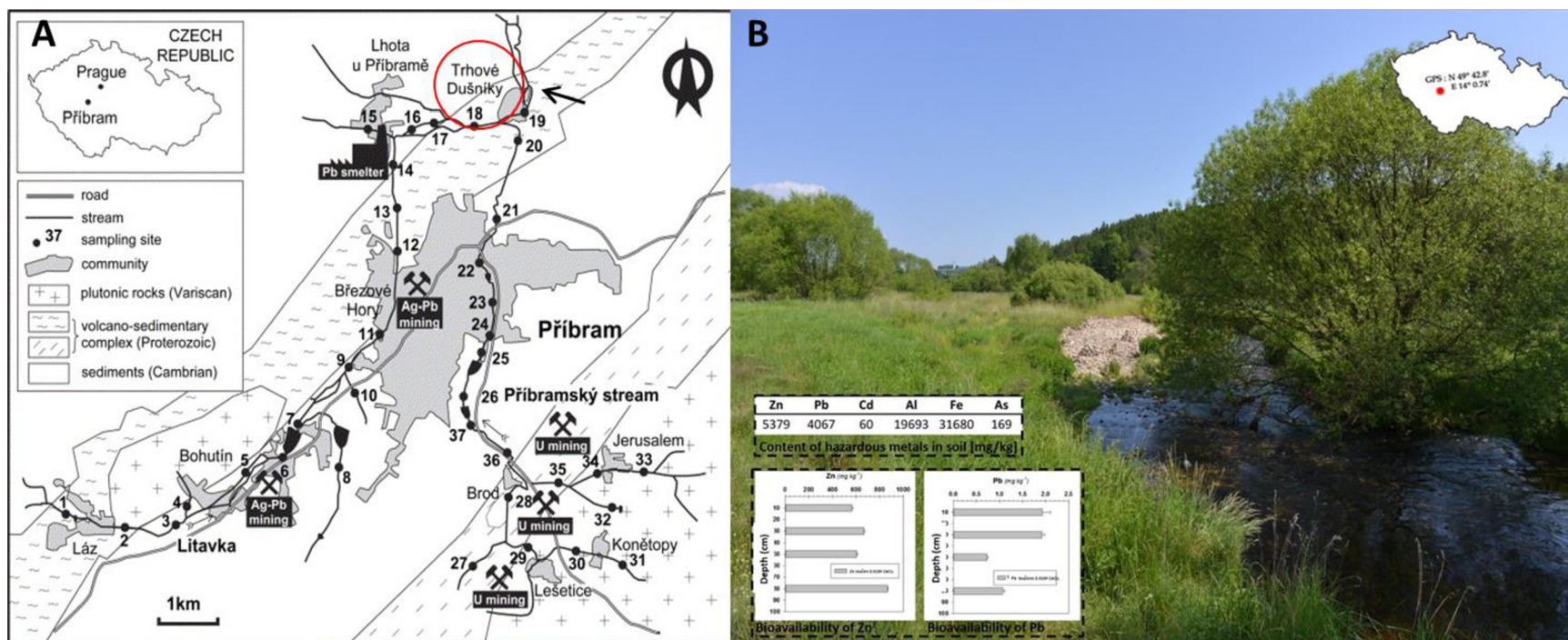
Supplementary material

Fig.S. 5-1 Sampling site. A- Graphic based on Ettler et al. 2006. B -Photography

Basic kinetic experiments

Solution	Initial concentration (mmol/l)
Experiment: Zn	0.2
Experiment: Pb	1
Experiment: Zn + Pb	0.5

Fig.S. 5-2 Initial solution concentrations used for kinetic experiments

Sorption isotherm

Solution	Concentration range (mmol/l)
Experiment: Zn	
Experiment: Pb	0.5 - 6
Experiment: Zn + Pb	

Fig.S. 5-3 Concentration range used for isotherm experiment

Column experiments

Inflow solution concentration and time

Solution	Saturation	Pause(no flow)	Extraction 1	Pause(no flow)	Extraction 2
Experiment: Zn	6 mM 0 − 82 h	68 h	0.01 M 150 - 232 h	68 h	0.43 M 300 - 382 h
Experiment: Pb	12 mM 0 − 82 h	68 h	0.01 M 150 - 232 h	68 h	0.43 M 300 - 382 h
Experiment: Zn + Pb	6 + 12 mM 0 − 82 h	68 h	0.01 M 150 - 232 h	68 h	0.43 M 300 - 382 h

Fig.S. 5-4 Scheme of column experiment time and concentrations

Column experiment - tracer test

Solution	Solution concentration (mmol/l)	Time [h]	Volumetric flux [ml/h]
Pure water	0	until saturation	60
NaCl	1000	start - 0.16	150
Pure water	0	0.16 - 180	150

Fig.S. 5-5 Experimental scheme of tracer test
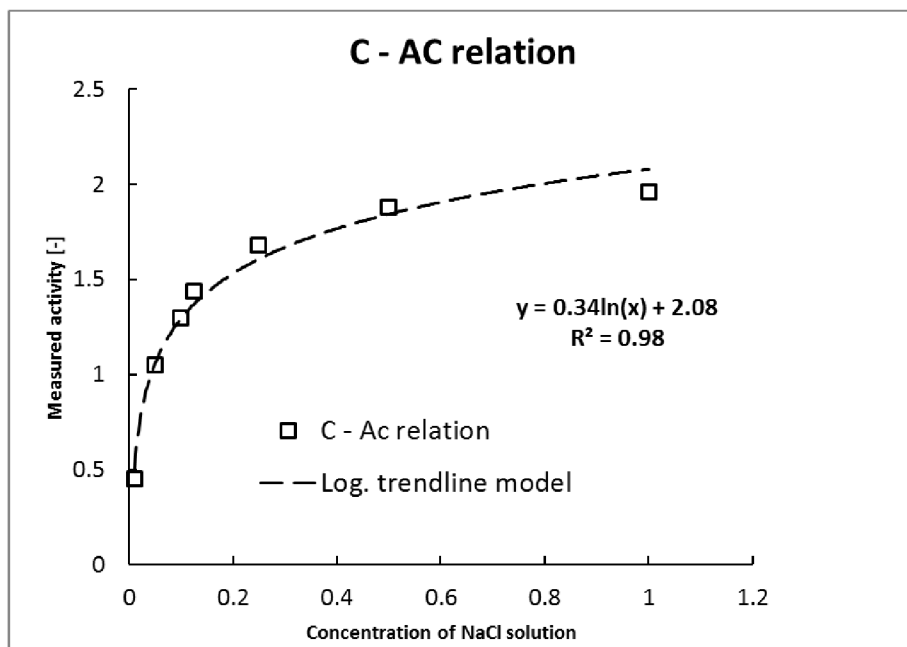
Fig.S. 5-6 Measured activities to concentrations conversion

Table S. 5-1 **Particle size distribution and soil classification**

Particle size distribution

sand	75%
silt	20%
clay	5%

<u>Loamy sand - sandy loam</u>

Table S. 5-2 Measured Soil hydraulic parameters

	measured values		van Genuchten fitting		
Material	Bulk density [g/cm3]	K_s [cm/h]	θ_s [-] * 100	α [1/cm]	n [-]
CONTROL	1.14 ± 0.01	1.43 ± 0.13	50.54	0.033	1.28
BCH	1.11 ± 0.08	1.29 ± 0.22	51.08	0.034	1.31
BCH + AMO	1.13 ± 0.03	1.34 ± 0.15	58.22	0.067	1.39

Cummulative leaching of Zn
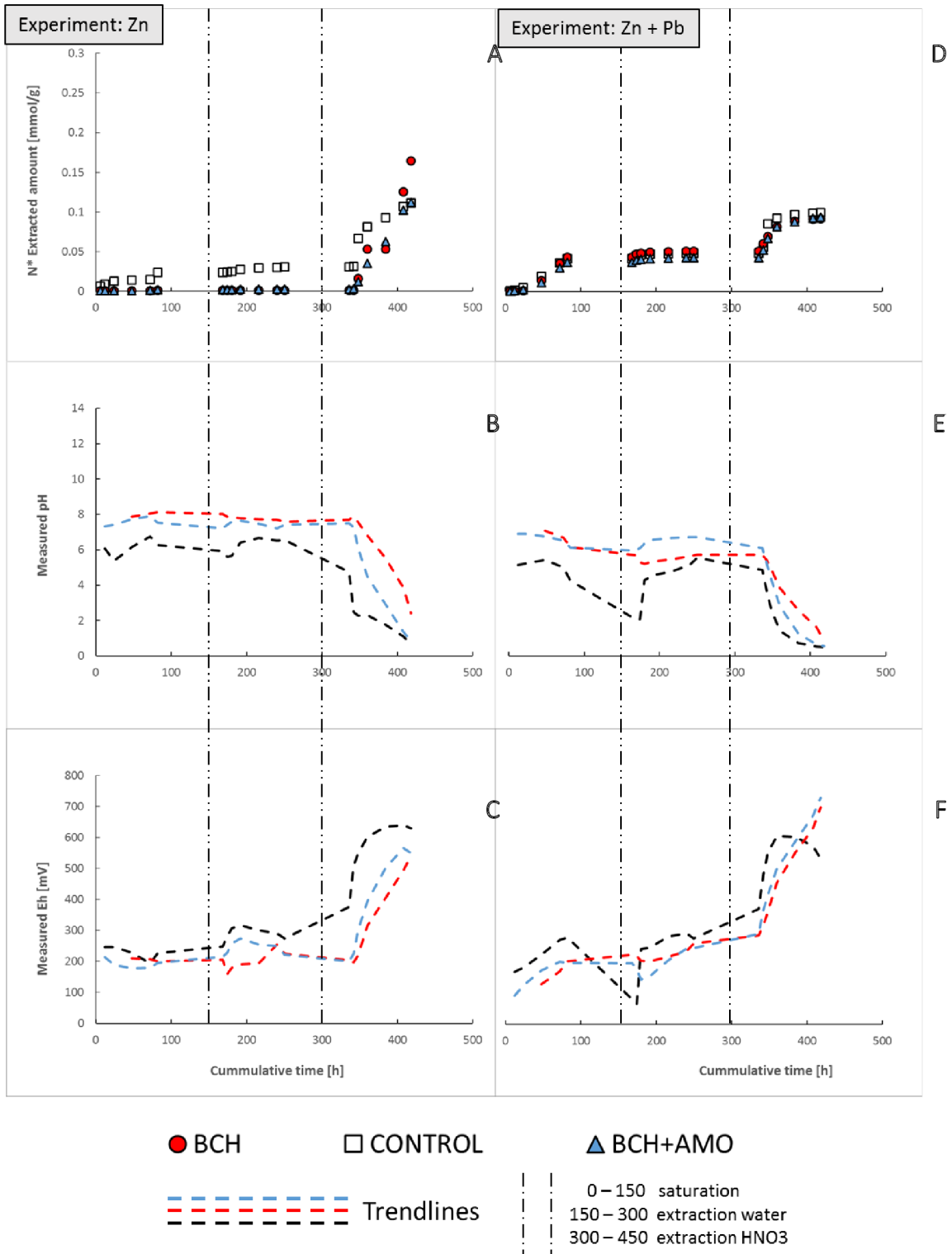
Fig.S. 5-7 Leaching of Zn from columns during experiment

Cummulative leaching of Pb
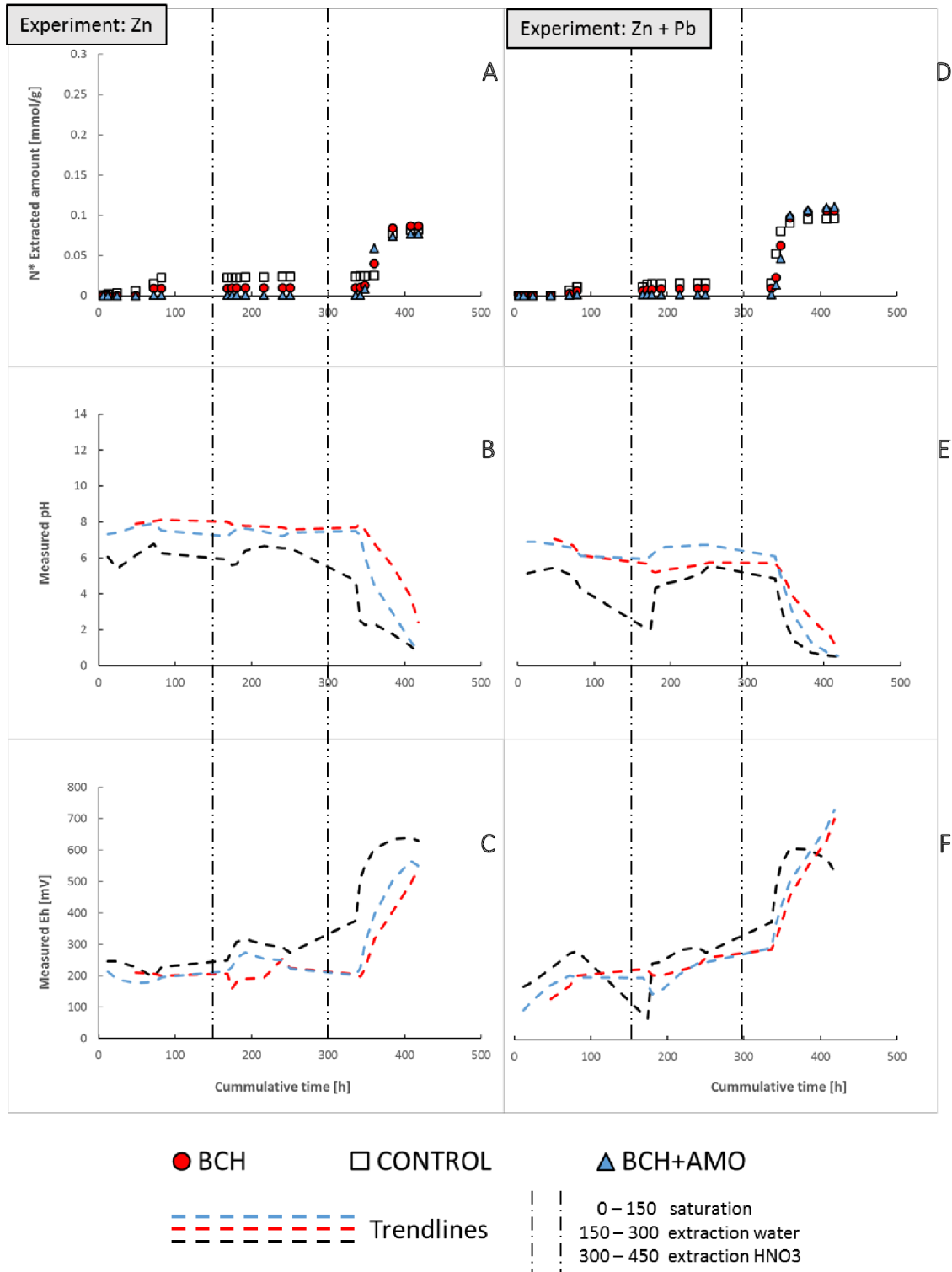
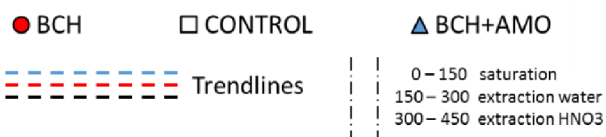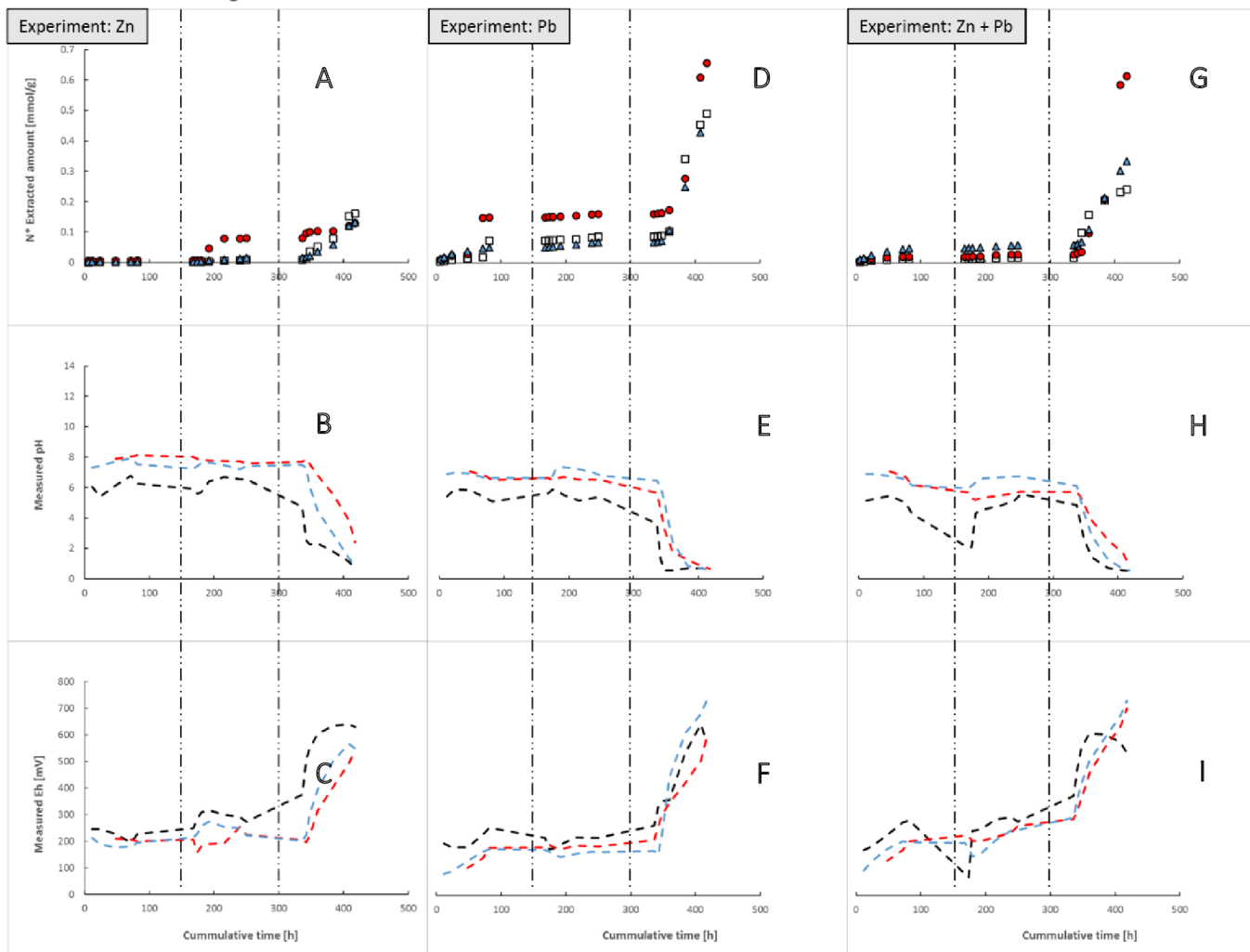Fig.S. 5-8 Leaching of Pb from columns during experiment

Table S.5-3 Modelled sorption parameters

Material	Metal	Freundlich model			Langmuir model		
		K_F [(mmol/kg^{-1})(l mmol)$^{1/\beta}$]	β[-]	R^2	K_L [l/kg]	S_{MAX} [mmol/kg]	R^2
Control	Zn (single)	6.24	0.590	0.98	0.344	24.28	0.98
	Zn (bimetal Zn x Pb)	**not fitted**			**not fitted**		
	Pb (single)	66.58	0.346	0.94	4.753	87.67	0.93
	Pb(bimetal Pb x Zn)	58.05	0.305	0.95	6.080	75.24	0.93
BCH	Zn (single)	16.56	0.449	0.92	1.836	30.75	0.95
	Zn (bimetal Zn x Pb)	5.41	0.318	0.93	**not fitted**		
	Pb (single)	78.76	0.347	0.90	31.656	73.60	0.93
	Pb(bimetal Pb x Zn)	56.00	0.326	0.91	7.725	66.23	0.96
BCH + AMO	Zn (single)	20.39	0.603	0.94	0.704	56.51	0.97
	Zn (bimetal Zn x Pb)	9.48	0.282	0.94	9.244	12.59	0.90
	Pb (single)	101.56	0.338	0.94	56.167	98.92	0.94
	Pb(bimetal Pb x Zn)	87.50	0.305	0.91	16.493	93.67	0.93

Table S. 5-4 Measured and optimized K_s [cm/h]

	CONTROL			BCH			BCH + AMO		
	measured	optimized	R2	measured	optimized	R2	measured	optimized	R2
Experiment: Zn	3.352	2.500	0.92	2.020	0.074	0.85	2.691	1.660	0.92
Experiment: Pb	3.380	2.498	0.89	2.123	2.115	0.81	2.792	2.310	0.89
Experiment: Zn + Pb	3.334	2.585	0.93	2.141	2.322	0.81	2.741	2.521	0.89

Cummulative leaching of C
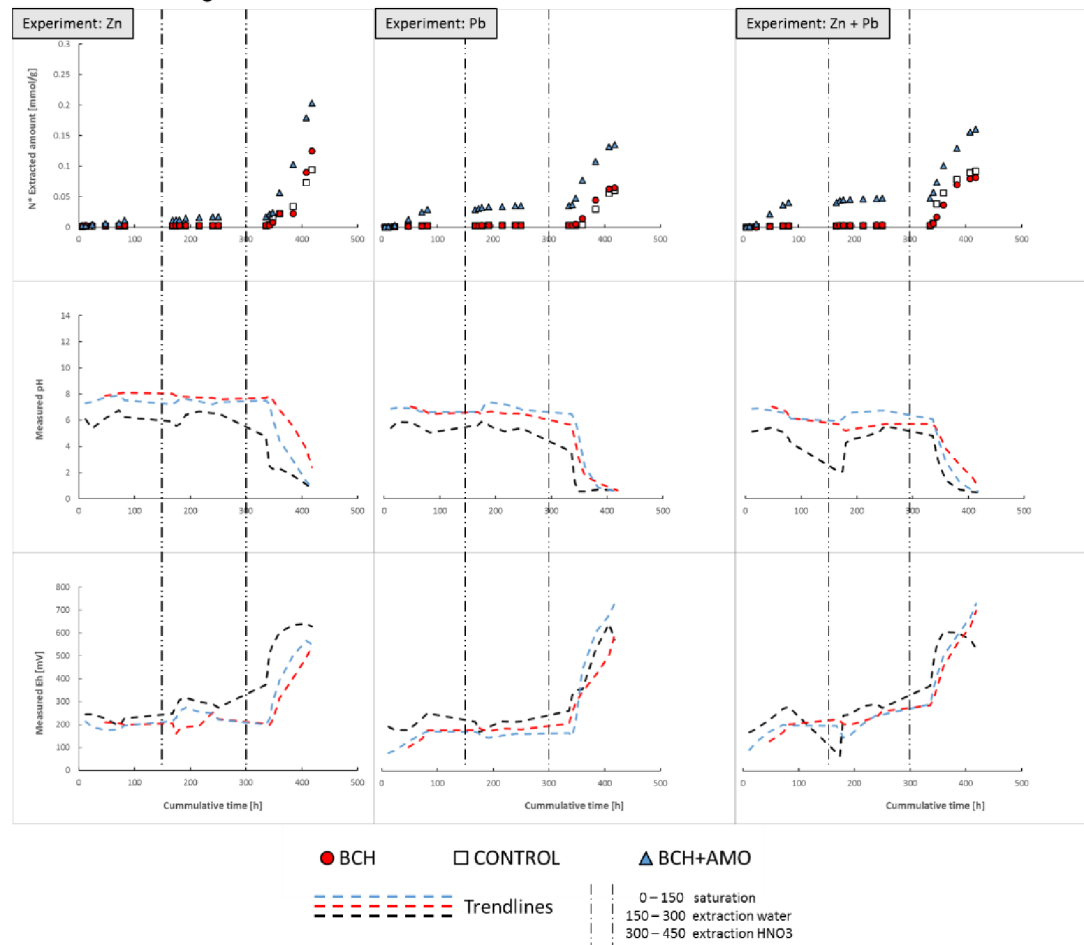
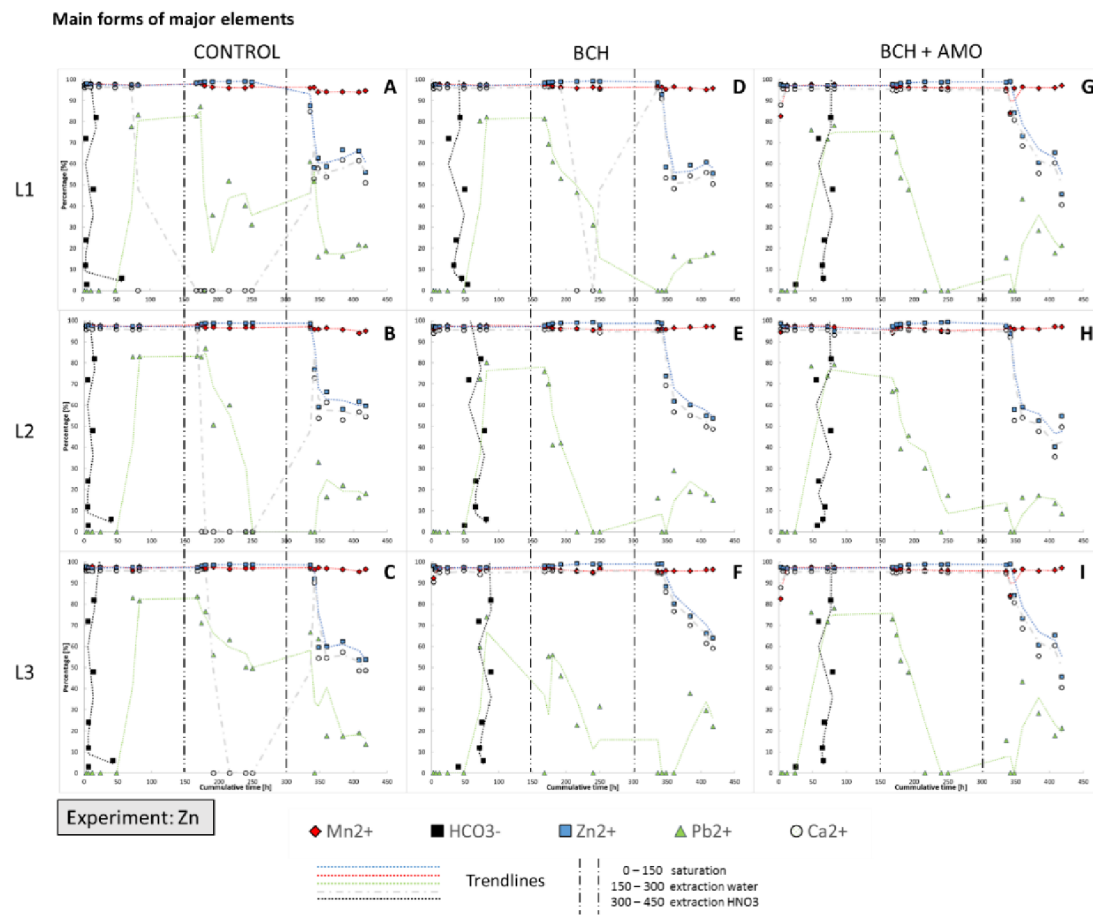**Fig.S. 5-9** Leaching of Mn from columns during experiment

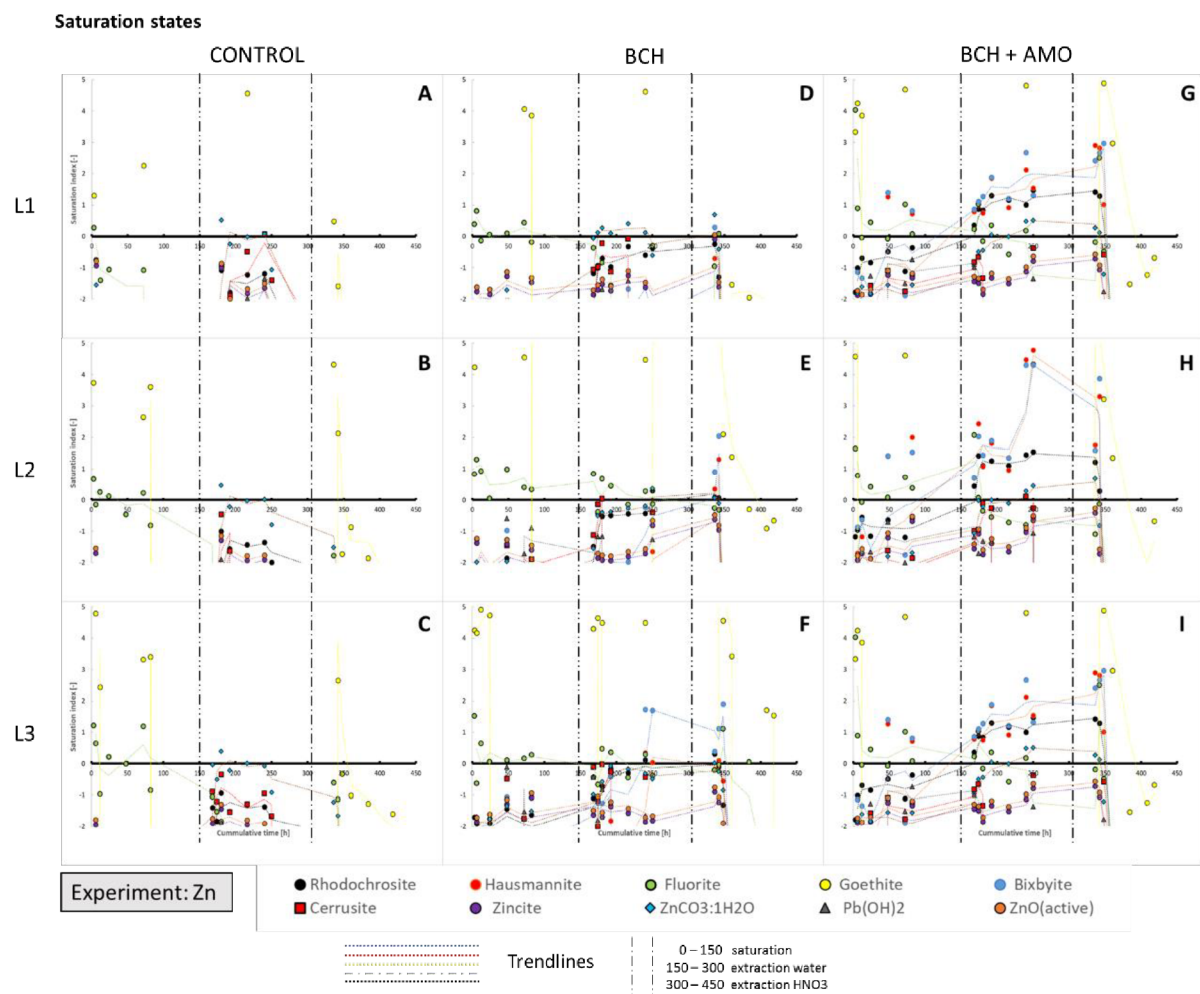Fig.S. 5-10 Speciation of major observed elements during bimetal (Zn) experiment.

Fig.S. 5-11 Saturation index of observed mineral phases during single metal (Zn) sorption experiment.
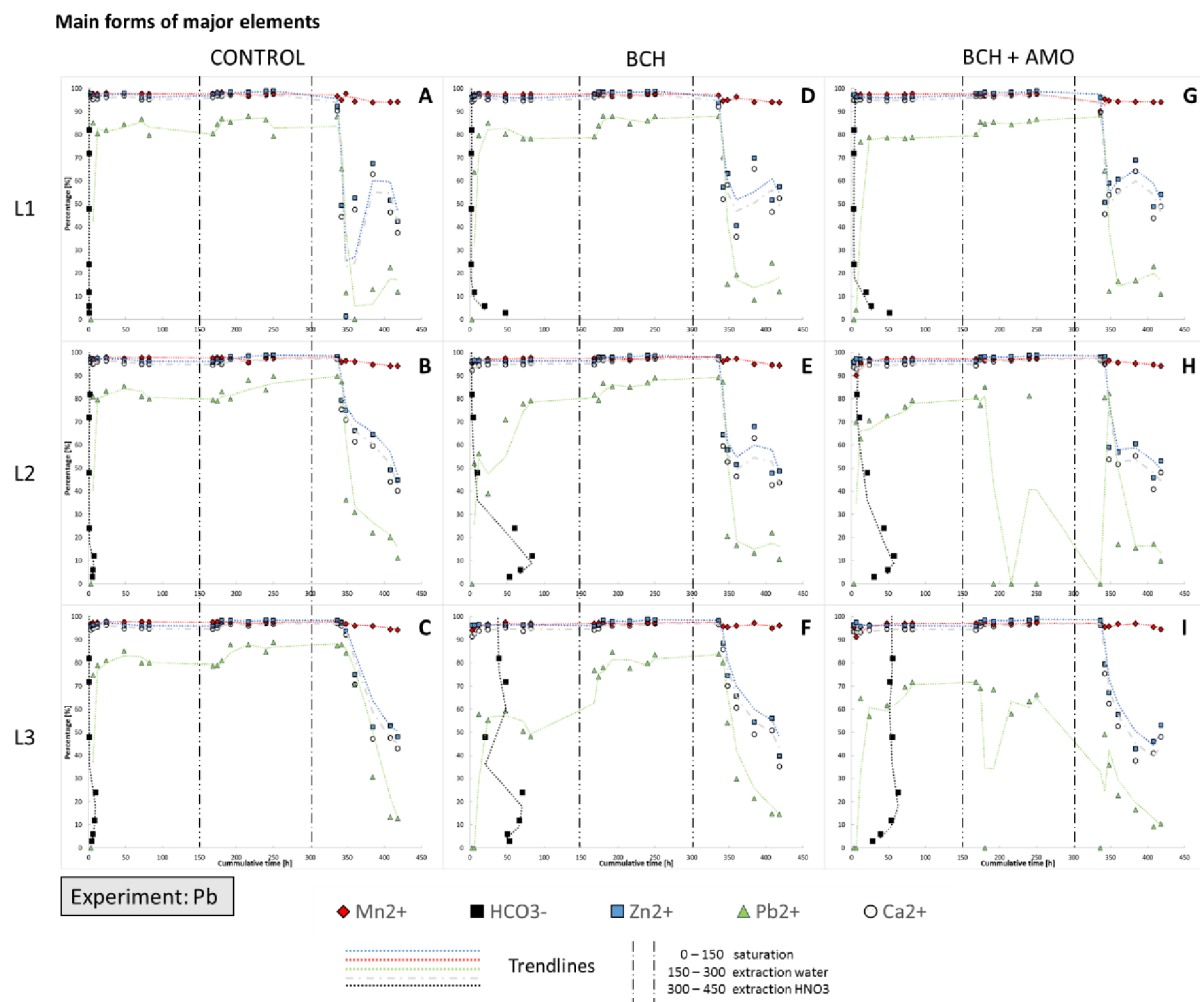
Main forms of major elements

Fig.S. 5-12 Speciation of major observed elements during bimetal (Pb) experiement.
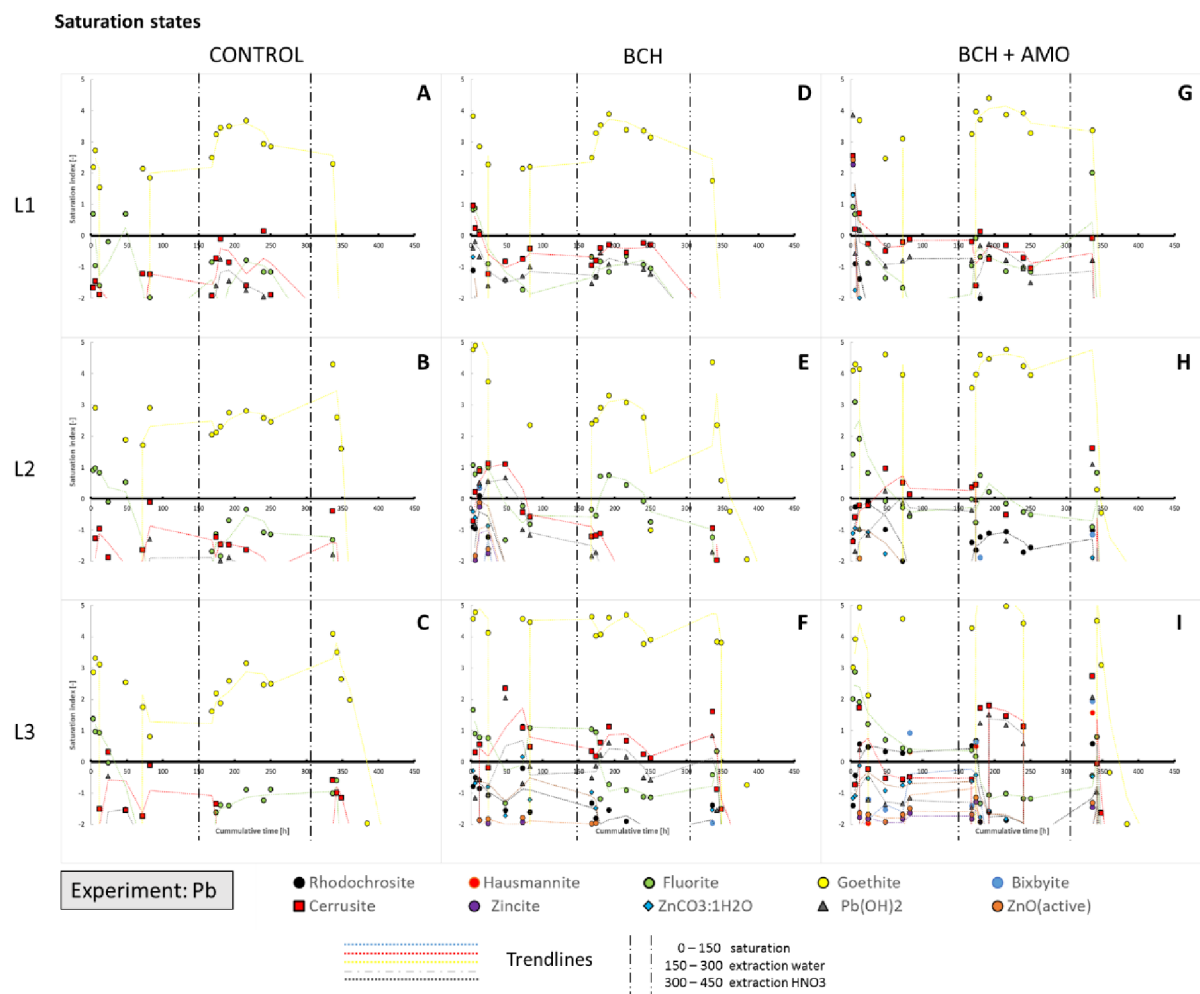
199

Fig.S. 5-13 Saturation index of observed mineral phases during single metal (Pb) sorption experiment.
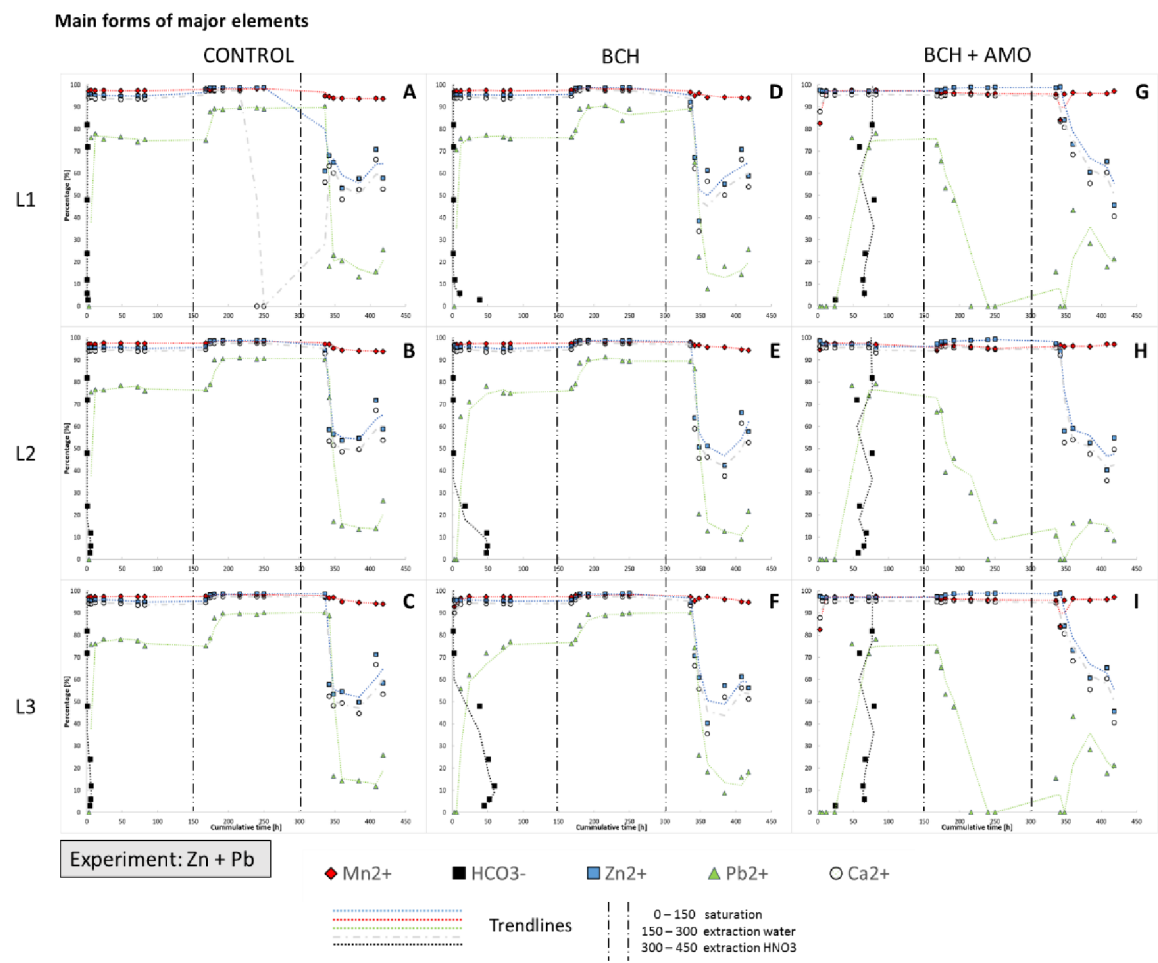
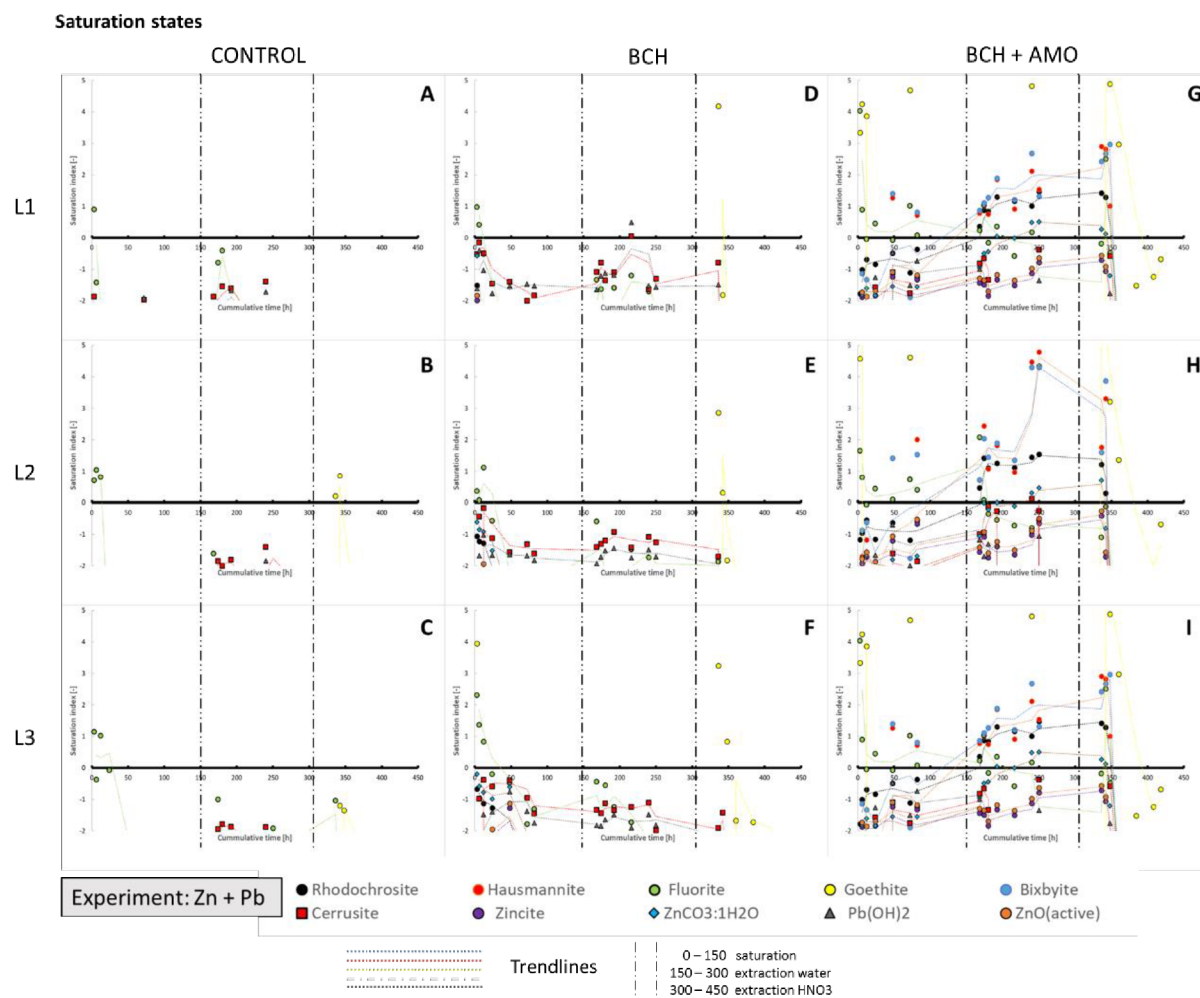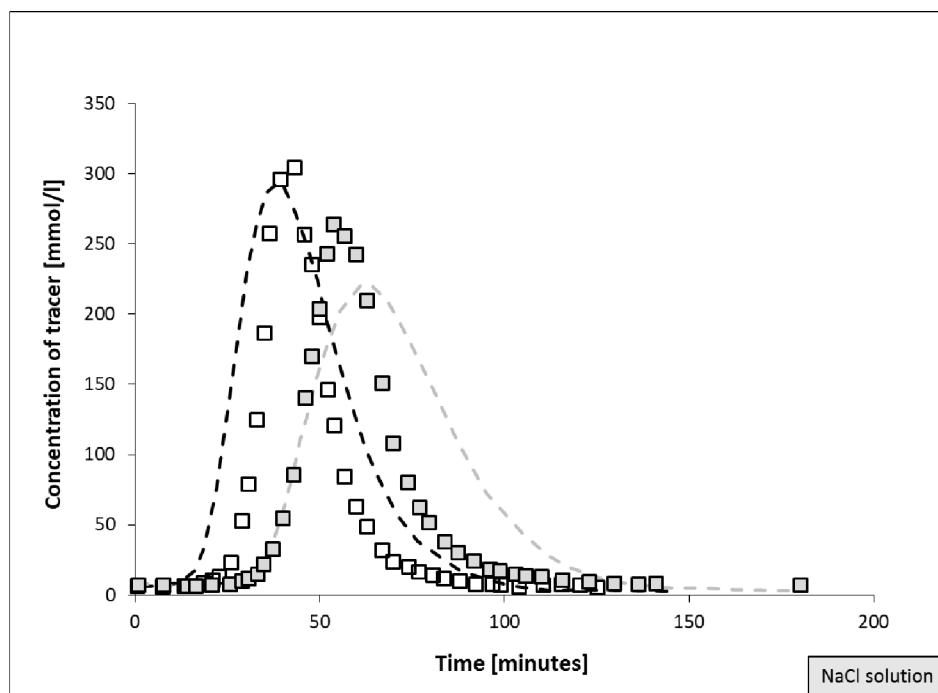Fig.S. 5-14 Speciation of major observed elements during bimetal (Zn + Pb) experiement.

Fig.S. 5-15 Saturation index of observed mineral phases during bimetal (Zn x Pb) sorption experiment.

Tracer experiment

Fig.S. 5-16 Tracer experiment. Observed values and model fitting

Table S. 5-5 Optimized equilibrium model parameters

	CONTROL			BCH			BCH+AMO		
	K_D	Nu	R^2	K_D	Nu	R^2	K_D	Nu	R^2
Experiment: Zn	0.44	15.00	0.83	0.30	5.00	0.85	4.00	40.00	0.99
Experiment: Pb	4.70	90.00	0.21	5.00	73.60	0.98	10.00	10.00	0.99
Experiment: Zn + Pb, Zn	0.61	5.00	0.46	0.55	5.00	0.32	5.00	8.00	0.17
Experiment: Zn + Pb, Pb	4.00	80.00	0.99	6.00	60.00	0.99	5.00	105.00	0.96

Chapter VII

Summary

The main objective of this work was to assess biochar based amendments in terms of detailed study of their crucial parameter and to present a suitable modelling approach after their application to soil conditions. Biochar based amendments were selected because biochar is a potentially very suitable material (easy production, versatility) to solve various environmental problems and its appropriate modification (e.g., by Mn oxides) can further improve its specific applicability. Biochar based amendments can be used in problems connected to the overall decrease of soil sustainability (Cha et al., 2016) and can be used to decrease contamination of the environment with hazardous metals (Masindi and Muedi, 2018) and metalloids (Ng, 2005). The creation of functional and robust models plays an important role in the subsequent easier applicability of the material in real environmental technologies. The term "model" in this study means the construction of a reaction-transport model that will enable to describe the processes after application of biochar based amendment to the soil. In order to build a reaction-transport model, it is necessary to have very well mapped parameters of the computational domain (the environment in which the experiment takes place, e.g., soil in the case of this study), initial and boundary conditions (e.g., saturation state, solution concentration, irrigation intensity, etc.). For this reason, a significant part of this thesis was focused on the characteristics of biochar and biochar based amendments and their behavior in soil and water environments as parameters that are essential for the model. These are water flux parameters (describing the movement of the flow medium through the porous media (un)treated by biochar) and solute transport parameters (describing the behavior of biochar based amendments in interaction with metal(loid)s). A basic description of the models has been summarized in the first chapter (**CHAPTER 1**). The next chapters of this thesis, i.e., individual scientific studies, are then devoted to detailed description of important biochar properties, modifications and, finally, the creation of the reaction-transport model itself.

In the first research study presented in this thesis (**CHAPTER 2**), the effect of grape stalks biochar on the hydraulic properties of two different contrasting soil types was studied (i.e., water flux parameters). At the same time, the effect of different weight doses of biochar was also investigated compared to the untreated variant. The results of this research showed a decrease in K_s, which was positively correlated with the

dose of biochar (i.e., higher dose causes higher decrease). The swelling effect was observed in the case of soil samples treated with biochar when saturated with water. From a microscopic point of view, this was an effect where the biochar surface binds water molecules through the hydrogen bonds to O–H and C–O–H groups. This effect causes a decrease in the bulk density of the soil to which the biochar was added (i.e., the sample volume increases but the weight remains the same). The binding of water to the biochar surface also increases the WHC of the soil and this effect again positively correlated with the biochar dose. Thus, biochar could be used as a tool to reduce the risk of drought stress in soils. Based on the results of this section, a further understanding of parameters for water flux was derived. In subsequent parts of this thesis, the research focused on the other solute transport parameters, such as sorption.

Biochar has been previously identified as a potentially highly effective sorbent for various metals in both water and soil (Martins et al., 2019). However, pristine biochar is not an adequate sorbent for metalloids (e.g., As) and shows insignificant sorption compared to untreated variants (Agrafioti et al., 2014b). Therefore, the suitable modification of biochar to improve the sorption properties against As was the objective of next part of the study (**CHAPTER 3**). A novel sorbent made from biochar and amorphous Mn oxides (AMO), noted here as AMOchar, was compared with the pristine biochar for removing various metal(loid)s (e.g., As, Cd, Pb) from aqueous solutions using basic adsorption experiments and further detailed characterization using solid-state analyses. Compared with the pristine biochar, AMOchar composites were able to remove more significant quantities of various metal(loid)s from the aqueous solutions. In the terms of structure on microscopic scale, Mn oxides in form of Mn–oxalates covered the surface of pristine biochar forming an efficient and well-proportioned surface for subsequent adsorption. Without its stabilization on the biochar surface, AMO showed significant Mn leaching, in common with the observations of other studies, e.g., Michálková et al. (2016), Ettler et al. (2015) and Della Puppa et al. (2013); such leaching may be a a subsequent environmental problem due to Mn contamination of ground water (Gillispie et al., 2016) in the case of field application. This study proved that stabilization of AMO on the biochar surface, i.e., formation of AMOchar composite, led to a significant decrease in the Mn leaching compared to the pure AMO. Additionally, this study also proposed an optimal ratio between pristine biochar and

manganese oxides for the modification procedure, which is crucial to prepare both sufficiently effective and profitable product.

To refine the modified biochar further, to improve its cost and material efficiency, and increase its longevity further modification of biochar and AMO were studied in the next part of the thesis (**CHAPTER 4**). The preparation of pure AMO and AMOchar based on the original procedure published by Della Puppa et al.(2013) was evaluated as not very suitable due to the low yield of the final product and higher chemical consumption than is required for successful AMO synthesis. At the same time, the economic aspect of the selected chemicals was also emphasized and the original expensive reactant (glucose) was replaced by cheaper alternatives (sucrose, molasses). Moreover, obtained results significantly showed that sucrose and molasses-based AMOs and AMO/BC composites presented similar or higher sorption efficiencies for metals compared to the original AMO and/or modified AMO. Moreover, material stability were assessed by parametrization of observed data, which made it possible to create a stability model. The model was used for prediction of short-term stability in various pH levels and fully saturated conditions. Based on the observed data and performed simulations, Mn leaching from the structure of the new AMOs and AMOChar was negligible compared to that observed for the glucose-based AMOs. In this study as well as in other studies dealing with glucose-based AMOs (Della Puppa et al., 2013; Michálková et al., 2016c; Trakal et al., 2018a). Thus, using molasses as reducing agent during AMO synthesis in this study, dramatically decreased the total cost of the final materials compared to original materials. The presented optimization gives a promising possibility to use these amendments in real applications.

In the final part of the thesis (**CHAPTER 5**), the research was focused on validation of the findings from previous parts in systems closer to natural conditions (i.e., dynamic system with more than one pollutant). The aim was to build up a reaction-transport model with an emphasis on simplicity (based on calibration data) and easy applicability. The majority of sorption studies in the current literature are primarily describing sorption using batch equilibrium sorption experiments performed under ideal conditions (i.e., constant pH, constant temperature (Alberti et al., 2012; Salvestrini et al., 2014)). However, this assumption may lead to different/inconsistent result compared to systems closer to reality (i.e., non-

equilibrium, dynamic systems). Most studies consider only single metal sorption, which may overestimate a performance of studied sorbent in real conditions (Esfandiar et al., 2022). Therefore, biochar based amendments (biochar and its modification by AMO) mixed with soil were tested here using batch (equilibrium system) and laboratory columns (dynamic system) during single and bimetal sorption experiments to compare it with the untreated variant. Both batch equilibrium and dynamic column experiments showed a significant increase in sorption efficiency in soils treated with amendments for single sorption and also competitive bimetal sorption. To understand the observed processes and changes during the sorption experiments, a speciation model in PHREEQC has been set with respect to the received data. Based on the simulations of this model, it was possible to evaluate the different dominant forms of the observed elements and to analyze the potentially precipitating mineral phases. Based on the results from the measurements and observations, calibration data were prepared for the HYDRUS 1D transport model. The aim was to achieve a highly valid model of dynamic system with non-equilibrium sorption using dynamic data with initial values from equilibrium experiments. This approach is innovative and has not been sufficiently studied in the literature, mainly due to strict adherence to equilibrium and non-equilibrium models (Carnahan and Remer, 1984). In terms of physical validity, it is assumed that any attempt to simulate these non-equilibrium conditions using an equilibrium model should not be valid. However, in order to build a valid model of a dynamic system with non-equilibrium sorption, it is necessary to collect and record highly complex data, which is relatively difficult to obtain. If this process could be partially generalized and simplified into equilibrium modeling, it would be invaluable in terms of creating more feasible simulations. The calibration results showed that this approach is fully valid if specific constraints are fulfilled. If the process can be considered as a pseudo-equilibrium, then replacing the non-equilibrium system with such a system is effective. In the case of this study, the successful calibration was performed only in the layer closest to the upper boundary condition in terms of the computational domain. The second fact that must be taken into account is the sorption mechanism of biochar based amendments. These processes consist of several different physicochemical subprocesses and it is not possible to successfully summarize all of them in a low-parametric model such as the Freundlich or Langmuir

isotherms. Therefore, more complex models, that can be further included in reaction-transport models, are still necessary.

Based on the results of this thesis, it can be summarized that the studied biochar based amendments showed significantly higher sorption efficiency and/or stability compared to pristine materials, together with a significant positive effect of the biochar matrix on soil water retention in soils compared to the untreated ones; further studies with novel composites are now recommended. Although the reaction-transport model presented in this study proved to be valid, its use is limited and cannot sufficiently incorporate all relevant parameters. Therefore, a comprehensive complex geochemical model is needed to monitor the individual speciation, saturation indices of all ions during transport modelling, their individual concentrations. At the same time, such a model should allow prediction of external chemical (e.g., pH, temperature,..) and physical (e.g., K_s, θ_s,..) parameters during transport in a porous system. However, another important task is also the parametrization of biochar and biochar based amendments themselves, i.e., to include the most relevant physicochemical processes that can take place during sorption to the material surface (i.e., cation exchange, chemisorption, physical sorption, precipitation, etc.) and effectively convert them to model parameters. The findings of this thesis further the possibility to include all these tasks in the framework of linking the HYDRUS (transport) and PHREEQC (speciation, geochemistry) models with the implementation of Model WHAM VII, which has not been fully studied yet (Tipping et al., 2011). The implementation of such a complex model in the future studies should help in the subsequent selection and screening procedure of suitable biochar and biochar based amendments based on their individual properties for specific purposes, and therefore will be beneficial to select remediation agents applicable to specific contaminated areas.

References

" Z. Für Anal., 2007. 3051A - 1 Revision 1 February 2007 METHOD 3051A MICROWAVE ASSISTED ACID DIGESTION OF SEDIMENTS, SLUDGES, SOILS, AND OILS. Chem 111.

Adina, C., Florinela, F., Abdelmoumen, T., Carmen, S., 2010. Application of FTIR spectroscopy for a rapid determination of some hydrolytic enzymes activity on sea buckthorn substrate. Rom. Biotechnol. Lett.

Adriano, D.C., 2001. Bioavailability of Trace Metals. Trace Elem. Terr. Environ. 61–89. https://doi.org/10.1007/978-0-387-21510-5_3

Agrafioti, E., Kalderis, D., Diamadopoulos, E., 2014a. Ca and Fe modified biochars as adsorbents of arsenic and chromium in aqueous solutions. J. Environ. Manage. 146, 444–450. https://doi.org/10.1016/j.jenvman.2014.07.029

Agrafioti, E., Kalderis, D., Diamadopoulos, E., 2014b. Arsenic and chromium removal from water using biochars derived from rice husk, organic solid wastes and sewage sludge. J. Environ. Manage. 133, 309–314. https://doi.org/10.1016/j.jenvman.2013.12.007

Ahalya, N., Kanamadi, R.D., Ramachandra, T.V., 2005. Biosorption of chromium (VI) from aqueous solutions by the husk of Bengal gram (Cicer arientinum). Electron. J. Biotechnol. 8, 258–264. https://doi.org/10.2225/vol8-issue3-fulltext-10

Ahmad, M., Rajapaksha, A.U., Lim, J.E., Zhang, M., Bolan, N., Mohan, D., Vithanage, M., Lee, S.S., Ok, Y.S., 2014. Biochar as a sorbent for contaminant management in soil and water: A review. Chemosphere 99, 19–33. https://doi.org/10.1016/j.chemosphere.2013.10.071

Ahmed, M., Faisal, M., Ihsan, A., Naseer, M.M., 2019. Fluorescent organic nanoparticles (FONs) as convenient probes for metal ion detection in aqueous medium. Analyst 144, 2480–2497. https://doi.org/10.1039/C8AN01801D

Ahmed, M.B., Zhou, J.L., Ngo, H.H., Guo, W., Chen, M., 2016. Progress in the preparation and application of modified biochar for improved contaminant

removal from water and wastewater. Bioresour. Technol. 214, 836–851. https://doi.org/10.1016/J.BIORTECH.2016.05.057

Ajayi, A.E., Holthusen, D., Horn, R., 2016. Changes in microstructural behaviour and hydraulic functions of biochar amended soils. Soil Tillage Res. 155, 166–175.

Alberti, G., Amendola, V., Pesavento, M., Biesuz, R., 2012. Beyond the synthesis of novel solid phases: Review on modelling of sorption phenomena. Coord. Chem. Rev. 256, 28–45. https://doi.org/10.1016/j.ccr.2011.08.022

Ali, S., Rizwan, M., Qayyum, M.F., Ok, Y.S., Ibrahim, M., Riaz, M., Arif, M.S., Hafeez, F., Al-Wabel, M.I., Shahzad, A.N., 2017. Biochar soil amendment on alleviation of drought and salt stress in plants: a critical review. Environ. Sci. Pollut. Res. 24, 12700–12712. https://doi.org/10.1007/s11356-017-8904-x

Altdorff, D., Galagedara, L., Abedin, J., Unc, A., 2019. Effect of Biochar Application Rates on the Hydraulic Properties of an Agricultural-Use Boreal Podzol. Soil Syst. 3, 53. https://doi.org/10.3390/soilsystems3030053

Ambaye, T.G., Vaccari, M., van Hullebusch, E.D., Amrane, A., Rtimi, S., 2021. Mechanisms and adsorption capacities of biochar for the removal of organic and inorganic pollutants from industrial wastewater. Int. J. Environ. Sci. Technol. 18, 3273–3294. https://doi.org/10.1007/s13762-020-03060-w

Amoah-Antwi, C., Kwiatkowska-Malina, J., Thornton, S.F., Fenton, O., Malina, G., Szara, E., 2020. Restoration of soil quality using biochar and brown coal waste: A review. Sci. Total Environ. 722, 137852. https://doi.org/10.1016/j.scitotenv.2020.137852

Antoniadis, V., Shaheen, S.M., Levizou, E., Shahid, M., Niazi, N.K., Vithanage, M., Ok, Y.S., Bolan, N., Rinklebe, J., 2019. A critical prospective analysis of the potential toxicity of trace element regulation limits in soils worldwide: Are they protective concerning health risk assessment? - A review. Environ. Int. 127, 819–847. https://doi.org/10.1016/j.envint.2019.03.039

Arabyarmohammadi, H., Darban, A.K., Abdollahy, M., Yong, R., Ayati, B., Zirakjou, A., van der Zee, S.E.A.T.M., 2018. Utilization of a Novel Chitosan/Clay/Biochar Nanobiocomposite for Immobilization of Heavy Metals in Acid Soil Environment. J. Polym. Environ. 26, 2107–2119. https://doi.org/10.1007/s10924-017-1102-6

Atkinson, C.J., 2018. How good is the evidence that soil-applied biochar improves water-holding capacity? Soil Use Manag. 34, 177–186. https://doi.org/10.1111/sum.12413

B. Duwiejuah, A., J. Cobbina, S., Bakobie, N., 2017. Review of Eco-Friendly Biochar Used in the Removal of Trace Metals on Aqueous Phases. Int. J. Environ. Bioremediation Biodegrad. 5, 27–40. https://doi.org/10.12691/ijebb-5-2-1

Barnes, R.T., Gallagher, M.E., Masiello, C.A., Liu, Z., Dugan, B., 2014. Biochar-induced changes in soil hydraulic conductivity and dissolved nutrient fluxes constrained by laboratory experiments. PLoS One 9. https://doi.org/10.1371/JOURNAL.PONE.0108340

Bayu, D., Tadesse, M., Amsalu, N., 2016. Effect of biochar on soil properties and lead (Pb) availability in a military camp in South West Ethiopia. African J. Environ. Sci. Technol. 10, 77–85. https://doi.org/10.5897/AJEST2015.2014

Beesley, L., Dickinson, N., 2011. Carbon and trace element fluxes in the pore water of an urban soil following greenwaste compost, woody and biochar amendments, inoculated with the earthworm Lumbricus terrestris. Soil Biol. Biochem. 43, 188–196. https://doi.org/10.1016/j.soilbio.2010.09.035

Beesley, L., Moreno-Jiménez, E., Gomez-Eyles, J.L., 2010. Effects of biochar and greenwaste compost amendments on mobility, bioavailability and toxicity of inorganic and organic contaminants in a multi-element polluted soil. Environ. Pollut. 158, 2282–2287. https://doi.org/10.1016/j.envpol.2010.02.003

Beesley, L., Moreno-Jiménez, E., Gomez-Eyles, J.L., Harris, E., Robinson, B., Sizmur, T., 2011. A review of biochars' potential role in the remediation, revegetation and restoration of contaminated soils. Environ. Pollut. 159, 3269–3282. https://doi.org/10.1016/j.envpol.2011.07.023

Bernal, M., Haro, J.M., Bernert, S., Brugha, T., de Graaf, R., Bruffaerts, R., Lépine, J.P., de Girolamo, G., Vilagut, G., Gasquet, I., Torres, J.V., Kovess, V., Heider, D., Neeleman, J., Kessler, R., Alonso, J., 2007. Risk factors for suicidality in Europe: Results from the ESEMED study. J. Affect. Disord. 101, 27–34. https://doi.org/10.1016/j.jad.2006.09.018

Berns, A.E., Flath, A., Mehmood, K., Hofmann, D., Jacques, D., Sauter, M., Vereecken,

H., Engelhardt, I., 2018. Numerical and Experimental Investigations of Cesium and Strontium Sorption and Transport in Agricultural Soils. Vadose Zo. J. 17, 170126. https://doi.org/10.2136/vzj2017.06.0126

Bezirtzoglou, E., Panagiou, A., Savvaidis, I., Maipa, V., 1997. Distribution ofClostridium perfringensin Polluted Lake Environments. Anaerobe 3, 169–172. https://doi.org/10.1006/anae.1997.0101

Bird, J.A., Kleber, M., Torn, M.S., 2008. 13C and 15N stabilization dynamics in soil organic matter fractions during needle and fine root decomposition. Org. Geochem. 39, 465–477. https://doi.org/10.1016/j.orggeochem.2007.12.003

Blanco-Canqui, H., 2017. Biochar and Soil Physical Properties. Soil Sci. Soc. Am. J. 81, 687–711. https://doi.org/10.2136/sssaj2017.01.0017

Bolan, N., Kunhikrishnan, A., Thangarajan, R., Kumpiene, J., Park, J., Makino, T., Kirkham, M.B., Scheckel, K., 2014a. Remediation of heavy metal(loid)s contaminated soils - To mobilize or to immobilize? J. Hazard. Mater. 266, 141–166. https://doi.org/10.1016/j.jhazmat.2013.12.018

Bolan, N., Kunhikrishnan, A., Thangarajan, R., Kumpiene, J., Park, J., Makino, T., Kirkham, M.B., Scheckel, K., 2014b. Remediation of heavy metal(loid)s contaminated soils – To mobilize or to immobilize? J. Hazard. Mater. 266, 141–166. https://doi.org/10.1016/j.jhazmat.2013.12.018

Bolan, N.S., Adriano, D.C., Kunhikrishnan, A., James, T., McDowell, R., Senesi, N., 2011. Dissolved Organic Matter. pp. 1–75. https://doi.org/10.1016/B978-0-12-385531-2.00001-3

Bossy, A., Grosbois, C., Beauchemin, S., Courtin-Nomade, A., Hendershot, W., Bril, H., 2010. Alteration of As-bearing phases in a small watershed located on a high grade arsenic-geochemical anomaly (French Massif Central). Appl. Geochemistry. https://doi.org/10.1016/j.apgeochem.2010.10.004

Boudesocque, S., Guillon, E., Aplincourt, M., Marceau, E., Stievano, L., 2007. Sorption of Cu(II) onto vineyard soils: Macroscopic and spectroscopic investigations. J. Colloid Interface Sci. 307, 40–49. https://doi.org/10.1016/j.jcis.2006.10.080

Bresler, E., Hanks, R.J., 1969. Numerical Method for Estimating Simultaneous Flow of Water and Salt in Unsaturated Soils. Soil Sci. Soc. Am. J. 33, 827–832.

https://doi.org/10.2136/sssaj1969.03615995003300060013x

Buergisser, C.S., Cernik, M., Borkovec, M., Sticher, H., 1993. Determination of nonlinear adsorption isotherms from column experiments: an alternative to batch studies. Environ. Sci. Technol. 27, 943–948. https://doi.org/10.1021/es00042a018

Burrell, L.D., Zehetner, F., Rampazzo, N., Wimmer, B., Soja, G., 2016. Long-term effects of biochar on soil physical properties. Geoderma 282, 96–102. https://doi.org/10.1016/J.GEODERMA.2016.07.019

Butnan, S., Deenik, J.L., Toomsan, B., Antal, M.J., Vityakon, P., 2015. Biochar characteristics and application rates affecting corn growth and properties of soils contrasting in texture and mineralogy. Geoderma 237–238, 105–116. https://doi.org/10.1016/j.geoderma.2014.08.010

Butto, N., Cabrera-Barjas, G., Neira-Carrillo, A., 2018. Electrocrystallization of CaCO3 crystals obtained through phosphorylated chitin. Crystals. https://doi.org/10.3390/cryst8020082

Cantrell, K.B., Hunt, P.G., Uchimiya, M., Novak, J.M., Ro, K.S., 2012. Impact of pyrolysis temperature and manure source on physicochemical characteristics of biochar. Bioresour. Technol. 107, 419–428. https://doi.org/10.1016/j.biortech.2011.11.084

Cao, Y., Gao, Y., Qi, Y., Li, J., 2018. Biochar-enhanced composts reduce the potential leaching of nutrients and heavy metals and suppress plant-parasitic nematodes in excessively fertilized cucumber soils. Environ. Sci. Pollut. Res. 25, 7589–7599. https://doi.org/10.1007/s11356-017-1061-4

Carnahan, C.L., Remer, J.S., 1984. Nonequilibrium and equilibrium sorption with a linear sorption isotherm during mass transport through an infinite porous medium: Some analytical solutions. J. Hydrol. 73, 227–258. https://doi.org/10.1016/0022-1694(84)90002-7

Cesarano, G., De Filippis, F., La Storia, A., Scala, F., Bonanomi, G., 2017. Organic amendment type and application frequency affect crop yields, soil fertility and microbiome composition. Appl. Soil Ecol. 120, 254–264. https://doi.org/10.1016/j.apsoil.2017.08.017

Cha, J.S., Park, S.H., Jung, S.C., Ryu, C., Jeon, J.K., Shin, M.C., Park, Y.K., 2016. Production and utilization of biochar: A review. J. Ind. Eng. Chem. 40, 1–15. https://doi.org/10.1016/j.jiec.2016.06.002

Chatterjee, A., Schiewer, S., 2014. Effect of Competing Cations (Pb, Cd, Zn, and Ca) in Fixed-Bed Column Biosorption and Desorption from Citrus Peels. Water, Air, Soil Pollut. 225, 1854. https://doi.org/10.1007/s11270-013-1854-0

Chemerys, V., Baltrėnaitė, E., 2016. MODIFIED BIOCHAR: A REVIEW ON MODIFICATIONS OF BIOCHAR TOWARDS ITS ENHANCED ADSORPTIVE PROPERTIES, in: Proceedings of the 19th Conference for Junior Researchers „Science – Future of Lithuania". VGTU Technika. https://doi.org/10.3846/aainz.2016.03

Chen, H., Ye, Y., Tong, W., Fang, J., Gong, H., 2020. Formation of allylated quaternary carbon centers: Via C-O/C-O bond fragmentation of oxalates and allyl carbonates. Chem. Commun. https://doi.org/10.1039/c9cc07072a

Chen, T., Luo, L., Deng, S., Shi, G., Zhang, S., Zhang, Y., Deng, O., Wang, L., Zhang, J., Wei, L., 2018. Sorption of tetracycline on H_3PO_4 modified biochar derived from rice straw and swine manure. Bioresour. Technol. 267, 431–437. https://doi.org/10.1016/j.biortech.2018.07.074

Chen, W.Y., Mattern, D.L., Okinedo, E., Senter, J.C., Mattei, A.A., Redwine, C.W., 2014. Photochemical and acoustic interactions of biochar with CO_2 and H_2O: Applications in power generation and CO_2 capture. AIChE J. 60, 1054–1065. https://doi.org/10.1002/AIC.14347

Chen, X., Dai, Y., Fan, J., Xu, X., Cao, X., 2021. Application of iron-biochar composite in topsoil for simultaneous remediation of chromium-contaminated soil and groundwater: Immobilization mechanism and long-term stability. J. Hazard. Mater. 405, 124226. https://doi.org/10.1016/j.jhazmat.2020.124226

Ching, S., Petrovay, D.J., Jorgensen, M.L., Suib, S.L., 1997. Sol-gel synthesis of layered birnessite-type manganese oxides. Inorg. Chem. 883–890.

Ching, S., Tabet, E.A., Dudek, R.C., Magiera, J.P., 1995. Synthesis and Reactivity of Modified Electrodes Derived from $TiCl_4$ and Other Early-Transition-Metal Complexes. Chem. Mater. https://doi.org/10.1021/cm00050a027

Claoston, N., Samsuri, A., Ahmad Husni, M., Mohd Amran, M., 2014. Effects of pyrolysis temperature on the physicochemical properties of empty fruit bunch and rice husk biochars. Waste Manag. Res. J. a Sustain. Circ. Econ. 32, 331–339. https://doi.org/10.1177/0734242X14525822

Colombani, N., Gervasio, M.P., Castaldelli, G., Mastrocicco, M., 2020. Soil conditioners effects on hydraulic properties, leaching processes and denitrification on a silty-clay soil. Sci. Total Environ. 733, 139342. https://doi.org/10.1016/j.scitotenv.2020.139342

Crane-Droesch, A., Abiven, S., Jeffery, S., Torn, M.S., 2013. Heterogeneous global crop yield response to biochar: a meta-regression analysis. Environ. Res. Lett. 8, 44049.

de Pasquale, C., Marsala, V., Berns, A.E., Valagussa, M., Pozzi, A., Alonzo, G., Conte, P., 2012. Fast field cycling NMR relaxometry characterization of biochars obtained from an industrial thermochemical process. J. Soils Sediments 12, 1211–1221. https://doi.org/10.1007/S11368-012-0489-X

Della Puppa, L., Komárek, M., Bordas, F., Bollinger, J.C., Joussein, E., 2013. Adsorption of copper, cadmium, lead and zinc onto a synthetic manganese oxide. J. Colloid Interface Sci. 399, 99–106. https://doi.org/10.1016/J.JCIS.2013.02.029

DeLuca, T.H., Gundale, M.J., MacKenzie, M.D., Jones, D.L., 2015. Biochar effects on soil nutrient transformations. Biochar Environ. Manag. Sci. Technol. Implement. 2, 421–454.

Di Leo, P., Pizzigallo, M.D.R., Ancona, V., Di Benedetto, F., Mesto, E., Schingaro, E., Ventruti, G., 2012. Mechanochemical transformation of an organic ligand on mineral surfaces: The efficiency of birnessite in catechol degradation. J. Hazard. Mater. https://doi.org/10.1016/j.jhazmat.2011.11.054

Dias, B.O., Silva, C.A., Higashikawa, F.S., Roig, A., Sánchez-Monedero, M.A., 2010. Use of biochar as bulking agent for the composting of poultry manure: Effect on organic matter degradation and humification. Bioresour. Technol. 101, 1239–1246. https://doi.org/10.1016/j.biortech.2009.09.024

Ding, Y., Liu, Y., Liu, S., Li, Z., Tan, X., Huang, X., Zeng, G., Zhou, L., Zheng, B., 2016. Biochar to improve soil fertility. A review. Agron. Sustain. Dev. 36, 36.

https://doi.org/10.1007/s13593-016-0372-z

Domingues, R.R., Trugilho, P.F., Silva, C.A., De Melo, I.C.N.A., Melo, L.C.A., Magriotis, Z.M., Sánchez-Monedero, M.A., 2017. Properties of biochar derived from wood and high-nutrient biomasses with the aim of agronomic and environmental benefits. PLoS One. https://doi.org/10.1371/journal.pone.0176884

Dong, D., Feng, Q., McGrouther, K., Yang, M., Wang, H., Wu, W., 2015. Effects of biochar amendment on rice growth and nitrogen retention in a waterlogged paddy field. J. Soils Sediments 15, 153–162. https://doi.org/10.1007/s11368-014-0984-3

Dong, C. Di, Chen, C.W., Hung, C.M., 2017. Synthesis of magnetic biochar from bamboo biomass to activate persulfate for the removal of polycyclic aromatic hydrocarbons in marine sediments. Bioresour. Technol. https://doi.org/10.1016/j.biortech.2017.08.204

Doumer, M.E., Rigol, A., Vidal, M., Mangrich, A.S., 2016. Removal of Cd, Cu, Pb, and Zn from aqueous solutions by biochars. Environ. Sci. Pollut. Res. 23, 2684–2692. https://doi.org/10.1007/s11356-015-5486-3

Duan, Y., Sorescu, D.C., 2010. CO2 capture properties of alkaline earth metal oxides and hydroxides: A combined density functional theory and lattice phonon dynamics study. J. Chem. Phys. https://doi.org/10.1063/1.3473043

Edeh, I.G., Mašek, O., Buss, W., 2020. A meta-analysis on biochar's effects on soil water properties – New insights and future research challenges. Sci. Total Environ. 714, 136857. https://doi.org/10.1016/j.scitotenv.2020.136857

El-Shafey, E., Cox, M., Pichugin, A., Appleton, Q., 2002. Application of a carbon sorbent for the removal of cadmium and other heavy metal ions from aqueous solution. J. Chem. Technol. Biotechnol. 77, 429–436. https://doi.org/10.1002/jctb.577

Eren, E., Gumus, H., 2011. Characterization of the structural properties and Pb(II) adsorption behavior of iron oxide coated sepiolite. Desalination. https://doi.org/10.1016/j.desal.2011.01.004

Esfandiar, N., Suri, R., McKenzie, E.R., 2022. Competitive sorption of Cd, Cr, Cu, Ni, Pb and Zn from stormwater runoff by five low-cost sorbents; Effects of co-

contaminants, humic acid, salinity and pH. J. Hazard. Mater. 423, 126938. https://doi.org/10.1016/j.jhazmat.2021.126938

Esmaeelnejad, L., Shorafa, M., Gorji, M., Hosseini, S.M., 2016. Enhancement of physical and hydrological properties of a sandy loam soil via application of different biochar particle sizes during incubation period. Spanish J. Agric. Res. 14, e1103--e1103.

Ettler, V., Knytl, V., Komárek, M., Puppa, L. Della, Bordas, F., Mihaljevič, M., Klementová, M., Šebek, O., 2014a. Stability of a novel synthetic amorphous manganese oxide in contrasting soils. Geoderma 214–215, 2–9. https://doi.org/10.1016/j.geoderma.2013.10.011

Ettler, V., Knytl, V., Komárek, M., Puppa, L. Della, Bordas, F., Mihaljevič, M., Klementová, M., Šebek, O., 2014b. Stability of a novel synthetic amorphous manganese oxide in contrasting soils. Geoderma 214–215, 2–9. https://doi.org/10.1016/j.geoderma.2013.10.011

Ettler, V., Tomášová, Z., Komárek, M., Mihaljevič, M., Šebek, O., Michálková, Z., 2015. The pH-dependent long-term stability of an amorphous manganese oxide in smelter-polluted soils: Implication for chemical stabilization of metals and metalloids. J. Hazard. Mater. 286, 386–394. https://doi.org/10.1016/J.JHAZMAT.2015.01.018

Ettler, V., Vaněk, A., Mihaljevič, M., Bezdička, P., 2005. Contrasting lead speciation in forest and tilled soils heavily polluted by lead metallurgy. Chemosphere 58, 1449–1459. https://doi.org/10.1016/j.chemosphere.2004.09.084

Farkas, É., Feigl, V., Gruiz, K., Vaszita, E., Fekete-Kertész, I., Tolner, M., Kerekes, I., Pusztai, É., Kari, A., Uzinger, N., Rékási, M., Kirchkeszner, C., Molnár, M., 2020. Long-term effects of grain husk and paper fibre sludge biochar on acidic and calcareous sandy soils − A scale-up field experiment applying a complex monitoring toolkit. Sci. Total Environ. 731, 138988. https://doi.org/10.1016/j.scitotenv.2020.138988

Fiol, N., Villaescusa, I., 2008. Determination of sorbent point zero charge: usefulness in sorption studies. Environ. Chem. Lett. 2008 71 7, 79–84. https://doi.org/10.1007/S10311-008-0139-0

Gillispie, E.C., Austin, R.E., Rivera, N.A., Bolich, R., Duckworth, O.W., Bradley, P., Amoozegar, A., Hesterberg, D., Polizzotto, M.L., 2016. Soil Weathering as an Engine for Manganese Contamination of Well Water. Environ. Sci. Technol. 50, 9963–9971. https://doi.org/10.1021/acs.est.6b01686

Głąb, T., Palmowska, J., Zaleski, T., Gondek, K., 2016. Effect of biochar application on soil hydrological properties and physical quality of sandy soil. Geoderma 281, 11–20.

Glaser, B., Lehr, V.-I., 2019. Biochar effects on phosphorus availability in agricultural soils: A meta-analysis. Sci. Rep. 9, 9338. https://doi.org/10.1038/s41598-019-45693-z

Godlewska, P., Bogusz, A., Dobrzyńska, J., Dobrowolski, R., Oleszczuk, P., 2020. Engineered biochar modified with iron as a new adsorbent for treatment of water contaminated by selenium. J. Saudi Chem. Soc. 24, 824–834. https://doi.org/10.1016/j.jscs.2020.07.006

Golui, D., Datta, S.P., Dwivedi, B.S., Meena, M.C., Trivedi, V.K., 2020. Prediction of free metal ion activity in contaminated soils using WHAM VII, baker soil test and solubility model. Chemosphere 243, 125408. https://doi.org/10.1016/j.chemosphere.2019.125408

Gregory, S.J., Anderson, C.W.N., Camps Arbestain, M., McManus, M.T., 2014. Response of plant and soil microbes to biochar amendment of an arsenic-contaminated soil. Agric. Ecosyst. Environ. 191, 133–141. https://doi.org/10.1016/j.agee.2014.03.035

Gu, X., Liu, C., Jiang, X., Ma, X., Li, L., Cheng, K., Li, Z., 2014. Thermal behavior and kinetics of the pyrolysis of the raw/steam exploded poplar wood sawdust. J. Anal. Appl. Pyrolysis 106, 177–186. https://doi.org/10.1016/j.jaap.2014.01.018

Gustafsson, J.P., 2013. Visual MINTEQ, Version 3.1 Division of Land and Water Resources. R. Inst. Technol. Stock. Sweden http//www2. lwr. kth. se/English/Oursoftware/vminteq/download. html.

Hailegnaw, N.S., Mercl, F., Pračke, K., Száková, J., Tlustoš, P., 2019. Mutual relationships of biochar and soil pH, CEC, and exchangeable base cations in a model laboratory experiment. J. Soils Sediments 19, 2405–2416.

https://doi.org/10.1007/s11368-019-02264-z

Han, Z., Sani, B., Mrozik, W., Obst, M., Beckingham, B., Karapanagioti, H.K., Werner, D., 2015. Magnetite impregnation effects on the sorbent properties of activated carbons and biochars. Water Res. 70, 394–403. https://doi.org/10.1016/J.WATRES.2014.12.016

Hardie, M., Clothier, B., Bound, S., Oliver, G., Close, D., 2014. Does biochar influence soil physical properties and soil water availability? Plant Soil 376, 347–361. https://doi.org/10.1007/S11104-013-1980-X

Hasan Khan Tushar, M.S., Mahinpey, N., Khan, A., Ibrahim, H., Kumar, P., Idem, R., 2012. Production, characterization and reactivity studies of chars produced by the isothermal pyrolysis of flax straw. Biomass and Bioenergy 37, 97–105. https://doi.org/10.1016/j.biombioe.2011.12.027

Herath, H.M.S.K., Camps-Arbestain, M., Hedley, M., 2013. Effect of biochar on soil physical properties in two contrasting soils: An Alfisol and an Andisol. Geoderma 209–210, 188–197.

Hettiarachchi, G.M., Pierzynski, G.M., Ransom, M.D., 2000. In situ stabilization of soil lead using phosphorus and manganese oxide. Environ. Sci. Technol. https://doi.org/10.1021/es001228p

Hillel, D., 1998. Environmental soil physics: Fundamentals, applications, and environmental considerations. Elsevier.

Horel, Á., Tóth, E., Gelybó, G., Dencső, M., Farkas, C., 2019. Biochar Amendment Affects Soil Water and CO2 Regime during Capsicum Annuum Plant Growth. Agronomy 9, 58. https://doi.org/10.3390/agronomy9020058

Horgan, G.W., 1996. A review of soil pore models.

Hou, X., Zhang, L., 2007. Saliency detection: A spectral residual approach, in: Proceedings of the IEEE Computer Society Conference on Computer Vision and Pattern Recognition. https://doi.org/10.1109/CVPR.2007.383267

Hu, X., Ding, Z., Zimmerman, A.R., Wang, S., Gao, B., 2015. Batch and column sorption of arsenic onto iron-impregnated biochar synthesized through hydrolysis. Water Res. 68, 206–216. https://doi.org/10.1016/j.watres.2014.10.009

Huang, X., Liu, M., Belongie, S., Kautz, J., 2018. Multimodal Unsupervised Image-to-image TranslationXun_Huang_Multimodal_Unsupervised_Image-to-image_ECCV_2018_paper. Eccv.

Huang, Y., Xia, Y., Tan, X., 2017. On the pattern of CO_2 radiative forcing and poleward energy transport. J. Geophys. Res. Atmos. https://doi.org/10.1002/2017JD027221

Hudcová, B., Fein, J.B., Tsang, D.C.W., Komárek, M., 2022. Mg-Fe LDH-coated biochars for metal(loid) removal: Surface complexation modeling and structural change investigations. Chem. Eng. J. 432, 134360. https://doi.org/10.1016/j.cej.2021.134360

Hudcová, B., Osacký, M., Vítková, M., Mitzia, A., Komárek, M., 2021. Investigation of zinc binding properties onto natural and synthetic zeolites: Implications for soil remediation. Microporous Mesoporous Mater. 317, 111022. https://doi.org/10.1016/j.micromeso.2021.111022

Hudcová, B., Veselská, V., Filip, J., Číhalová, S., Komárek, M., 2018. Highly effective Zn(II) and Pb(II) removal from aqueous solutions using Mg-Fe layered double hydroxides: Comprehensive adsorption modeling coupled with solid state analyses. J. Clean. Prod. https://doi.org/10.1016/j.jclepro.2017.10.104

Hudcová, B., Veselská, V., Filip, J., Číhalová, S., Komárek, M., 2017. Sorption mechanisms of arsenate on Mg-Fe layered double hydroxides: A combination of adsorption modeling and solid state analysis. Chemosphere. https://doi.org/10.1016/j.chemosphere.2016.11.031

Hussain, M., Farooq, M., Nawaz, A., Al-Sadi, A.M., Solaiman, Z.M., Alghamdi, S.S., Ammara, U., Ok, Y.S., Siddique, K.H.M., 2017. Biochar for crop production: potential benefits and risks. J. Soils Sediments 17, 685–716. https://doi.org/10.1007/s11368-016-1360-2

Hussain, R., Ravi, K., Garg, A., 2020. Influence of biochar on the soil water retention characteristics (SWRC): Potential application in geotechnical engineering structures. Soil Tillage Res. 204, 104713. https://doi.org/10.1016/j.still.2020.104713

Inyang, M., Gao, B., Zimmerman, A., Zhou, Y., Cao, X., 2015. Sorption and cosorption

of lead and sulfapyridine on carbon nanotube-modified biochars. Environ. Sci. Pollut. Res. 22, 1868–1876. https://doi.org/10.1007/s11356-014-2740-z

J. W. Gaskin, C. Steiner, K. Harris, K. C. Das, B. Bibens, 2008. Effect of Low-Temperature Pyrolysis Conditions on Biochar for Agricultural Use. Trans. ASABE 51, 2061–2069. https://doi.org/10.13031/2013.25409

Jačka, L., Pavlásek, J., Kuráž, V., Pech, P., 2014. A comparison of three measuring methods for estimating the saturated hydraulic conductivity in the shallow subsurface layer of mountain podzols. Geoderma 219–220, 82–88.

Jačka, L., Trakal, L., Ouředníček, P., Pohořelý, M., Šípek, V., 2018. Biochar presence in soil significantly decreased saturated hydraulic conductivity due to swelling. Soil Tillage Res. 184, 181–185. https://doi.org/10.1016/j.still.2018.07.018

Jeffery, S., Meinders, M.B.J., Stoof, C.R., Bezemer, T.M., van de Voorde, T.F.J., Mommer, L., van Groenigen, J.W., 2015. Biochar application does not improve the soil hydrological function of a sandy soil. Geoderma 251–252, 47–54.

Jian, Z., Bai, Y., Chang, Y., Liang, J., Qu, J., 2019. Removal of micropollutants and cyanobacteria from drinking water using KMnO4 pre-oxidation coupled with bioaugmentation. Chemosphere. https://doi.org/10.1016/j.chemosphere.2018.10.013

Jin, H., Capareda, S., Chang, Z., Gao, J., Xu, Y., Zhang, J., 2014. Biochar pyrolytically produced from municipal solid wastes for aqueous As(V) removal: Adsorption property and its improvement with KOH activation. Bioresour. Technol. 169, 622–629. https://doi.org/10.1016/j.biortech.2014.06.103

Jindo, K., Audette, Y., Higashikawa, F.S., Silva, C.A., Akashi, K., Mastrolonardo, G., Sánchez-Monedero, M.A., Mondini, C., 2020. Role of biochar in promoting circular economy in the agriculture sector. Part 1: A review of the biochar roles in soil N, P and K cycles. Chem. Biol. Technol. Agric. 7, 15. https://doi.org/10.1186/s40538-020-00182-8

Jindo, K., Mizumoto, H., Sawada, Y., Sanchez-Monedero, M.A., Sonoki, T., 2014. Physical and chemical characterization of biochars derived from different agricultural residues. Biogeosciences 11, 6613–6621. https://doi.org/10.5194/bg-11-6613-2014

Joseph, S., Kammann, C.I., Shepherd, J.G., Conte, P., Schmidt, H.-P., Hagemann, N., Rich, A.M., Marjo, C.E., Allen, J., Munroe, P., Mitchell, D.R.G., Donne, S., Spokas, K., Graber, E.R., 2018. Microstructural and associated chemical changes during the composting of a high temperature biochar: Mechanisms for nitrate, phosphate and other nutrient retention and release. Sci. Total Environ. 618, 1210–1223. https://doi.org/10.1016/j.scitotenv.2017.09.200

Kanungo, B.P., Glade, S.C., Asoka-Kumar, P., Flores, K.M., 2004. Characterization of free volume changes associated with shear band formation in Zr- and Cu-based bulk metallic glasses, in: Intermetallics. https://doi.org/10.1016/j.intermet.2004.04.033

Keske, C., Godfrey, T., Hoag, D.L.K., Abedin, J., 2020. Economic feasibility of biochar and agriculture coproduction from Canadian black spruce forest. Food Energy Secur. 9. https://doi.org/10.1002/fes3.188

Khan, Ibrahim, Saeed, K., Khan, Idrees, 2019. Nanoparticles: Properties, applications and toxicities. Arab. J. Chem. 12, 908–931. https://doi.org/10.1016/j.arabjc.2017.05.011

Khan, S., Naushad, M., Govarthanan, M., Iqbal, J., Alfadul, S.M., 2022. Emerging contaminants of high concern for the environment: Current trends and future research. Environ. Res. 207, 112609. https://doi.org/10.1016/j.envres.2021.112609

Kim, J., Song, J., Lee, S.-M., Jung, J., 2019. Application of iron-modified biochar for arsenite removal and toxicity reduction. J. Ind. Eng. Chem. 80, 17–22. https://doi.org/10.1016/j.jiec.2019.07.026

Kodešová, R., 2012. Modelování v pedologii. Česká zemědělská univerzita v Praze.

Komárek, M., Vaněk, A., Ettler, V., 2013. Chemical stabilization of metals and arsenic in contaminated soils using oxides − A review. Environ. Pollut. 172, 9–22. https://doi.org/10.1016/J.ENVPOL.2012.07.045

Kong, F., Chen, Y., Huang, L., Yang, Z., Zhu, K., 2021. Human health risk visualization of potentially toxic elements in farmland soil: A combined method of source and probability. Ecotoxicol. Environ. Saf. 211, 111922. https://doi.org/10.1016/j.ecoenv.2021.111922

Kutílek, M., Nielsen, D.R., others, 1994. Soil hydrology: texbook for students of soil science, agriculture, forestry, geoecology, hydrology, geomorphology and other related disciplines. Catena Verlag.

Laird, D., Rogovska, N., 2015. Biochar effects on nutrient leaching, in: Biochar for Environmental Management. Routledge, pp. 553–574.

Laird, D.A., Fleming, P., Davis, D.D., Horton, R., Wang, B., Karlen, D.L., 2010. Impact of biochar amendments on the quality of a typical Midwestern agricultural soil. Geoderma 158, 443–449.

Lal, R., Shukla, M.K., 2004. Principles of soil physics. CRC Press.

Lamb, D.T., Ming, H., Megharaj, M., Naidu, R., 2009. Heavy metal (Cu, Zn, Cd and Pb) partitioning and bioaccessibility in uncontaminated and long-term contaminated soils. J. Hazard. Mater. 171, 1150–1158. https://doi.org/10.1016/j.jhazmat.2009.06.124

Lawrinenko, M., Laird, D.A., 2015. Anion exchange capacity of biochar. Green Chem. https://doi.org/10.1039/c5gc00828j

Lehmann, J., Abiven, S., Kleber, M., Pan, G., Singh, B.P., Sohi, S.P., Zimmerman, A.R., 2015. Persistence of biochar in soil, in: Biochar for Environmental Management. Routledge, pp. 267–314.

Lehmann, J., Gaunt, J., Rondon, M., 2006. Bio-char Sequestration in Terrestrial Ecosystems – A Review. Mitig. Adapt. Strateg. Glob. Chang. 11, 403–427. https://doi.org/10.1007/s11027-005-9006-5

Lenoble, V., Laclautre, C., Serpaud, B., Deluchat, V., Bollinger, J.C., 2004. As(V) retention and As(III) simultaneous oxidation and removal on a MnO2-loaded polystyrene resin. Sci. Total Environ. 326, 197–207. https://doi.org/10.1016/J.SCITOTENV.2003.12.012

Li, B., Yang, L., Wang, C. quan, Zhang, Q. pei, Liu, Q. cheng, Li, Y. ding, Xiao, R., 2017. Adsorption of Cd(II) from aqueous solutions by rape straw biochar derived from different modification processes. Chemosphere 175, 332–340. https://doi.org/10.1016/J.CHEMOSPHERE.2017.02.061

Li, R., Deng, H., Zhang, X., Wang, J.J., Awasthi, M.K., Wang, Q., Xiao, R., Zhou, B., Du, J.,

Zhang, Z., 2019. High-efficiency removal of Pb(II) and humate by a CeO2–MoS2 hybrid magnetic biochar. Bioresour. Technol. https://doi.org/10.1016/j.biortech.2018.10.053

Li, R., Liang, W., Wang, J.J., Gaston, L.A., Huang, D., Huang, H., Lei, S., Awasthi, M.K., Zhou, B., Xiao, R., Zhang, Z., 2018a. Facilitative capture of As(V), Pb(II) and methylene blue from aqueous solutions with MgO hybrid sponge-like carbonaceous composite derived from sugarcane leafy trash. J. Environ. Manage. https://doi.org/10.1016/j.jenvman.2017.12.034

Li, R., Wang, J.J., Zhang, Z., Awasthi, M.K., Du, D., Dang, P., Huang, Q., Zhang, Y., Wang, L., 2018b. Recovery of phosphate and dissolved organic matter from aqueous solution using a novel CaO-MgO hybrid carbon composite and its feasibility in phosphorus recycling. Sci. Total Environ. https://doi.org/10.1016/j.scitotenv.2018.06.092

Lie, K.-A., Mallison, B.T., 2015. Mathematical Models for Oil Reservoir Simulation, in: Encyclopedia of Applied and Computational Mathematics. Springer Berlin Heidelberg, Berlin, Heidelberg, pp. 850–856. https://doi.org/10.1007/978-3-540-70529-1_277

Lim, T.J., Spokas, K.A., Feyereisen, G., Novak, J.M., 2016. Chemosphere Predicting the impact of biochar additions on soil hydraulic properties. Chemosphere 142, 136–144. https://doi.org/10.1016/j.chemosphere.2015.06.069

Liu, B., Abouimrane, A., Ren, Y., Balasubramanian, M., Wang, D., Fang, Z.Z., Amine, K., 2012. New anode material based on SiO-SnxCoyCz for lithium batteries. Chem. Mater. https://doi.org/10.1021/cm3017853

Liu, L., Li, W., Song, W., Guo, M., 2018. Remediation techniques for heavy metal-contaminated soils: Principles and applicability. Sci. Total Environ. 633, 206–219. https://doi.org/10.1016/j.scitotenv.2018.03.161

Liu, P., Ptacek, C.J., Blowes, D.W., 2019. Mercury Complexation with Dissolved Organic Matter Released from Thirty-Six Types of Biochar. Bull. Environ. Contam. Toxicol. 103, 175–180. https://doi.org/10.1007/s00128-018-2397-2

Liu, X., Zhang, A., Ji, C., Joseph, S., Bian, R., Li, L., Pan, G., Paz-Ferreiro, J., 2013. Biochar's effect on crop productivity and the dependence on experimental

conditions-a meta-analysis of literature data. Plant Soil. https://doi.org/10.1007/s11104-013-1806-x

Lu, Y., Wei, X.-Y., Cao, J.-P., Li, P., Liu, F.-J., Zhao, Y.-P., Fan, X., Zhao, W., Rong, L.-C., Wei, Y.-B., Wang, S.-Z., Zhou, J., Zong, Z.-M., 2012. Characterization of a bio-oil from pyrolysis of rice husk by detailed compositional analysis and structural investigation of lignin. Bioresour. Technol. 116, 114–119. https://doi.org/10.1016/j.biortech.2012.04.006

Major, J., Rondon, M., Molina, D., Riha, S.J., Lehmann, J., 2012. Nutrient Leaching in a Colombian Savanna Oxisol Amended with Biochar. J. Environ. Qual. 41, 1076–1086. https://doi.org/10.2134/jeq2011.0128

Manigandan, R., Giribabu, K., Munusamy, S., Praveen Kumar, S., Muthamizh, S., Dhanasekaran, T., Padmanaban, A., Suresh, R., Stephen, A., Narayanan, V., 2015. Manganese sesquioxide to trimanganese tetroxide hierarchical hollow nanostructures: Effect of gadolinium on structural, thermal, optical and magnetic properties. CrystEngComm. https://doi.org/10.1039/c4ce02390k

Manisalidis, I., Stavropoulou, E., Stavropoulos, A., Bezirtzoglou, E., 2020. Environmental and Health Impacts of Air Pollution: A Review. Front. Public Heal. 8. https://doi.org/10.3389/fpubh.2020.00014

Mankasingh, U., Choi, P.-C., Ragnarsdottir, V., 2011. Biochar application in a tropical, agricultural region: A plot scale study in Tamil Nadu, India. Appl. Geochemistry 26, S218–S221. https://doi.org/10.1016/j.apgeochem.2011.03.108

Mansoor, S., Kour, N., Manhas, S., Zahid, S., Wani, O.A., Sharma, V., Wijaya, L., Alyemeni, M.N., Alsahli, A.A., El-Serehy, H.A., Paray, B.A., Ahmad, P., 2021. Biochar as a tool for effective management of drought and heavy metal toxicity. Chemosphere 271, 129458. https://doi.org/10.1016/j.chemosphere.2020.129458

Martins, D.D. dos santos, Serra, J.C.V., Zukowski Junior, J.C., Pedroza, M.M., 2019. Efficiency of biochars in the removal of heavy metals. Acta Bras. 3, 131. https://doi.org/10.22571/2526-4338242

Masindi, V., Muedi, K.L., 2018. Environmental Contamination by Heavy Metals, in: Heavy Metals. InTech. https://doi.org/10.5772/intechopen.76082

Mensah, A.K., Frimpong, K.A., 2018. Biochar and/or Compost Applications Improve Soil Properties, Growth, and Yield of Maize Grown in Acidic Rainforest and Coastal Savannah Soils in Ghana. Int. J. Agron. 2018, 1–8. https://doi.org/10.1155/2018/6837404

Meyer, S., Glaser, B., Quicker, P., 2011. Technical, Economical, and Climate-Related Aspects of Biochar Production Technologies: A Literature Review. Environ. Sci. Technol. 45, 9473–9483. https://doi.org/10.1021/es201792c

Michálková, Z., Komárek, M., Šillerová, H., Della Puppa, L., Joussein, E., Bordas, F., Vaněk, A., Vaněk, O., Ettler, V., 2014. Evaluating the potential of three Fe- and Mn-(nano)oxides for the stabilization of Cd, Cu and Pb in contaminated soils. J. Environ. Manage. 146, 226–234. https://doi.org/10.1016/J.JENVMAN.2014.08.004

Michálková, Z., Komárek, M., Veselská, V., Číhalová, S., 2016a. Selected Fe and Mn (nano)oxides as perspective amendments for the stabilization of As in contaminated soils. Environ. Sci. Pollut. Res. 23, 10841–10854. https://doi.org/10.1007/s11356-016-6200-9

Michálková, Z., Komárek, M., Veselská, V., Číhalová, S., 2016b. Selected Fe and Mn (nano)oxides as perspective amendments for the stabilization of As in contaminated soils. Environ. Sci. Pollut. Res. 2016 2311 23, 10841–10854. https://doi.org/10.1007/S11356-016-6200-9

Michálková, Z., Komárek, M., Vítková, M., Řečínská, M., Ettler, V., 2016c. Stability, transformations and stabilizing potential of an amorphous manganese oxide and its surface-modified form in contaminated soils. Appl. Geochemistry. https://doi.org/10.1016/j.apgeochem.2016.10.020

Michálková, Z., Komárek, M., Vítková, M., Řečínská, M., Ettler, V., 2016d. Stability, transformations and stabilizing potential of an amorphous manganese oxide and its surface-modified form in contaminated soils. Appl. Geochemistry 75, 125–136. https://doi.org/10.1016/j.apgeochem.2016.10.020

Michálková, Z., Martínez-Fernández, D., Komárek, M., 2017. Interactions of two novel stabilizing amendments with sunflower plants grown in a contaminated soil. Chemosphere 186, 374–380.

https://doi.org/10.1016/j.chemosphere.2017.08.009

Miheretu, B., 2020. Soil acid Management using Biochar: Review. Int. J. Agric. Sci. Food Technol. 211–217. https://doi.org/10.17352/2455-815X.000076

Mitchell, K., Trakal, L., Sillerova, H., Avelar-González, F.J., Guerrero-Barrera, A.L., Hough, R., Beesley, L., 2018. Mobility of As, Cr and Cu in a contaminated grassland soil in response to diverse organic amendments; a sequential column leaching experiment. Appl. Geochemistry 88, 95–102. https://doi.org/10.1016/j.apgeochem.2017.05.020

Moene, F.A., van Dam, C.J., 2014. Transport in the Atmosphere-Vegetation-Soil Continuum. Cambridge university press, New York.

Mohamed, B.A., Ellis, N., Kim, C.S., Bi, X., Emam, A.E.R., 2016. Engineered biochar from microwave-assisted catalytic pyrolysis of switchgrass for increasing water-holding capacity and fertility of sandy soil. Sci. Total Environ. 566–567, 387–397.

Mohan, D., Kumar, H., Sarswat, A., Alexandre-Franco, M., Pittman, C.U., 2014a. Cadmium and lead remediation using magnetic oak wood and oak bark fast pyrolysis bio-chars. Chem. Eng. J. 236, 513–528. https://doi.org/10.1016/J.CEJ.2013.09.057

Mohan, D., Kumar, S., Srivastava, A., 2014b. Fluoride removal from ground water using magnetic and nonmagnetic corn stover biochars. Ecol. Eng. 73, 798–808. https://doi.org/10.1016/j.ecoleng.2014.08.017

Mohan, D., Sarswat, A., Ok, Y.S., Pittman, C.U., 2014c. Organic and inorganic contaminants removal from water with biochar, a renewable, low cost and sustainable adsorbent – A critical review. Bioresour. Technol. 160, 191–202. https://doi.org/10.1016/J.BIORTECH.2014.01.120

Mollon, L.C., Norton, G.J., Trakal, L., Moreno-Jimenez, E., Elouali, F.Z., Hough, R.L., Beesley, L., 2016. Mobility and toxicity of heavy metal(loid)s arising from contaminated wood ash application to a pasture grassland soil. Environ. Pollut. 218, 419–427. https://doi.org/10.1016/J.ENVPOL.2016.07.021

Moreno-Jiménez, E., Beesley, L., Lepp, N.W., Dickinson, N.M., Hartley, W., Clemente, R., 2011. Field sampling of soil pore water to evaluate trace element mobility and associated environmental risk. Environ. Pollut. 159, 3078–3085.

https://doi.org/10.1016/j.envpol.2011.04.004

Mukherjee, A., Zimmerman, A.R., Harris, W., 2011. Surface chemistry variations among a series of laboratory-produced biochars. Geoderma 163, 247–255.

Nag, S.K., Kookana, R., Smith, L., Krull, E., Macdonald, L.M., Gill, G., 2011. Poor efficacy of herbicides in biochar-amended soils as affected by their chemistry and mode of action. Chemosphere 84, 1572–1577. https://doi.org/10.1016/j.chemosphere.2011.05.052

Ng, J.C., 2005. Environmental Contamination of Arsenic and its Toxicological Impact on Humans. Environ. Chem. 2, 146. https://doi.org/10.1071/EN05062

Nigussie, A., Kissi, E., Misganaw, M., Ambaw, G., 2012. Effect of biochar application on soil properties and nutrient uptake of lettuces (Lactuca sativa) grown in chromium polluted soils. Am. J. Agric. Environ. Sci. 12, 369–376.

Nurchi, V.M., Villaescusa, I., 2008. Agricultural biomasses as sorbents of some trace metals. Coord. Chem. Rev. 252, 1178–1188. https://doi.org/10.1016/j.ccr.2007.09.023

Ociński, D., Jacukowicz-Sobala, I., Mazur, P., Raczyk, J., Kociołek-Balawejder, E., 2016. Water treatment residuals containing iron and manganese oxides for arsenic removal from water - Characterization of physicochemical properties and adsorption studies. Chem. Eng. J. https://doi.org/10.1016/j.cej.2016.02.111

Omondi, M.O., Xia, X., Nahayo, A., Liu, X., Korai, P.K., Pan, G., 2016. Quantification of biochar effects on soil hydrological properties using meta-analysis of literature data. Geoderma 274, 28–34. https://doi.org/10.1016/j.geoderma.2016.03.029

Palansooriya, K.N., Shaheen, S.M., Chen, S.S., Tsang, D.C.W., Hashimoto, Y., Hou, D., Bolan, N.S., Rinklebe, J., Ok, Y.S., 2020. Soil amendments for immobilization of potentially toxic elements in contaminated soils: A critical review. Environ. Int. 134, 105046. https://doi.org/10.1016/j.envint.2019.105046

Parkhurst, D.L., Appelo, C.A.J., others, 2013. Description of input and examples for PHREEQC version 3—a computer program for speciation, batch-reaction, one-dimensional transport, and inverse geochemical calculations. US Geol. Surv. Tech. methods 6, 497.

Peake, L.R., Reid, B.J., Tang, X., 2014. Quantifying the influence of biochar on the physical and hydrological properties of dissimilar soils. Geoderma 235–236, 182–190.

Pérez, R., Tapia, Y., Antilén, M., Casanova, M., Vidal, C., Silambarasan, S., Cornejo, P., 2021. Rhizosphere Management for Phytoremediation of Copper Mine Tailings. J. Soil Sci. Plant Nutr. 21, 3091–3109. https://doi.org/10.1007/s42729-021-00591-0

Pinsino, A., Matranga, V., Carmela, M., 2012. Manganese: A New Emerging Contaminant in the Environment, in: Environmental Contamination. https://doi.org/10.5772/31438

Pütün, A.E., Uzun, B.B., Apaydin, E., Pütün, E., 2005. Bio-oil from olive oil industry wastes: Pyrolysis of olive residue under different conditions. Fuel Process. Technol. 87, 25–32. https://doi.org/10.1016/j.fuproc.2005.04.003

Qin, G., Niu, Z., Yu, J., Li, Z., Ma, J., Xiang, P., 2021. Soil heavy metal pollution and food safety in China: Effects, sources and removing technology. Chemosphere 267, 129205. https://doi.org/10.1016/j.chemosphere.2020.129205

Rabbi, S.M.F., Minasny, B., Salami, S.T., McBratney, A.B., Young, I.M., 2021. Greater, but not necessarily better: The influence of biochar on soil hydraulic properties. Eur. J. Soil Sci. 72, 2033–2048. https://doi.org/10.1111/ejss.13105

Rajapaksha, A.U., Chen, S.S., Tsang, D.C.W., Zhang, M., Vithanage, M., Mandal, S., Gao, B., Bolan, N.S., Ok, Y.S., 2016. Engineered/designer biochar for contaminant removal/immobilization from soil and water: Potential and implication of biochar modification. Chemosphere 148, 276–291. https://doi.org/10.1016/J.CHEMOSPHERE.2016.01.043

Rapp, L., Bergmann, F., Zimmermann, W., 2016. Pattern orientation in finite domains without boundaries. EPL (Europhysics Lett. 113, 28006.

Rawat, J., Saxena, J., Sanwal, P., 2019. Biochar: A Sustainable Approach for Improving Plant Growth and Soil Properties, in: Biochar - An Imperative Amendment for Soil and the Environment. IntechOpen. https://doi.org/10.5772/intechopen.82151

Rawls, W.J., Pachepsky, Y.A., Ritchie, J.C., Sobecki, T.M., Bloodworth, H., 2003. Effect

of soil organic carbon on soil water retention. Geoderma 116, 61–76.

Razzaghi, F., Obour, P.B., Arthur, E., 2020. Does biochar improve soil water retention? A systematic review and meta-analysis. Geoderma 361, 114055. https://doi.org/10.1016/j.geoderma.2019.114055

Regmi, P., Garcia Moscoso, J.L., Kumar, S., Cao, X., Mao, J., Schafran, G., 2012. Removal of copper and cadmium from aqueous solution using switchgrass biochar produced via hydrothermal carbonization process. J. Environ. Manage. 109, 61–69. https://doi.org/10.1016/j.jenvman.2012.04.047

Rehman, M.Z. ur, Khalid, H., Akmal, F., Ali, S., Rizwan, M., Qayyum, M.F., Iqbal, M., Khalid, M.U., Azhar, M., 2017. Effect of limestone, lignite and biochar applied alone and combined on cadmium uptake in wheat and rice under rotation in an effluent irrigated field. Environ. Pollut. 227, 560–568. https://doi.org/10.1016/j.envpol.2017.05.003

Rogovska, N., Laird, D.A., Rathke, S.J., Karlen, D.L., 2014. Biochar impact on Midwestern Mollisols and maize nutrient availability. Geoderma 230–231, 340–347.

Román-Ross, G., Cuello, G.J., Turrillas, X., Fernández-Martínez, A., Charlet, L., 2006. Arsenite sorption and co-precipitation with calcite. Chem. Geol. https://doi.org/10.1016/j.chemgeo.2006.04.007

Salvestrini, S., Leone, V., Iovino, P., Canzano, S., Capasso, S., 2014. Considerations about the correct evaluation of sorption thermodynamic parameters from equilibrium isotherms. J. Chem. Thermodyn. 68, 310–316. https://doi.org/10.1016/j.jct.2013.09.013

Santos, A., Fangueiro, D., Moral, R., Bernal, M.P., 2018. Composts Produced From Pig Slurry Solids: Nutrient Efficiency and N-Leaching Risks in Amended Soils. Front. Sustain. Food Syst. 2. https://doi.org/10.3389/fsufs.2018.00008

Shahbaz, M., Ashraf, M., 2013. Improving Salinity Tolerance in Cereals. CRC. Crit. Rev. Plant Sci. 32, 237–249. https://doi.org/10.1080/07352689.2013.758544

Shakoor, M.B., Ali, S., Rizwan, M., Abbas, F., Bibi, I., Riaz, M., Khalil, U., Niazi, N.K., Rinklebe, J., 2020. A review of biochar-based sorbents for separation of heavy metals from water. Int. J. Phytoremediation 22, 111–126.

https://doi.org/10.1080/15226514.2019.1647405

Sharma, G., Naushad, M., 2020. Adsorptive removal of noxious cadmium ions from aqueous medium using activated carbon/zirconium oxide composite: Isotherm and kinetic modelling. J. Mol. Liq. 310, 113025. https://doi.org/10.1016/j.molliq.2020.113025

Shetty, R., Prakash, N.B., 2020. Effect of different biochars on acid soil and growth parameters of rice plants under aluminium toxicity. Sci. Rep. 10, 12249. https://doi.org/10.1038/s41598-020-69262-x

Shi, G., Shen, Y., Liu, J., Wang, C., Wang, Y., Song, B., Hu, J., Fang, H., 2015. Molecular-scale Hydrophilicity Induced by Solute: Molecular-thick Charged Pancakes of Aqueous Salt Solution on Hydrophobic Carbon-based Surfaces. Sci. Rep. 4, 6793. https://doi.org/10.1038/srep06793

Simonich, S.L., Hites, R.A., 1995. Global Distribution of Persistent Organochlorine Compounds. Science (80-.). 269, 1851–1854. https://doi.org/10.1126/science.7569923

Šimůnek, J., Genuchten, M.T., Šejna, M., 2016. Recent Developments and Applications of the HYDRUS Computer Software Packages. Vadose Zo. J. 15, 1–25. https://doi.org/10.2136/vzj2016.04.0033

Šimůnek, J., Genuchten, M.T., Šejna, M., 2008. Development and Applications of the HYDRUS and STANMOD Software Packages and Related Codes. Vadose Zo. J. 7, 587–600. https://doi.org/10.2136/vzj2007.0077

Šimůnek, J., Jarvis, N.J., Van Genuchten, M.T., Gärdenäs, A., 2003. Review and comparison of models for describing non-equilibrium and preferential flow and transport in the vadose zone. J. Hydrol. 272, 14–35.

Singh, J., Upadhyay, S.K., Pathak, R.K., Gupta, V., 2011. Accumulation of heavy metals in soil and paddy crop (Oryza sativa), irrigated with water of Ramgarh Lake, Gorakhpur, UP, India. Toxicol. Environ. Chem. 93, 462–473. https://doi.org/10.1080/02772248.2010.546559

Smebye, A., Alling, V., Vogt, R.D., Gadmar, T.C., Mulder, J., Cornelissen, G., Hale, S.E., 2016. Biochar amendment to soil changes dissolved organic matter content and composition. Chemosphere 142, 100–105.

https://doi.org/10.1016/j.chemosphere.2015.04.087

Soja, G., Bücker, J., Gunczy, S., Kitzler, B., Klinglmüller, M., Kloss, S., Watzinger, A., Wimmer, B., Zechmeister-Boltenstern, S., Zehetner, F., 2014. Economic feasibility of biochar application to soils in temperate climate regions, in: EGU General Assembly Conference Abstracts, EGU General Assembly Conference Abstracts. p. 8421.

Song, Z., Lian, F., Yu, Z., Zhu, L., Xing, B., Qiu, W., 2014. Synthesis and characterization of a novel MnOx-loaded biochar and its adsorption properties for Cu2+ in aqueous solution. Chem. Eng. J. 242, 36–42. https://doi.org/10.1016/J.CEJ.2013.12.061

Sparks, D.L., 2003. Environmental soil chemistry. Elsevier.

Steefel, C.I., Appelo, C.A.J., Arora, B., Jacques, D., Kalbacher, T., Kolditz, O., Lagneau, V., Lichtner, P.C., Mayer, K.U., Meeussen, J.C.L., Molins, S., Moulton, D., Shao, H., Šimůnek, J., Spycher, N., Yabusaki, S.B., Yeh, G.T., 2015. Reactive transport codes for subsurface environmental simulation. Comput. Geosci. 19, 445–478. https://doi.org/10.1007/s10596-014-9443-x

Streubel, J.D., Collins, H.P., Garcia-Perez, M., Tarara, J., Granatstein, D., Kruger, C.E., 2011. Influence of Contrasting Biochar Types on Five Soils at Increasing Rates of Application. Soil Sci. Soc. Am. J. 75, 1402–1413. https://doi.org/10.2136/SSSAJ2010.0325

Su, Q., Pan, B., Wan, S., Zhang, W., Lv, L., 2010. Use of hydrous manganese dioxide as a potential sorbent for selective removal of lead, cadmium, and zinc ions from water. J. Colloid Interface Sci. https://doi.org/10.1016/j.jcis.2010.05.052

Takagi, H., Maruyama, K., Yoshizawa, N., Yamada, Y., Sato, Y., 2004. XRD analysis of carbon stacking structure in coal during heat treatment. Fuel. https://doi.org/10.1016/j.fuel.2004.06.019

Tammeorg, P., Simojoki, A., Mäkelä, P., Stoddard, F.L., Alakukku, L., Helenius, J., 2014. Biochar application to a fertile sandy clay loam in boreal conditions: Effects on soil properties and yield formation of wheat, turnip rape and faba bean. Plant Soil 374, 89–107. https://doi.org/10.1007/S11104-013-1851-5

Tipping, E., Lofts, S., Sonke, J.E., 2011. Humic Ion-Binding Model VII: a revised

parameterisation of cation-binding by humic substances. Environ. Chem. 8, 225. https://doi.org/10.1071/EN11016

Tipping, E., Rieuwerts, J., Pan, G., Ashmore, M.R., Lofts, S., Hill, M.T.R., Farago, M.E., Thornton, I., 2003. The solid–solution partitioning of heavy metals (Cu, Zn, Cd, Pb) in upland soils of England and Wales. Environ. Pollut. 125, 213–225. https://doi.org/10.1016/S0269-7491(03)00058-7

Trakal, L., Bingöl, D., Pohořelý, M., Hruška, M., Komárek, M., 2014a. Geochemical and spectroscopic investigations of Cd and Pb sorption mechanisms on contrasting biochars: Engineering implications. Bioresour. Technol. 171, 442–451. https://doi.org/10.1016/J.BIORTECH.2014.08.108

Trakal, L., Bingöl, D., Pohořelý, M., Hruška, M., Komárek, M., 2014b. Geochemical and spectroscopic investigations of Cd and Pb sorption mechanisms on contrasting biochars: Engineering implications. Bioresour. Technol. 171, 442–451. https://doi.org/10.1016/j.biortech.2014.08.108

Trakal, L., Komárek, M., Száková, J., Tlustoš, P., Tejnecký, V., Drábek, O., 2012. Sorption Behavior of Cd, Cu, Pb, and Zn and Their Interactions in Phytoremediated Soil. Int. J. Phytoremediation 14, 806–819. https://doi.org/10.1080/15226514.2011.628714

Trakal, L., Michálková, Z., Beesley, L., Vítková, M., Ouředníček, P., Barceló, A.P., Ettler, V., Číhalová, S., Komárek, M., 2018a. AMOchar: Amorphous manganese oxide coating of biochar improves its efficiency at removing metal(loid)s from aqueous solutions. Sci. Total Environ. https://doi.org/10.1016/j.scitotenv.2017.12.267

Trakal, L., Michálková, Z., Beesley, L., Vítková, M., Ouředníček, P., Barceló, A.P., Ettler, V., Číhalová, S., Komárek, M., 2018b. AMOchar: Amorphous manganese oxide coating of biochar improves its efficiency at removing metal(loid)s from aqueous solutions. Sci. Total Environ. 625, 71–78. https://doi.org/10.1016/j.scitotenv.2017.12.267

Trakal, L., Raya-Moreno, I., Mitchell, K., Beesley, L., 2017a. Stabilization of metal(loid)s in two contaminated agricultural soils: Comparing biochar to its non-pyrolysed source material. Chemosphere. https://doi.org/10.1016/j.chemosphere.2017.04.064

235

Trakal, L., Raya-Moreno, I., Mitchell, K., Beesley, L., 2017b. Stabilization of metal(loid)s in two contaminated agricultural soils: Comparing biochar to its non-pyrolysed source material. Chemosphere 181, 150–159. https://doi.org/10.1016/j.chemosphere.2017.04.064

Trakal, L., Šigut, R., Šillerová, H., Faturíková, D., Komárek, M., 2014c. Copper removal from aqueous solution using biochar: Effect of chemical activation. Arab. J. Chem. 7, 43–52. https://doi.org/10.1016/j.arabjc.2013.08.001

Trakal, L., Veselská, V., Šafařík, I., Vítková, M., Číhalová, S., Komárek, M., 2016. Lead and cadmium sorption mechanisms on magnetically modified biochars. Bioresour. Technol. 203, 318–324. https://doi.org/10.1016/J.BIORTECH.2015.12.056

Tran, H.N., Lee, C.K., Nguyen, T.V., Chao, H.P., 2018. Saccharide-derived microporous spherical biochar prepared from hydrothermal carbonization and different pyrolysis temperatures: synthesis, characterization, and application in water treatment. Environ. Technol. (United Kingdom). https://doi.org/10.1080/09593330.2017.1365941

Tufféry, S., 2011. Data mining and statistics for decision making. Wiley Chichester.

Uchimiya, M., Chang, S., Klasson, K.T., 2011. Screening biochars for heavy metal retention in soil: Role of oxygen functional groups. J. Hazard. Mater. 190, 432–441. https://doi.org/10.1016/j.jhazmat.2011.03.063

Uzoma, K.C., Inoue, M., Andry, H., Zahoor, A., Nishihara, E., others, 2011. Influence of biochar application on sandy soil hydraulic properties and nutrient retention. J. Food, Agric. Environ. 9, 1137–1143.

Van Genuchten, M.T. van, Leij, F.J., Yates, S.R., others, 1991. The RETC code for quantifying the hydraulic functions of unsaturated soils.

Vasiliki Maipa, Yannis Alamanos, E., 2001. Seasonal fluctuation of bacterial indicators in coastal waters. Microb. Ecol. Health Dis. 13, 143–146. https://doi.org/10.1080/089106001750462687

Verheijen, F., Jeffery, S., Bastos, A.C., der Velde, M., Diafas, I., 2010. Biochar application to soils. A Crit. Sci. Rev. Eff. soil Prop. Process. Funct. EUR 24099, 162.

Volesky, B., Holan, Z.R., 1995. Biosorption of heavy metals. Biotechnol. Prog. 11, 235–250. https://doi.org/10.1021/bp00033a001

Walker, D.J., Clemente, R., Roig, A., Bernal, M.P., 2003. The effects of soil amendments on heavy metal bioavailability in two contaminated Mediterranean soils. Environ. Pollut. 122, 303–312. https://doi.org/10.1016/S0269-7491(02)00287-7

Wang, C., Walter, M.T., Parlange, J.Y., 2013. Modeling simple experiments of biochar erosion from soil. J. Hydrol. 499, 140–145.

Wang, D., Li, C., Parikh, S.J., Scow, K.M., 2019. Impact of biochar on water retention of two agricultural soils – A multi-scale analysis. Geoderma 340, 185–191. https://doi.org/10.1016/j.geoderma.2019.01.012

Wang, H.-Y., Chen, P., Zhu, Y.-G., Cen, K., Sun, G.-X., 2019. Simultaneous adsorption and immobilization of As and Cd by birnessite-loaded biochar in water and soil. Environ. Sci. Pollut. Res. 26, 8575–8584. https://doi.org/10.1007/s11356-019-04315-x

Wang, H., Gao, B., Wang, S., Fang, J., Xue, Y., Yang, K., 2015. Removal of Pb(II), Cu(II), and Cd(II) from aqueous solutions by biochar derived from KMnO4 treated hickory wood. Bioresour. Technol. 197, 356–362. https://doi.org/10.1016/J.BIORTECH.2015.08.132

Wang, M.C., Sheng, G.D., Qiu, Y.P., 2015. A novel manganese-oxide/biochar composite for efficient removal of lead(II) from aqueous solutions. Int. J. Environ. Sci. Technol. https://doi.org/10.1007/s13762-014-0538-7

Wang, Q., Zhang, Z., Xu, G., Li, G., 2021. Magnetic porous biochar with nanostructure surface derived from penicillin fermentation dregs pyrolysis with K2FeO4 activation: Characterization and application in penicillin adsorption. Bioresour. Technol. 327, 124818. https://doi.org/10.1016/j.biortech.2021.124818

Wang, S., Gao, B., Li, Y., Mosa, A., Zimmerman, A.R., Ma, L.Q., Harris, W.G., Migliaccio, K.W., 2015a. Manganese oxide-modified biochars: Preparation, characterization, and sorption of arsenate and lead. Bioresour. Technol. 181, 13–17. https://doi.org/10.1016/J.BIORTECH.2015.01.044

Wang, S., Gao, B., Li, Y., Wan, Y., Creamer, A.E., 2015b. Sorption of arsenate onto

magnetic iron–manganese (Fe–Mn) biochar composites. RSC Adv. 5, 67971–67978. https://doi.org/10.1039/C5RA12137J

Wang, S., Gao, B., Zimmerman, A.R., Li, Y., Ma, L., Harris, W.G., Migliaccio, K.W., 2015c. Removal of arsenic by magnetic biochar prepared from pinewood and natural hematite. Bioresour. Technol. 175, 391–395. https://doi.org/10.1016/j.biortech.2014.10.104

Werdin, J., Fletcher, T.D., Rayner, J.P., Williams, N.S.G., Farrell, C., 2020. Biochar made from low density wood has greater plant available water than biochar made from high density wood. Sci. Total Environ. 705, 135856. https://doi.org/10.1016/j.scitotenv.2019.135856

Winiwarter, W., Erisman, J.W., Galloway, J.N., Klimont, Z., Sutton, M.A., 2013. Estimating environmentally relevant fixed nitrogen demand in the 21st century. Clim. Change 120, 889–901. https://doi.org/10.1007/s10584-013-0834-0

WU, Y., YANG, A., ZHAO, Y., LIU, Z., 2019. SIMULATION OF SOIL WATER MOVEMENT UNDER BIOCHAR APPLICATION BASED ON THE HYDRUS-1D IN THE BLACK SOIL REGION OF CHINA. Appl. Ecol. Environ. Res. 17, 4183–4192. https://doi.org/10.15666/aer/1702_41834192

Xiao, R., Ali, A., Xu, Y., Abdelrahman, H., Li, R., Lin, Y., Bolan, N., Shaheen, S.M., Rinklebe, J., Zhang, Z., 2022. Earthworms as candidates for remediation of potentially toxic elements contaminated soils and mitigating the environmental and human health risks: A review. Environ. Int. 158, 106924. https://doi.org/10.1016/j.envint.2021.106924

Xie, W., Zhao, D., 2016. Controlling phosphate releasing from poultry litter using stabilized Fe-Mn binary oxide nanoparticles. Sci. Total Environ. https://doi.org/10.1016/j.scitotenv.2015.09.063

Xu, G., Zhang, Y., Sun, J., Shao, H., 2016. Negative interactive effects between biochar and phosphorus fertilization on phosphorus availability and plant yield in saline sodic soil. Sci. Total Environ. 568, 910–915. https://doi.org/10.1016/j.scitotenv.2016.06.079

Xu, K., Wang, Z., Du, X., Safdar, M., Jiang, C., He, J., 2013. Atomic-layer triangular WSe2 sheets: Synthesis and layer-dependent photoluminescence property.

Nanotechnology. https://doi.org/10.1088/0957-4484/24/46/465705

Xu, Q., Cheng, B., Yu, J., Liu, G., 2017. Making co-condensed amorphous carbon/g-C3N4 composites with improved visible-light photocatalytic H2-production performance using Pt as cocatalyst. Carbon N. Y. https://doi.org/10.1016/j.carbon.2017.03.052

Xu, X., Cao, X., Zhao, L., Wang, H., Yu, H., Gao, B., 2013. Removal of Cu, Zn, and Cd from aqueous solutions by the dairy manure-derived biochar. Environ. Sci. Pollut. Res. 20, 358–368. https://doi.org/10.1007/s11356-012-0873-5

Xu, X., Kan, Y., Zhao, L., Cao, X., 2016. Chemical transformation of CO2 during its capture by waste biomass derived biochars. Environ. Pollut. 213, 533–540. https://doi.org/10.1016/J.ENVPOL.2016.03.013

Xue, Y., Gao, B., Yao, Y., Inyang, M., Zhang, M., Zimmerman, A.R., Ro, K.S., 2012. Hydrogen peroxide modification enhances the ability of biochar (hydrochar) produced from hydrothermal carbonization of peanut hull to remove aqueous heavy metals: Batch and column tests. Chem. Eng. J. 200–202, 673–680. https://doi.org/10.1016/j.cej.2012.06.116

Yao, Y., Gao, B., Chen, J., Zhang, M., Inyang, M., Li, Y., Alva, A., Yang, L., 2013. Engineered carbon (biochar) prepared by direct pyrolysis of Mg-accumulated tomato tissues: Characterization and phosphate removal potential. Bioresour. Technol. 138, 8–13. https://doi.org/10.1016/j.biortech.2013.03.057

Yousaf, B., Liu, G., Wang, R., Zia-ur-Rehman, M., Rizwan, M.S., Imtiaz, M., Murtaza, G., Shakoor, A., 2016. Investigating the potential influence of biochar and traditional organic amendments on the bioavailability and transfer of Cd in the soil–plant system. Environ. Earth Sci. 75, 374. https://doi.org/10.1007/s12665-016-5285-2

Yu, Z., Qiu, W., Wang, F., Lei, M., Wang, D., Song, Z., 2017. Effects of manganese oxide-modified biochar composites on arsenic speciation and accumulation in an indica rice (Oryza sativa L.) cultivar. Chemosphere 168, 341–349. https://doi.org/10.1016/j.chemosphere.2016.10.069

Yu, Z., Zhou, L., Huang, Y., Song, Z., Qiu, W., 2015. Effects of a manganese oxide-modified biochar composite on adsorption of arsenic in red soil. J. Environ.

Manage. 163, 155–162. https://doi.org/10.1016/j.jenvman.2015.08.020

Zama, E.F., Reid, B.J., Arp, H.P.H., Sun, G.-X., Yuan, H.-Y., Zhu, Y.-G., 2018. Advances in research on the use of biochar in soil for remediation: a review. J. Soils Sediments 18, 2433–2450. https://doi.org/10.1007/s11368-018-2000-9

Zhang, A., Li, X., Xing, J., Xu, G., 2020. Adsorption of potentially toxic elements in water by modified biochar: A review. J. Environ. Chem. Eng. 8, 104196. https://doi.org/10.1016/j.jece.2020.104196

Zhang, M., Gao, B., Varnoosfaderani, S., Hebard, A., Yao, Y., Inyang, M., 2013. Preparation and characterization of a novel magnetic biochar for arsenic removal. Bioresour. Technol. 130, 457–462. https://doi.org/10.1016/j.biortech.2012.11.132

Zhang, M., Gao, B., Yao, Y., Xue, Y., Inyang, M., 2012. Synthesis of porous MgO-biochar nanocomposites for removal of phosphate and nitrate from aqueous solutions. Chem. Eng. J. 210, 26–32. https://doi.org/10.1016/j.cej.2012.08.052

Zhang, S., Grip, H., Lövdahl, L., 2006. Effect of soil compaction on hydraulic properties of two loess soils in China. Soil Tillage Res. 90, 117–125.

Zhang, X., Wang, H., He, L., Lu, K., Sarmah, A., Li, J., Bolan, N.S., Pei, J., Huang, H., 2013. Using biochar for remediation of soils contaminated with heavy metals and organic pollutants. Environ. Sci. Pollut. Res. 20, 8472–8483. https://doi.org/10.1007/s11356-013-1659-0

Zheng, Q., Yang, L., Song, D., Zhang, S., Wu, H., Li, S., Wang, X., 2020. High adsorption capacity of Mg–Al-modified biochar for phosphate and its potential for phosphate interception in soil. Chemosphere 259, 127469. https://doi.org/10.1016/j.chemosphere.2020.127469

Zhou, Y., Gao, B., Zimmerman, A.R., Chen, H., Zhang, M., Cao, X., 2014. Biochar-supported zerovalent iron for removal of various contaminants from aqueous solutions. Bioresour. Technol. 152, 538–542. https://doi.org/10.1016/j.biortech.2013.11.021

Zhou, Y., Gao, B., Zimmerman, A.R., Fang, J., Sun, Y., Cao, X., 2013. Sorption of heavy metals on chitosan-modified biochars and its biological effects. Chem. Eng. J. 231, 512–518. https://doi.org/10.1016/j.cej.2013.07.036

Zimmerman, A.R., Gao, B., Ahn, M.-Y., 2011. Positive and negative carbon mineralization priming effects among a variety of biochar-amended soils. Soil Biol. Biochem. 43, 1169–1179. https://doi.org/10.1016/j.soilbio.2011.02.005

Curriculum vitae & List of publications

Petr Ouředníček

Born: 1ˢᵗ June, 1989, Brno (Czech Republic)

Address: Lánice 47, 595 01, Velká Bíteš, Czech Republic

E-mail: ourednicek@fzp.czu.cz

Education

2015 – present: Ph.D. studies

Applied and landscape ecology, Faculty of Environmental Sciences

Czech University of Life Sciences, Prague, Czech Republic

Thesis: *Biochar based amendments in the environment; different modeling approaches*

2012 – 2015:   Master study program

Environmental Modelling, Faculty of Environmental Sciences

Czech University of Life Sciences, Prague, Czech Republic

Thesis: *Simulation of Pb and Zn transport through the soil profile after amorphous manganese oxide (AMO) treating*

2008 – 2012:   Bachelor study program

Applied Ecology, Faculty of Environmental Sciences

Czech University of Life Sciences, Prague, Czech Republic

Thesis: *Grape stalk waste as a low-cost sorbent of hexavalent chromium*

244

Publications

Jačka L., Trakal L., **Ouředníček P.,** Pohořelý M., Šípek V. (2018) Biochar presence in soil significantly decreased saturated hydraulic conductivity due to swelling. Soil and Tillage Research,184:181-185

Trakal L., Michálková Z., Beesley L., Vítková M., **Ouředníček P.,** Barceló A. P., Ettler V., Číhalová S., Komárek M.(2018) AMOchar: Amorphous manganese oxide coating of biochar improves its efficiency at removing metal(loid)s from aqueous solutions. Science of the Total Environment, Volume 625: 71-78

Hudcová B., Vítková M., **Ouředníček P.,** Komárek, M. (2018) Stability and stabilizing efficiency of Mg-Fe layered double hydroxides and mixed oxides in aqueous solutions and soils with elevated As(V), Pb(II) and Zn(II) contents. Science of the Total Environment, Volume 648: 1511-1519

Ouředníček,P., Hudcová B., Trakal L., Pohořelý M., Komárek M. (2019) Synthesis of modified amorphous manganese oxide using low-cost sugars and biochars: Material characterization and metal(loid) sorption properties. Science of the Total Environment, Volume 670: 1159 – 1169

Grants and projects

- Principal investigator on grant: Development and production of innovative materials from waste products for stabilization of metals and metalloids: A comprehensive experimental and model approach
  CIGA 20174204 (Czech University of Life Sciences)

- Principal investigator on grant: Modelling transport of Zn through the soil profile using laboratory columns
  IGA 20174242 (Czech University of Life Sciences)

- Investigator on project: Ministry of Education, Youth and Sports of the Czech Republic (projects no. CZ.07.1.02/0.0/0.0/16_040/0000368 and CZ.02.1.01/0.0/0.0/16_026/0008403)

- Investigator on project: Ministry of Education, Youth and Sports of the Czech Republic (COST CZ LD13068) and the Czech Science Foundation (GAČR 14-02183P)

Teaching activities

- Environmental Soil Chemistry – laboratory course
- Environmental hydrogeology
- Workshop for EGS (HYDRUS and PHREEQC modelling)
- Field Practise for EGS – laboratory course
- Supervision of 4 bachelor theses
- Consultant of 5 master theses

Voluntary and other activities

- Representative of the Czech Republic in rowing 2007 - 2021 (national champion, academic champion of the Czech Republic, participant of the European and World Rowing Championships)

- European Champion and Vice-Champion in indoor rowing (2020)

- World record holder on the indoor rowing machine in the 24-hour race (2021)